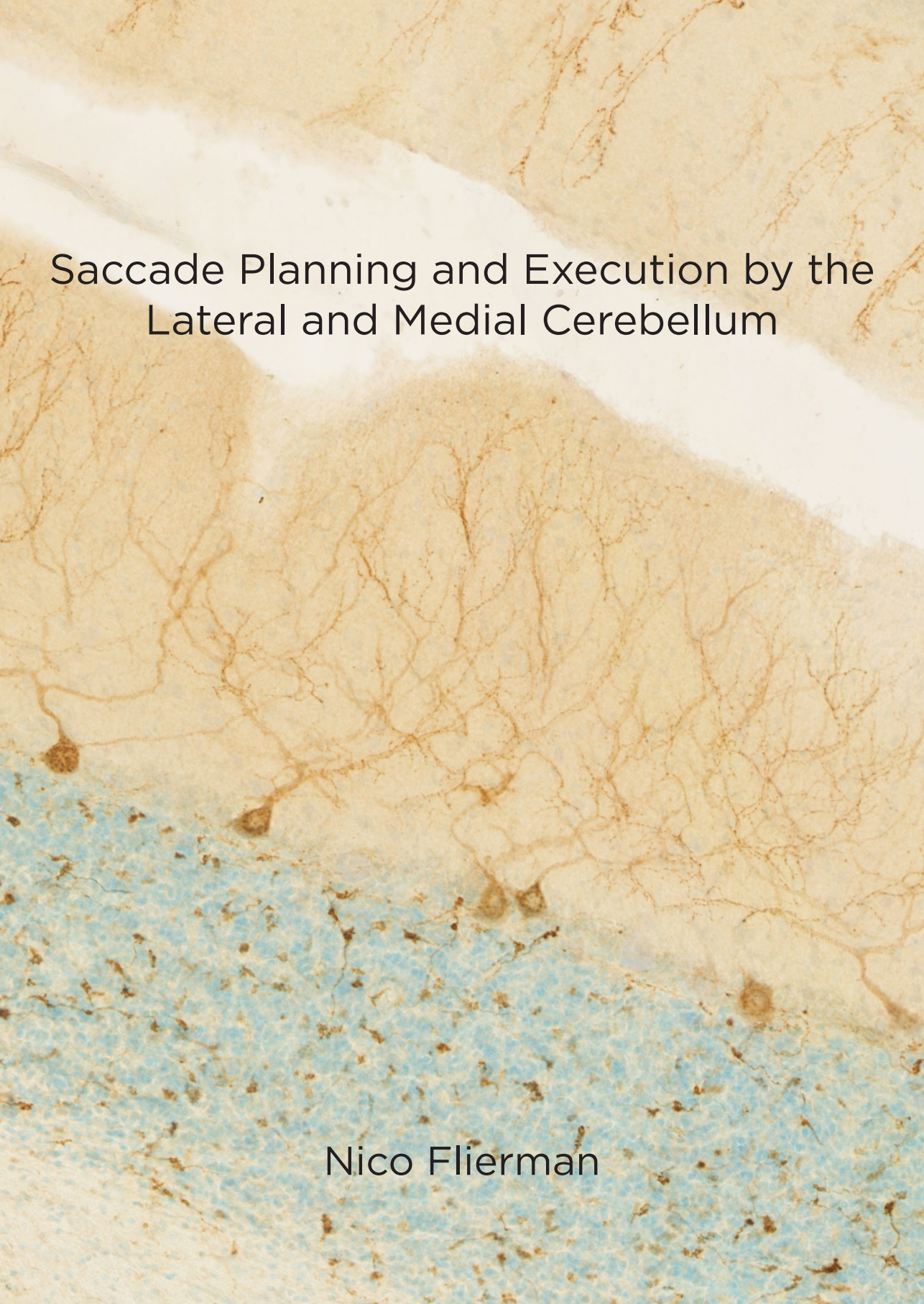

Saccade Planning and Execution by the Lateral and Medial Cerebellum

Nico Flierman

Saccade Planning and Execution by the Lateral and Medial Cerebellum

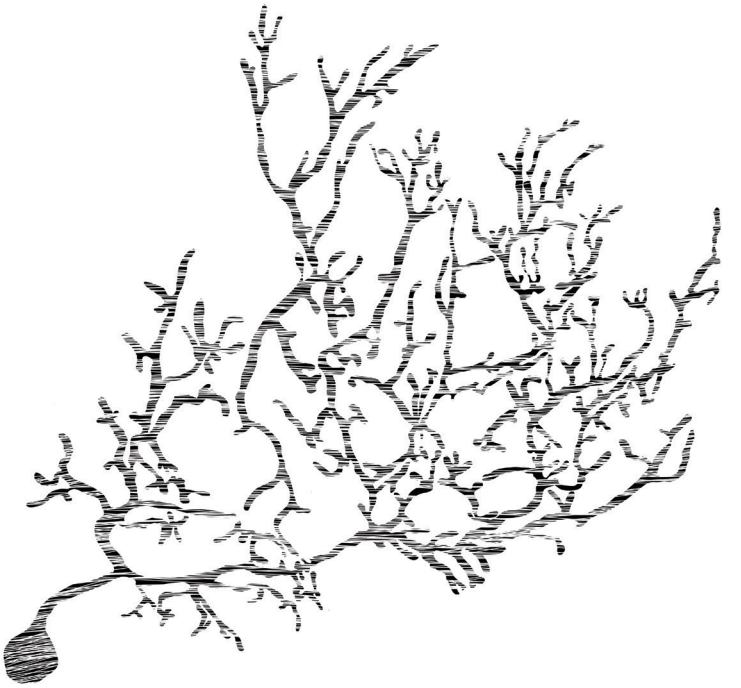

Nico Flierman

The research described in this thesis was conducted at the Netherlands Institute for Neuroscience, Amsterdam, The Netherlands. This work was supported by the Netherlands Organisation for Scientific Research (NWO).

About the cover: Staining of retrogradely labelled Purkinje cells with CtB, photographed in the lateral cerebellum. These cells are part of a network in the cerebellum that is at the intersection between visual and motor functions. For details see Chapter 4.

Illustrations and layout: Nico Flierman

Printed by: Ridderprint | www.ridderprint.nl
ISBN: 978-94-6416-732-0

Saccade Planning and Execution by the Lateral and Medial Cerebellum

Preparatie en uitvoering van saccades door het laterale en mediale cerebellum

Proefschrift
ter verkrijging van de graad van doctor aan de
Erasmus Universiteit Rotterdam
op gezag van de rector magnificus
Prof. dr. F.A. van der Duijn Schouten
en volgens besluit van het College voor Promoties

De openbare verdediging zal plaatsvinden op
dinsdag 14 September 2021 om 15.30 uur

door
Nico Adriaan Flierman
Geboren te Hilversum

Erasmus University Rotterdam

Promotiecommissie:

Promotor:	Prof. dr. C.I. de Zeeuw
Overige leden:	Dr. T.J.H. Ruigrok Dr. J. Goossens Prof. dr. S. Spijker
Copromotor:	Dr. A.M. Badura

For my mother

Table of contents

Abbreviations

ALM	anterolateral motor cortex
ANOVA	analysis of variance
AP	anterior posterior
Avg	average
BBG	brainstem burst generator
BDA10 kDa	biotinylated dextran amine molecular weight 10 kDa
BOLD	blood oxygen level dependent
CAD	computer-aided design
CDF	cumulative distribution function
CF	climbing fiber
CFU	controlled fluid uptake
CR	conditioned response
CS	complex spike
CT	computerized tomography
CtB	cholera toxin subunit B
CV	coefficient of variation
DAB	3,3'-Diaminobenzidine
DAN	dorsal attention network
DCN	deep cerebellar nuclei
dlPFC	dorsolateral prefrontal cortex
DN	dentate nucleus
EBN	excitatory burst neurons
EEG	electroencephalogram
EPSP	excitatory postsynaptic potential
FEF	frontal eye fields
fMRI	functional magnetic resonance imaging
FN	fastigial nucleus
FOR	fastigial oculomotor region
GC	granule cell
GC	Golgi cell
HA	hydroxyapatite
i.m.	intramuscular
i.v.	intravenous
IBN	inhibitory burst neurons
IN	interposed nuclei
IO	inferior olive
IPSP	inhibitory postsynaptic potential
ITI	intertrial interval
KS	Kolmogorov-Smirnov

LIP	lateral intraparietal area
LTD	long-term depression
LTP	long-term potentiation
M1	primary motor cortex
MF	mossy fiber
ML	medio-lateral
MLI	molecular layer interneuron
MRI	magnetic resonance imaging
NHP	non-human primate
NRTP	nucleus reticularis tegmenti pontis
OMV	oculomotor vermis
PBS	phosphate buffered saline
PC	Purkinje cell
PCA	principal component analysis
PEEK	polyetheretherketone
PEF	parietal eye field
PF	parallel fiber
PFA	paraformaldehyde
PN	pontine nuclei
PR	positive reinforcement
PSO	post-saccadic oscillation
Rwd	reward
SC	superior colliculus
SCHEER	Scientific Committee on Health, Environ mental and Emerging Risks
SD	standard deviation
SEF	supplementary eye fields
SEM	standard error of the mean
SS	simple spike
US	unconditioned stimulus
VOR	vestibulo-ocular reflex
VTA	ventral tegmental area
ZII	zebrin II

Chapter 1:
Introduction

1.0 General introduction

The study of the brain, neuroscience, is a relatively young field of science. Modern neuroscience is often said to have originated in the late nineteenth century with the work of the neuroanatomist Ramon y Cajal (1852–1934) and that of the founder of modern neurophysiology Lord D. Edgar Adrian (1889–1977). However, the history of the study of brain functions is much older. How different types of head injuries can lead to different symptoms was described by the author of the Edwin Smith Surgical Papyrus as early as 1000 BCE (Gross, 2009). The history of the *cerebellum*, the area under study in this thesis, is a bit more recent. The term *cerebellum*, Latin for *little brain*, was used in the second century CE as a diminutive of the *cerebrum*, to represent the small brains of small animals. The anatomical term as reference to the area in the back of the brain that is currently in use is said to be introduced by Leonardo da Vinci. However, a close study by Voogd and De Zeeuw (2020) of his works revealed no mention of the term. Instead, the authors suggest that the first use appears to be by Magnus Hundt in his *Anthropologia* from 1501. Much later, many cerebellar functions were mapped by the preeminent neurosurgeon Gordon Holmes, who studied gun-shot injuries and other traumas to the head of soldiers during World War I (Head and Holmes, 1911; Holmes, 1917; Lepore, 1994). His studies mainly cover motoric aspects of cerebellar injuries, e.g. gait problems, tremor, dystonia and voluntary movement disorders. At that time, clinical and experimental descriptions of cerebellar involvement in nonmotor functions already existed (Leiner et al., 1986, 1993), yet they only rose to interest in recent decades with advances in brain imaging (Schmahmann, 2016). Cerebellar stroke, cerebellar cortical atrophy and developmental disorders were indeed found to lead to cognitive impairments. Additionally, cerebellar abnormalities have been observed in autism spectrum disorders, schizophrenia and ADHD (Schmahmann, 1991). Thus, much of what we know today about the cerebellar involvement in higher cognition is derived from clinical and brain imaging studies. In contrast, many motoric functions of the cerebellum are understood on a cellular level, since the homology of the network allows for thorough neurophysiological investigations in animal models. In the next decades we will hopefully gain a similar level of understanding of the cognitive functions of the cerebellum.

1.1 The cerebellum

1.1.1 Gross anatomy

The cerebellum is a brain structure about the size of a peach, situated at the back of the head in the posterior fossa dorsal from the brainstem. Regardless of its relatively small size, adding up to around 10% of the volume of the brain, it is incredibly dense, containing more than half the number of neurons of the entire brain. In addition to its density, its most prominent macroscopical feature is the highly uniform and foliated structure. This extreme foliation enables compacting an immense surface area into a small volume. If we were to unfold all the folia of the human cerebellum, its total length would reach almost two meters (Braitenberg et al., 1997). Under the cerebellar surface a repetitive homogenous circuit exists, which facilitates massive parallel processing of information coming from numerous sources (Doya, 1999). The cerebellum is grossly divided into two parts: medially the vermis (''worm'' in Latin), with lateral hemispheres on both sides (**Fig. 1**). The paramedian sulcus, a shallow groove along the exterior surface, divides the two regions (Voogd and Marani, 2016). Along the transverse axis the cerebellum is divided by fissures into ten lobules denoted I-X, which

make up the anterior lobe (I-V) and the posterior lobe (V-IX), separated by the primary fissure and the flocculo-nodular lobe (X) separated from the posterior lobe by the posterolateral fissure. The division based on roman numbers was first introduced by Larsell in the early 50' (Larsell, 1952) (**Fig. 1B**). At closer inspection these lobules are made up of even smaller folds called folia.

The cerebellar cortex surrounds the deep cerebellar nuclei, consisting of medial to lateral of the fastigial nucleus, emboliform and globose nucleus together forming the interposed nuclei, and lastly the dentate nucleus (**Fig. 1A**). These nuclei receive topographically ordered input from the cortex and represent the output pathway of the cerebellum.

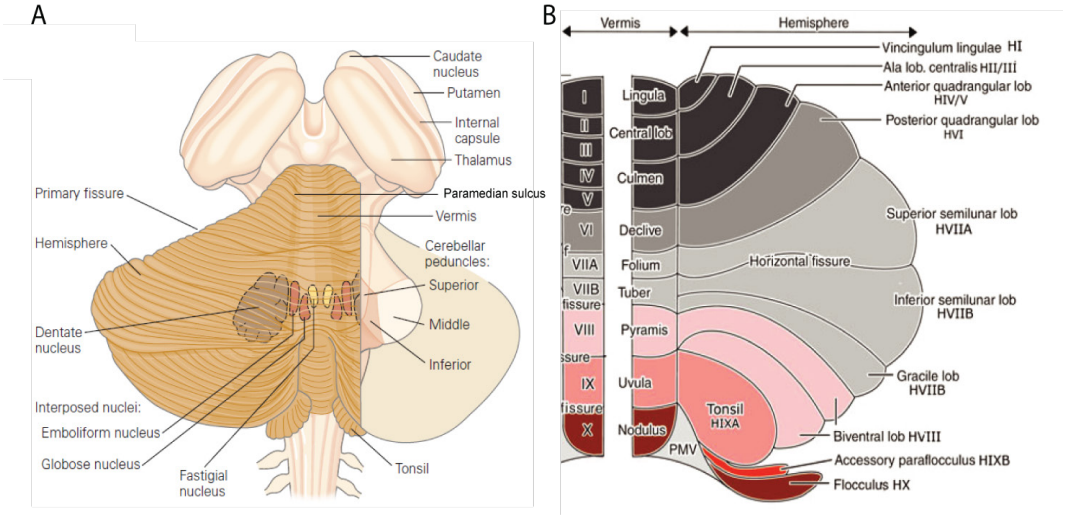

Figure 1. The cerebellum *A) Macroscopic drawing of dorsal view of the cerebellum including the spinal cord and striatum. Through the cerebellar surface the deep nuclei can be found. B) Schematic drawing of unfolded cerebellar lobuli (A, from Kandel 2000. B, from Voogd and Marani 2016).*

1.1.2 Cerebellar cortex

When cutting vertically through a folium the cerebellar cortex is revealed to consist of three layers. The inner layer is the granule cell layer, containing millions of small densely packed granule cells, and much larger, sparse Golgi cells, unipolar brush cells and Lugaro cells. The Purkinje cell (PC) layer, named after large PCs that form a one neuron thick plane, is located above the granule cell layer. The dendritic arbors of the PCs extend into the topical layer; the molecular layer. Next to the PC dendrites, the molecular layer contains parallel fibers (PF), the axons of granule cells, and interneurons, which innervate the PCs. This characteristic architecture is identical throughout the entire cerebellar cortex.

One main source of excitatory input to the cerebellum comes via mossy fibers from a variety of pre-cerebellar nuclei containing a wide variety of sensory and motor signals (Huang et al., 2013). Mossy fibers form a unique synapse with granule cells embedded in a so-called glomerulus, which is made up from the bulbous axon terminal of a mossy fiber, the axons of several Golgi cells and

granules cell dendrites (Palay and Chan-Palay, 1974). Golgi cells are large interneurons that receive excitatory input from both mossy fibers and granule cell axons providing in turn both feedforward and feedback inhibition onto granule cells as well as onto other Golgi cells (Hull and Regehr, 2012). Granule cells are small excitatory cells, which project into the molecular layer. Here, the granule cell axons bifurcate and travel in parallel along the long axis of the folium as parallel fibers where they synapse onto Golgi cells, molecular layer interneurons (MLIs), and PCs (**Fig. 2**). Due to the planar dendritic trees of PCs, which are oriented perpendicular to the parallel fibers, one parallel fiber makes synapses with many PCs over its 6 mm length in primates (Mugnaini, 1983). Stemming from this arrangement and the massive number of parallel fibers in the molecular layer, parallel fibers make roughly 200.000 synapses on an individual PC (Napper and Harvey, 1988). Glutamatergic PF afferents cause an increase in discharges in the intrinsically active PCs. PFs and mossy fibers also contact two types of MLIs, basket and stellate cells, which suppress Purkinje cell firing rates by feedforward inhibition through synaptic release of GABA. The PFs also innervate dendrites of Golgi cells and Lugaro cells (**Fig. 2**). Lastly there are also excitatory interneurons in the granular layer; these are called unipolar brush cells, after their brush-like dendrites, and they are most prominently distributed in the vestibulocerebellum (i.e., the flocculus and nodulus) and vermis (van Dorp and De Zeeuw, 2014). The second main afferent input to the cerebellar cortex is the climbing fiber (CF) pathway (**Fig. 2**). CFs are axons of inferior olivary (IO) cells and their discharge elicits complex spikes (CS) in PCs, which are strong depolarizations distinct from regular depolarizations called simple spikes (SS) (**Fig. 3**). Each PC is innervated by one CF, which makes contact over the PCs entire dendritic tree with approximately 500 to 1500 excitatory synapses; discharge of a CF always causes a CS (Palay and Chan-Palay, 1974).

1.1.3 Electrophysiology of Purkinje cells

The IO is the only source of CF input to Purkinje cells. IO cells fire at ~1 Hz in vivo, causing complex spikes, consisting of one large discharge followed by a variable number of smaller high frequency discharges called spikelets (**Fig. 3**). The CS is followed by the CF pause in which no SS's are discharged by the PC for roughly 20 ms. The CS discharges are accompanied by a huge calcium influx into the dendritic tree, which has an influence on the PF-PC synapses (Yang and Lisberger, 2014). In general, increases in CF activity induce long-term depression at conjunctively active parallel fiber synapses, which has long been regarded as the sole or at least main mechanism for motor learning through an anti-Hebbian form of synaptic pruning of erroneous synapses (Ito, 2001). However, plasticity rules are a lot more complex than that (Gao et al., 2012). Dependent on PF-CF activity timing intervals, PF simulation frequency, order of CF and PF stimulation, simultaneous activity of MLIs and even the region of the cerebellum, plasticity is influenced (for extensive overviews of plasticity rules at the PF-PC synapse see (Suvrathan and Raymond, 2018)). In the oculomotor vermis (OMV), CF activity can be triggered through motor errors. Activity at the PF to PC synapse when followed by a CS, causes that synapse to weaken probably partly through long-term depression (Catz et al., 2005). As such, this CS is classically regarded as an 'error' or 'teacher' signal, however this definition is too narrow since CS's are also directly associated with non-error signals, including motor output, sensorimotor predictions, and expected reward sizes and history of movement errors (Simpson et al., 2002; De Gruijl et al., 2014; Heffley et al., 2018; Junker et al., 2018; Larry et al., 2019).

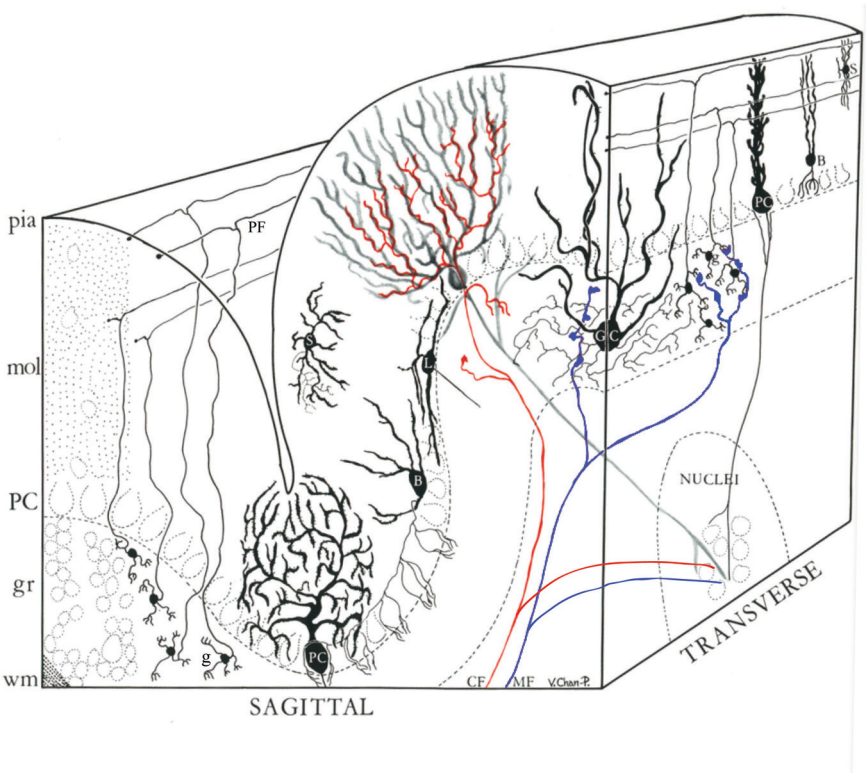

Figure 2. Sagittal section through a folium of the cerebellar cortex revealing the granule layer (gr), Purkinje cell layer (PC) and molecular layer (mol). *Climbing fiber (CF) and mossy fiber (MF) pathways are highlighted in red and blue respectively and project to the cerebellar cortex and deep nuclei. A variety of neuronal subtypes can be observed including Purkinje cell (PC), stellate cell (S), basket cell (B), Lugaro cell (K), Golgi cell (GC) and lastly granule cells (g). These give rise to the parallel fibers (PF). (Adapted from Paley and Chan-Paley 1974).*

The dynamic range of PCs' SS frequency is large; even though on average they are spontaneously active at ~60 Hz, they can completely suppress their activity for hundreds of milliseconds and then again burst up to 400 Hz (Monsivais et al., 2005). In vivo they produce spike trains with highly irregular inter-spike intervals, whereas in vitro when PF afferents are cut, they are highly regular (Shin et al., 2007; De Schutter and Steuber, 2009). In behavior related contexts PCs show many different modulation patterns, including bursts, pauses, burst-pause combinations and phasic modulation, which vary inversely with CS rates (Yakhnitsa and Barmack, 2006; Badura et al., 2013). PCs that receive the same parallel fiber inputs, called on-beam, show high degrees of synchronicity in their activity (Heck et al., 2007). These SS patterns are well known for their temporally precise linear coding of movement kinematics across different behaviors, such as whisker position, eye velocity, arm velocity, or eye blinks (Coltz et al., 1999; Herzfeld et al., 2015; Chen et al., 2016; Broersen, 2019). During tracking of a pseudo-randomly moving cursor with arm movements,

SS firing encodes both predictions of upcoming movements and feedback of kinematics. In the large majority of these PCs the SS rates also signal a form of performance errors such as position error, radial error (magnitude of the position error vector) or directional error (Popa et al., 2012). Strength of encoding of performance error is robust and comparable to encoding of movement kinematics. These two properties are not split into different subpopulations of neurons, indicating that integration of task and task error occurs at the level of individual neurons (Popa et al., 2012; Streng et al., 2018).

The complex patterns of CS and SS signals converge their inhibitory input onto the deep cerebellar nuclei cells (DCN) in a ratio of ~40 PCs to one DCN cell. It should be noted that PC axons branch out and thus make connections with tens of DCN neurons (Palkovits et al., 1977; Person and Raman, 2011). This pathway through the DCN provides the sole output of the cerebellum, which in turn reaches back to the cerebral cortex (via the thalamus), the spinal cord and a variety of

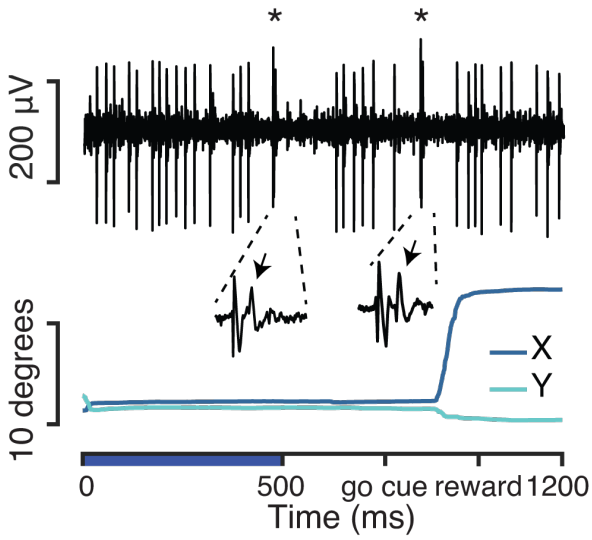

brainstem motor nuclei (Sparks, 2002; Kelly and Strick, 2003).

Figure 3. Purkinje cell activity during an antisaccade trial recorded in macaque Crus I/II. *Top, trace of extracellularly recorded Purkinje cell, with high frequency simple spikes and low frequency complex spike marked with *. In the magnification of the complex spikes, black arrows indicate spikelets. Bottom, the accompanying eye position and timeline. The blue bar in the timeline represents the instruction period of the task (for details see chapter 3).*

1.1.4 Deep cerebellar nuclei

At the heart of the cerebellum, under the cerebellar cortex and white matter we find the deep cerebellar nuclei. These nuclei provide the sole output of the cerebellar cortex to a wide variety of targets ranging from motor nuclei in the brainstem to the cerebral cortex via the thalamus.

They receive input from PCs in the cortex, mossy fibers and the IO (Ruigrok, 1997; Sparks, 2002; Kelly and Strick, 2003). Six different populations of cells are defined in the DCN, four types of projection neurons and two types of interneurons (Uusisaari and Knöpfel, 2012). Of the two types of interneurons, one is GABA/glycinergic, the other glutamatergic. However, most of the cells in the DCN are projection neurons (>95%), reinforcing the idea that they act as the output channel of the cerebellum. There are GABAergic, glutamatergic and two types of glycinergic projection neurons. The GABAergic group projects to the IO and mostly consists of small cells with somata smaller than 20 μm (Ruigrok, 1997). The glutamatergic group are the largest neurons, comparable in size with Purkinje cells that fire at high rates (up 60 Hz *in vivo*) and are known to project mostly outside of the cerebellum, among others to the thalamus and red nucleus (Rowland and Jaeger, 2005). Lastly, there are two types of glycinergic projection neurons, one that sends its projections to the cerebellar cortical granule layer, and ones that are found in the fastigial nucleus and projects to the vestibular nuclei (Bagnall et al., 2009; Uusisaari and Knöpfel, 2012).

How information is transferred from PCs to the DCN still remains an active topic of debate. The high firing frequency and convergence of PCs onto DCN neurons would suggest that DCN neurons are largely inhibited unless PCs stop firing. Pauses in PC firing are indeed common and a well-studied mechanism of behavior encoding and information transduction to the DCN (De Schutter and Steuber, 2009). Regardless, when PCs are firing many DCN cells still remain intrinsically active and PC and DCN rates do not always vary inversely (McDevitt et al., 1987; Person and Raman, 2012). After inhibitory current injection from PCs, DCN neurons can show rebound depolarization of the membrane potential accompanied by firing an action potential (Llinás and Mühlethaler, 1988; Aizenman and Linden, 1999). Rebound firing has been hypothesized to be an mechanism to store and process information for motor coordination (Wulff et al., 2009; Witter et al., 2013). However, the true relevance and existence *in vivo* under physiological conditions is still under debate (Alviña et al., 2008; Reato et al., 2016). An alternative way of information transduction from PC to DCN was recently shown on basis of the high degree of synchronicity that is present between PCs (de Solages et al., 2008; Ramirez and Stell, 2016). *In vitro* asynchronous PC IPSPs suppress nuclear neuron activity. Synchronous activity on the other hand can reliably evoke nuclear neuron spiking (Person and Raman, 2011). This explanation provides an additional mechanism of information transmission to the DCN that does not discard the information present in PC rates, which would be discarded when DCN are only allowed to spike during pauses. Most probably, information transduction happens through all three mechanisms; synchrony, pausing, and rebound firing (Person and Raman, 2012).

1.1.5 Zonal organization of the cerebellum

Purkinje cell synchronicity is not only observed in SS patterns but also very reliably in CS activity. The cells in the inferior olive that produce the CS have dendrites that are electrically coupled by connexin 36 gap junctions, which enhance CS synchronicity (De Zeeuw et al., 2003). Complex spike synchronicity in PCs is strong in parasagittal zones in the cerebellar cortex, which are approximately 500 μm wide, but can stretch over multiple lobules. Zones are biochemically defined by expression of zebrin II (ZII+) or not (ZII-), which in turn can be subdivided into microzones (Apps and Garwicz, 2005). These microzones are 100 μm or 3-19 dendritic arbors wide (Schultz et al., 2009). PCs in ZII- zones have higher spontaneous SS firing rates than in ZII+ (60 vs 90 Hz) (Zhou et al., 2014). Consequently, PCs with higher intrinsic firing rates have more bandwidth in modulating their activity

downwards, whereas cells that operate at lower frequency have more bandwidth for modulation upwards (De Zeeuw, 2021). PCs in a microzone project to a specific part of the deep cerebellar nuclei. Beside the projections to extracerebellar targets, nuclear neurons also feed information back to the inferior olive, creating a closed loop (Ruigrok, 1997). These microzones are characterized by responsiveness to the same climbing fiber stimulation and are thus regarded as functional units of the cerebellum. Separate microzones that have functional similarity, but are on different parts of the cortex, can converge onto the same cerebellar nuclear neurons (Apps and Garwicz, 2000). These complexes are termed multizonal micro-complexes and through stimulation of one specific part of the nucleus interpositus can elicit multi-joint synergies, reliable and precise execution of which is critical for survival (Rispal-Padel et al., 1982; Ekerot et al., 1995).

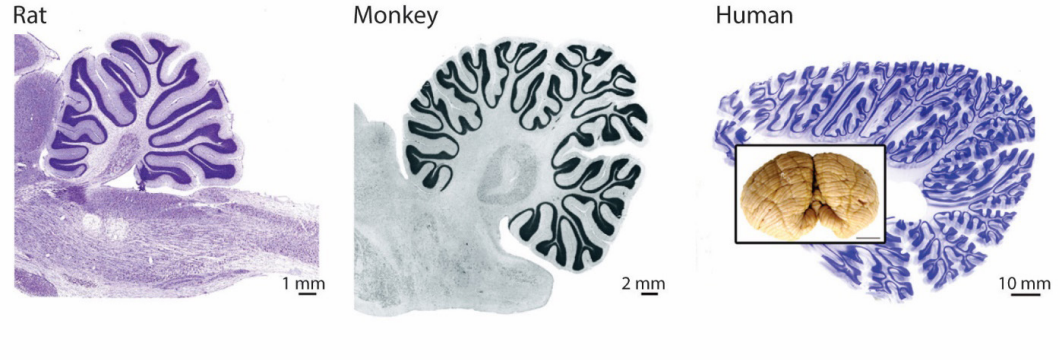

Figure 4. Cerebella from species that are often used as animal models for neuroscience research. *Adapted from (Baizer, 2014).*

1.2 The cerebellum throughout evolution

The cerebellum is remarkably conserved across species. Within roughly 50.000 extant species of vertebrates, a cerebellum has been identified in all classes (Krieg, 1967; Nieuwenhuys, 1967; Nieuwenhuys et al., 1998). Even in invertebrates a cerebellum or cerebellum-like structure is exceedingly common (Hodos, 2009). For example, fruit flies, a much-studied animal model in neurosciences, possess a similar structure called the mushroom bodies (Farris, 2011). A variety of functions have been attributed to the cerebellum across vertebrates; among others, regulation of proprioception and motor coordination in fish and amphibians (Sherrington, 1952). In electrical fish the cerebellum receives inputs from a large number of specialized electric receptive organs situated across its body's surface, compromising an electrical view of the world similar to that on a radar screen. In some of these fish such as mormyrid fish the cerebellum takes on such enormous proportions that it can become larger than the rest of the brain (Bullock et al., 2006). In mammals the cerebellum is known for motor adaptation (Catz et al., 2008), coordinating multi-joint movements (Hoogland et al., 2015), sequencing of movements (Khilkevich et al., 2018), predicting target trajectories (Broersen, 2019), perceiving time intervals (Broersen, 2019), perceiving self-motion (Laurens et

al., 2013a), and associative learning (ten Brinke et al., 2015). In primates, recent research has put a lot of emphasis on the contribution to higher cognition and also language in humans (Desmond and Fiez, 1998; Sendhilnathan et al., 2020). Despite the functional diversity the neural circuitry and cortical layout is highly homogeneous across all vertebrates **(Fig. 4)** (Krieg, 1967). Nevertheless, the cerebellum is not essential for immediate survival. Recently, it was discovered that a woman had lived her entire life without a cerebellum (Yu et al., 2015). Furthermore, cerebellectomies were historically performed in animals to investigate the ocular motor system (Westheimer and Blair, 1974), which may have limited the scientific scope. This apparent discrepancy poses the question: if the function of the cerebellum is not essential to stay alive, why is it so well conserved?

Like every biological function, the cerebellum is shaped through the pressure of natural selection. Considering the cerebellum's motor functions this was presumably based on predator-prey interaction (Paulin, 2005). This is a strong evolutionary pressure, since coming second in these types of interactions means either starving to death or getting eaten yourself. Reliable and fast extraction of information from sensory modalities and reacting upon it is fundamental for rapid pursuit and evasion. The cerebellum is highly efficient at filtering important sensory inputs and learning fast associations between sensory inputs and behavioral output (Dean et al., 2010; Ten Brinke et al., 2017). This type of associative learning is often studied in the model of eyeblink conditioning, where an initially neutral conditioned stimulus in the form of a flash of light is paired with an aversive stimulus in the form of an air puff to the eye. The air puff elicits eyelid closures; after learning the association with the light animals start closing the eye when the conditioned stimulus comes on to protect the eye. In the human brain information from around 200 million mossy fibers enters the cerebellum, which expands to roughly 50 billion granule cells, which in turn project to 15 million Purkinje cells (Shepherd, 2004). This huge divergence gives Purkinje cells an enormous amount of sensory signals, from which the most relevant can be selected (Ramnani, 2006). The relative size of the cerebellar circuit differs between species. Where the surface of the cerebellum is roughly one third of the surface of the cerebrum in Macaques, it is 78% of the surface in humans (Sereno et al., 2020).

Many mammalian species have developed high level cognitive performance over the course of evolution (Deaner et al., 2006). Distantly related lineages of apes, toothed whales (a parvorder including dolphins) and seals evolved a relative parallel expansion of the lateral cerebellum in contrast to the medial cerebellum (Smaers et al., 2018). Toothed whales require information processing geared towards auditory processing of echolocation, while in seals and primates, it has adapted towards vision (Dehnhardt et al., 1998; Scholtyssek et al., 2008; Hanke et al., 2009). This specialization might be reflected in the lobuli of the lateral cerebellum that have expanded over time; HIX in toothed whales versus HVII in primates and seals (Jansen and Jansen, 1969). Apes, dolphins and seals are among only a few species of mammals with the ability to learn new calls and vocalizations. The separate parallel evolutionary expansion of the lateral cerebellum in different species highlights its importance for learning (Smaers et al., 2018). Nevertheless, many of the higher cognitive functions studied in humans and primates have been attributed solely to the evolutionary expansion of the neocortex, although throughout evolution size changes to the neocortex and cerebellum happened in tandem. The highly correlated volumetric evolution of these regions indicates that these are not functionally separate but rather functionally and anatomically interdependent (Whiting and Barton, 2003; Smaers et al., 2011; Smaers and Vanier, 2019). Remarkably, there is a strong deviation in the branch of great apes from this otherwise tightly correlated evolution of the two structures. The evolutionary branch of the great apes is characterized by a significantly faster expansion of

the cerebellum relative to neocortical volume than the rest of the evolutionary tree (Barton and Venditti, 2014). This uneven expansion suggests that natural selection had a disproportionate effect on the ape cerebellar components of the cortico-cerebellar mechanisms. It has been proposed that this is caused by the specialized forage skills of and tool use by apes that require long and complex sequences of fine motor skills (Leiner, 2010; Sultan et al., 2010; Barton, 2012). Evidence from the field of cognitive neuroscience of the cerebellum highlights an extensive contribution to the capacity for planning execution and understanding of complex behavioral sequences, but also visual attention, working memory and language (Barton, 2012; Brissenden et al., 2018). Recent advances in systems neuroscience enable recordings from several areas simultaneously in high spatial and temporal resolution. These studies emphasize the functional cerebro-cerebellar connectivity in both motor planning as well as higher cognitive functions (Buckner, 2013; Sokolov et al., 2017; Brissenden et al., 2018; Gao et al., 2018).

1.3 Cerebellar control of behavior

1.3.1 Saccades

The retina of primates has a specialized region of roughly one visual degree at its center, called the fovea, containing the highest concentration of cone shaped retinal cells. This area produces extremely high visual acuity. In most cortical and subcortical structures, the fovea has a disproportionately large representation, highlighting its importance in visually based behavior (Dow et al., 1981). To be able to gain the full benefit of the high acuity of foveal vision, it is crucial to rapidly and accurately align the fovea with new targets that may appear unexpectedly. Also, the fovea needs to be aligned with the target long enough to perform a comprehensive analysis of the image. Therefore, the system needs to be able to move both eyes towards a target and suppress eye movements to irrelevant stimuli. To redirect the eyes, primates make saccades, allowing subsequent fixation on target.

Saccades are the fastest movements primates can make with speeds of over 700°/s (Fuchs, 1967). Due to this high speed, they are executed without online visual feedback, i.e., in a ballistic fashion. Additionally, non-human primate (NHP) studies have shown that proprioceptive feedback from eye muscles reflecting position signals nor visual feedback can be used to correct errors mid-flight (Zee et al., 1976; Guthrie et al., 1983; Lewis et al., 2001). Yet, saccades are sensitive to internal and external perturbations. For instance, distractors that appear in the periphery at the same time as the target, preceding the initiation of the saccade, cause saccade trajectories to be curved away from that direction (Doyle and Walker, 2001). Alternatively, internal errors can cause alterations in saccade trajectories causing them to over- or undershoot the final fixation points, appending a drift-like component to the end of the saccade called *glissade* (Flierman et al., 2019). Larger errors, where the eye completely misses the target, are corrected in the post-saccadic stage by the oculomotor system (Pélisson et al., 2010).

Adjusting saccade amplitude on the basis of previous errors is called saccadic adaptation and is studied by introducing an error through displacement of the target mid-flight a.k.a. the inter saccadic step (McLaughlin, 1967). Outward saccadic adaptation (i.e., lengthening of saccades) is critically dependent on the cerebellum and abolished after lesioning of the oculomotor vermis (lobulus VIc and VIIa) (Barash et al., 1999). Purkinje cells in the OMV encode eye velocities rather than eye position. Following from this, PCs do not have receptive fields, like pyramidal cells in the

visual cortex. Instead, they are sensitive to saccade direction (Ohtsuka and Noda, 1995; Herzfeld et al., 2015). This sensitivity is not directly clear from the SS firing patterns these cells display, but can be revealed when introducing an error through a backwards inter-saccadic step, which modulates complex spikes. The saccadic direction that elicits the highest probability of CS responses is the cells' preferred direction. The combined population activity of OMV Purkinje cells that are recorded for their preferred direction creates a meticulous prediction of the saccade velocity kinematics that are measured (Herzfeld et al., 2015). During saccadic adaptation PCs learn to correct errors on the basis of information received through the climbing fiber pathway. When CF input is received, the SS response and movement on the next trial are adapted along the vector of the cells' preferred direction. Markedly, when there is no CS in a trial with an error, the next trial will not show any change in velocity (Herzfeld et al., 2018). In conclusion, the SS population activity is reshaped on the basis of errors transmitted through the climbing fiber pathway to maintain optimal saccade precision.

1.3.2 Antisaccades

Antisaccades are a form of voluntary saccades in which the subject must make a saccade to the mirror position of the target (Hallett, 1978). They are used to investigate different aspects of oculomotor control, since they demand inhibition of a reflexive saccade to the target, transformation of the vector of the stimulus to the opposite location, and finally a volitional saccade to the opposite direction (Zhang and Barash, 2000). These demands are reflected by increased reaction times and error rates in comparison to saccades to targets (Munoz and Everling, 2004).

The saccade network is extensively described in NHPs through lesion studies, functional imaging and neurophysiology (Munoz and Everling, 2004). The great body of literature plus the relative ease of measuring saccades make the antisaccade task a great tool to study volitional behavior. Neurons that are active during fixations or during saccades have been identified in the frontal eye fields (FEF) and superior colliculus (SC). Fixation neurons are more active in antisaccades trials while the activity of saccade neurons is reduced, explaining the longer reaction times that are observed (Funahashi et al., 1993; Everling et al., 1999a; Everling and Munoz, 2000). The target vector inversion, necessary to calculate the mirror position, has been attributed to the lateral intraparietal cortex, an area that is situated on the intersection of sensory and motor processes. Single unit recordings during a memory guided antisaccade task demonstrate activity turns from the visual direction (i.e., the stimulus) to the motor direction (i.e. the antisaccade) in antisaccade trials, reflecting the inversion transformation necessary to correctly execute the task (Zhang and Barash, 2000). Furthermore, imaging studies show higher BOLD activity in frontal areas (FEF, DLPFC) in antisaccades than in prosaccades, which stems predominantly from differences in preparatory activity rather than motor activity (Connolly et al., 2002; DeSouza et al., 2003). More recent neurophysiological recordings in the dentate nucleus show that the cerebellum also has higher activity for antisaccades both during the preparatory period and the saccade. Inactivation of the region that was recorded with GABAA agonist muscimol resulted in a strong increase of errors in antisaccade trials, where the animal resorted to a prosaccade instead (Kunimatsu et al., 2016). These and more recent data suggest an import contribution of the cerebellum to motor preparation (Gao et al., 2018; Chabrol et al., 2019).

A contribution to this is made in the thesis by the investigation of the firing patterns of PCs in the lateral cerebellum and OMV during the preparation and execution of pro- and antisaccades

(**Chapter 3**).

1.3.3. The cerebellum and other motor functions

The cerebellum controls a wide variety of motor functions distributed over the entire body, ranging from the eye movements described above, to oro-fascial movements such as tongue and lip movements to full multi-jointed limb and trunk movements (Apps and Hawkes, 2009). Although the cerebellum controls all parts of the body, the exact nature of all basic operations performed remains unknown. The most studied topics of cerebellar motor control include, but are not limited to: movement timing, sensorimotor integration, classical conditioning, motor adaptation, sequencing of movements, motor predictions, ataxia of gait and posture, control of speech, control of grip and control of voluntary limb movements. For a more extensive overview see review by (Manto et al., 2012).

1.3.4 The cerebellum in non-motor behavior

One of the most influential studies of the last decades on the cognitive cerebellum is an anatomical study in cebus monkeys demonstrating a closed loop from CrusI/II of the lateral hemispheres of the cerebellum via the thalamus to prefrontal cortex and back via the pons (Middleton and Strick, 2000; Kelly and Strick, 2003). Whether the cerebellum actually contributes to cognitive processes or whether measured activity is motor or pre-motor related has long been a topic for discussion. In recent years, the convergence of anatomical (Kelly and Strick, 2003), evolutionary (Smaers et al., 2018), functional imaging (Brissenden et al., 2016, 2018), structural imaging (Yeo et al., 2011), clinical (Schmahmann, 2004), primate electrophysiology (Sendhilnathan et al., 2020), and rodent studies (Deverett et al., 2018; Carta et al., 2019; Kostadinov et al., 2019) have provided a definite confirming answer to this.

Investigations into non-motor functions of the cerebellum reveal contributions to domains as diverse as attention, language, executive function, social cognition, working memory, and even personality (Buckner, 2013). A common symptom of cerebellar movement disorders is dysmetria. For example, undershooting or overshooting of the eye after lesions to the OMV (Ignashchenkova et al., 2009). Keeping movements normometric (i.e. on target) is attributed to the idea that the cerebellum functions as a forward model, predicting sensory consequences of movements and learning to adjust those on basis of sensory prediction errors relayed through the climbing fiber pathway (Desmurget and Grafton, 2000). This idea has been extended to cognitive symptoms of damage to the lateral cerebellum or schizophrenia as dysmetria of thought (Andreasen et al., 1998). A behavioral function where dysmetria might be more directly applicable in a higher cognitive process is covert attention, classically attributed to the dorsal attention network in the cerebral cortex. Covert attention shifts are described as ‘’mental saccades’’ where one moves attention over the visual field without moving the eyes. Deficits to covert attention shifts are observed after cerebellar injury (Courchesne et al., 1994; Striemer et al., 2015). Recent work by Brissenden and colleagues (2016) beautifully connected the structural and functional imaging approaches in a covert attention task. They demonstrated that a cluster of voxels in lobules VII and VIII of the cerebellum showing increased BOLD responses during attentional shifts and visual working memory are the same voxels as the ones connecting to the dorsal attention network. This study showed that the cerebellum, which is usually omitted in fMRI studies due to technical difficulties, is an integral part of this network and contributes to

executing the visual attention and working memory tasks (Brissenden et al., 2016, 2018).

Neuronal systems learn in different ways according to what is most efficient given the information and the desired behavior. It is believed that the cerebral cortex learns in an unsupervised fashion, the basal ganglia learn through reinforcement, and the cerebellum learns in a supervised fashion (Doya, 1999). Recently the cerebellar cognitive field acquired many new insights in how the cerebellar cortex receives rewarding signals through its two main input pathways; the mossy fiber and climbing fiber paths. First, granule cells, whose primary input comes from mossy fibers, signal rewards or reward omissions whereas other cells selectively encode the anticipation of rewards (Wagner et al. 2017; Heffley and Hull 2019). These cells differentially modulate their activity for unexpected rewards signaling the context of the reward. Over time, sensory reward cells develop an anticipatory component, and omission related responses become stronger, indicating the entrainment of the network on a specific task instead of passive relaying of information (Wagner et al., 2017). Second, through the other main input to the cerebellum, the climbing fiber pathway, reward information is conveyed to Purkinje cells as well (Heffley and Hull, 2019; Larry et al., 2019). PCs in specific microzones receive climbing fiber input of either reward anticipation, delivery or omission. Depending on the zone, reward delivery suppresses activity in some zones and enhances activity in others, while both types of zones can be activated by reward omission. Just as in the granule cells, activity is modulated over time during learning. Responses to predictive reward are progressively suppressed during learning (Kostadinov et al., 2019). It should be noted that CF responses and granule cell responses were recorded in a different task and regions, making it difficult to directly compare the two. Still, these findings open the door to the idea that the cerebellum is not all about supervised error based learning, but also learns on the basis of reinforcement through reward(Sendhilnathan et al., 2020).

1.3.5 Studying cerebellar control of behavior in non-human primates

Studying the cerebellum in human subjects has the disadvantage that the possibilities for measurements and interventions are, except in very rare cases, limited to non-invasive measures, making functional investigation of the system very challenging. NHPs have played an essential role in medical and scientific progress over the past century and are of indispensable value thanks to their similarity to humans in physiology, neuroanatomy, development, cognition and social complexity. Many complex forms of behavior are not present to the same degree in other widely used animal models such as rodents. Techniques developed to study the brain in humans also have their disadvantages. Functional imaging, for instance, has severe temporal and spatial limitations and EEG can only precisely measure activity in cortex of the brain. Therefore, research on single cell activity of the NHP visual system through microelectrode recordings has elucidated many functional mechanisms underlying attention and vision that could not have been discovered otherwise (Roelfsema and Treue, 2014). To fully comprehend cerebellar contributions to higher cognitive functions, microelectrode recordings of the primate cerebellum can provide insights that are unattainable in other species. In this thesis I present results of my studies on the NHP cerebellum at the behavioral and electrophysiological level, so as to contribute to elucidating the mechanisms underlying its motor and nonmotor functions.

1.4 Scope of the thesis

Chapter 2: Measuring cerebellar processing and sensorimotor functions in non-human primates

In this chapter I will discuss in detail the techniques used in the thesis to set up and perform behavioral and physiological experiments in non-human primates. It covers structural imaging techniques and how these images can be used to build implants for head fixation and electrophysiology. A concise overview of surgical techniques is presented on how to implant these tools. Furthermore, an overview of experimental techniques is provided, including eye tracking, tracking oro-facial behavior, single-unit electrophysiological recordings, and pharmacological interventions.

Chapter 3: Purkinje cell activity during voluntary eye movements in medial and lateral cerebellum in Rhesus Macaques

In this chapter I examine the contribution of Purkinje cells to the classic antisaccade task and specifically if there are differences between the medial and lateral cerebellum. Antisaccades are a well-established task for the study of volitional motor behavior, the function of the lateral cerebellum in which, is currently a major issue in neuroscience research. Non-human primates were trained to perform randomly interleaved pro- and antisaccades in multiple directions while recordings from Purkinje cells in both regions were made. Comparisons of pro- and antisaccade related neural modulation between these brain regions are made in the instruction and the saccade epoch to elucidate some aspects of the question.

Chapter 4: Dentate nucleus neurons in rhesus macaques dynamically modulate their activity throughout a complex behavioral task

In this chapter the question how action potential trains of dentate nucleus neurons modulate in relation to a peripheral visual stimulus and reward is explored. Additionally, to better understand the properties of the network I investigate which regions of the inferior olive and cerebellar cortex produce afferent connections to the task related area of the dentate nucleus. The precise visual functions of the cerebellum are still relatively unexplored. With this study some of the cerebellar visual functions are brought to light. To this end non-human primates were trained to read the direction of the gap of a Landolt C presented in the periphery of the visual field while extracellular recordings were made.

Chapter 5: Glissades are altered by lesions to the oculomotor vermis but not by saccadic adaptation

How the cerebellum controls the execution of saccades is pretty well known. However, its part in glissades, the drift-like appendages that can occur at the end of saccades, is less well known. Therefore, I investigate the question how glissades are controlled by the oculomotor vermis (OMV). Accordingly, data from a lesion study of the OMV were used to examine the effect of ablation of the OMV on glissades and subsequent recovery of this effect. Furthermore, the relationship between saccade kinematics and glissades, and whether changes to glissades are dependent on the direction of the saccade is questioned. The last issue I investigate in this chapter is how saccadic adaptation

affects glissades in animals with a healthy OMV.

Chapter 6: General discussion

In this chapter I discuss the findings of the experimental chapters of this thesis in light of the literature and in context of each other. I also go further into the relevance of doing primate research in this day and age. Lastly, I draw conclusions from the combined results presented in this thesis.

Chapter 2:

Measuring cerebellar processing and sensorimotor functions in non-human primates

Nico A. Flierman[1,2], Eric Avila[3], Chris I. De Zeeuw[1,2], Aleksandra Badura[2]

Author affiliations:

[1]Netherlands Institute for Neuroscience, Amsterdam, The Netherlands.

[2]Department of Neuroscience, Erasmus MC, Rotterdam, The Netherlands.

[3]Center for Neural Science, New York University, New York, USA

Approved for publication as: ''Chapter 12: Measuring cerebellar processing and sensorimotor functions in non-human primates'' In *Neuromethods* edited by Roy Silitoe.

Expected: 2021

2.0 Abstract

Cerebellum is well known for integrating and processing sensory inputs to guide motor functions. Lesions to this brain region result in loss of movement precision, problems with balance and difficulty in acquiring new motor skills. Moreover, in recent years it has been shown that the cerebellum is also involved in many cognitive functions. In order to study the cerebellar neural mechanisms that underlie these processes we need to measure cerebellar activity accompanying these complex behaviors. We can achieve this by performing electrophysiological recordings from the neural tissue and collect signals from cerebellar neurons in awake, behaving animals. Even though many experimental questions can be addressed in rodents, some can only be answered by using non-human primates (NHPs). Particularly, the low acuity of the visual system and less developed neocortex, make rodents undesirable models when higher order sensorimotor functions are being probed. For analogous reasons NHPs are also indispensable when testing cortical prosthesis. In cerebellar research, NHPs have most commonly been used to study the role of Purkinje cell processing in integrating different forms of sensory information to acquire, plan and coordinate eye and limb movements. Our goal in this chapter is to provide the reader with guidelines on how to perform measurements of cerebellar function in NHPs, specifically using single-unit extracellular recordings. We highlight the advantages and limitations of this approach focusing on the surgical and technical aspects of these experiments, and we describe standard and novel approaches to quantify the behavior of NHPs during experimental manipulations.

2.1 Introduction

Neuroscience research employs a variety of species to study brain mechanisms underlying behaviors. Over the last few decades, the field has made incredible progress in studying even seemingly complex functions in worms (Stern et al., 2017) or flies (Guo et al., 2016). When it comes to the mammalian brain the most commonly used species are mice and rats. In fact, in 2015 over 30% of all neuroscience articles used rodents as the model organism (Keifer and Summers, 2016). While rodents in general and mice in particular offer many advantages, such as wide availability of genetic tools and high-resolution reference atlases (Wang et al., 2020a), many scientists argue that diversifying animal models is highly advantageous (Maximino et al., 2015; Keifer and Summers, 2016; Hale, 2019). Non-human primates (NHPs, predominantly rhesus macaques, i.e., *macaca mulatta*) represent model organisms closest to humans and are therefore indispensable for many lines of fundamental and applied research (Roelfsema and Treue, 2014; Jennings et al., 2016; Mitchell et al., 2018). This is of particular importance for studying the structure and function of neocortex as well as the way its activity drives movements of eyes and dexterities (Hutchison and Everling, 2012). A relatively prominent lateralization and interhemispheric connectivity are also distinctive features of the primate brain (Passingham, 2009; Procyk et al., 2016), although some evidence of lateralization has recently been shown in mice as well (Stoodley et al., 2017; Kelly et al., 2020). The opinion piece by Roelfsema and Treue compiles an extensive list of research topics where input from NHP studies is required to further our knowledge on brain functions in health and disease states (Roelfsema and Treue, 2014).

In cerebellar research NHPs have long been used to study oculomotor adaptation and visual functions (Optican and Robinson, 1980a; Thier et al., 2002; Ethier et al., 2008; Golla et al., 2008; Medina and Lisberger, 2009; Fuchs et al., 2010; Kunimatsu et al., 2016; Flierman et al., 2019). Notably, the eyes of some rodents, e.g., gerbils, possess features that resemble the primate macula (Huber et al., 2010), and research in mice can answer many fundamental questions about vision (Huberman and Niell, 2011). However, NHPs are uniquely fitted for this line of research because, unlike rodents, they have a fovea and use saccadic eye movements to track objects in their field of view, making them a perfect model organism for the human visual system (Zeki, 1978; Chen et al., 2019). Further, studies on the development of the upper limb neuroprosthetics are limited in rodents, and have been almost exclusively conducted in NHPs (Aggarwal et al., 2009; Adewole et al., 2016). In fact, many fundamental, cerebellar mechanisms that govern grasping and pointing motions have been uncovered thanks to NHP research (Wang et al., 1987; Ojakangas and Ebner, 1992; Albert et al., 2020). Sensorimotor integration of vestibular inputs is another area where studies done in NHPs aid in our understanding of how the cerebellum controls balance, coordination and self-motion (Angelaki et al., 2010; Cullen and Brooks, 2015; Laurens and Angelaki, 2020).

In the last ten years the insights gained from NHP research showed that the cerebellum is crucial for many functions that are highly relevant for understanding human behaviour. For example, it is involved in integrating sensory information to guide motor functions in simple and complex tasks, learning new motor sequences (Herzfeld and Shadmehr, 2014; Popa et al., 2016; Shadmehr, 2017), and processing of reward signals during ongoing acquisition of motor tasks (Sendhilnathan et al., 2020). Thus, while research on complex behaviors and cognitive processes can to a certain degree be also conducted in rodents (Gao et al., 2018; Chabrol et al., 2019), the superb level of NHPs' trainability and the anatomical similarities within the primate lineage (Van Essen et al., 2018) offer indispensable advantages so as to further our understanding of the human brain.

Above mentioned studies are not exhaustive and are merely representative examples of how cerebellar research benefits from NHP studies. This is in part due to the anatomical similarities between the human and NHP cerebellum. Even though the NHP cerebellum has only 33% of the surface area of the neocortex, as compared to 78% in human (Sereno et al., 2020), it is still most similar to the human one with the same neuronal cell types and conserved microcircuitry (Gerrits and Voogd, 1989; Clark et al., 2001). Particularly, the expansion of the dentate nucleus and the surface of the hemispheres, which expanded in parallel with the neocortex during evolution, are shared among the primates (Balsters et al., 2010; Barton and Venditti, 2014). The expansion of the cortices in primates results in extensive cerebello-cerebral connections, which have been studied using long-distance viral tracing predominantly in macaques (Caligiore et al., 2017). These studies indicated that the cerebellum is indeed not only a central hub in the motor-control system but is also a part of the non-motor circuitry (Strick et al., 2009).

Evident from the examples listed above, the ability to obtain neuronal signals from the NHP cerebellum and directly link it to the observed behaviors provides major insights to our understanding of higher cerebellar functions. However, neuronal recordings in NHPs in general, and from the cerebellum in particular, present many technical challenges. First, the surface of the cerebellum in NHPs is not readily accessible, which hampers the use of multielectrode arrays, commonly used for the neocortical recordings in NHPs (Spira and Hai, 2013; Rajan et al., 2015) or glass electrodes, used in rodents (Badura et al., 2013). In fact, the majority of cerebellar recordings from macaque monkeys have been obtained using tungsten electrodes, which on the one hand offer excellent signal isolation, but on the other hand can only record a single neuron at the time. Notably, several groups are actively working on incorporating novel multichannel recording methods into cerebellar research in NHPs, with first successful experiments performed in marmosets (Sedaghat-Nejad et al., 2019). Second, due to the location of the NHP cerebellum, electrodes have to travel through the neocortex to reach the cerebellar cortex or the cerebellar nuclei. Most commonly the electrodes are inserted in the guide tubes passing through the primary visual cortex. This is an important point of consideration, since repeated measurements can damage this structure. This is particularly important for visual tasks, and therefore careful calibration of the visual field acuity is strongly advised prior to performing any experiments. Third, because the surface of the cerebellar cortex is highly folded and visual inspection of the insertion point on the electrode is not possible, it is possible to miscalculate the final position of the electrode. This can be prevented by obtaining MRI image confirmation of an electrode placement.

In this chapter we will describe step-by-step procedures that enable successful cerebellar recordings in NHPs performing complex tasks. We will highlight techniques that allow for customization of the materials to an individual NHP, which in turn increases the comfort of the animal as well as the durability of the implants. We will also outline training methods and tools that allow quantification of behavioral output, with specific focus on the eye movements. Finally, we will illustrate how to perform electrophysiological recordings from the cerebellum and how its activity can be modulated pharmacologically.

2.2 Materials: Implants designs and manufacturing process

The importance of NHPs wellbeing used in research extends to all devices and implants used on them. Therefore, novel technological advancements such as CNC machines, 3D printers, biocompatible

materials, etc. are highly recommended to use in favor of the NHP health to increase the implants' longevity and provide better data acquisition. Creating personalized, skull-formed cranial implants for each animal has become the state-of-the-art standard and a critical and necessary step in the experimental planning process. Commercially available products do not account for individual differences between NHPs, which in turn may have a negative effect on the implant stability, bone health and precision of the neural target location. Customized implants, based on detailed anatomical scans, reduce the surgery duration, lower the chance of postoperative complications (e.g., granulation and bacterial growth) and improve the rate of osseointegration. Implementing such customized solutions is in line with the recommendation of the European Union Scientific Committee, which recommends adopting "the highest standards of NHP housing and husbandry and (...) scientific procedures" (SCHEER, (Scientific Committee on Health, Environmental and Emerging Risks), 2017).

2.2.1 CT/MRI image processing

In order to design customizable implants for chronic cerebellar recordings, 3D models of the skull and the cerebellum need to be generated. Obtaining proper imaging of a skull and brain areas to record from is critical to generate a suitable model, which in turn facilitates implant design, surgical planning and neurophysiological recordings. Computerized Tomography (CT) is fast, widely available and particularly well suited for obtaining high-resolution images of bone. It has exquisite contrast resolution and the ability to scan with metal objects. Depending on the scanner, ideal minimum spatial resolution should be of at least 0.5 mm. The imaging is done under anesthesia (see section 2.4.1.1). After obtaining the CT images, freely available software can be used to segment (i.e., isolate the structures of interest) to render a 3D image of a skull. Note that the process of segmentation and reconstruction of the surface of a skull is the same for both image sources (CT and MRI), however, the CT provides superior results for bone segmentation.

Magnetic resonance imaging (MRI) is an imaging technique that uses a magnetic field and radio waves to generate anatomical images. MRI is especially useful for soft tissues; hence, it is recommended to obtain head images using both technologies. If both are available, this step provides an extraordinary resource for three main reasons:

(1) The CT provides a high-resolution image of the skull to design a customized form-fitted implant;

(2) The MRI provides detailed soft tissue images to localize and map the areas to record for the subsequent electrode implantation;

(3) Obtaining anatomical high-quality images from both of these sources allows co-registration using landmarks. Our recommendation is using an MRI compatible stereotaxic device. In case it is not available, the second-best option is to use MRI-compatible ear bars and additional MRI-compatible markers (Laurens et al 2016; Avila et al. 2018) with visible interaural markers that will provide helpful alignment markers (**Fig. 1A, right column**). If none of these are available, one of the freely available software provides the best user-friendly approach to re-align the MRI and CT images.

Here we provide information to process the CT and MRI from two open source software systems developed to segment structures in 3D from medical images. They both offer similar features and results: ITK-Snap (http://www.itksnap.org/, (Yushkevich et al., 2006) and 3D slicer

(https://www.slicer.org/, (Kikinis et al., 2014). Both offer comprehensive tutorials online so we will only cover the main steps.

Import and re-alignment

3D Slicer: "Load Data" or "Add Data" tool to import image series, and adjust contrast and brightness. Save data as a medical record bundle (.mrb).

ITK-Snap: "Open main image" to import image series, and adjust contrast and brightness. Save the main image as a .nifti file (Neuroimaging Informatics Technology Initiative).

If no MRI-compatible stereotaxic frame was used and the image is rotated it needs to be re-aligned before proceeding to the next steps. This will allow alignment of the MRI images to a stereotaxic coordinate system. Having the MRI stereotaxically aligned will help to use an NHP reference brain atlas during surgery and electrophysiological recordings. This is particularly important for electrode position planning.

Here are the steps of the alignment using the 3D Slicer interactive tool:

1. Orientation labels: Make sure that the labels for orientation are correct (left-right, anterior-posterior). Go to the "Transforms" module and create a "New Linear Transform" and use the "Rotation" menu to rotate the MRI to its proper orientation. Start by doing it +/- 90˚. Once completed, go to the bottom section "Apply transform", select the MRI you are working on and click on the right arrow, so the name of the MRI moves to the right. Check now whether the labels are correct in the 3D view of the MRI. Lock the changes by clicking the "Harden transform" in the "Apply transform" menu section.

2. Fiducial markers: Fiducial markers can be created in the "Markups" module to be able to align the MRI in a stereotaxic plane. Create a new Markups fiducial list and position 4 fiducials, 2 in the ear canals in each side (external *meatus acusticus*) where the bony part begins, and 2 in the lower ridge of the orbit. Lock the fiducials. If a frameless stereotaxic device was used, the fiducial markers can be placed on the tip of the ear bars. Make sure that the 2D projection is toggled on (Advanced menu of the "Markups" module). This will allow visibility for all fiducial markers in all views.

3. MRI rotation: This step allows to rotate and align the ear and eye fiducials in the same plane. This is achieved in the "Transforms" module. Under "Transformable", select the MRI and the recently created fiducials and click on the right green arrow. Then, use the "Rotation" sliders to align the fiducial markers to the same plane. You can use the crosshairs as a visual help tool. Once completed, "Harden" the transform.

4. Reset to stereotaxic origin: This function sets all the MRI slices to stereotactic coordinates. Create a new fiducial marker at the stereotactic origin (midline at the intersection of the ear plane and the eye plane). Place the fiducial marker at the center of that intersection. The location of this fiducial marker (R, A, and S) will be used to translate the MRI to the stereotaxic coordinates. Open the "Transforms" module, create a new transform, move from "Transformable" all previous transformations and input in the "Translation" section, with the opposite sign (!), the stereotaxic origin fiducial marker location (i.e., if positive, input negative in R in LR, A in PA,

and S in IS), and harden transform. Note, if done correctly, when checking the fiducial marker location again, this should now be at the origin (0, 0, 0).

Segmentation

Segmentation (i.e., isolating the regions of interest) is achieved by labeling the skull and the target areas for recordings (**Fig. 1**).

ITK-Snap: After adjusting the contrast and brightness, this process can be completed first using automatic segmentation and then manual segmentation. Adjusting contrast and brightness will significantly help the algorithm to consider the intensities of the image. Progress and current state of the segmentation can be observed in the lower left window by clicking the "update" button. After automatic segmentation is done, manually scroll through the cuts to assess the result. If there are any gaps, fill in manually. For CT this is rarely the case, but more commonly found for MRI. Depending on the brain area, the target areas for electrophysiology can be automatically segmented. However, the cerebellum often needs to be manually segmented.

3D Slicer: For CT, select the CT and go to the "Volumes" module. Select the CT-brain view under display. Then, go to the "Segment Editor" module and click on "+ add" to add a segmentation. Under the "Effects" menu, select "Threshold" and adjust the range slider until the colored part only includes the skull. Click on "Apply". Due to the low contrast between tissues in the MRI, segmenting the skull will require automatic and manual segmentation. Select the MRI and go to the "Segment Editor" module and click on "+ add" to add a segmentation. Under the "Effects" menu, select "Threshold" and adjust the range slider until the colored part only includes the outside of the skull, subcutaneous tissue and skin. Click on "Apply". Using the sagittal or coronal cut, select "Islands" under the "Effects" menu, select "Keep selected island" and click anywhere on the colored segmentation in the MRI. Now, click on "Margin" in the "Effects" menu, and then "Apply". Now, create a second segmentation ("+Add"), select the "Scissors" tool and cut in the middle of the previous segmentation to leave the top of the skull free. This doesn't need to be exact, and do it all around the skull. Once this is completed, the selected region will be highlighted in a separate color. Select again "Margin", and select the option "Shrink", then click "Apply". Click on "Islands" to remove the outer segmentation and just leave the inner selection. Click once more on "Margin", and this time select the option "Grow", and then "Apply". The outside surface of the second segmentation will conform to the surface of the skull. The inner segmented area can now be erased. Another way to segment out the skull, is to use the "Threshold" effect. This will isolate most of the skull and the remaining segments need to be adjusted manually.

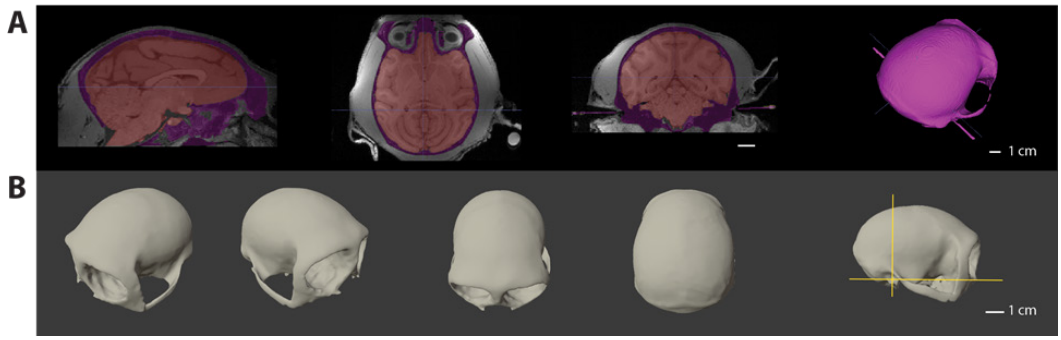

Figure 1. Segmentation and 3D reconstruction. A*) Segmentation of skull (magenta) and brain (red) from an MRI of one monkey using ITK-Snap.* **B***) Digital skull reconstruction by ITK-Snap (exported as .stl) as observed in any 3D computer graphics software. Yellow lines in the rightmost image show the stereotaxic planes.*

Export of the 3D structures (File format: .stl or .obj)

Once the previous steps are completed, the skull and brain structures can be exported to multiple file formats. The most commonly used are: .stl and .obj.

ITK-Snap: Menu Segmentation>Export as Surface Mesh enables exporting all labels created as separate files. Once you hit "Next", the file format and the directory can be selected.

3D Slicer: Go to the "Segmentations" module. Under the "Export/Import" models and labelmaps" select "Export", "Models" and "Export to new model hierarchy".

Go to Menu File>Save will open a window with every element created, the file format and the directory to be saved.

To ease comparison and take advantage of the two imaging methods, the segmented and aligned CT can be co-registered with the MRI to identify the brain regions of interest (Tek et al., 2008). To achieve this, both datasets can be loaded into 3D Slicer and, using the same landmark registration procedure described above, stereotaxically aligned to the same landmarks. The accuracy of the co-registration will directly depend on the user's ability to place the markers in the corresponding landmarks. The alignment can be achieved using bony structures (stereotaxic planes) and brain structures as a reference frame (Avila et al., 2019). All horizontal slices can be aligned to the horizontal plane passing through the interaural line and the infraorbital ridge (stereotaxic plane); all coronal slices can be aligned to the vertical plane passing through the interaural line (ear-bar zero, stereotaxic plane). Brain structures commonly used to align the same planes are the anterior and posterior commissure, as well as the genu and splenium of the corpus callosum (Dubowitz and Scadeng, 2011; Frey et al., 2011). These landmarks can be used to index any position in a standard macaque brain atlas (Paxinos et al., 2000; Saleem and Logothetis, 2012; Reveley et al., 2017). After successful registration the location of the chamber can be determined on the basis of the MRI images and macaque atlases.

2.2.2 Adapting implant design to CT/MRI images

There are numerous computer-aided design (CAD) software solutions to create and/or modify designs. They can be used to create headposts and chambers for the electrophysiological recordings of the cerebellum in NHPs. For this purpose the surface mesh or object containing the NHP head images is used to shape the base of the implant to the skull. We will briefly discuss how to shape the bottom of any design to the shape of the skull in SolidWorks (Dassault Systemes) and Inventor (Autodesk). Both softwares have the same approach and tools.

After designing the headpost or chamber (discussed below) and importing the 3D image of the reconstructed skull, described in section 2.2.1, the base of the design (body and legs) is shaped to perfectly fit the skull. This is achieved by moving the implant to the intended position on the skull and intersecting one another. For cerebellar recordings the most common position of the headposts is fronto-parietal. However, given the advancement of technology and possibilities to record simultaneously from multiple brain regions, the headpost position and leg shape can vary accordingly. The chamber is generally placed over the occipital bone and the exact position of the chamber is based on the intended recording location(s). The location is planned on a monkey-by-monkey basis and numbers will change based on intended recording location and chamber size. The bottom base of the design needs to be thick enough as it will be subtracted from the shape of the skull.

SolidWorks: Select the implant, go to Insert>Features>Combine, and under operation select "Subtract", under "Main Body" select your implant and under "Bodies to Subtract" select the skull. The main image will highlight the area that is going to be subtracted so this is a good time to adjust the area of the implant that will be deleted. Click "Ok" (the green check mark on the left menu) and the workspace will show the subtracted body. The subtracted body can be added at any time again. If you do not want for it to be deleted, you can use the tool "Indent" instead. To properly move the two bodies go to Insert>Features>Move/Copy, select the body to move, and then click on "Translate/Rotate" at the bottom of the left menu. You can flip the alignment and manually rotate them and click on "Add". Select the two body faces that are intersecting and need to be added, and subsequently click on "Ok". Now go to the menu Insert>Features>Indent. In the same way as before, select your Target Body (implant), the Tool Body region (skull) and select the option "Cut" underneath this last menu.

Inventor: the approach and tools are the same. Once the implant and skull are in the workspace, click on "Combine" indicated on the left side menu. Select the implant as the "Base" and the skull as the "Toolbody"; click on "Ok". This is a good moment to save the implant again.

2.2.3 Headpost

Commercial head posts have been used for a long time in primate neurobiology. However, the problem with these implants is that the "feet" of the headpost that adhere to the skull have to be bent to fit the skull during the surgery. This is a delicate and time-consuming process and even when performed by experts can still result in implants having an imperfect contact with the skull. Moreover, even if good alignment is achieved the base of the implant remains flat. The gaps between the skull and the implant make osseointegration harder and thus the strength of the implant worsens over time and could result in an infection (see Notes 1).

Custom implants: Standard headposts generally have 4 main feet, which are placed in a way so that they can support forces from all angles. Customized headposts generally also have 3-4 feet, which are designed in a way to efficiently redistribute the force that the headpost is exerting onto the skull from all directions (**Fig. 2**). Ideally, space and skull-shape permitting, each foot should have at least 2-3 screws; too few screws can cause major problems when one of them comes out. The general design of a headpost is the same across all animals. Particularly, the top part of the post that is fitted in the head fixation frame forms the standard part to which the recording equipment can be attached. The customized part is the exact shape of the headpost feet and their bottom side, which adhere to the skull. The goal is to make it fit perfectly to the NHP skull anatomy (see section 2.2.2 for details on how this is achieved).

Advances in 3D printing technology allow fast and affordable creation of individualized implants from a large range of materials. Most commonly the design is printed in grade 1 titanium, with a resolution of 50 μm. When designing implants that are MRI compatible, Polyetheretherketone (PEEK) is currently the material of choice, which can be attached to the skull with ceramic screws (for details on design implants in PEEK see (Mulliken et al., 2015; Ortiz-Rios et al., 2018). Custom headposts are designed based on the individual NHP's skull shape, reconstructed using CT and MRI scans (see section 2.2.1). For headposts CT images are usually sufficient. When planning the location of the customized headposts the front legs of the head posts should be positioned close to but not less than ~2 mm from the anterior-most part of the supraorbital ridge (also known as the eyebrow bone; (Chen et al., 2017).

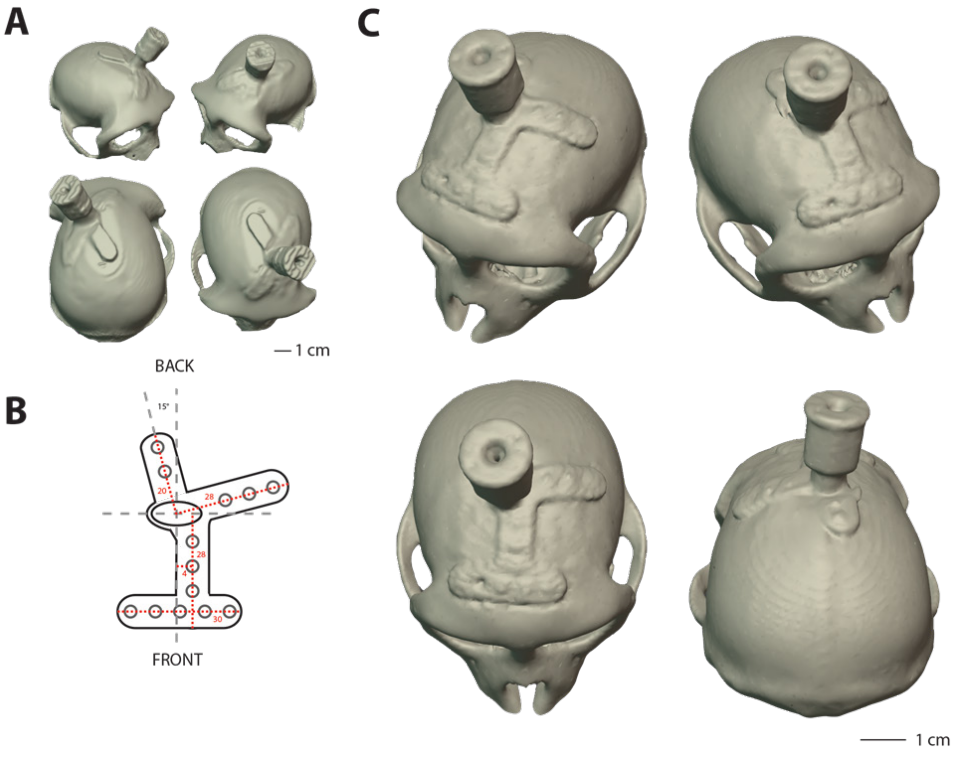

Figure 2. Headpost design. A*) A CT scan of an implanted standard headpost with 4 feet.* **B***) Design of a customized headpost that accommodates recording chambers or multi-electrode array implants over the cerebellum and frontal eye field.* **C***) A CT scan of the implanted headpost shown in B.*

2.2.4 Chamber

Recording chambers for NHPs can also be purchased commercially. However, commercial chambers do not connect perfectly to the contour of the skull. This results in manual adjustment of legs and filling of gaps with dental acrylic (Jet Acrylic, Lang, Illinois, USA) during surgery. These fixes are susceptible to bacterial growth and/or could break over time (McAndrew et al., 2012). Moreover, heat generation during curing of dental cement could damage osseointegration of titanium implants (Ormianer et al., 2000). Thus, a chamber that connects closely to the skull is preferred. Similar to the headposts the chambers are most commonly made from grade 1 titanium (unless MRI compatible materials are required). The walls of the chamber are usually 1 mm thick. For the outside of the chamber the 3D printer resolution of 50 μm is smooth enough, however this inside is electropolished to a roughness of Ra < 0.05 μm to aid cleaning and reduce the risk of infection.

Custom chambers are designed based on individual NHP's skull shape reconstructed using CT and MRI scans (see section 2.2.1). While the CT is superior in determining the exact shape of the skull the MRI is used to plan the location of the implants relative to the brain areas of interest. Therefore, it is advisable to use both techniques together for the chamber design. The size and shape of the chamber should allow the experimenters to reach the brain areas of interest and fit the contour of the skull. Small round recording chambers can be attached by 6 feet that are 1 mm thick and have one screw each. Such chambers are sufficient to record from one side of the cerebellum when implanted over one of the occipital bones. Yet, larger chambers that go past the midline are preferable for cerebellar recordings as they enable electrode insertion in the entire cerebellum (**Fig. 3**). They are secured with 1mm feet with 2 or 3 screws. The top of the chamber should remain level to allow attachment of the electrode drivers. Here, we present a chamber that allows for recording in any region of the cerebellum (20 x 40 mm), located based on stereotaxic coordinates at Anterior-Posterior (AP) -11 mm (front edge), AP -28 mm (hind edge), right Medio-Lateral (ML) 18 mm, and left ML 22 mm. It should be noted that the smaller chambers cannot be subjected to much force, neither are they compatible with multiple feet, which may cause scalp retraction from the chamber wall (Adams et al., 2011).

2.2.5 Coatings

Similar to medical implants used in humans, the bottom of chamber and headpost implants is coated with Hydroxyapatite which is a synthetic calcium phosphate. This technique is commonly used to enhance the stability of dental implants. Coating different types of metals and their alloys, such as stainless steel, titanium, and magnesium, requires specific surface pretreatment. Acid etching is most commonly used as pretreatment for implants. For titanium, the surface pretreatments improve the thickness of the TiO2 passive layer, improving adhesion and bonding of the hydroxyapatite (HA) coating (Huynh et al., 2019). Since these preprocessing steps require a high level of expertise, they are commonly outsourced (i.e., Medicoat AG, Mägenwil, Switzerland, which offer coating and pretreatment for around 200 euros per implant). Notably, the effectiveness of these coatings is still

debated (Welch et al., 2007; Adams et al., 2011; Lanz et al., 2013; Overton et al., 2017; Ortiz-Rios et al., 2018). In vitro studies of HA coatings show that they can improve osseointegration and have a significant effect on the bone regeneration process through enhancement of cellular adhesion, proliferation and differentiation thus helping stability and longevity of the implant (Surmenev et al., 2014). In vivo studies do not always report all details of techniques used to enhance the functionalization of the coatings; factors that should be considered include: microroughness and thickness of coating, calcium phosphate solubility and nanotopography. These details might contribute to the mixed reporting of effectiveness, (for review see (Bral and Mommaerts, 2016). Futhermore, Furthermore, there is little data on the use of these coatings specifically in monkeys.

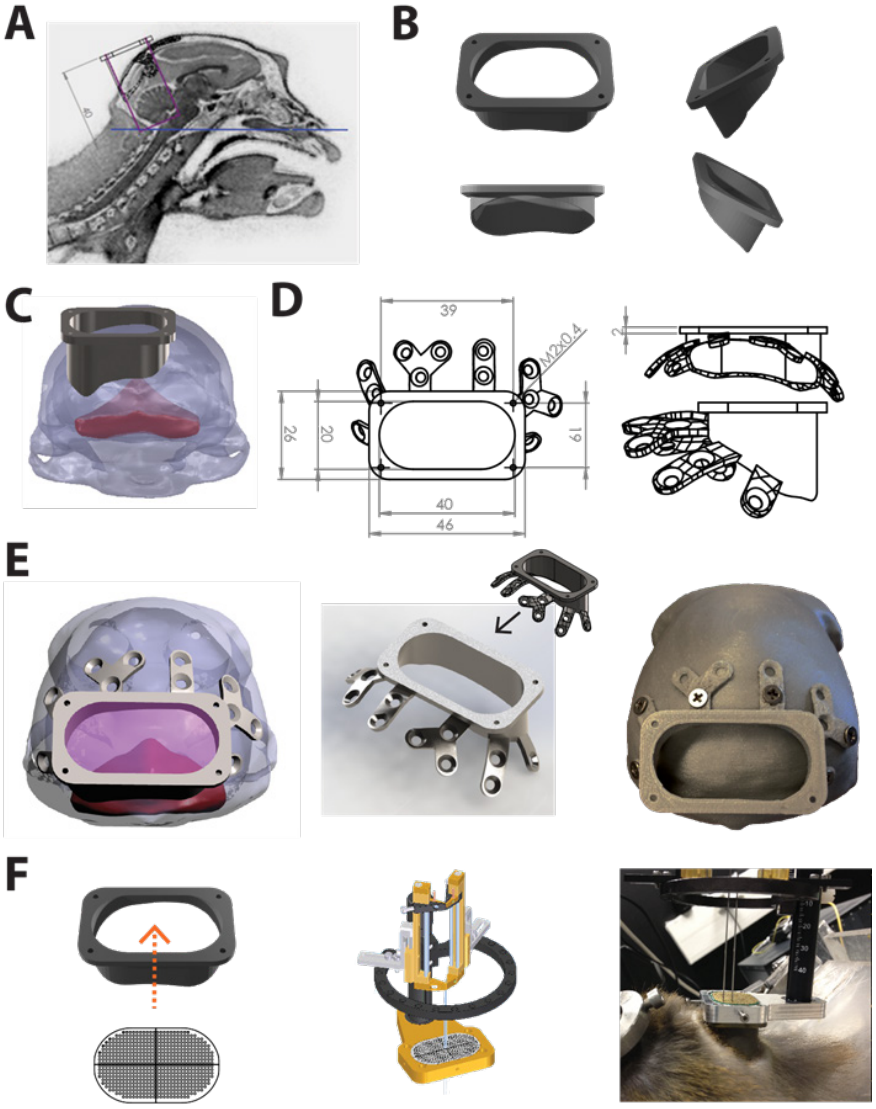

Figure 3. Customized chamber for cerebellar recordings. A*) Chamber angle and depth plan from MRI sagittal cut. Based on the MRI, we calculated the chamber size and angle to be able to reach all vermal lobules and left lateral cerebellum. This can be easily expanded to cover the whole right cerebellum.* **B***) Custom cerebellar chamber rendered after shaping the bottom to the skull.* **C***) Posterior view of the chamber fitted on the MRI reconstructed skull (gray) and cerebellar (red) target locations.* **D***) Engineering drawing of the chamber with the legs to be screwed onto the skull. The legs were also skull-fitted.* **E***)* **Left***; Posterior view of the chamber with the legs fitted on the skull on top of the occipital bone.* **Middle***; After having completed the CAD chamber, the chamber was printed in 3D printed in Grade 5 Titanium alloy.* **Right***; Plastic 3D printed skull and chamber that facilitated surgery preparation.* **F***)* **Left***; Custom two-sided grid (to cover all the available recording space in the chamber) to guide electrode recordings. Every hole is 1 mm x 1 mm apart.* **Middle***; Custom grid mounted on the FlexMT microdrive (Alpha Omega). The microdrive screwed onto the four corners of the chamber that also served to screw the lid to cover the chamber when not in use.* **Right***; Photograph of an actual cerebellar recording in a monkey implanted with the chamber using two electrodes.*

2.3 Methods: CT and MRI scans

A computer tomography (CT) scan should be obtained to allow 3D models of the NHP's skull to be constructed. CT images have excellent contrast for bone and are thus very suitable for reconstruction of the skull. Magnetic resonance imaging (MRI) is especially useful for visualizing soft tissues and is therefore indispensable in designing the recording chambers. MRI is also very helpful in determining the exact electrode position post-chamber implantation (**Fig. 4**). This step is particularly useful for cerebellar recordings since the electrode has to travel a long distance through the visual cortex and the tentorium to reach the cerebellum, enhancing the chances for potential errors in reaching the target. The CT/MRI scans often have to be repeated several times throughout the duration of the experiments (see Note 2). For this procedure the animal is lightly anesthetized while in the cage (2.4.4.1). When the animal is sedated, he is transported in a cage to the scanner location.

2.4 Methods: Surgical procedures

2.4.1 Anesthesia

Repeated anesthesia can cause discomfort and therefore minor procedures, such as cleaning the chamber or wound treatment post-op, are performed without anesthesia (see section 2.4.4).

2.4.1.1 Anesthesia minor procedures

Minor procedures that do not take longer than 90 minutes, and do not require intubation, have a lighter anesthesia protocol. Types of procedures that require this form of anesthesia are: thinning of the dura, removal of stitches, small adjustments to implants, such as replacing a screw, and removal of the dental tartar. Throughout the procedure the animal's temperature is regulated through a heating mat. The animal is weighed prior to the procedure to ensure the correct dose is used. Anesthesia is given through a combination of just medetomidine (0.08mg/kg body weight) or medetomidine

mixed with ketamine (7mg/kg body weight), administered intramuscularly (i.m.). After every 20-30 minus another 4 mg/kg ketamine is given to maintain the proper level of anesthesia. At the end of the procedure atipamezole 0.5 mg/kg i.m. is given as an anesthesia antidote to wake the animal up. NHPs are anesthetized in their home cage, and then transferred to the CT/MRI scanner. After the procedure they are returned to their home cage, where they are monitored and allowed to recover from anesthesia.

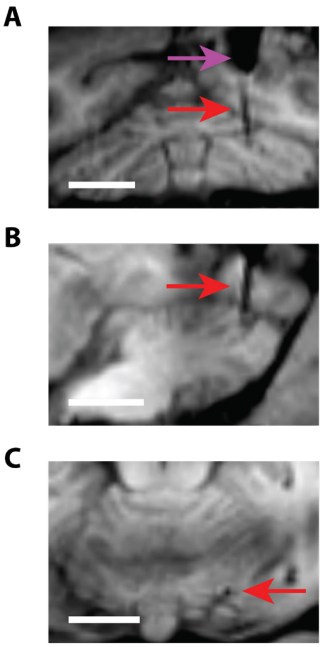

Figure 4. Confirmation of the electrode placement. A*) Coronal MR image of cerebellum with tungsten electrode indicated by the red arrow. Purple arrow indicates artefact from titanium guide tube in visual cortex.* **B***) Sagittal section of the same image stack as A.* **C***) Transverse section of the same image stack as A & B. Scale bars indicate 1 cm in all panels.*

2.4.1.2 Anesthesia major procedures

To sedate an NHP a combination of ketamine and medetomidine (7 mg/kg, 0.08 mg/kg respectively, i.m.) is administered while the animal is still in the cage. The animal is secured in the stereotaxic apparatus with ear stifts that are prepared with the topical analgesic xylocaine. Eye ointment is put on the cornea to prevent dehydration. The animal is intubated and fully anesthetized with 0.8 - 1.5% isoflurane combined with 20% O_2 and 80% air and 0.5 mg/kg intravenous (i.v.) administration of midazolam. For general analgesia the animal receives 0.005mg/kg of fentanyl i.v. To prevent dehydration the animal is put on an i.v. drip of Ringer-glucose of 15ml/kg/hr.

During the surgery the animal is constantly monitored through ECG, heart frequency, external blood pressure, SpO2, CO2, body temperature and breathing frequency. If the skull is opened for the implantation of a recording chamber, the animal receives 0.25 mg/kg dexamethasone i.v. 30 minutes before the opening of the skull, which is repeated every 30 minutes when the skull is open. If brain edema occurs it is treated with maximally 50 ml of mannitol in bolus through the i.v. drip. If the heart rate drops below 75 bpm 0.2 ml of atropine is administered i.v. and the anesthesia is adjusted. 10 minutes before the surgery is finished the animal receives i.v. 0.003 mg/kg buprenorphine, which partially antagonizes the fentanyl. The respirator is set to manual breathing and the animal is released from the stereotaxic apparatus. Lastly, when isoflurane is stopped and the animal starts to wake up, the i.v. drips are removed. The animal is then transported back to the cage and put under a heat lamp. If there was no intracranial procedure the animal receives pain relief with finadyne, (1-2 mg/kg) once every two days for 6 days total. If an intracranial procedure was performed the animal will also receive antibiotics on consultation of the veterinary for 10 days along with 5 days of dexamethasone in decreasing concentration (from 0.7 mg/kg to 0.1 mg/kg, i.m.).

After an intracranial procedure the animal receives 0.003 mg/kg i.m. buprenorphine as pain relief for 2 days; thereafter the finadyne, 1-2 mg/kg i.m., once every two days for 6 days total. Alternatively, other anti-inflammatory drugs can be given orally. If an animal was socially housed before the procedure, it will be single housed for up to 9 days or until deemed fit again to be housed socially.

2.4.2 Headpost implantation

Before surgery the headpost, screws and tools are sterilized in an autoclave. Headpost implantation is performed under general anesthesia and analgesia. The animal is head-fixed with ear-bars into the stereotaxic apparatus and the scalp is shaved and prepped with alternating betadine and alcohol sponges. An incision is made in the scalp and the skin is gently pulled aside at the location where the headpost will be placed. The fit of the head-post is tested and if necessary some bone is removed with a dental drill to ensure perfect contact. If the fit is good, the screw holes are drawn on the skull through the holes of the headpost. The holes are pre-drilled with a hand or mechanical drill. Subsequently, the headpost is placed on the skull and fastened into place with a torque measuring screwdriver until the 1.4 Nm tension is reached (alternatively: two-finger tightness). The skin is closed over the feet to fit as closely as possible around the headpost and sutured. After the headpost surgery the animal is trained at the task of interest (1-6 months). Only when the task performance is sufficient the recording chamber is implanted.

2.4.3 Chamber placement and craniotomy

Before the surgery, the chamber, Ti screws and all tools are sterilized in an autoclave. Craniotomy and chamber placement are carried out under general anesthesia and analgesia, and the animal also receives drugs that reduce intracranial pressure during the operation (e.g., mannitol, dexamethasone; for dosage see above). The duration of the procedure is approximately 1-2 hours. The animal is head-fixed with ear bars in a stereotaxic device and the scalp is shaved and disinfected with alternating scrubs of betadine and alcohol. An incision is made in the scalp and the skin is retracted. Based on the stereotactic coordinates, the chamber is placed on top of the skull and the location of the screw holes is marked on the skull with a marker pen. When the recording chamber is

placed on the marked location the chamber should follow the contours of the skull perfectly. Before opening the skull, screw holes of appropriate diameter are made with a hand or motor drill. Before the chamber is screwed in place, the craniotomy is made with a trephin or motor drill in the marked location, leaving the dura intact. Then the chamber is placed over the craniotomy and fastened into place with a torque measuring screwdriver until the 1.4 Nm tension is reached. To make the inside of the chamber water tight, dental cement should be applied at the intersection between the skull and the chamber. The skin is sutured up tightly surrounding the chamber, the animal is taken off the anesthesia and transported back to its cage.

2.4.4 Post-operative care

After any type of anesthesia, the animals are left in the front part of the cage where they can't climb and fall due to after-effects of the anesthesia. After major procedures the animals are treated with an infrared warmth lamp overnight. The NHPs are left in the cage to recover from the chamber implantation for one to two weeks before recordings are made, or until the implant wound completely heals. However, during that time, the chamber must be cleaned every 2-3 days to prevent infection. Throughout the duration of the experiments, the chamber is cleaned every day before and after the recording session. This procedure takes place while the animal is sitting in the primate chair. The chamber lid is removed and the interior of the chamber is flushed with anti-bacterial solutions such as chlorhexidine. Finally, the chamber is flushed with sterile saline. The total duration of the cleaning procedure is around 5 minutes and it causes minimal discomfort. The chamber should be filled with several milliliters of sterile saline at all times to prevent the dura mater from drying up or scabbing.

2.5 Methods: Behavior

2.5.1 Eye tracking

To link the cerebellar activity to sensorimotor behavior it is essential to monitor one or more behavioral parameters. Almost all primate neurophysiology studies record eye movements. In the context of cerebellar recordings, eye movements need to be recorded as precisely as possible, since the cerebellum is involved in the execution of all types of eye movements (Hong et al., 2016; Popa et al., 2017). In order to parse saccadic eye movements into their minute components or study their kinematic properties, the data must be acquired at a high spatial and temporal resolution (e.g., amplitude of glissades is usually ± 0.2°, red segment of the trace in **Figure 5A-B**, and speed of a saccade is between 30 and 70 ms). Historically, eye movements are tracked using sclera implanted search coils (Robinson, 1963). Search coils have excellent spatial and temporal resolution and do not suffer from some of the artefacts such as pupil wobble, which can be observed in pupil trackers (Kimmel et al., 2012; Nyström et al., 2013). Therefore, coils are particularly useful for studies of eye movement kinematics. On the other hand, the coil system is a lot more labor intensive, invasive and can lead to altered saccade kinematics (Frens and van der Geest, 2002; Kimmel et al., 2012). More commonly used methods of tracking the eye movements rely on non-invasive infrared trackers (Machado and Nelson, 2011; Ryan et al., 2019).

One well-known infrared eye movement tracker is the Eyelink 1000 plus system. It allows

measurements of the position of the pupil at 1000 Hz at a precision of 0.01° (SR Research, www.sr-research.com; **Figure 5C**). Given the high temporal resolution of the visual system, tasks that rely on visual cues require a monitor with a high refresh rate. Usually the animal is placed at a viewing distance of approximately 52 cm from a monitor, e.g., a CRT monitor (100 Hz, 1152 x 864 pixels; (Flierman et al., 2019). At the beginning of every experiment the eye tracker is calibrated with the standard 5-point eyelink calibration at 10° eccentricity. Saccades are detected online by the eye tracker when eye velocity exceeds 30°/s. Data is stored offline in the form of x-y coordinates and can be further analyzed offline using e.g., MATLAB (MathWorks Inc.).

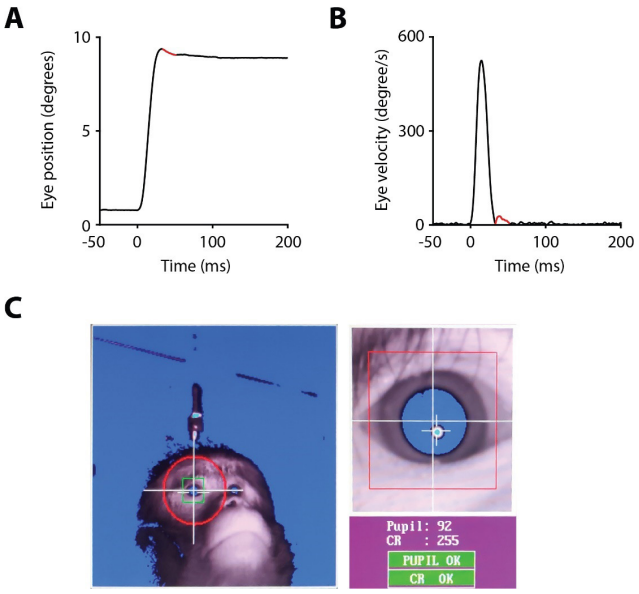

Figure 5. Eye tracking. A*) Saccadic eye movement recorded with infrared video eye tracker. Glissades are marked in red.* **B***) Velocity trace of the same saccadic eye movement as in A.* **C***) Tracking of the left pupil with eyelink 1000+ system. White cross in the top view displays the center of the pupil. In the bottom view the large white cross represents the center of the pupil and the small white cross through the light blue dot represents the corneal reflection.*

2.5.2 Oro-facial behavior

Recent research has shown that the cerebellum is actively involved in many cognitive tasks (D'Angelo and Casali, 2012; Caligiore et al., 2017; Sendhilnathan et al., 2020). Therefore, it is increasingly important to monitor the movement and position of many body parts to distinguish the neural signals triggered by motor activity from those related to sensory information, reward signals or attention. Particularly when it comes to reward signals it is necessary to record covariates such as tongue movements and mouth openings, as NHPs are most commonly rewarded by a drop of juice delivered via a lick spout. In some laboratories the lick spout is equipped with an infrared (Tsutsui et al., 2016), or a capacitive touch sensor (Sendhilnathan et al., 2020) that can detect the licks. However, modern tracking technologies offer an opportunity to directly measure all facial

movements (**Fig. 6**). To track facial behavior an industrial camera can be used (e.g., The Imaging Source, GmbH), triggered by a TTL pulse coming from the Eyelink (the example data shown in **Figure 6** was recorded at 40 Hz and 640x480 pixels). It is important to only capture as many frames and pixels as are of interest, since otherwise computational power needed quickly increases. Data from the camera is fed into a trained neural network to extract facial markers with high precision. For this purpose we use DeepLabCut, an open source and an easy to use machine learning algorithm (Mathis et al., 2018). We have recently developed a new version of the tracking software capable of extracting oro-facial movements from NHPs (Liu et al., 2020). Most of these programs have their own manual and are easy to set up even for those not computationally inclined.

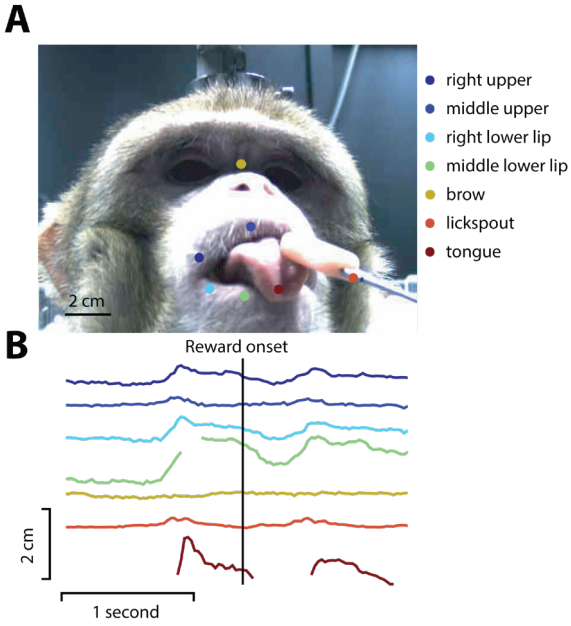

Figure 6. Tracking of oro-facial behavior. A*) Different points in the frame are annotated for tracking of mouth movements and tongue protrusion. The brow and lick spout can be used as reference.* **B***) Output of DeepLabCut analysis. Tracking of the points shown in A aligned to reward onset. If the point is occluded the line is not visible.*

2.5.3 Hand and whole-body tracking

As described above, video tracking of different body parts or the whole body is a complementary, non-intrusive method to quantify behavior. The advent of continuous, unrestrained, more naturalistic tasks (Huk et al., 2018) puts 3D markerless tracking at the forefront of behavioral estimation (Mathis et al., 2018; Bala et al., 2020; Berger et al., 2020; Liu et al., 2020). Hand and body tracking can be achieved just by using a single camera for tracking hand movements using a joystick (Heimbauer et al., 2012) to 62 or more synchronized cameras (Bala et al., 2020). Hand and whole-body tracking videos can be recorded using an industrial monochrome CCD camera (DMK 23U445, The Imaging Source LLC, North Carolina, USA) capturing a 1280 x 960 video at 30 frames/s (1.2 Megapixels) or

a color camera (BFS-U3-23S3C-C) capturing 1920 x 1200 video at 163 FPS (2.3 MP) among others. Careful considerations must be taken in selecting lenses when cameras are placed at short distances and low light conditions. The start and end of the video recording is synchronized with other behavioral data using a trigger pulse sent by the behavioral PC controller. The storing of the video can be done using common video formats (such as .avi) or saving every frame and reconstructing them offline. To extract pose estimation or the trajectory of hand movements, identifiable features in the hand (i.e.., the wrist and fingers) are labeled to be tracked in a random subset of frames. Next, the researcher has to train a deep neural network model, for example using the DeepLabCut (Mathis et al., 2018) or OpenMonkey Studio (Bala et al., 2020), and extract the time course of the spatial locations of the marked features.

2.5.4 Training of the behavioral tasks

Training non-human primates on complex tasks can be quite challenging. Therefore, a project-based training program with clear objectives and trained using positive reinforcement (PRT) will give the best results. Training is usually split into small segments in a build-up fashion, using the last learned behavior to continue to the next goal. PRT technique is used to obtain the desired behavior and helps to establish a positive relationship with the NHPs. If a NHP presents an undesired behavior withholding a reward is commonly used. Sometimes, an acutely applied, negative reinforcement is used (e.g., unpleasant sensory stimulus). However, this should not be the norm and should be used only sporadically, so as not to cause stress that can result in a discouragement in the task. Most countries nowadays only allow PRT methods, i.e., punishment is forbidden. Undesired behavior can thus only be reduced by a time out, disallowing the animal to receive the next reward. When a small segment of the task is ingrained, the task is made more complex by adding the next step and reinforcing good behavior again.

In head-fixed, visually-guided behavioral tasks animals are seated in a primate chair. This is a chair on wheels that fits inside the setup, so the only physical act that is required of the animal is climbing in the chair. For this to happen, efficient cooperative training must be accomplished. This can sometimes be a stressful process for the animal, so selecting the optimal training approach must be planned in advance and dedicated to the type of chair and task to be accomplished. In addition, developing a positive interaction with the animal before any training begins will facilitate training and cooperation (Bliss-Moreau et al., 2013; McMillan et al., 2014). Each training will depend on the type of chair selected for the experiment and the required behavior. Typical NHP chairs, where the monkey is “guided” to the chair, either using a pole-collar technique or chain, will require desensitization to the chair and to the element attached to his neck. Desensitization to these elements can be done early on in the process, while the animal is acclimating to their new space. To name a few, guiding a monkey to a chair using a chain can take 1-1.5 weeks, while pole and collar can take up to 5-6 weeks due to the pole being a more stressful object for the monkey. Training duration times can be variable and depends on each animal (McMillan et al., 2014). Training can be performed twice a day for a duration of 15-20 min, although some reports suggest that once a day training may increase success (Fernström et al., 2009). The training includes desensitization to the chain or pole, chair, chain or pole on collar training, chain or pole on collar guidance to chair and finally closing the chair. Training a monkey to freely cooperate, this means, with no guiding object or method of head or neck restraining, training the monkey to fully cooperate to come into the chair by themselves could take between 6-8 weeks. Providing the animal with behavioral choices using

PRT, the trainer facilitates motivating effects that positively impact the behavior of NHPs during experiments (Laule et al., 2003; Reinhardt, 2003, 2004).

To start the experiments, first the animals are habituated to the setup, by exposing them to the environment for increasing amounts of time, whilst building a positive association by giving fruit juice or treats in the form of (dried) fruit. When habituated to the setup, the same procedure is repeated but with head-fixation through the head-post in a stepwise procedure, where on the first day the animal is head-fixed for 15 min, then 25-30 min and so on, adding 10-15 min to the fixation time with each step. Subsequently, the animal is trained to fixate their eyes at a dot at the center of the screen for increasing amounts of time, which is monitored by an eye tracker. From this point the animals have to input their own behavior instead of passive habituation. To improve performance the water intake is controlled prior to training. During the training or experimental sessions, the animals can earn the water in the form of fruit juice. This is a form of positive reinforcement where the behavior is strengthened by removing a passively applied aversive stimulus, i.e., thirst. Juice is more suitable than food rewards, since it can be stretched out over thousands of trials by giving small drops of juice for every correct trail and there is no chance of disturbance of electrophysiological measurements from chewing. Notably, some laboratories use fruit puree or food pellets instead of the juice and do not control the water or food intake prior to training/experiments (Prescott et al., 2010; Westlund, 2015).

For traditional tasks, when an animal is consistently fixating, real task elements can be added. For instance, a saccade target or a distractor. Interestingly, several laboratories have demonstrated that fixation in the center position is not always necessary (Lakshminarasimhan et al., 2020) and in fact the natural eye movements can reveal the NHP's internal states. More naturalistic tasks also lack a fixation point (Knöll et al., 2018). Regardless of the presence or absence of the center fixation point, the amount of task elements or distractors is very slowly built up, only if performance is constantly above chance level for multiple days. Other tools include increasing or decreasing the brightness of a stimulus that should be paid attention to or ignored. When a stimulus causes a forced choice later on in the task, this element should be introduced in the simplest way possible, generally in the central fixation position. When fully integrated, the element can be presented for shorter periods of time or gradually moved to an eccentric position on the screen. A possible flowchart of the procedures carried on for cerebellar neural measurements in a behaving NHPs is shown in **Figure 7.** The levels of discomfort given here are estimated by the Dutch Ethical Animal Committee.

Besides the classical type of setups involving a primate chair, an eye tracker and a screen, a world of behavioral manipulations exists. Many cerebellar tasks either directly probe the oculomotor system or rely on the eye movements as a behavioral readout. Numerous different behavioral manipulations have been described. These include the use of touchscreens (Norris et al., 2011), an arm manipulandum, which measures and alters the force exerted (Miall et al., 1987), primate chairs that can introduce tilt, translation and roll to affect vestibular input (Laurens et al., 2013b; Streng et al., 2018). Together, they provide a complete toolbox to study cerebellar behaviors.

A common strategy in the NHP laboratories is to use the animals for several experimental protocols. Usually starting at easier tasks and slowly progressing to the most complex ones. In the context of cerebellar research that could mean studying processing of reflexive responses (e.g., reflexive eye movements) before proceeding to volitional behaviors.

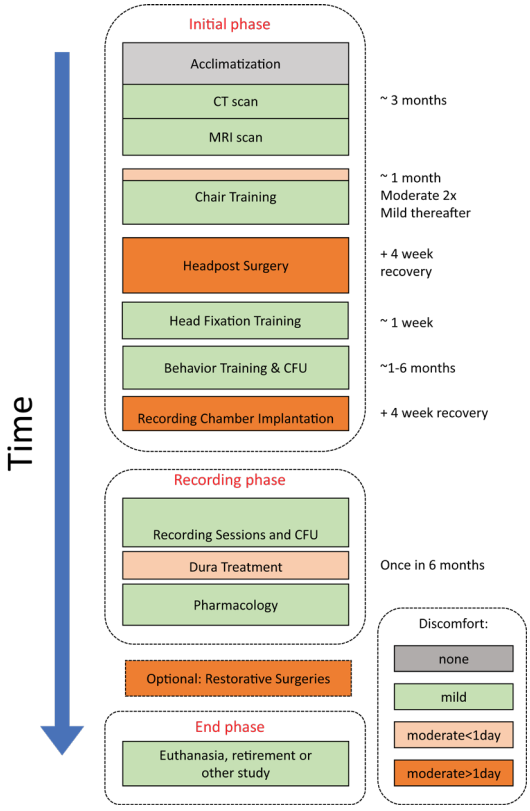

Figure 7. Flowchart primate experiments. *Initial phase: after arrival primates go through an extensive preparation and habituation phase (time estimates to the left). Recording phase: data collection according to experimental protocol. Endphase: euthanasia, retirement to a sanctuary or allocation to another study (pending Animal Ethical Committee approval). Colors represent levels of discomfort. Abbreviation: controlled fluid uptake (CFU).*

2.6 Methods: Cerebellar electrophysiology

To date, cerebellar neuronal signals from the NHPs have predominantly been obtained using single cell, extracellular electrophysiological recording techniques. Although we recognize that novel methods, such as multichannel arrays (Sedaghat-Nejad et al., 2019) are being introduced to NHP cerebellar research (although currently mainly in small primates such as marmosets). Here, we will focus on the single-unit recording technique, which is most commonly used.

Single-unit recordings are most commonly obtained using tungsten glass-coated electrodes (1-2 MΩ, e.g., Alpha Omega Engineering, Nazareth, Israel) through a sterile 23-gauge guide tube, which is inserted through the dura. A motorized microdriver (Alpha Omega Engineering, Nazareth, Israel) with a 1-mm spaced grid can be used to introduce the electrode and map the recording sites.

The electrode inside the guide tube is carefully moved across the visual cortex and the dura, which causes a brief moment of mild discomfort and it is therefore advisable to administer a few drops of juice during this step to encourage the NHP to sit still. Alternatively, a few drops of Lidocaine 2% can be placed on top of the dura a few minutes before inserting the guide tube to provide local analgesia. Subsequently, the electrode is moved into the cerebellar tissue in micrometer increments outside the guide tube. Thus, the tentorium can be passed with just the tungsten electrode (250 μm width 60° beveled tip), not requiring the guide tube to be moved past the dura and thereby minimizing the damage to the visual cortex and the cerebellum. Subsequently the electrode is moved in 2-5 μm increments in the grey matter and 10-50 μm increments in the white matter, until the activity of a single cell is found (see Note 3). The Alpha Omega software allows for real-time spike sorting, rasters and peristimulus histograms. The rasters and histograms can be aligned to any of the digital inputs of the signal processing box, and are thus very useful tools for discriminating if a unit is task related (see Note 4). Extracellular recordings are digitized and sampled at 44 kHz and subsequently stored during the experiment. Under good conditions cells can easily be recorded for 20 minutes, with outliers of over 45 minutes, yielding hundreds of trials depending on the task.

Purkinje cells can be distinguished by the presence of spontaneous firing of simple spikes (SS) and complex spikes (CS) (**Fig. 8A**), as well as the presence of a concurrent short pause in SS firing following a CS (i.e., climbing fiber pause; see (De Zeeuw et al., 2011), as distinguished online using for example Multi-Spike Detector (MSD, Alpha Omega Engineering). Raw traces are offline spike sorted again for higher precision discrimination between SS, CS and noise. Spike events are detected by a manual set positive and negative amplitude threshold for tracers and their derivatives. This threshold is set for every recording session individually based on the signal quality. Threshold crossings are aligned to the peak of the derivative, which is more consistent than the peak of the raw signal, since SS have a larger negative amplitude and CS have a larger positive amplitude when the tip of the electrode is close to the cell body of the Purkinje cell. Spike waveforms are cut out around the peak from -0.5 to +6 ms for Purkinje cells, because CS have a long duration, and -0.5 to +2 for cerebellar nuclei cells, which do not show CS (**Fig. 8B**).

Waveforms belonging to putative Purkinje cells are analyzed through Principal Component Analysis (PCA) to distinguish the SS and CS waveforms. The first three components are used to select exemplary SS and CS to train a probabilistic neural network in a supervised machine learning fashion. This trained neural network is used to determine the class of the rest of the cutout spike waveforms (see Note 4 and 5).

If pharmacological agents are used, these will be applied via a combined recording electrode/pipette (**Fig. 8C**), as described in the next section. The animals will perform the same tasks as outlined above. The duration of daily sessions is usually limited to 3 to 4 hours, but can be prolonged depending on the type of experiment (pharmacological interventions with concurrent electrophysiological recordings can last up to 8 hours with preparations). The total duration of the experimental time is quite variable across laboratories but on average data is collected for several years, although the chamber remains usable after this time-period.

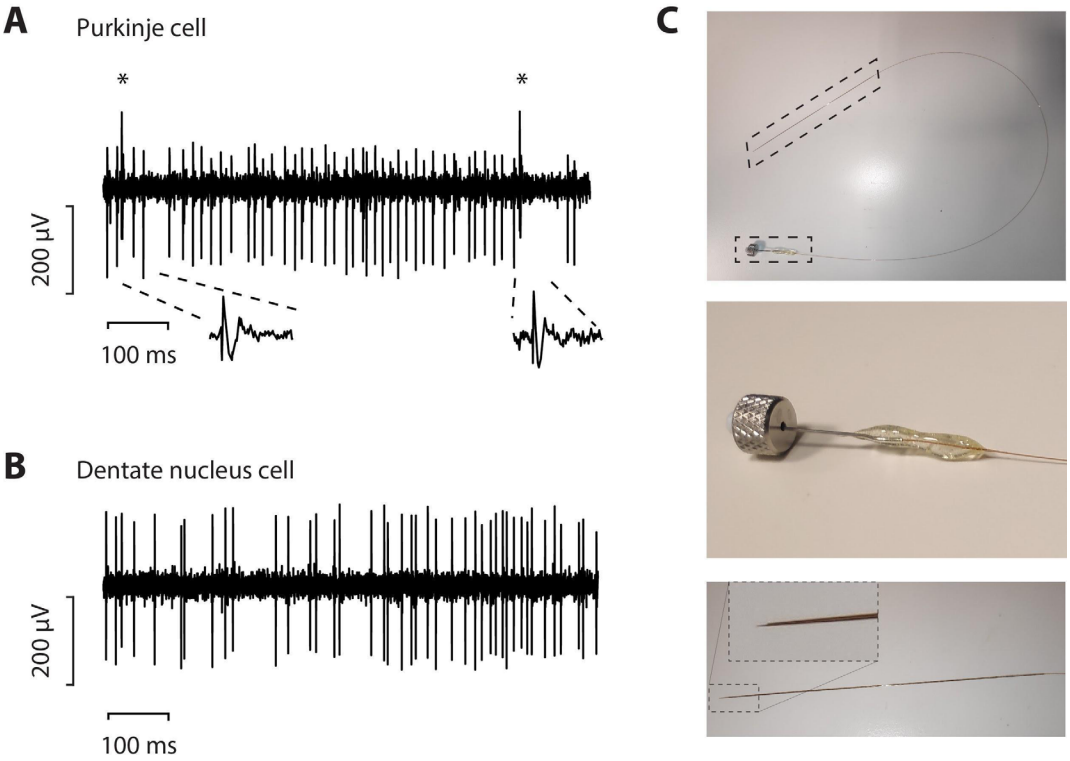

Figure 8. Cerebellar single unit recordings. A*) example trace of Purkinje cell recording exhibiting simple spikes and complex spikes (denoted with *).* **B***) Example trace of dentate nucleus cell.* **C***) Injectrode used for pharmacological interventions. Top panel shows the entire injection line with in the top dashed box a tungsten electrode attached to the capillary tube and in the bottom dashed box a removable needle from Hamilton syringe attached to the capillary. Middle panel shows magnification of the removable needle. Bottom panel shows magnification of the electrode and a further magnified inset of the tip.*

2.7 Methods: Pharmacological interventions

Reversible pharmacological agents can be applied locally through the implanted recording chamber, to the area of the cerebellum where task related neurons are recorded from. If the site of application is in the cortex, a sharp glass pipette or combined electrode/pipette will be lowered across the dura in the same manner as a recording electrode. In case of deeper structures, a glass pipette doesn't work. Instead, an injectrode can be made by attaching a capillary tube (150 µm outer diameter, 40 µm inner diameter (Molex Polymicro) to a tungsten electrode (AlphaOmega) (**Fig. 8C**). This injectrode is connected to the needle of a 10 µl syringe (Hamilton, model 701), which is used to inject the pharmacological agents. This injectrode can be lowered to the target in the same way as the electrode. The pharmacological agent will either be slowly injected using pressure or iontophoresis.

The approach used will depend upon the properties of the drug to be applied and the desired volume of the effect; iontophoresis produces a more local effect, whereas pressure injections can affect larger volumes.

To estimate to what extent a cerebellar region that is being recorded from might be causally related to a particular behavior, inactivation studies can be informative (Kunimatsu et al., 2016, 2018; Sendhilnathan et al., 2020). Most of the published studies use muscimol, a potent, selective agonist of the GABAA receptors, which inhibits activity in Purkinje cells, i.e., the sole output neurons of the cerebellar cortex (Caesar et al., 2003). Most commonly between 2 and 10 μl of 5 μg/ml muscimol is injected directly into the cerebellum (Monzée et al., 2004; Kunimatsu et al., 2016). Muscimol is dissolved in sterile saline and injected with a syringe pump with an average speed of 1μl per 10 min. The injection is preceded by the same injection with only saline to ensure any effect was not based on volumetric tissue displacement. The behavior of interest is recorded before and directly after the injection. If the injection is correctly targeted, a behavioral effect should be visible after 15 minutes, and the effect size could increase up to 60 minutes (Kunimatsu and Tanaka, 2010; Kunimatsu et al., 2018). Depending on the type of drug, suppression of activity can be up to 24 hours, therefore no more than 3 sessions per week can be performed to ensure complete washout before starting a session.

2.8 Notes

Note 1: The edge skin near the implant will often retract somewhat over time. This could uncover the feet of the implant and make the areas with imperfect contact between implant and skull a place of infection that is very difficult to keep clean. Therefore, a customized post, which adheres tightly to the skull, is favorable. In general, skin retraction is a known effect of cranial implants, especially the ones that use acrylic and titanium. This happens because skin cannot adhere to these materials well. In addition, if the implant causes some skin tension, this effect will be amplified. When this happens, it is a common practice to cover the exposed area with acrylic or any other type of cement like Metabond. There are a few things that can be done to try to prevent this, depending on the type of implant: (1) Leaving space between the "legs" of the implant so the skin can bond to the skull; (2) positioning the screws inside the implant when possible; and (3) improving the surgical technique. Specifically, the tissue should be properly positioned ("wrapped") around the implant to decrease skin tension; this gives a chance for the skin to adhere to the underlying tissue. This can be achieved by opening the skin layer by layer and attaching it back in the same fashion.

Note 2: The precise number of MRI scans depends on several variables:

(1) The reliability of the localization of the brain structures involved; in case of cerebellar recordings it is advisable to get at least one scan with the electrode present conforming to the targeted location.

(2) The growth rate and age of the NHP; since the experiments usually take several years, the skull can change the shape considerably in that period. This is particularly important if the implant has to be adjusted at some point. Scans are performed under ketamine anesthesia (see section 2.4.1.1) with an electrode and titanium guide-tube (typically a 28-30G needle) in place when determining the recording location. Scanning with electrodes in the brain is a well-known technique (Logothetis et al., 2001), and there is no real risk on implant heating for titanium implants (Buchli et al., 1988); when using limited, yet sufficient, time to visualize electrode position, artifacts remain usually local,

i.e., close to the implant/guide tube itself (see **Figure 4** for details). It should be noted though that the artifact can be substantially larger than the electrode, which is 250 um in diameter.

Note 3: When the sound of a neuronal unit can be seen or heard ramping up quickly there is some movement in the tissue, this can be accounted for by retracting the electrode 50-100 um or more if necessary to prevent penetrating the cell.

Note 4: It should be noted that single-unit recordings from Purkinje cells or interneurons in the cerebellar cortex of NHPs can differ from those in other animals such as rodents or fish due to the different sizes of the molecular, granular and Purkinje cell layers involved. For example, even though the amplitudes of the spikes of Purkinje cells can be substantially higher in NHPs, it is often relatively difficult to record complex spikes and simple spikes of a single Purkinje cell at the same time in NHPs.

Note 5: When performing electrophysiological recordings, it is essential to analyze the data as soon as possible to see whether the recorded cell shows any task related activity. If this is not sufficiently clear on the online rasters, it should be done offline immediately after the recording.

2.9 Conclusions

Measurements of single neuron activity in awake and behaving NHPs offer a unique insight into the brain of a species most closely resembling that of a human. Considering that electrophysiological measurements in humans *in vivo* are predominantly performed intraoperatively and never in healthy individuals, NHP research is the only alternative in studying the primate brain. Techniques presented in this chapter allow researchers to answer relevant questions about the role of the cerebellum in planning, learning and coordination of sensorimotor tasks. Historically, NHP cerebellar recordings have been instrumental in defining many characteristics of such tasks; for example: encoding of saccade kinematics, movement predictions, and error-based adjustment of future performance (Herzfeld et al., 2015; Hong et al., 2016; Junker et al., 2018; Streng et al., 2018). Although the field of movement control and learning is far from solved and many experiments are still focused on these functions, there is an observable shift in the field towards more cognitive functions of the cerebellum. In recent years, the techniques we describe in this chapter have provided insights into the role of the cerebellum in behaviors classically attributed to cerebral cortex and basal ganglia, such as reward processing, attention, working memory and reinforcement learning (Kunimatsu et al., 2018; Sendhilnathan et al., 2020). Developments in other fields, such as machine learning, have been incorporated into the field of NHP research of the cerebellum, further fueling this shift. For instance, the oro-facial behavior tracking shown in **Figure 7** is applied to distinguish motor-related neuronal activity (such as licking) from reward signals. Notably, the use of camera methods for behavior tracking omits the necessity to put markers on the animals.

Similarly, techniques previously only available in rodent research are slowly starting to become accessible to primate neuroscientists. Several studies using optogenetics in cortical neurons have been published in recent years (Jazayeri et al., 2012; Chernov et al., 2018). Calcium imaging and chemogenetic manipulations have also made their first appearances in the literature together with the use of high density silicon probes and arrays (Seidemann et al., 2016; Mitz et al., 2017; Deffains et al., 2020). The latter have successfully been applied in the cerebellar research (Sedaghat-Nejad et al., 2019). Advances in the 3D printing technology, described in detail in this chapter,

have made it possible to fully customize the headposts and record chambers, which offers much improvement with respect to the older, non-customized models. The use of these custom-made implants leads to fewer rejections, shorter recovery times and less infections, which all contribute to the overall increase in the wellbeing of the animal and success in research efforts. In conclusion, the techniques described here provided the guide to study motor and cognitive behavior in combination with cellular activity in NHPs, specifically in rhesus macaques.

Chapter 3:

Purkinje cell activity during voluntary eye movements in medial and lateral cerebellum in Rhesus Macaques

Eric Avila[1,2#], Nico A. Flierman[1,2#], Peter J. Holland[3], Pieter Roelfsema[1,4,5], Maarten Frens[2], Aleksandra Badura[1,2*] and Chris I. De Zeeuw[1,2*]

Author affiliations:

[1] Netherlands Institute for Neuroscience, Amsterdam, The Netherlands

[2] Department of Neuroscience, Erasmus MC, Rotterdam, The Netherlands

[3] School of Psychology, University of Birmingham, Birmingham, UK

[4] Department of Integrative Neurophysiology, VU University, Amsterdam, The Netherlands

[5] Department of Psychiatry, Academic Medical Centre, Amsterdam, The Netherlands

[#/*]These authors contributed equally to this work.

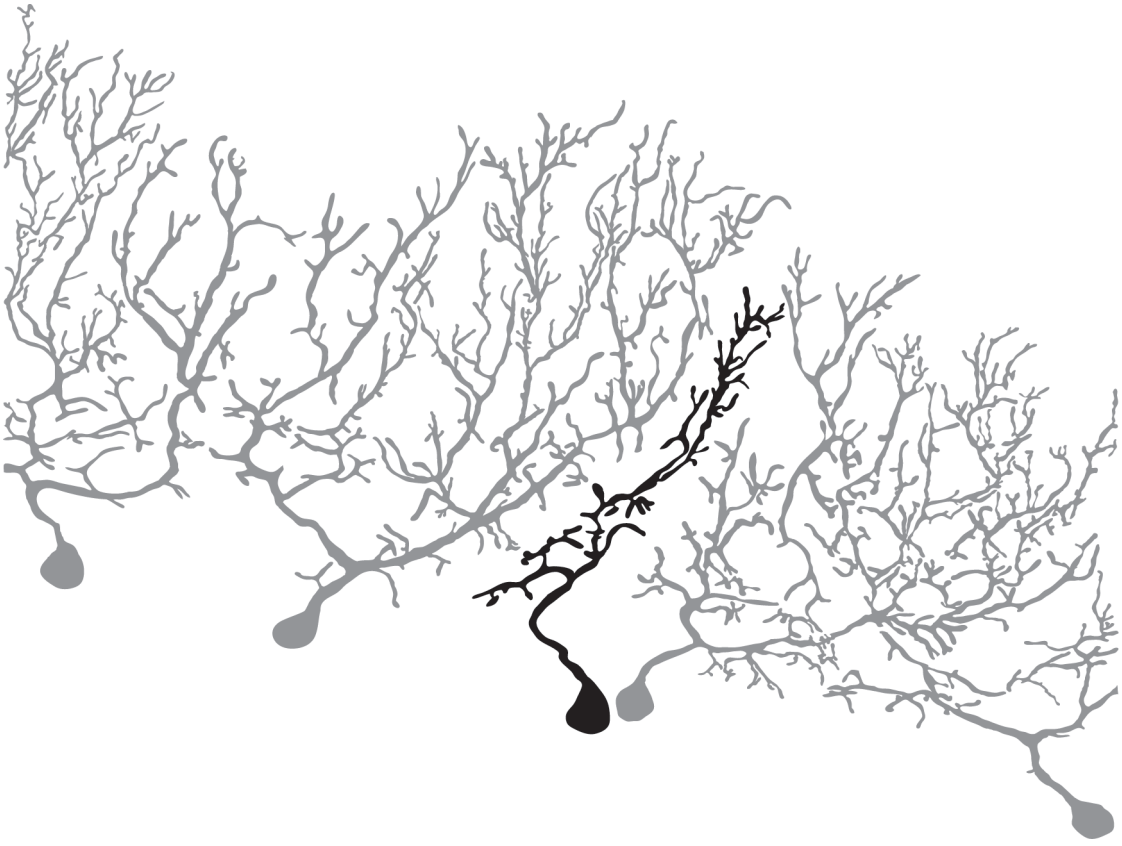

3.0 Abstract

To what extent different parts of cerebellum play differential or complementary roles in higher behavioral functions remains an open question. Here, we monitored Purkinje cell activity in medial and lateral cerebellum of non-human primates during prosaccades towards a target and antisaccades, which requires to inhibit a response to a target and instead look to a mirrored virtual target. This is a behavioral task that taps into volitional control of action, a hallmark of top-down executive control. We found that Purkinje cells in both cerebellar regions modulated their activity throughout the entire task for both types of eye movement. Simple spike activity modulated in a facilitating or suppressing manner, which was different in the two cerebellar areas. Cells in the lateral region also showed more prominent saccade-related activity at the population level. Purkinje cells in the medial cerebellum were more sensitive to trial history. Complex spike activity also modulated in both regions throughout the task, but at a higher level of reciprocity with respect to simple spike modulation in the lateral cerebellum. Our data indicate that Purkinje cells in medial and lateral cerebellum are simultaneously, yet differentially, involved in preparation and control of simple movements and complex movements.

3.1 Introduction

In a dynamic environment, volitional control of behavior is necessary to make flexible, well-adapted choices. In order to accomplish internal goals, voluntary behavior often requires suppression of reflexive responses to external stimuli, a hallmark of conscious, executive control (Diamond, 2013). For example, when we focus our visual attention in everyday life, we suppress our natural tendency to make a saccade to nearby moving or static objects in order to keep our gaze fixed on the target of choice (Munoz and Everling, 2004). In a laboratory setting, we can measure this complex behavior using the antisaccade task. It requires participants to refrain from looking at a suddenly appearing target ('reflexive response') and instead execute a saccade to the unmarked mirror position of that target ('internal goal') (Everling and Fischer, 1998; Mitchell et al., 2002; Munoz and Everling, 2004). This ability to voluntarily inhibit the urge to look at the target and instead make a saccade away from it is part of executive control function and supports goal-directed behavior.

Similar to that of other volitional movements, antisaccade control is regarded to be organized top-down in that the cerebral cortex has been claimed to initiate such movements (Bunge et al., 2005; Everling and Johnston, 2013). This notion is supported by: (1) dysfunction in various neurological and psychiatric disorders and such as schizophrenia or attention-deficit hyperactivity disorder perform poorly on antisaccade tasks, showing marked difficulties in response inhibition and, (2) observations that antisaccade related activity has been found in various parts of the cortex, including dorsolateral prefrontal cortex (DLPFC), frontal eye fields (FEFs), and supplementary eye fields (SEFs) (Funahashi et al., 1993; Schlag-Rey et al., 1997; Gottlieb and Goldberg, 1999; Bunge et al., 2005; Hakvoort Schwerdtfeger et al., 2012; Everling and Johnston, 2013; Cutsuridis et al., 2014). However, given that all these regions are both downstream and upstream connected with the cerebellum (Kelly and Strick, 2003), the cerebellum may well form an additional hub in this voluntary motor control circuitry (Tanaka et al., 2003; Peterburs et al., 2012; Brunamonti et al., 2014; Kunimatsu et al., 2016; Dacre et al., 2019). This possibility is corroborated by recent findings that the cerebellum does not only participate in movement execution, but also in movement planning (Ashmore and Sommer, 2013; Giovannucci et al., 2017; Deverett et al., 2018; Gao et al., 2018; Kostadinov et al., 2019). To what extent the execution and planning of movements are differentially controlled by the medial and lateral cerebellum has been an outstanding question for a long time (Miall et al., 1993; Thach, 2007; Ito, 2008; Gao et al., 2018, 2019; Chabrol et al., 2019; De Schutter, 2019). Some studies indicate that executions of simple, reflexive movements may be controlled by a relatively medial module of Purkinje cells (PCs), whereas complex behaviors, which require instruction, inhibition and planning (executive control), might be controlled by more lateral parts of the cerebellum (Strick et al., 2009; Caligiore et al., 2017; Chabrol et al., 2019; De Schutter, 2019; Sendhilnathan et al., 2020). Others however, advocate that both the execution and planning of a particular movement can be controlled by the same module regardless of the cerebellar area (Gao et al., 2018, 2019), the location of which in the cerebellar cortex is determined by the PC-to-effector pathway (De Zeeuw, 2020). Settling this argument would require simultaneous monitoring of spiking activity of PCs (Voogd et al., 2012) in both medial and lateral cerebellar areas during a motor task that includes both the execution of a simple reflex and a more complex form of planning of movement related to the same effector.

Here, we investigated the hypotheses that (1) PCs in the cerebellum do not only play a role in the execution of reflexive eye movement responses, but also during volitional eye movements; and (2) that PCs in medial and lateral cerebellum differentially contribute to these two tasks. More

specifically, we set out to study PC modulation in the medial (oculomotor vermis or OMV) and lateral (crus-I/II) cerebellum of non-human primates (macaca mulatta) during the generation of both prosaccades and antisaccades (**Fig. 1**). The animals were trained to make either a prosaccade or an antisaccade to a mirror 'invisible' target depending on an initial color cue. During the entire paradigm we recorded both simple spike (SS) and complex spike (CS) activity of PCs, which are mediated by the mossy fiber and climbing fiber pathway, respectively (Voogd et al., 2012).

We found that SS modulation during the instruction and the execution periods of prosaccade and antisaccade eye movements was prominent in PCs of both medial and lateral cerebellum. SS activity in both regions modulated in both a facilitating and suppressing manner, a feature that is common in sensorimotor tasks that require bidirectional control in the PC-to-effector pathway (Heiney et al., 2014; Yang and Lisberger, 2014; Herzfeld et al., 2015, 2018; ten Brinke et al., 2015; Ten Brinke et al., 2017; De Zeeuw, 2020). In both regions, the PCs of the *facilitation* category showed a prominent increase in firing rate just before target appearance during the instruction period. In addition, in both regions SS activity displayed distinct, time-ordered, sequences that were stable across many trials, which can be considered a recurring motif of population activity when keeping track of timing is critical (Ikegaya et al., 2004; Jin et al., 2009; Harvey et al., 2012). However, various other parameters of the SS activity modulations differed between medial and lateral cerebellum. PCs in the lateral cerebellum showed a greater firing rate during the execution of saccades. In addition, the same cells in the lateral cerebellum displayed modulated SS signals in the instruction period in both pro- and antisaccade trials, and showed more prominent saccade-related activity at the population level. PCs in the medial cerebellum were more sensitive to trial history, and PCs of the *suppression* category in this region showed a relatively late SS modulation during execution of both pro- and antisaccades, in line with previous findings (Ashmore and Sommer, 2013; Herzfeld et al., 2015, 2018). CS activity modulated during pro- and antisaccade trials in both cerebellar regions throughout the task, but it showed a higher level of reciprocity with respect to SS activity in the lateral cerebellum. Our results indicate that PCs in the OMV of the medial cerebellum and those in crus-I/II of the lateral cerebellum differentially contribute to the instruction and execution of reflexive behavior and the suppression thereof. This finding highlights that different cerebellar regions can contribute to the same simple and complex forms of related behaviors. Yet different propensities add to the growing evidence of the role of the cerebellum in executive control and into conditions where response inhibition is hampered.

3.2 Results

Behavior during pro- and antisaccades

We trained two adult, male rhesus macaques (referred to as monkeys Mo and Mi) to perform a randomized, interleaved pro- and antisaccade task. Correct behavior required either the execution of a saccade to a single visual target in one of 8 directions (prosaccade) or the suppression of the prepotent saccade to a visible target and redirection of gaze to an unmarked mirror position (antisaccade, **Fig. 1a**). A trial started with the appearance of a central fixation point and the trial condition was indicated by the fixation point color (red for prosaccade, presented in figures in magenta; green for antisaccade, presented in figures in blue; colors were adjusted for presentation to accommodate color-blind readers). After this instruction period (300-500 ms), a target would appear randomly at 1 of 8 different locations separated 45˚ from each other, while monkeys

maintained fixation for 100 ms more before the central fixation point turned gray (referred to as motor planning period), serving as the "go-cue". Animals had 500 ms to execute the pro- or antisaccade (execution or saccade period) before the trial was aborted. This task design temporally separates the initial neural representation of the stimulus from the subsequent motor preparation and execution (Amador et al., 1998).

We removed trials with saccades with reaction times of less than 100 ms to avoid contamination from anticipatory saccades; these reflect a visual, involuntary reflex towards a novel stimulus in the environment and do not represent correctly planned saccades, during which the monkeys delay their eye movements until the presentation of the "go-cue" (Goldring and Fischer, 1997; Coe and Munoz, 2017). We also removed error trials, as we did not have enough power to analyze them due to the accuracy across the experiments (94.1 ± 5.6% and 94.4 ± 5.3% for Mo and Mi, respectively). The eye movements during antisaccades exhibited longer reaction times, lower peak velocities, larger amplitudes, and longer durations than prosaccades (**Fig. 1c**).

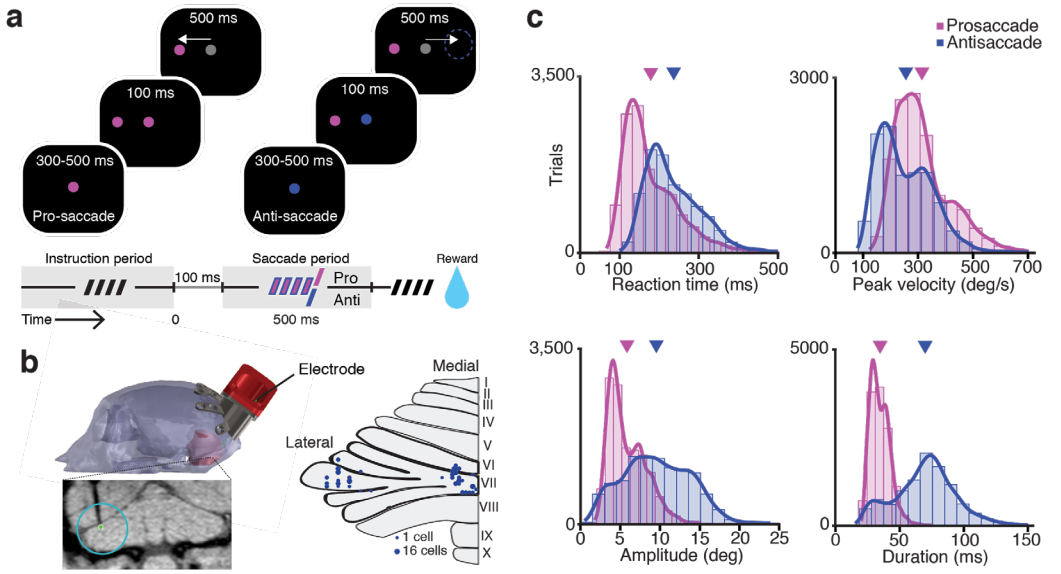

Figure 1. Task, recording location and saccade kinematics. a, *A scheme representing the different periods of the task. Trial condition was indicated by the color of the fixation point. After a random delay between 300-500 ms (i.e., instruction period) a target appeared in one of 8 locations, while monkeys were required to maintain fixation for 100 ms (i.e., planning period). Next, the fixation target switched to gray and monkeys were given 500 ms to execute a saccade (i.e., execution or saccade period) towards the target (prosaccade) or the mirror position of the target (antisaccade).* **b**, **left,** *MRI-based 3D-reconstruction of the skull of monkey Mi;* **bottom**, *coronal MRI section showing the localization of a temporarily implanted single electrode in the left lateral cerebellum;* **right**, *overview of localization of recordings sites in medial cerebellum (lobules VIc and VII) and lateral cerebellum (crus-I/II, left hemisphere).* **c**, *Features of kinematics of all prosaccades (magenta; monkey Mo n = 6114, monkey Mi n = 6670) and antisaccades (blue; Mo n = 4114, Mi n = 6305) for all trials. Antisaccades were characterized by longer reaction times (pro- mean 178.4 ms ± 70.6 s.d.; anti- mean 236.6 ms ± 72.7 s.d.; p < 0.0001), lower peak velocities (pro- mean 311.8 °/s ± 102.6 s.d.; anti- mean*

253.4˚/s ± 103.1 s.d.; p < 0.0001), bigger amplitudes (pro- mean 5.8˚ ± 2.3 s.d.; anti- mean 9.5˚ ± 4.1 s.d.; p < 0.0001), and longer durations (pro- mean 34.7 ms ± 7.9 s.d.; anti- mean 69.8 ms ± 24 s.d.; p < 0.0001). Triangles in magenta and purple indicate means of pro- and antisaccade movement parameters, respectively.

Purkinje cells in both medial and lateral cerebellum modulate their activity during execution of pro- and antisaccades, but with different characteristics

While the monkeys performed the task, we recorded from 90 PCs in medial and 72 PCs in lateral (Crus-I/II) cerebellum during 122 sessions (**Fig. 1b**); recording sessions started when the animals reached a performance of at least 80% after the initial weeks of training. A neuron was considered to be task-related if SS activity during the beginning of the saccade period (i.e., from saccade onset to 150 ms after saccade onset) was significantly different from the intertrial interval period (see **Methods**). Approximately half of the cells recorded in both areas fulfilled this criterion [n = 40 (43%) for medial cerebellum and n = 38 (53%) for lateral cerebellum]. All subsequent analyses were performed only for these cells (n = 78 PCs).

Many PCs showed SS modulations in relation to peak velocity, amplitude and duration of pro- and/or antisaccades, but on average no significant differences were observed between medial and lateral cerebellum in this respect. We regressed the firing rate in the two areas with either amplitude or peak velocity and compared the firing rate for pro- and antisaccades in both areas. There were no correlations between firing rate and either saccade amplitude or saccade peak velocity in the two areas between the two conditions and allowed us to first directly compare them by pooling the mean firing rate for each cell during pro- and antisaccades **(Supplementary Figure 1a-d** and **Supplementary Table 1**). Activity of PCs obtained during the first 150 ms after saccade onset, was significantly higher in the lateral cerebellum in both conditions (mean and s.d., medial pro 66.7 ± 30 spks/s, lateral pro 69.3 ± 39 spks/s; medial anti 68 ± 36 spks/s, lateral anti 71.8 ± 39 spks/s, p<0.05 for both, Wilcoxon rank sum test)

We classified the PCs into two different groups depending on whether they decreased (*suppression* PCs) or increased (*facilitation* PCs) their firing rate after saccade onset and we also observed subtle differences between medial and lateral cerebellum (**Figure 2**). The activity profile of the PCs was the same during pro- and antisaccades in both areas except for two PCs in the lateral cerebellum. These two cells were included in their respective category (*facilitation* or *suppression*) for further analyses. The mean latencies of SS activity of suppression PCs within medial and lateral cerebellum during prosaccades, defined as the largest trough after saccade onset, were similar to those during antisaccades (mean ± s.d.: Medial pro 87 ± 70 ms vs Medial anti 93 ± 67 ms, p = 0.83, Wilcoxon Rank sum test; Lateral pro 139 ± 40 ms vs Lateral anti 127 ± 42 ms, p = 0.1, Wilcoxon Rank sum test; **Supplementary Figure 2**). However, when we compared the two regions, we found that the latencies of the *suppression* PCs in the lateral cerebellum (mean ± s.d: 133 ± 40 ms) were significantly longer than those in the medial cerebellum (89 ± 68 ms; p = 0.01, Wilcoxon rank sum). In contrast, *facilitation* PCs peaked their activity after saccade onset on average at similar times during pro- and antisaccades and similarly in both medial and lateral cerebellum (medial vs lateral for pro- and antisaccade cells p = 0.2 and p = 0.9, respectively, Wilcoxon Rank sum test; **Fig. 2e-f**); all occurring approximately 100 ms after saccade onset (mean ± s.d.: Medial pro: 105 ± 41 ms vs Lateral pro 84 ± 48 ms; Medial anti: 104 ± 33 ms vs Lateral anti 106 ± 43 ms).

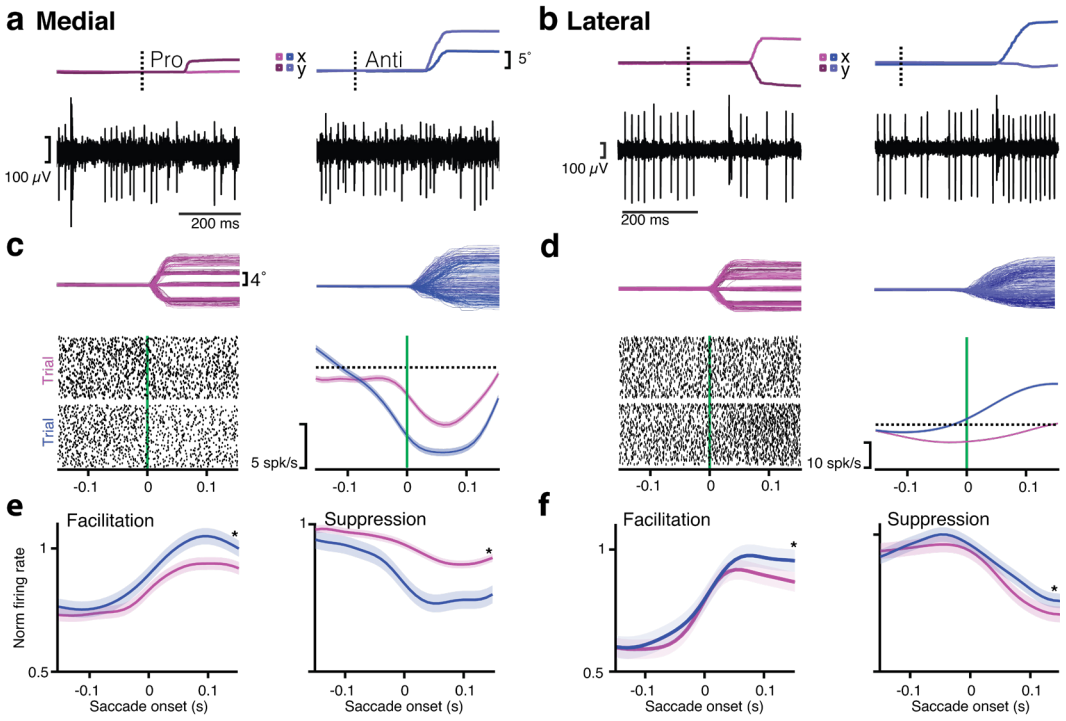

Figure 2. PCs in both medial and lateral cerebellum modulate their activity during the saccade period. a Top, *Eye trace for an example trial during saccade onset for a pro- (left) and antisaccade (right). Dashed line indicates the time of the "go" cue. Dark and light magenta and blue show the x and y position (horizontal and vertical components) of the eye trace for pro- and antisaccades respectively.* **a Bottom**, *traces of activity recorded from a PC in medial cerebellum for a single trial aligned to the eye trace indicated above. Note that the traces include many simple spikes (SSs; smaller spikes) and only a few complex spikes (CSs, bigger spikes).* **b**, *Same as in (a) but for lateral cerebellum.* **c Top**, *Eye traces in all 8 directions for all trials for an example cell during the saccade period for pro- and antisaccade trials.* **c Bottom**, *raster plots (on the left) showing the time of SS action potentials of this cell sorted by go-time aligned to saccade onset, and the corresponding response time-course (on the right) averaged for all correct trials. Shaded regions denote s.e.m. dotted line is average baseline firing frequency* **d,** *Same as in (c) but for lateral cerebellum.* **e**, *Time-course of normalized responses averaged for all neurons in medial cerebellum that either increased their firing (facilitation cells) or decreased it (suppression cells) after saccade onset (facilitation pro vs anti: $p = 1.61x10^{-7}$, suppression pro vs anti: $p = 5.3x10^{-23}$).* **f**, *Same as in (e) for lateral cerebellum (facilitation pro vs anti: $p = 1.08x10^{-17}$, suppression pro vs anti: $p = 4.4x10^{-9}$). Prosaccades are denoted in magenta and antisaccades in blue for all panels.*

Purkinje cells in both medial and lateral cerebellum modulate their activity during instruction of pro- and antisaccades, but with different characteristics

We next assessed SS activity during the instruction period for the PCs that modulated their activity up or down during the saccade period (for details, see **Methods**). Given the variable duration of the instruction period, which varied between 300 and 500 ms, we analyzed the last 300 ms of

this epoch, before the onset of the target, for all cells (**Fig. 1a**). Here, we also encountered diverse neural responses in both regions and classified the activity of these neurons in the same way as for the saccade period depending on whether they increased (*facilitation* cells) or decreased (*suppression* cells) their firing after instruction onset compared to the activity during the intertrial interval. In the medial cerebellum, the percentages of PCs that responded with increases (10%) or decreases (11%) of their SS activity during instruction of prosaccades were similar to those during the instruction of antisaccades (11% and 7%, respectively, **Fig. 3a**, **Supplementary Table 2**). The same was true for lateral cerebellum, where the percentages of *facilitation* and *suppression* PCs were similar in the prosaccade and antisaccade trials (17% and 14% prosaccade; 18% and 15% antisaccade, *facilitation* and *suppression* respectively, **Supplementary Table 2**). Overall, we found more significantly modulated PCs during the instruction period in the lateral cerebellum than in the medial cerebellum (Medial vs Lateral, $p = 0.03$; Mann-Whitney test), suggesting a more prominent role for PC modulation in the lateral cerebellum during instruction. This is congruent with the finding that in the lateral cerebellum, the levels of PCs modulation during the execution period, of both types of trials, are higher than during the instruction period (**Fig. 3b-c**). Accordingly, we found for both prosaccades and antisaccades in the lateral cerebellum, but only for prosaccades in the medial cerebellum, that the maximum firing rate of the neurons was significantly lower during the instruction period than the execution period (Medial pro $p = 0.03$, anti $p = 0.07$, Lateral pro $p = 0.002$, anti $p = 0.01$, **Fig. 3c**). In addition to the differences between PC activities in the medial and lateral cerebellum associated with the instruction period highlighted above, there were also several interesting differences that were not related to the region involved. For example, SS modulation during the instruction period in both cerebellar areas was more prominent during the instruction for antisaccades than that for prosaccades. The changes in SS firing rate were significantly greater for the antisaccade trials as compared to those for the prosaccade trials in both areas (medial: *facilitation* $p = 4.4 \times 10^{-04}$, *suppression* $p = 1.03 \times 10^{-16}$; lateral: *facilitation* $p = 0.01$, *suppression* $p = 0.04$; K-S test, **Fig. 3a**). Unlike the execution period, which was dominated by suppression cells, during instruction the contribution of the *facilitation* cells to preparation of the antisaccades appeared most prominent. Indeed, when we subtracted the prosaccade SS modulation from the SS modulation during antisaccades (antisaccade SS activity-prosaccade SS activity), *facilitation* PCs of both medial and lateral cerebellum showed a prominent change in firing rate just before target appearance during the instruction period (**Fig. 3b**) and these changes were significantly less pronounced for *suppression* cells (*facilitation* PCs versus *suppression* PCs in medial cerebellum $p = 4.4x10\text{-}6$; *facilitation* PCs versus *suppression* PCs in lateral cerebellum $p = 0.004$; Wilcoxon Rank sum test).

SS activity modulation bridged the interval between the instruction and the saccade epoch through ramping (**Fig. 3d**). We quantified the ramping of SS activity by fitting a linear model to the firing rate during the last 300 ms of the instruction period, cells were classified as having bridging modulation when R^2 was higher than 0.75, we found that bridging modulation was quite rare in the medial cerebellum and more prevalent in the lateral cerebellum (**Fig. 3e**); this held true for both prosaccade and antisaccade trials (both comparisons $p = 0.02$; Chi^2 test, medial: n (pro) = 3, n (anti) = 2; lateral: n (pro) = 11, n (anti) = 10).

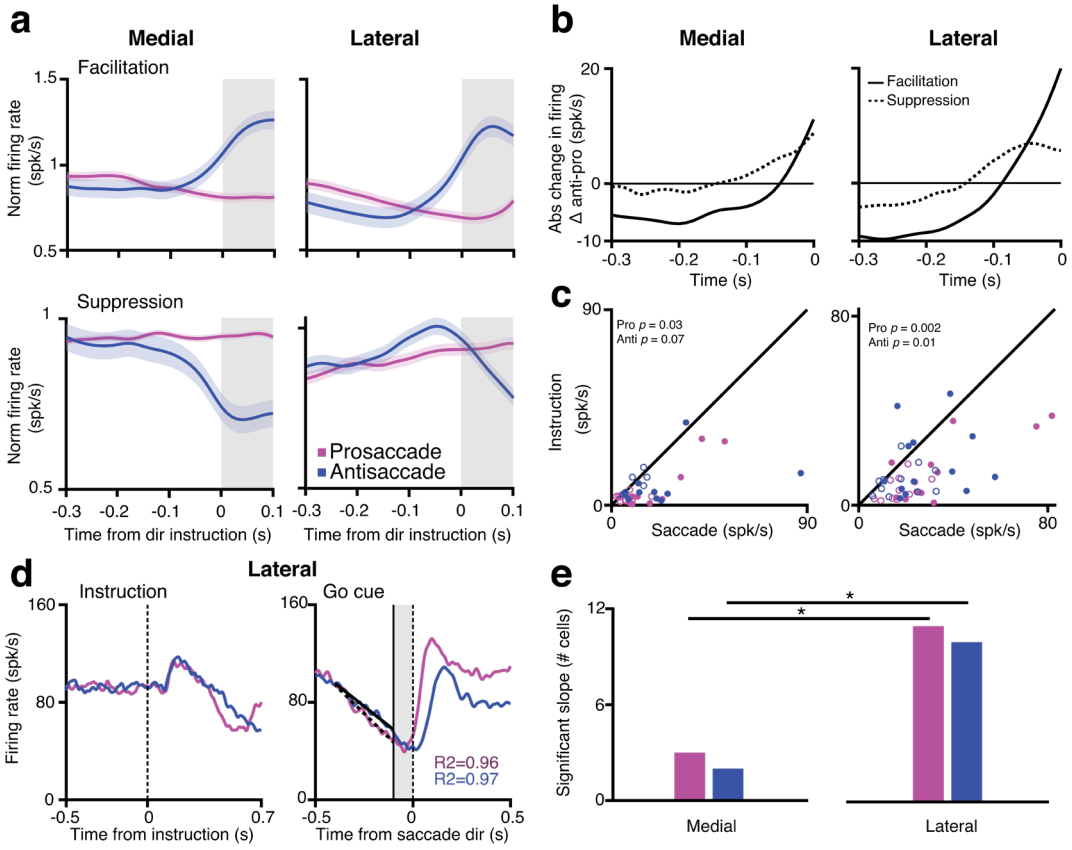

Figure 3. Saccade modulated PCs in both medial and lateral cerebellum modulate their activity up and down during the instruction period. a, *Time-course of normalized responses averaged for all selected neurons aligned to the end of instruction period for prosaccade (magenta) or antisaccade (blue). Responses from medial cerebellum (left) and lateral cerebellum (right) are sorted based on changes in the firing frequency during the saccade period (facilitation, top; suppression, bottom). Grey shaded areas show time after the instruction period when the target appears, but the monkeys have to keep fixating at a central dot (referred to as the planning period).* **b**, *Absolute difference in change in firing rate between pro- and antisaccades for facilitation and suppression neurons in medial (left) and lateral (right) cerebellum. Note the change in firing rate just before target appearance in the facilitation cells.* **c**, *Scatter plots of maximum simple spike firing rate of the Purkinje cells during the instruction period vs. that during the saccade period (in spks/s) for pro- and antisaccades in medial (left) and lateral (right) cerebellum. Inset shows p-values for the comparison between facilitation and suppression neurons in each trial condition. Filled and open circles represent facilitation and suppression neurons, respectively.* **d**, *Explanation of slope calculations used for panel e. Left, Time-course of responses during prosaccades (magenta) and antisaccades (blue) for an example neuron in the lateral cerebellum aligned to instruction onset (vertical line at zero); right, activity of the same neuron but now aligned to the "go" cue (vertical dotted line at zero; solid line represents the end of the instruction period, shaded area is direction instruction same as in a). A linear regression model was fitted (diagonal dotted and solid*

line for pro- and antisaccades, respectively) to the firing rate 300 ms before the end of the instruction period to the end to calculate the slopes. **e***, Number of cells with significant slope modulation in the medial and lateral cerebellum (*Chi² *test for proportions) are higher in the lateral cerebellum for both prosaccade (magenta) and antisaccade (blue) trials (p = 0.02 for both comparisons).*

We conclude that PCs in both medial and lateral cerebellum modulate their activity during instruction of pro- and antisaccades, with a relatively prominent role for the *facilitation* cells during the instruction of antisaccades. Yet, PCs in the lateral cerebellum differ from those in the medial cerebellum in that they have a relatively stronger modulation in both the instruction and execution periods.

Population of Purkinje cells in the lateral, but not in medial, cerebellum denotes trial identity based on simple spike activity

Given the response profiles described above we wondered to what extent the trial conditions were represented by the population activity of PCs in the medial and lateral cerebellum. We compared the differences in neural activity between pro- and antisaccades in both areas by computing a modulation ratio between the responses during the saccade period in the two types of trials, defined as the ratio between the response during pro- and antisaccades (**Fig. 4a**, **Methods**). Values of 1 mean that both responses are the same, values higher than 1 mean that prosaccade activity was higher, and below 1 that antisaccade activity was higher. Medial PCs had somewhat different responses when comparing pro- and antisaccade activity in contrast to lateral PCs (mean of *facilitation* PCs in medial cerebellum 0.91 ± 0.1 s.d. versus that in lateral cerebellum 0.88 ± 0.3, $p = 0.03$; mean of *suppression* PCs in medial cerebellum 1.16 ± 0.2 versus that in lateral cerebellum 1 ± 0.2, $p = 8.02 \times 10^{-04}$; one-tailed K-S test).

To further quantify the differences between the medial and lateral cerebellum and address their potential meaning, we computed a binomial proportion test as a function of time between pro- and antisaccades for the same neurons to better capture the time at which the spiking was significantly different and show if, and how well, single PCs discriminate between both conditions in both regions. The responses of single PCs differ strikingly between the two areas and the two different activity populations, especially for the PCs that showed significantly different activity between pro- and antisaccades (**Fig. 4b**). This is for neurons that changed their firing during the saccade execution period and had a firing rate significantly different between the two conditions. Unlike *suppression* PCs, *facilitation* PCs in the lateral, but not in the medial, cerebellum exhibited prominent contrasting activity mainly present around saccade onset (**Fig. 4b-c**). Apparently, at the population level, the activity of medial cerebellum could not discriminate between pro- and antisaccade trials, even though individual PCs in that region showed significant differences between the conditions (**Fig. 4b**). In contrast, the population of PCs in the lateral cerebellum was able to effectively discriminate between the two types of trials during saccade execution only, reaching peak separation at 70 ms after saccade onset (**Fig. 4c**). This is quite surprising, because both types of PCs (i.e., *facilitation* and *suppression* cells) in both areas exhibit saccade-related activity, but only the *facilitation* cells in the lateral parts of the cerebellum contain information about the trial at the population level.

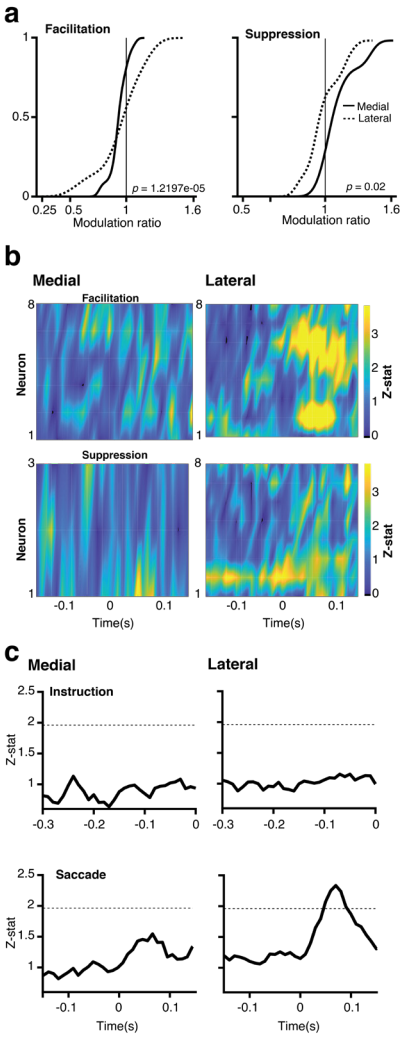

Figure 4. Population encoding of SS modulations in lateral versus medial cerebellum. a, *Cumulative distribution of the SS modulation ratio for medial and lateral cerebellum for facilitation and suppressive PCs. Insets show p-values for the comparison between medial and lateral cerebellum (two sample K-S test).* **b**, *Z-statistic of a binomial probability distribution comparison between pro- and antisaccades for significant PCs in medial (left) and lateral (right) cerebellum separate for facilitation and suppressive responses (top and bottom respectively). Color bar is set at twice the significance value (1.96).* **c**, *Z-statistic of a binomial proportion test during the saccade period as a function of time for pro- and antisaccades for medial (left) and lateral (right) cerebellum during the instruction (top) and saccade (bottom) period for significantly different neurons (***Methods***).*

Purkinje cells in medial cerebellum are sensitive to trial history

It has been suggested that the PC response on a given trial may be modulated by the recent history of different trial types (Herzfeld et al., 2018). We showed above that the population response in lateral cerebellum areas is different for pro- and antisaccades, we wanted to know if the PC modulation was sensitive to trial history, given that the monkeys exhibit a low error performance. We performed trial-by-trial analysis of the SS firing rate of all PCs, comparing the absolute difference in SS spiking activity between trial *n* and one trial back (*n*-1), and trial *n* and two trials back (*n*-2). We included in our analysis one or two trials back to assess if there is an influence of previous trial(s) on the current one, especially when the last trial(s) switched from prosaccade to antisaccade or vice versa (current trial-1 or current trial-2). We did not observe any significant changes during the instruction period (**Supplementary Figure 3a**). During the execution period however, the PCs in the medial, but not in the lateral cerebellum, were indeed sensitive to trial history (**Supplementary Figure 3b**). The PCs of the medial cerebellum showed a significant increase in firing frequency when the identity of a trial differed from that of the previous trial (trial *n* vs. *n-1* $p = 9.26 \times 10^{-9}$, trial *n* vs. *n-2* $p = 1.76 \times 10^{-7}$, Kruskal-Wallis test). Specifically, in comparison to both one (*n*-1) and two trials back (*n*-2), trial *n* showed the least amount of change in PC activity when a prosaccade condition was also preceded by a prosaccade trial (post-hoc Tukey-Kramer test). These results indicate that, in line with our hypothesis, PC modulation in the medial, more so than in the lateral cerebellum, depends on trial history including the type of saccade that is executed.

Purkinje cells in both medial and lateral cerebellum display sequential simple spike firing throughout the task

To further investigate the temporal response dynamics of the PCs in both regions during the saccade period, we plotted the normalized SS firing rate of all recorded neurons for pro- and antisaccade trials sorted by the time of their maximum response for both *facilitation* and *suppression* neurons (**Fig. 5a, b**). Close observation revealed a broad distribution of the peak responses of the individual PCs around saccade onset with each of them showing a preferred maximum response time. In both medial and lateral cerebellum, the timing of the occurrence of maximum firing rates were similar for pro- and antisaccade trials. We plotted the timing for all the neurons for pro and anti-saccades in each area and then compared for each neuron the timing of maximum response between pro and antisaccade (**Fig. 5c-f**). We did not observe significant difference between the mean peak response timings in the medial and lateral cerebellum (cells *facilitating* for both pro- and antisaccades in medial cerebellum versus those *facilitating* for both pro- and antisaccade in the lateral cerebellum $p = 0.3$; cells *suppressing* for both pro- and anti saccades in the medial cerebellum versus those of the lateral cerebellum $p = 0.1$; *facilitation* cells of the medial cerebellum during prosaccade trials versus those of the lateral cerebellum under the same condition $p = 0.15$; *facilitation* cells of the medial cerebellum during antisaccade trials versus those of the lateral cerebellum under the same condition $p = 0.9$; *suppression* cells of the medial cerebellum during prosaccade trials versus those of the lateral cerebellum under the same condition $p = 0.14$; and *suppression* cells of the medial cerebellum during antisaccade trials versus those of the lateral cerebellum under the same condition $p = 0.51$) (**Fig. 5e-f**).

To test if the measured time of the responses did not represent an observation by chance, we randomly drew 50% of the trials and calculated to what extent PCs conserve their position in the sequence following a 100 time repetition (**Supplementary Figure 4a** and **b**). We computed the cosine

similarity index between the patterns of SS maximum firing rates for all trials and compared it to the randomly resampled trials in four 75 ms time windows around saccade onset (two before and two after saccade onset; see **Methods** for details). Neurons with perfectly matched patterns would be assigned an index of "1", whereas no similarity between the sequences would be assigned a "0". We found that the time at which each PC fires maximally is quite robust with the mean similarity index for both pro- and antisaccades being higher in the 4th window after the saccade window in both the medial and lateral cerebellum (medial pro: w3 = 0.78 ± 0.12, w4 = 0.91 ± 0.05; medial anti: w3 = 0.51 ± 0.04, w4 = 0.93 ± 0.01; lateral pro: w3 = 0.91 ± 0.07, w4 = 0.93 ± 0.05; lateral anti: w3 = 0.74 ± 0.01, w4 = 0.88 ± 0.01 see **Supplementary Figure 4c** for example neuron with maximum response at the end of the window). These results indicate that PCs in both medial and lateral cerebellum have a preference to fire at specific times during the task and that this pattern is relatively well preserved across trials.

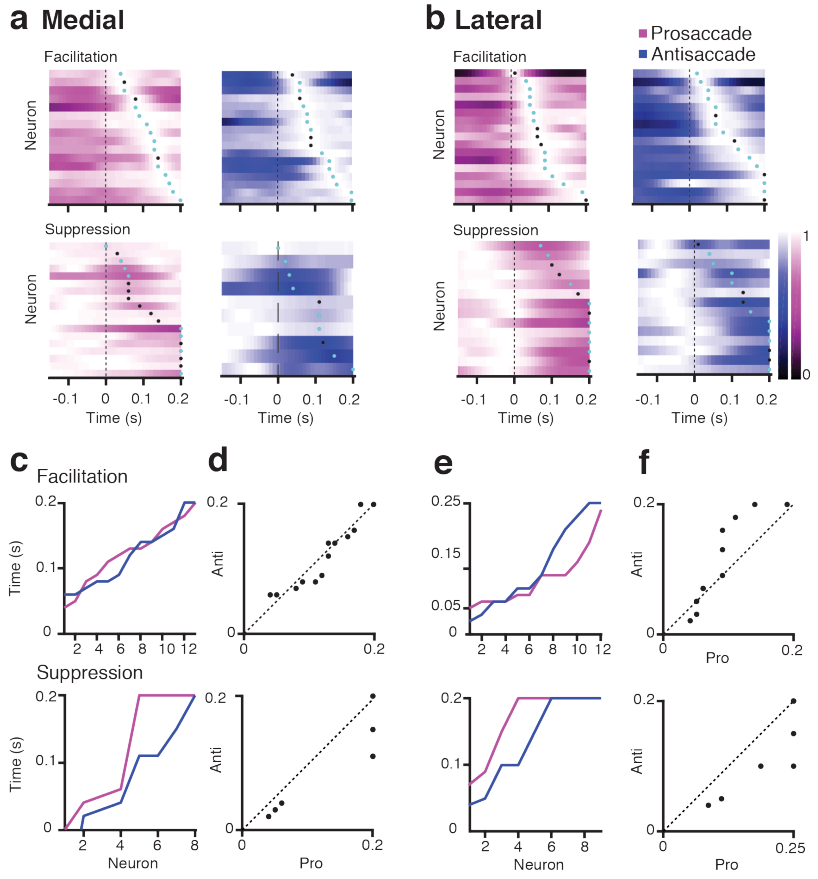

Figure 5. PCs discharge are temporally organized. a, top *Each row shows normalized mean SS responses for facilitation PCs in medial cerebellum aligned to saccade onset for pro- and antisaccade sorted by the time of the peak response. Dots depict the time of maximum response for each cell; cyan color denotes selected shared cells with significant activity in both pro- and antisaccades.* **bottom,** *same as top but now for suppression cells.* **b**, *Same as* **a** *for lateral cerebellum.* **c, top**, *Maximum firing rate times during the saccade period for pro- (magenta) and antisaccades (blue) for all facilitation neurons in the medial cerebellum.* **bottom,** *same as top for suppression neurons.* **d**, **top**, *Scatter plot of maximum firing rate times during the saccade period between pro- and antisaccades for facilitation neurons.* **bottom,** *same as top for suppression neurons.* **e** *and* **f**, *Same as c and d, but for lateral cerebellum.*

Complex spike responses of PCs in lateral cerebellum show most prominent directional tuning and reciprocal firing

In a subset of recorded PCs, we were able to reliably isolate and analyze CS responses throughout the recording (**Supplementary Table 1**). We restricted the CS analysis only to cells with average CS firing rates higher than 0.5 Hz over the duration of the complete recording and at least 5 trials per direction for both prosaccades and antisaccades. Similar to the SS analyses, we examined the CS responses separately in the medial and lateral cerebellum during the instruction and execution periods (**Fig. 6a-b**). The average CS activities during execution (1.11 Hz ± 0.50 s.d., n=11) and instruction (1.10 Hz ± 0.47 s.d., n=11) in the medial cerebellum were not significantly different from those in the lateral cerebellum (1.13 Hz ± 0.52 s.d., n=18 and 1.15 Hz ± 0.33 s.d., n=18, respectively, p = 0.36 and p = 0.87 for comparison medial versus lateral during execution and instruction, respectively).

The interaction between CS and SS responses was first quantified in the context of their directional preference during the execution period. Directional preference was determined by fitting a sinusoid to the CS and SS rates as a function of the direction of the saccade (**Fig. 6 c-f**). If the coefficient of determination (R^2) from the sinusoidal fit for CS responses was higher than 0.4, the cell was deemed directionally tuned and was included for further analyses (see **Methods**). **Figure 6c** shows the direction preference of an exemplary neuron recorded in the medial cerebellum. We shifted the peak CS direction to 0 degrees and plotted the corresponding SS responses for the same neurons in the same way. When we did this for all the selected PCs of the medial cerebellum that were included based on their sinusoidal fits (5/38 pro- and 4/38 antisaccades), there seemed to be no clear pattern of significant relations between CS and SS responses in the context of directional modulation (**Fig. 6d, Supplementary Table 3**). To test if CS and SS directional preferences are from the same population, we performed a Watson Williams test, a circular analog to the ANOVA, on the directional responses of PCs in the medial cerebellum during prosaccades. No difference could be detected between the preferred direction of SS and CS responses in the medial cerebellum for prosaccades (p = 0.12, n=5) (**Fig. 6g**, left). The same was the case during antisaccades (p = 0.91, n=4) (**Fig. 6g**, right). Possibly, these findings obtained in the medial cerebellum reflect the low number of cells, or that robust CS modulation in the OMV is triggered by errors while these are correct trials (Herzfeld et al., 2015; Sendhilnathan et al., 2020). Unfortunately, we did not have sufficient error trials for an analysis of those. In the lateral cerebellum, directional tuning was more prominent (**Fig. 6b, 6e-f,** and **6h**). In the lateral cerebellum 12 and 9 out of 40 PCs showed significant saccade direction-sensitive modulation for pro- and antisaccades, respectively. Compared to medial PCs, the preferred directions of the CS responses of PCs in the lateral cerebellum were relatively often opposite to those of the SS responses (see **Fig. 6e-f**, for single neuron and population data, respectively). When comparing the directional preferences of the CS and SS responses by means of a Williams-Watson test this difference did hold for both pro- and antisaccades (p = 0.0014, n=12 and p = 0.006, n=9, respectively) (**Fig. 6h**). Moreover, the vector averages of the CS and SS responses of PCs in the lateral cerebellum during prosaccades appeared opposite to those during antisaccades (**Fig. 6h**).

Next, we quantified the interaction between CS and SS responses during the instruction period (**Fig. 6a** and **b,** left panels). For every PC of both medial and lateral cerebellum with sufficient CS responses we calculated the maximum change in CS firing rate from baseline in the instruction window and the maximum change in SS firing rate from baseline in the 300 ms window around the

time of the peak CS rate. Similar to the execution period, this was done for the pro- and antisaccade trials separately. When calculating the Pearson correlation coefficients between the peak CS and associated SS responses for the PCs in the medial cerebellum, no significant correlation was found (R = 0.21, p = 0.54, for prosaccades; and R = 0.15, p = 0.67 for antisaccades; n = 11 for both). However, when we applied the same procedure to PCs of the lateral cerebellum, a significant negative correlation between CSs and SSs was found during the instruction period for prosaccade trials (R = -0.59, p = 0.01; n = 18), but not during antisaccade trials (R = -0.21, p = 0.41; n = 18). When we compared this reciprocity between the instruction and the saccade period, we observed that the cells in the lateral cerebellum that show reciprocity in the instruction period are the same ones that show reciprocity in the saccade period (**Supplementary Figure 5**). Together, the data obtained during the instruction and execution of pro- and antisaccades suggest that the reciprocal modulation of CS and SS activity of PCs in the lateral cerebellum is more prominent than that in the medial cerebellum.

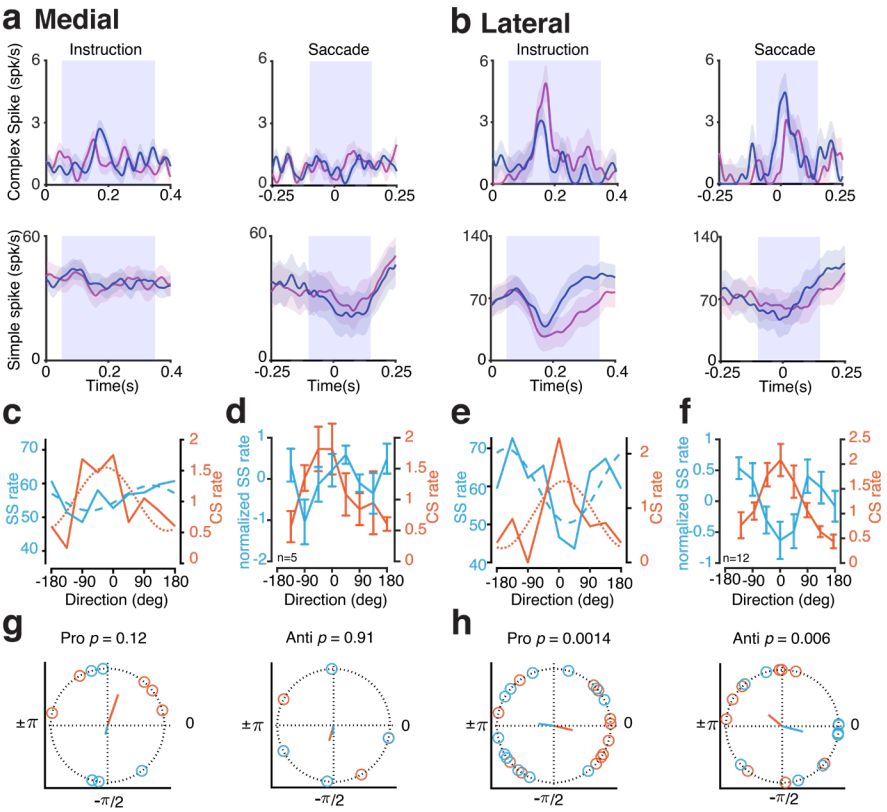

Figure 6. Complex spike and simple spike interaction during pro- and antisaccade trials. a, **top** *Average CS rate of PCs in medial cerebellum during prosaccades (magenta) and antisaccades (blue) aligned to the onset of the instruction (left) and execution (right) period. Bottom panels show the associated SS responses. Shaded areas represent s.e.m. rectangular patches indicate the windows* **b**, *Same as a, but for neurons recorded in the lateral cerebellum.* **c**, *Directional tuning of an example neuron recorded in the medial cerebellum for prosaccades. The direction of the peak CS response is set*

at 0 degrees; simple spikes are aligned to the direction of the peak CS response. Orange and blue lines show directional tuning for CS and SS, respectively. Dotted and dashed lines represent sinusoidal fits for the CS and SS response, respectively (CS: $R^2 = 0.5$, SS: $R^2 = 0.43$). **d***, Average CS (orange) response for all cells in the medial cerebellum during prosaccade trials. Peak CS set at 0 degrees in the same way as in panel c. Cells are included if the sinusoidal fit $R^2 > 0.4$. The corresponding SS responses of the same cells are indicated in blue. Error bars represent s.e.m.* **e***, Same as c, but for an exemplary cell in the lateral cerebellum (CS: $R^2 = 0.48$, SS: $R^2 = 0.53$).* **f***, Same as d, but for all included PCs of the lateral cerebellum.* **g***, Preferred directions of CS (orange) and SS (blue) responses of PCs in medial cerebellum according to the sinusoidal fits (same cells as in d); orange and blue lines represent vector averages. (P values from Watson Williams test between SS and CS direction preferences).* **h***, Same as g, but for lateral cerebellum. Note that the PCs in the lateral cerebellum show a more pronounced level of reciprocity.*

Facilitation and suppression Purkinje cells in medial and lateral cerebellum operate at different baseline frequencies

The presence of both *facilitating* and *suppressing* cells in both medial and lateral cerebellum indicates that the cells recorded here contain cells from both downbound and upbound modules (De Zeeuw, 2020). Given that downbound and upbound modules of PCs in the cerebellar cortex of rodents have been hypothesized to operate at a relatively high and low baseline SS firing frequency, respectively (De Zeeuw, 2020), we investigated whether the *suppression* and *facilitation* cells recorded here also differed in this respect. Cells were categorized as *suppressing* or *facilitating* based on their responses during the execution period (0-150 ms after saccade onset) to all trial types, pooling both pro- and antisaccades. This provides an estimate whether the cell's general preference is upbound or downbound. We then compared the baseline firing frequencies of these putative upbound and downbound units. It appears that *suppressive* cells started at a relatively high baseline SS firing frequency in both the medial and lateral cerebellum (62.43 ± 3.76 spks/s and 69.6 ± 6.12 spks/s, respectively), and that *facilitating* cells started at a significantly lower baseline SS firing frequency in both regions (56.36 ± 3.65 spks/s and 54.72 ± 3.76 spks/s, $p < 0.05$ for both; one-tailed Wilcoxon rank-sum test). In line with other saccade studies that focused on the medial cerebellum, these data imply that PCs of non-human primates, contain both upbound and downbound modulates (Sun et al., 2017; Herzfeld et al., 2018; Soetedjo et al., 2019).

3.3 Discussion

The antisaccade task has served to investigate hubs of flexible behavioral control and their interaction, where a correct suppression of a prosaccade followed by a response to the opposite direction forms a feature of executive control (Mokler and Fischer, 1999; Mitchell et al., 2002). We found evidence for cerebellar involvement in volitional control of this behavior in both medial (i.e., OMV) and lateral (i.e., crus I/II) cerebellum by recording the activity PCs during pro- and antisaccades in non-human primates. Our findings add to the growing literature of evidence pointing to an important contribution of the cerebellum to cognitive processes in general and voluntary behavior in particular. We demonstrated that PCs in both areas modulate their activity depending on the trial type, and that SS responses of populations of PCs in the lateral cerebellum are able to discriminate the type of trial. Even though the lateral cerebellum is not traditionally viewed as a saccade-control area, our

findings support early reports where saccades are elicited following electrical stimulation to lateral regions of the hemispheres, especially in crus I/II (Ron and Robinson, 1973).

Antisaccades exhibit saccade kinematic properties that differ from standard prosaccades, a result consistent with previous reports in human and non-human primates (Amador et al., 1998; Munoz and Everling, 2004). Even so, the preferential modulations of both SS and CS responses in the PCs were not highly correlated to any of those kinematic changes (**Supplementary Figure 1**). This suggests that the observed neuronal activity was not merely an efference copy of the motor command. Specifically, we argue that the observed activity during the instruction period reflects the preparatory or planning phase of the voluntary movement in which the PC firing is determined by the cue. This is in line with recent findings in cerebellar atrophy patients who show impairments when making goal-oriented movements (Piu et al., 2019).

Various parameters of PC activity differed between medial and lateral cerebellum. SS activity of PCs in the lateral cerebellum (1) showed a greater firing rate during the execution of saccades, (2) exhibited more prominent saccade-related signals at the population level, and (3) displayed more signal separation/selectivity for pro- and antisaccades during the instruction period. Likewise, their CS activity showed a higher level of reciprocity with respect to simple spike activity, during both the execution and instruction period. In contrast, PCs in the medial cerebellum were more sensitive to trial history, and those of the *suppression* category showed a relatively early SS modulation during execution of both pro- and antisaccades. Together, these data indicate that different modules of different cerebellar regions can both contribute to the same complex behaviour, yet with different propensities.

SS and CS modulation during instruction period

Studies of the eye movements from patients with cerebellar lesions suggest that the role of the cerebellum might not be in the initiation of saccades, but in the correct and accurate execution of them (Kornhuber, 1971; Thier et al., 2002). Our results indicate that PCs in lateral cerebellum receive information about the trial identity. Although only a small fraction of neurons in Crus I/II exhibited significantly different SS activity between both conditions, we showed that these contain sufficient information to distinguish a pro- from an antisaccade (**Fig. 3** and **Fig. 4**). This is in part supported by a previous study showing that the posterior part of the dentate nucleus fires more during the preparation of antisaccades and that local inactivation promotes more antisaccade errors (Kunimatsu et al., 2016). This instruction-related activity in antisaccade trials is thought to be relayed to the superior colliculus (SC) and related nuclei in the brainstem that are engaged in curtailing reflexive saccades (Everling et al., 1999b). Together with the existing data on the dentate nucleus and its downstream structures, the persistent SS modulation of PCs in the lateral cerebellum upon cue presentation during the instruction period suggests that they may maintain and update an internal model for well-timed activity during motor planning (Gao et al., 2018). This in turn suggests that this part of the cerebellum, through its projections to the prefrontal cortex, participates in optimizing not only the execution of saccades, but also the preparation thereof.

Correct decoding of a visual stimulus is an essential component of the pro- and antisaccade task. Visual responses in the cerebellum have been reported in several areas including the floccular complex, crus I/II and the inferior semilunar lobe (VII/VIII) (Marple-Horvat and Stein, 1990). Our results of PCs in the lateral cerebellum show direct CS signals timed to the onset of the visual cue

related to the correct execution of the subsequent pro- or antisaccade. Many cells in this region showed a CS drive during both the instruction and execution epoch, complementing the findings that their CS-SS reciprocity and simple spike modulation are also prominently spread throughout the task. Dentate nucleus neurons have activity bridging the period from task instructions to motor execution (Kunimatsu et al., 2016), which could be derived from the same population of PC's as we recorded in the lateral cerebellum. The results from our current study raise the possibility that CS responses play a similar role in decoding of visual stimuli for the preparation of ensuing movements.

Contemporary models of antisaccade decision-making require evidence accumulation to reach a decision boundary in the frontal cortex (Munoz and Everling, 2004). The PC's in the cerebellum receive an enormous amount of diverse sensory and motor information through their parallel fiber inputs, which may also facilitate efficient evidence accumulation. Classical models of cerebellar function dictate that PCs pick relevant parallel fiber inputs to drive SS firing through means of climbing fiber inputs, which cause plasticity at the parallel fiber to PC synapse (Gao et al., 2012). The PCs that we measured in the lateral cerebellum carry both SS and CS signals during the instruction period of the antisaccade task. We hypothesize that through the pre-learned associations of the right parallel fiber input based on the CS, relevant evidence from the stimulus (i.e., dot color in instruction) for the selection of the required action (i.e., pro- or antisaccade) can be rapidly relayed from the lateral cerebellum to the frontal saccade areas (e.g., SEF, FEF, DLPFC). In cerebellar patients, latencies for antisaccades are prolonged, indicating a less efficient decision-making process in absence of cerebellar input (Piu et al., 2019). When the decision is made in the cortical areas, projections from FEF to the SC and OMV of the medial cerebellum will generate a fast and accurate execution of the eye movement.

SS and CS modulation during saccade execution

Single PCs modulated their SS activity during the execution of pro- and antisaccades in both medial and lateral cerebellum, but only lateral cerebellar PCs were able to successfully discriminate the type of trial. Despite the heterogeneity of the responses, neurons that facilitated or suppressed their response after saccade onset exhibited differential activity during both conditions (**Fig. 3**). As a population, PC responses were different when executing a saccade towards a visible target than when using an internally generated goal. This is particularly interesting for two reasons: Firstly, the medial cerebellum has always been identified as a motor and timing controller for the different types of saccades, interacting with cortical and brainstem brain areas (McElligott and Keller, 1984; Noda and Fujikado, 1987; Thier and Möck, 2006), while the role of the lateral cerebellum in saccade control has remained under debate. Indeed, lesions to the lateral cerebellum can delay onsets of saccades between 10 and 60 ms and result in variable hypo- and hypermetria (Ohki et al., 2009), but the contribution of Purkinje cell activity in the lateral cerebellum to proactive control of saccades and flexible behavior in general has not been completely elucidated. Secondly, the differential cerebellar activity during antisaccades implies that it contains neural signatures to modulate preparation and execution by encoding information about the current context of the upcoming action (saccade), which is necessary for the fast classification of the response as correct or erroneous. This finding is in line with the impact of focal cerebellar lesions in humans on the changes in potentials observed during performance monitoring in an antisaccade task (Peterburs et al., 2012).

The CS responses in the medial cerebellum have been shown to encode errors in movement execution, enabling PCs to correct errors in subsequent movements by pruning SS responses (Catz

et al., 2008). Unlike prosaccades, the antisaccades do not have a visual target. Therefore, keeping them accurate is more challenging, which is displayed in the broader range of saccade amplitudes in **Figure 1**. Furthermore, antisaccade accuracy monitoring depends on internal estimates of saccade amplitudes, which could explain why adaptation of antisaccades poorly transfers to prosaccades (Cotti et al., 2009). Taking this into account it seems most likely that antisaccade amplitude is monitored upstream of the medial cerebellum (Lévy-Bencheton et al., 2013).

In line with other studies on CS responses of PCs in lateral cerebellum during visual pursuit, we found that they also modulate during saccades (Marple-Horvat and Stein, 1990). Similar to the SSs, their activity is modulated depending on the trial-type. In the saccade period, the CS activity in the lateral PCs shows direction selectivity similar to that observed in the medial cerebellum (Marple-Horvat and Stein, 1990). This implies that the saccade-related CS activity found in the lateral cerebellum is not only involved in the preparation of the motor response, but also in its execution. To what extent well-timed CS synchrony in the lateral cerebellum, which can contribute to coordination of complex movements (Welsh et al., 1995; Van Der Giessen et al., 2008), also contributes to the generation of pro- and antisaccades remains to be shown.

Cerebellar modules operate in parallel

The data on *suppression* PCs in the medial cerebellum showing a relatively late SS modulation during execution of both pro- and antisaccades as well as those on *facilitation* PCs in the lateral cerebellum showing a prominent modulation at the end of the instruction of antisaccades indicate that different modules of different cerebellar regions can simultaneously contribute to the same complex behaviour, yet with different particularities. A similar conclusion was drawn from a recent study on delay eyeblink conditioning (Wang et al., 2020b). Even though this form of conditioning is classically considered to be controlled solely by modules in lobule simplex of the lateral cerebellum (De Zeeuw, 2020), Wang and colleagues have shown that modules of the medial cerebellum are equally essential, yet also contributing in a slightly differential fashion, possibly regulating mainly muscle tone (Wang et al., 2020b). Interestingly, similar to the current pro- and antisaccade tasks, during eyeblink conditioning the medial and lateral cerebellum also both engage *facilitation* and *suppression* cells and they also operate at relatively low and high baseline firing frequencies, respectively (ten Brinke et al., 2015; Wang et al., 2020b). Our current finding that *facilitation* and *suppression* cells appear to play a more dominant role during the instruction and execution of the saccade task, respectively, further highlights the differential functional relevance of the upbound and downbound modules (De Zeeuw, 2020).

Previous reports of activity in the dentate nucleus, which is the main target of PCs in the lateral cerebellum, have shown mixed evidence regarding the direction of modulation during saccade-related behavior (Ashmore and Sommer, 2013; Kunimatsu et al., 2018). Kunimatsu and colleagues found only upward modulating units during self-initiated saccades (Kunimatsu et al., 2018), whereas Ashmore and Sommer revealed groups of both facilitating and suppressing cells during delayed saccades (Ashmore and Sommer, 2013). Possibly, these differences reflect differences in the behavioral paradigms and/or the different time windows analyzed. In our dataset, the modulation exhibited by PCs is bidirectional in both medial and lateral cerebellum with populations of both *facilitation* and *suppression* cells.

PC activity in both medial and lateral cerebellum displays stable time-ordered sequences

Sequence activation of neurons is a feature observed in different brain areas. Typically, neurons exhibit their maximum response at discrete time points during structured behaviors, often reflecting the connectivity of the network (Ikegaya et al., 2004; Harvey et al., 2012). This also holds for the cerebellum, where the sequences of activity may serve to enhance motor timing (Ten Brinke et al., 2017; Deverett et al., 2018; Gao et al., 2018). Here, we observed structured sequenced SS responses in both medial and lateral cerebellum during both types of saccades. These sequences could be interpreted as a mechanism to control the timing of eye movements, including their duration and the moment of their peak amplitude. Lesions of medial and lateral cerebellum are in line with this notion (Ohki et al., 2009). In addition, these sequences could represent a distributed computational resource to aid in saccade execution. To test this hypothesis future experiments need to perform PC recordings while the monkeys learn the pro- and antisaccade task to observe the formation of sequences during the training of the task (Sendhilnathan et al., 2020).

In this study we investigated how Purkinje cells of the medial and lateral cerebellum contribute to the planning and execution of pro- and antisaccades. We report clear differences in SS responses to pro- and antisaccades in the lateral cerebellum on both population and single cell level around the time of the saccade, but in the medial cerebellum these are limited to the single cell level and less frequent. Moreover, the lateral cerebellum displayed striking bridging of activity between the instruction and saccade epoch, thereby highlighting its role in connecting the saccade planning and execution processes. Finally, the interplay between CS and SS responses in a direction selective manner implies reciprocity between these responses, the direction of which is a defining feature of whether a module learns in an upbound or downbound fashion.

3.4 Methods

Animals

All procedures complied with the NIH Guide for the Care and Use of Laboratory Animals (National Institutes of Health, Bethesda, Maryland), and were approved by the institutional animal care and use committee of the Royal Netherlands Academy of Arts and Sciences. Two adult male rhesus non-human primates (Macaca mulatta), Mi and Mo, were used in this study.

Surgical procedures

Animals were prepared for eye movement and awake, extracellular single unit recordings in the cerebellum using surgical and electrophysiological techniques in a two-step procedure (Roelfsema et al., 2012). Under general anesthesia induced with ketamine (15 mg/kg, i.m.) and maintained under intubation by ventilating with a mixture of 70% N2O and 30% O2, supplemented with 0.8% isoflurane, fentanyl (0.005 mg/kg, i.v.), and midazolam (0.5 mg/kg • h, i.v.), we first implanted a titanium head holder to painlessly immobilize the monkey's head. Four months later, once the monkeys had mastered the behavioral task (see below), a custom-made 40 mm chamber was implanted under the same anesthesia conditions as described above to gain access to the cerebellum with a 25 angle (**Fig. 1b**). Animals recovered for at least 21 days before training was resumed.

Behavioral task

Animals were trained to perform a randomized interleaving pro- and antisaccade task in 8 different directions (cardinal and diagonal directions), with amplitudes between 5 and 14 (**Fig. 1a**). All recordings were conducted with the monkey in complete darkness. During training and experiments, monkeys were seated in a primate chair (Crist Instrument, USA) with their head restrained at 100 cm from a screen with a resolution of 1,024 x 768 pixels. Visual stimuli were presented by a CRT-Projector Marquee 9500 LC (VDC Display Systems, Florida, USA) with a refresh rate of 100 Hz. Binocular vision was unrestricted. A trial started when the monkey fixated on a red or green fixation point at the center of the screen for a random time between 300-500 ms. Next, a red target appeared in one of 8 different target locations. After 100 ms the fixation point changed to gray and the monkey had to perform either a prosaccade toward the target (when fixation point was red) or antisaccade in the opposite direction with the same amplitude as the target, (when fixation point was green) within 500 ms. Colors of fixation point and target were changed to blue and magenta in the figures to accommodate colorblind readers.

The animals received liquid reward if they performed a correct saccade (within 6 of the (anti-)target) and maintained fixation for 100 ms. Within a single block the 8 (targets) * 2 (pro/anti) possible configurations were presented in a random order.

Recordings

Position of the right eye was recorded with an infrared video-based eye tracker (iViewX Hi-Speed Primate, SMI GmbH, Germany) at a sampling rate of 350 Hz. The eye tracker was calibrated before every recording session by having the animal look at 1˚ target grid consisting of 9 points (one at the center of the screen and 8 points 10˚ apart) to adjust offset of X and Y position by hand. Pre and post-surgical MRI-images were used to build a 3D model of the skull and cerebellum for anatomical localization of cerebellar oculomotor vermis (lobules VI and VII) and lateral cerebellum (crus I/II, **Fig.1b**, Saleem and Logothetis, 2006). Single-unit recordings were obtained using tungsten glass-coated electrodes (1-2 MΩ, Alpha Omega Engineering, Nazareth, Israel) through a 23-gauge guide tube, which was inserted only through the dura. A motorized microdriver (Alpha Omega Engineering, Nazareth, Israel) with a 1-mm spaced grid was used to introduce the electrode and map the recording sites with a maximum resolution of 0.25 mm.

Extracellular recordings were digitized and sampled at 44 kHz and subsequently stored during the experiment using a Multi-Channel Processor (Alpha Omega Engineering, Nazareth, Israel). Single units were determined to be a Purkinje cell by the presence of spontaneous firing of simple spikes (SS) and complex spikes (CS) as well as the presence of a concurrent short pause in SS firing following a CS (i.e. climbing fiber pause; see De Zeeuw et al., 2011), as discriminated online using Multi-Spike Detector (MSD, Alpha Omega Engineering). The discovery of a saccade-related site was often guided by the modulating multi- unit signals generated by granule cells during saccades. Trial history, horizontal and vertical eye position and electrophysiological data were concurrently stored for offline analysis.

Data Analysis Software

All analyses were performed off-line using custom programs written in Matlab (The Mathworks,

Natick, MA, USA).

Eye movement analysis

Eye position was sampled at 350 Hz with an infrared video eye tracker which tracked the pupil center of mass. Noise was reduced using a finite impulse response filter and a savitzky-golay filter (20 ms window). Eye velocity and acceleration traces were created by differentiating the signal. Eye acceleration was further processed using a median filter. Saccade onset and offset were detected using an adaptive threshold based on 6 s.d. of the noise during fixation from the recording session of that day as described in Nyström and Holmqvist (2010). Trials with reaction times less than 80 ms were excluded, as these were thought to represent anticipatory actions.

Electrophysiological analysis and statistics: Simple spikes

In order to perform statistical analysis, neurons were required to have at least 10 recorded trials per direction. Note that only correct trials and saccade-related neurons were incorporated in the analyses. This was due to the fact that both monkey Mo and Mi exhibited an expert level performance reaching >90% correct responses. Therefore, we lacked statistical power to analyze the incorrect trials. A neuron was considered to be saccade-related when SS firing during the baseline period, defined as a window 400 to 50 ms before trial onset in the intertrial interval was significantly different from the saccade execution period activity defined to be 150 ms after saccade onset (Wilcoxon rank test; $p < 0.05$) for at least one of the 8 directions. We then computed the instantaneous SS firing rate of the neurons using a continuous spike density function (SDF) generated by convoluting the spike train with a Gaussian function of $\sigma = 50$ ms width and averaging all the individual spike density functions (Silverman, 1986, Dash et al., 2013). We compared the number of spikes for all pro- and antisaccade trials of each PC using a Kolmogorov-Smirnov test which determined if the activity of a PC was significantly different between a pro- and antisaccade with a p value <0.05. The characteristics of the saccade-related activity, as previously reported in PC recordings, was quite heterogeneous. On that account, we categorized the PCs if their activity increased after instruction or saccade onset as *facilitation*, or decreased as *suppression*. For the instruction period, we compared the mean firing rate of each cell from a window 400 ms before instruction onset to a period of 300 ms at the end of the instruction period. For the saccade period we compared the mean firing rate of each cell from a window 150 ms before saccade onset to a window from saccade onset to 150 ms after saccade onset (Wilcoxon signed rank, p value of < 0.05). To determine the correlation between kinematic parameters and neuronal activity we determined Pearson's correlation coefficient (r) for all neurons in the two tasks. Modulation ratio for both areas was obtained by computing the ratio between the response during pro- and antisaccades.

Change in firing rate during the instruction period was computed by taking the difference between the mean firing rate during the baseline period separate for pro- and antisaccade trials. For the saccade period, we compared the mean activity 150 ms before the saccade onset to a period 150 ms after saccade onset.

To compare the dynamics in the temporal responses of PCs, we trial-averaged the responses during the saccade period, normalized and sorted the activity of each PC by their maximum response. To test that the time of the responses was not an observation by chance, we randomly picked 50%

of the trials, and plotted their maximum firing rate times. We repeated this procedure 100 times. To test whether the neurons change substantially their maximum firing location, we classified their position as 1 or 0 if they fired maximally in one of 4 windows around saccade onset: -150 to -75 ms, -75 to 0 ms, 0 to 75 ms, 75 to 150 ms (**Supplementary Figure 3**). Similarity index between all and redrawn trials maximum location times was computed by estimating the cosine similarity between strings of binary classification patterns (B_i and B_j) obtained by comparing two windows at a time (all trials v.s. randomly drawn). Similarity index:. Identical classification patterns have an index of 1.

To test how well a single PC can discriminate between a pro- or antisaccade we computed a binomial proportion test over time. This will show if a PC contains information about the trial condition and the time points at which the discrimination is more pronounced. We first computed the probability of a spike in every trial in every condition in bins of 10 ms. Then, we computed a binomial proportion test: , where and is the probability of a spike in a pro- and antisaccade respectively: , is the number of trials in prosaccades and is the number of trials of antisaccade trials.

To test if the identity of previous trials had an effect on the current trial (*n*), we computed the absolute difference in SS between the current trial *n* and one previous trial (*n*-1) or two previous trials (*n*-2). We first identified all correct trials where all possible combinations presented in at least 10 repetitions and computed the absolute difference in SS activity for all cells in medial and lateral cerebellum (Kruskall-Wallis test).

Electrophysiological analysis and statistics: Complex spikes

Cells were included into the analysis for complex spikes if they had a CS firing rate of between 0.5 and 2 hz over the entire recording session and at least 5 trials for every of the 8 pro and antisaccade directions. To determine if the CS modatuled to the one of the task epochs we calculated the baseline firing rate ± 3 standard deviations. Baseline firing was considered a period of 500 ms of inter-trial activity. When the CS rate exceeded this upper or lower limit during either the instruction or the saccade window (50 - 350 ms after onset of the instruction and -150 to +150 ms around the onset of the saccade) the unit was considered as modulating.

To determine if cells had any directional modulation a sinusoid was fitted on the SS and CS firing rate in the saccade window as a function of the direction using formula: . When fitting, b was fixed at 1 so that only one period was fitted. The phase shift found as c was used in **figure 6g,h** to compare preferred directions. If the R^2 of the sinusoidal fit for was higher than cutoff value 0.4 the cell was deemed direction-selective. To avoid constraining the analysis too much, we included the cells in further analysis of directional reciprocity if the cell had CS directional selectivity. Cells were aligned to their preferred CS direction and the Pearson correlation coefficients were calculated to determine if there was directionally dependent reciprocity between SS and CS rates in the different groups of cells. Lastly to determine if there was a difference between CS and SS directionality the Watson Williams test was used on the unaligned CS and SS directions to determine if they were from different groups.

Acknowledgements

We thank Kor Brandsma and Anneke Ditewig for their excellent biotechnical assistance; Beerend Winkelman for providing the Matlab code for spike sorting; Chris van der Togt for providing assistance with stimulus presentation; Mario Negrello for providing the Matlab code for saccade detection; Geert Springeling, Peter Thier, Peter W. Dicke, Ruud Smith for their help with anatomical scans and 3D model building; and Kaushik J. Lakshminarasimhan for helpful comments in the analysis. This research was supported by FP7-C7 European Commission, the Marie Curie Initial Training Network ITN-GA-2009-238214, Van Raamsdonk Fonds, ZonMw, Netherlands Organization for Scientific Research, European Research Council (Advanced Grant, and Proof of Concept Grant), Medical NeuroDelta Programme, Topsector Life Sciences & Health (Innovative Neurotechnology for Society or INTENSE), and the Albinism Vriendenfonds Netherlands Institute for Neuroscience.

Author contributions

CIDZ, AB, MF, NAF and EA designed the study and analysis. EA and PR performed surgeries on the animals. EA and NAF executed the experiments and EA, NAF, AB and PJH analysed the data. EA, NAF, AB and CIDZ wrote the first draft. All authors edited the manuscript.

Competing interests

The authors declare no competing interests.

Data and code availability

The data that support the findings of this study and code for analysis of in vivo eye movement and Purkinje cell recordings are available from the corresponding author upon reasonable request.

3.5 Supplementary data

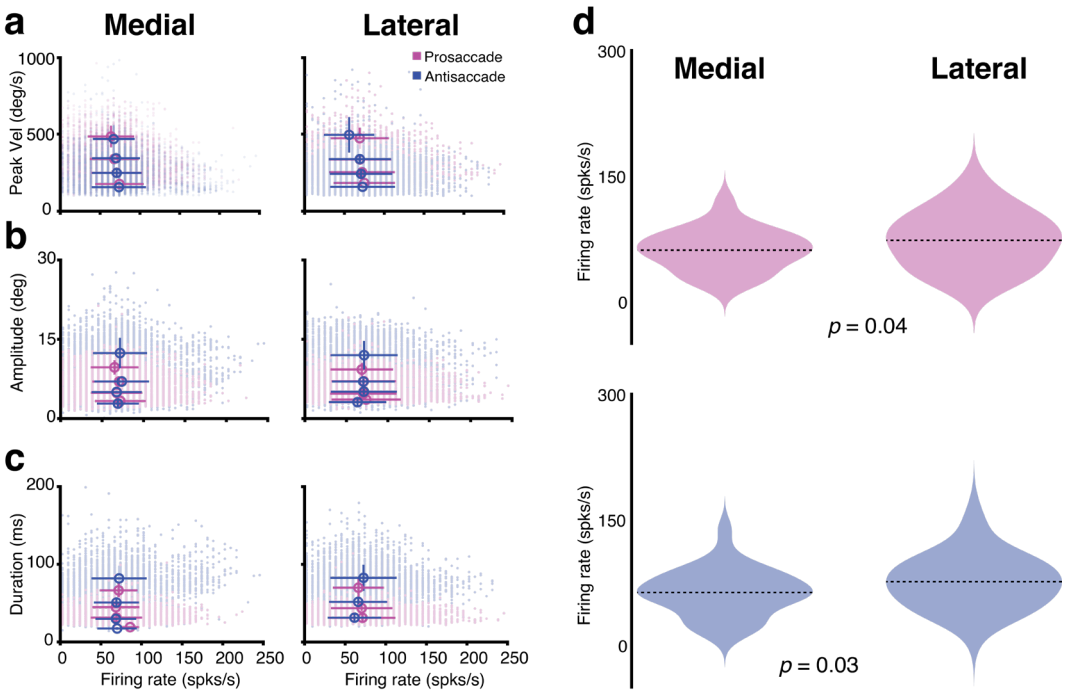

Supplementary Figure 1. PCs in medial (left) and lateral cerebellum (right) modulate similarly with saccade parameters, but fire differently during pro and antisaccades. **a**, *Amplitude (deg).* **b**, *Peak velocity.* **c**, *Duration for all saccades (correct and incorrect) plotted against simple spike firing rates for all trials in pro- (magenta) and antisaccades (blue). Open circles show the firing rate mean and s.d. for 4 different predetermined blocks in each saccade kinematics: (a) 4, 6, 8, and >8 deg, (b) 200, 300, 400, and >400 deg/s, (c) 20, 40, 60, and >60 ms. Pearson correlations for medial cerebellum: Amplitude pro- r = -0.05, anti- r = 0.04; duration pro- r = 0.007, anti- r = 0.14; and peak velocity pro- r = 0.11, anti- r = -0.08. Pearson correlations for crus-I/II: Amplitude pro- r = 0.01, anti- r = -0.04; duration pro- r = 0.005, anti- r = -0.05; and peak velocity pro- r = -0.01, anti- r = -0.03. Error bars denote s.e.m.* **d**, *Violin plots show the mean average firing rate for all cells during prosaccades (top) and antisaccades (bottom) for medial (left) and lateral (right) cerebellum. Dashed lines depict the mean value for the population. The p values in the figure are for a Wilcoxon rank sum test for each condition comparison between medial vs lateral.*

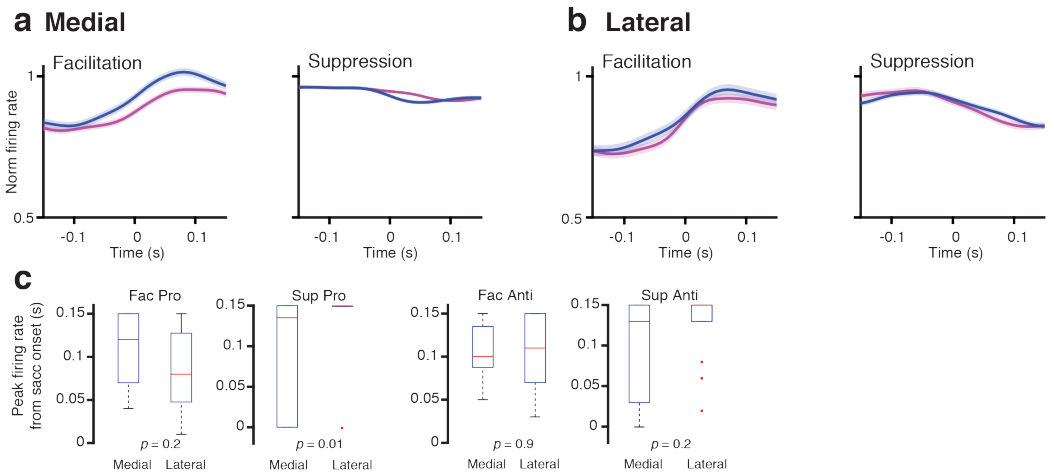

Supplementary Figure 2. Time-course of responses for different types of activity. a, *Time-course of response averaged for all neurons in the medial cerebellum that either increased their firing during both conditions (facilitation) or decreased it (suppression) after the instruction onset. Shaded regions denote s.e.m.* **b**, *Same as* **a** *for lateral cerebellum. c) Time of peak responses separate by the type of activity exhibited by PCs in medial and lateral cerebellum.*

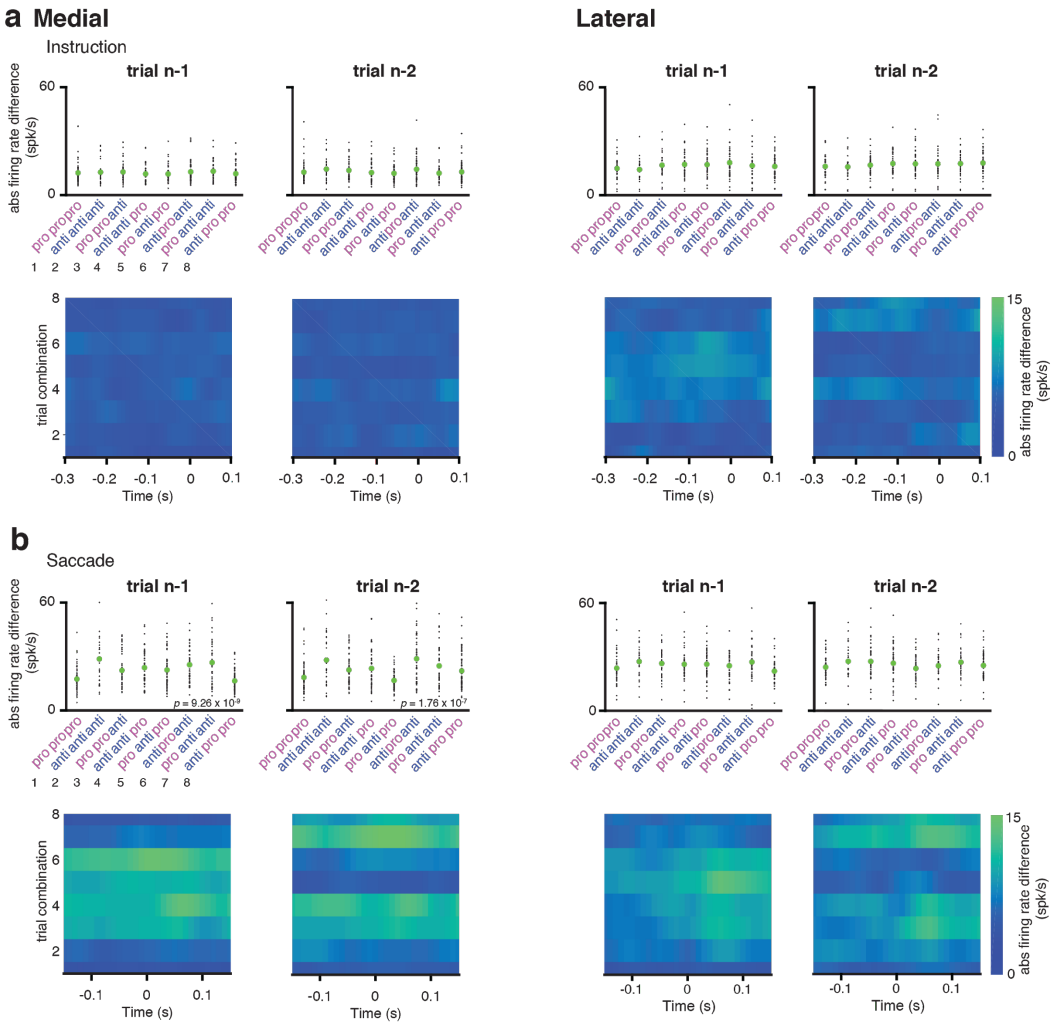

Supplementary Figure 3. Trial history modulates PC activity of medial cerebellum during execution (i.e., saccade) period. a top, *Absolute difference in spiking activity during the instruction period for trial n compared to one trial back (trial n -1) and two trials back (trial n -2) for all cells in medial (n = 81; left) and lateral cerebellum (n = 68; right). Green dots depict mean activity. Inset shows p-value for a Kruskal-Wallis test.* **a bottom,** *Heat maps show absolute firing difference estimated between the PSTH in trial n and trial n-1 and n-2 for every combination.* **b,** *Same as (a) for the saccade period.*

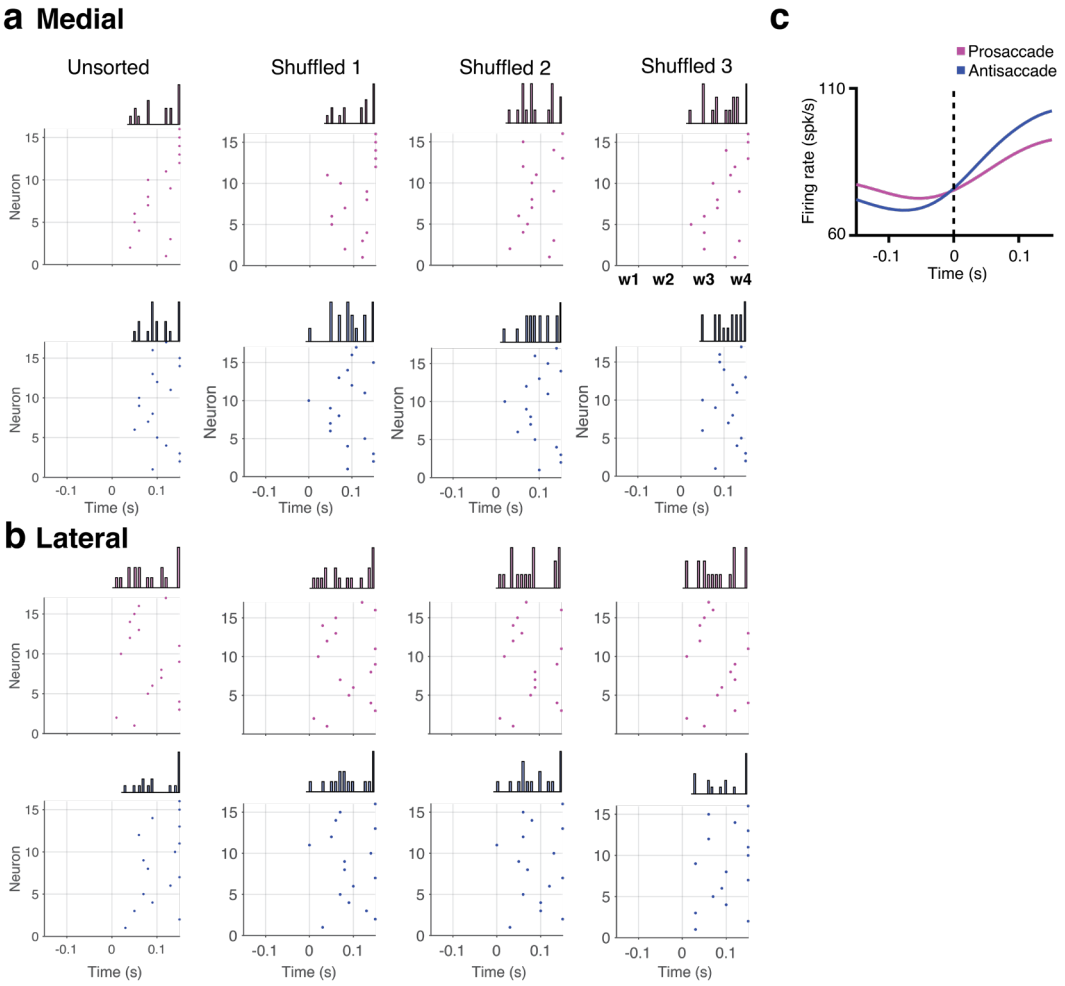

Supplementary Figure 4. PC maximum responses are stable across trials. a, *Leftmost panel shows unsorted maximum response time for all medial cells including all trials. Rest of the panels were calculated by shuffling the order of the trials and selecting only 50% of them.* **b**, *Same as (a) for lateral cerebellum.* **c**, *One example cell from lateral cerebellum showing maximum responses at the end of the saccade window.*

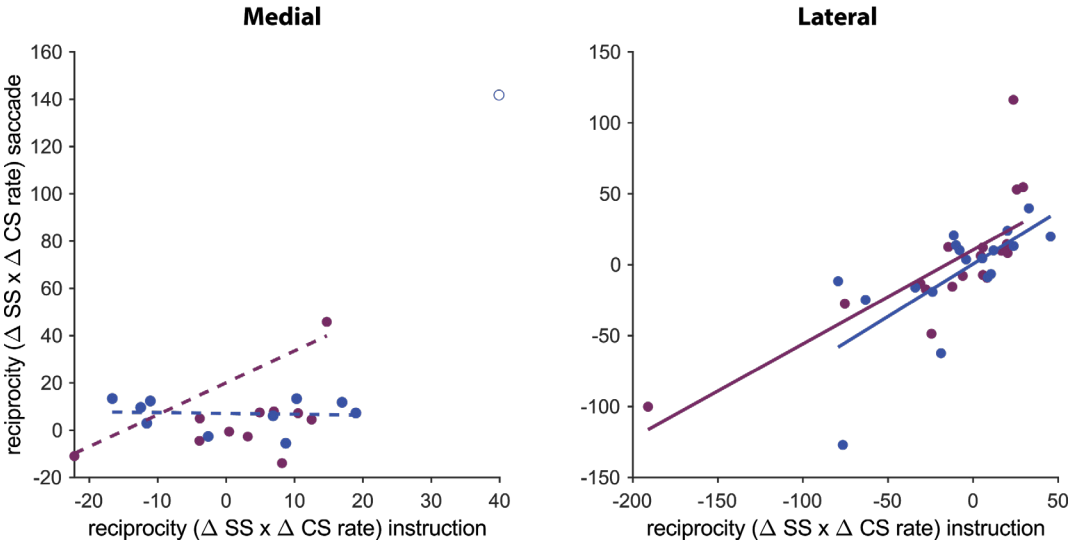

Supplementary Figure 5. Shared reciprocity between instruction period and saccade period. *To quantify the reciprocity between CS and SS responses the maximum change in CS firing rate in the windows of interest (instruction and saccade) were calculated. Subsequently, the associated maximum change in SS rate in a window of 300 ms around the peak CS rate was found. To quantify the reciprocity, we calculated the product (Δ CS rate x Δ SS rate). If there is a positive modulation of CS and negative modulation of SS and thus reciprocity this will give a negative value. If both CS and SS have positive modulation and thus no reciprocity this will give a positive value. Every dot represents one cell. One outlier was removed from the medial anti-saccade group because it changed the coefficient of determination from R^2 = 0.44 to R^2=0.01 when removing the outlier, indicating that the whole association depended on that one value. For other coefficients of determination see table below.*

	R^2
Medial pro	0.30
Medial anti	0.01
Lateral pro	0.59
Lateral anti	0.48

		Medial		Lateral	
		pro	anti	pro	anti
Simple spikes	Firing rate	61.4 (± 22.6)	62.9 (± 24.7)	68 (± 30)	69.3 (± 31.3)
	# trials	75 (± 49) 6801	71 (± 47) 6431	80 (± 52) 5784	76 (± 50) 5471
	# cells	90		72	
Complex spikes	Firing rate	1.08 (± 0.55)	1.11 (± 0.48)	0.91 (± 0.23)	0.92 (± 0.22)
	# trials	192(± 187) 2114	127(± 93) 1401	120(± 38) 2343	112(± 39) 2213
	# cells	11		18	

Supplementary Table 1. Summary of quantitative statistics of total population of neurons describing average firing rate of all neurons during the saccade period (Methods), number of trials per cell and grand total of trials, and number of cells per category. *Complex spike responses were only analyzed if the cell's CS firing rates was between 0.5 and 2.5 Hz over the entire recording and at least 5 correct trials were recorded per direction (8 pro direction and 8 anti directions).*

All		Execution period		Instruction period
		All	Selected	Selected
Medial (n = 90)	Facilitation	Pro 37 (˜41%) Anti 40 (˜44%)	Pro 16 (˜18%) Anti 17 (˜19%)	Pro 9 (10%) Anti 10 (˜11%)
	Suppression	Pro 53 (˜59%) Anti 50 (˜56%)	Pro 18 (˜20%) Anti 10 (˜11%)	Pro 10 (˜11%) Anti 6 (˜7%)
Lateral (n = 72)	Facilitation	Pro 37 (˜51%) Anti 34 (˜48%)	Pro 17 (˜23%) Anti 16 (˜22%)	Pro 12 (˜17%) Anti 13 (˜18%)
	Suppression	Pro 35 (˜49%) Anti 38 (˜52%)	Pro 14 (˜20%) Anti 14 (˜20%)	Pro 10 (˜14%) Anti 11 (˜15%)

Supplementary Table 2. Quantification of SS activity profiles in medial and lateral cerebellum. *PCs were classified into two groups based on whether their activity during execution (left columns) or instruction (right columns) increased (Facilitation) or decreased (Suppression) its neural activity (for definitions of time windows, see* **Methods***). A cell could have a significant suppression activity for antisaccades but not for prosaccades. Columns indicated by "Selected" show the number of cells for which the modulation was significant, not the total number of cells.*

		Medial cerebellum 40 cells	Lateral cerebellum 38 cells
SS directionaliry	**prosacade trials only**	10 (˜25%)	9 (˜24%)
	antisaccade trials only	6(˜15%)	9 (˜24%)
	pro- and antisaccade	9 (˜23%)	13 (˜34%)
	no modulation	15 (˜38%)	7 (˜18%)
	total cells	40 (100%)	38 (100%)
		11 cells	**18 cells**
CS directionallirty	**prosacade trials only**	3 (27%)	4 (˜22%)
	antisaccade trials only	3(˜18%)	1 (˜6%)
	pro- and antisaccade	2 (˜18%)	8 (˜44%)
	no directionality	4 (˜36%)	5 (˜28%)
	total cells	**11 (100%)**	**18 (100%)**

Supplementary Table 3. Neuronal populations with directional preference for saccades split between SSs and CSs. *A sinusoidal was fitted to the firing frequency in the saccade window. If the R^2 of the fit was higher than 0.4 it was deemed significant. Inclusion criteria CS are the same as the previous table. Cells were only included if SS responses were on average over the whole between 15 and 170 hz and at least 5 correct trials were available per direction (8 pro directions and 8 anti directions).*

Chapter 4:

Dentate nucleus neurons in rhesus macaques dynamically modulate their activity throughout a complex behavioral task

Nico A. Flierman[1,2], Bastiaan van Hoogstraten[2], Aleksandra Badura[2*], and Chris I De Zeeuw[1,2*]

Author affiliations:

[1]Netherlands Institute for Neuroscience, Amsterdam, The Netherlands.

[2]Department of Neuroscience, Erasmus MC, Rotterdam, The Netherlands.

* These authors contributed equally to this work.

4.0 Abstract

Cerebellar activity has historically been measured during a performance of relatively uncomplicated motor tasks studying one effector. In recent years various lines of research have shown cerebellar neurons contribute to a wide variety of cognitively challenging behaviors. To study the cerebellar contribution to complex behaviors we recorded extracellular activity of cerebellar dentate neurons in two non-human primates (NHPs) performing a visual covert attention task. Specifically, we trained the NHPs to perform a task in which they had to read the direction of a peripheral visual stimulus, while maintaining fixation at the center of the visual field. Following a delay period, the animals reported the perceived direction by performing a saccade eye movement to the direction-relevant target. Correct trials were rewarded. We found that neurons in the dentate nucleus modulated strongly over the entire time course of the task, often bridging different trial events that were temporally separated. The cells can respond in a movement or visually direction-selective manner almost a second before an upcoming saccade. In addition, they also often respond to reward or the absence thereof. The task related activity of these neurons was highly restricted to the recording region. Retrograde labeling of afferents to the recording location indicates that these cells receive inputs from Purkinje cells in the D1 region of the cerebellar cortex and the principal nucleus of the inferior olive. This cerebellar module is known to connect to the frontal eye fields, supporting the idea that this area might contribute to the planning of saccades and possibly the deployment of covert attention shifts. Together, our results highlight that neurons in the dentate nucleus can dynamically modulate their activity during a complex task, comprising sensorimotor as well as cognitive components.

4.1 Introduction

The cerebellum performs a wide variety of visual sensorimotor functions, such as planned and compensatory eye movements or movement perception (Ivry and Diener, 1991; Kunimatsu et al., 2016; Inoshita and Hirano, 2018). Accumulating evidence over the last few decades have implicated involvement of the lateral hemispheres of the cerebellum in cognitive visual functions (Courchesne et al., 1994; Nicolson et al., 2001; Baier et al., 2010; Voogd et al., 2012; Brissenden et al., 2016). The different ways in which the cerebellum uses visual information to guide these functions are slowly starting to become clear. Covert spatial attention is an example of this, which causes biases in perception of behaviorally relevant stimuli in the periphery of the visual field, in the absence of overt eye movements. The brain accomplishes this by providing stimuli that are covertly attended to with enhanced weight in the visual processing stream (Moore et al., 2003). This behavior has been extensively used in the context of neocortical attention networks (for review see (Moore and Zirnsak, 2017)). Cerebellar involvement in the regulation of this task has been less extensively studied. Human fMRI studies found activation in the lateral hemispheres during a covert attention tasks that required participants to eyes fixated at a central target, and thus did not require eye movements (Allen, 1997; Baier et al., 2014; Brissenden et al., 2016, 2018; van Es et al., 2019). The voxels that are activated during a multiple object tracking covert attention task are functionally connected with the dorsal attention network (DAN) in the cerebrum, implying that this region of the cerebellum is an integral part of the DAN (Brissenden et al., 2016, 2018). Moreover, patients with developmental disorders or lesions of the lateral cerebellum exhibit visual attention impairments (Townsend et al., 1996b; Bosse et al., 2007; Baier et al., 2010).

Covert attention is a function that is advantageous for visual goal directed behavior and thus the acquisition of a reward. Reward related modulation has been demonstrated throughout the cerebellar circuit, from reward expectation being encoded in granule cells, to signaling of reward magnitudes relayed onto Purkinje cells (PC) by climbing fibers (Wagner et al., 2017; Larry et al., 2019). In fact, reward signals are represented throughout the whole brain. Reward representation is also found in different cortical regions varying from high level cortical areas to the primary visual cortex, where the neural response to a stimulus can be persistently enhanced when it is repetitively associated with a reward (Henschke et al., 2020). Visual scenes usually contain considerably more information than the visual system can process. Therefore, saccades are made to align the fovea, the region of the retina with highest visual acuity, and also the largest representation in the visual cortex, with the target of interest. Because of this it is critical to plan saccades in an efficient way. A great deal of neuroimaging evidence exists that implies that mechanisms of covert attention overlap with those that control the programming of saccades (Corbetta et al., 1998; Nobre et al., 2000). This is collectively called the ''premotor theory of attention'' and proposes that the same circuit that is used for generating movements, is also active during attention shifts (Rizzolatti et al., 1987). More recent work shows that visual cells in the frontal eye fields (FEF) respond to covert attention but not to saccades, implying that there is cell type specificity for responses to covert attention (Gregoriou et al., 2012). Nevertheless, there is a strong relation between the oculomotor system and spatial attention, which is demonstrated through the observation that the spatial location of exogenous, i.e., bottom up, covert attention stimuli is restricted by the position of the eye, since it is not possible to plan a saccade or move spatial attention outside the range of the oculomotor system (Craighero et al., 2004; Hanning and Deubel, 2020). Although neural control of control of eye movements by the cerebellum is an established field, its contribution to visual attention still remains elusive.

Activity in Purkinje cells of the lateral cerebellum bridges the time between the onset of a visual stimulus and the execution of a saccade, showing the convergence of visual and motor information onto these cells (**Chapter 3**). The cerebellum also contributes to planning of saccades, however, the exact mechanisms of this is still an active topic of research with many open questions. Planning of saccades is not achieved solely by the cerebellum, but rather in collaboration with other motor areas of the brains such as, FEF, lateral intraparietal area (LIP), superior colliculus, and the basal ganglia (Tanaka, 2006; Wardak et al., 2011; Gao et al., 2018; Kunimatsu et al., 2018; Scerra et al., 2019). Dentate nucleus (DN) neurons have been shown to incorporate delay activity in firing rates related to saccade contexts, such as memory guided or self-timed saccades (Ashmore and Sommer, 2013). This type of activity could be indicative of motor preparation. According to Svoboda and Li (2018) motor preparation should include the following three characteristics: First, activity modulation must precede movement onset; second, activity must be selective for movement specifics, such as direction; and third, the activity must predict aspects of the upcoming movement execution, such as velocity.

In this work we studied the activity of single units in the DN during a complex, peripheral Landolt C saccade task. The task comprised the following consecutive components: 1) reading of visual information, 2) planning of a saccade that depends on the visual information, 3) executing the saccade, and 4) receiving a reward depending on the correctness of the repons. We hypothesized that DN neurons would display activity during several of these four different epochs, so as to facilitate efficient task performance. Indeed, we found that neurons modulated their activity during all these epochs, often bridging multiple conditions. Furthermore, we provided anatomical evidence that these cells are connected to the FEF, a classical attention and saccade planning center in the neocortex.

4.2 Results

Task description and behavioral performance

Two rhesus macaques (Mo and Mi) were trained to perform a peripheral Landolt C task, during which single-unit recordings of 304 cells in the left DN were made (**Fig. 1A**). **Table 1** provides an overview of the properties of the neuronal population. We trained our monkeys to perform a covert attention task (Ignashchenkova et al., 2004). We used this task to assess how DN cells encode complex behavioral cues, preparatory motor activity, and reward. **Figure 1B** shows an example trial with all trial variables and durations. In short, the animals had to maintain central fixation throughout the trial as long as the fixation dot remained red (**Fig. 1B**, first sequence panel 1-6). First a cue was presented near the central fixation point to hint at the position of the upcoming target, which had been shown to improve task performance (Ignashchenkova et al., 2004). After a 500 ms pause, the C-target was presented in one of 4 directions called the *stimulus location* for the duration of 250 ms (**Fig. 1C,** left panel). The animals had to perceive the direction of the gap of the C, which was always perpendicular to the stimulus location, further referred to as the *action direction* (e.g., up or down when the stimulus location is to the right, or left or right if the stimulus location is up or down), without breaking fixation on the central point. In the example depicted in **Figure 1**, the stimulus is presented on the right and the gap points downwards. Therefore, the correct response is a downward saccade, which is then rewarded (**Fig. 1C**, right panel). After presentation the stimulus was masked for 100 ms to prevent retinal afterimages which could inform the animal of the gap-

direction. After a delay period (500 - 700 ms) in which the animals had to remember the correct *action direction*, two saccade targets at the same eccentricity but perpendicular to the C direction were shown. The correct saccade target was the same location as the gap direction and the other was presented as a distractor. If the animals made a saccade within 500 ms after the target onset, they received a juice reward. At the first correct trial the animal received 150 ms of juice, with each consecutive correct trial the amount of reward was increased by 50 ms until a maximum of 450 ms was reached. This strategy was introduced to motivate the animal to maintain consistent performance. The bonus was reset to 150 ms when an incorrect saccade target was chosen or when the animal would break fixation during the first part of the trial. DN neurons were recorded after the animals reached an above-chance performance level (60%, **Table 1**). An example trial with the corresponding neural activity is shown in **Figure 1D**; here the animal maintained fixation until the choice was presented, after which he made a saccade. During the presentation of the stimulus the DN cells responded with an action potential burst followed by a pause around the time of the saccade. This pattern was consistently observed in correctly executed trials (**Fig. 1E**, bottom panel, colors represent stimulus location, same cell as cell 2 in **Fig. 2**).

During acquisition of the data, we observed that many neurons continued the modulation of their firing until after the saccade (**Fig. 2**). Therefore, we also included reward omissions (10% of trials) and random rewards (10% of trials). Moreover, a camera was added to track the oro-facial behavior, specifically licking, during task performance.

	Mo	Mi
Neurons recorded	160	144
Avg. Firing rate	44 (±23) Hz	58 (±27) Hz
Avg. Trials per cell	132 (±108)	154 (±110)
% correct responses	86 (± 0.06)%	63 (±0.05)%
Neurons recorded with reward manipulations (random reward + omission)	125	67
Neurons recorded with video data	53	67

Table 1. *Overview of the properties of the recorded neurons. Variance is one SD.*

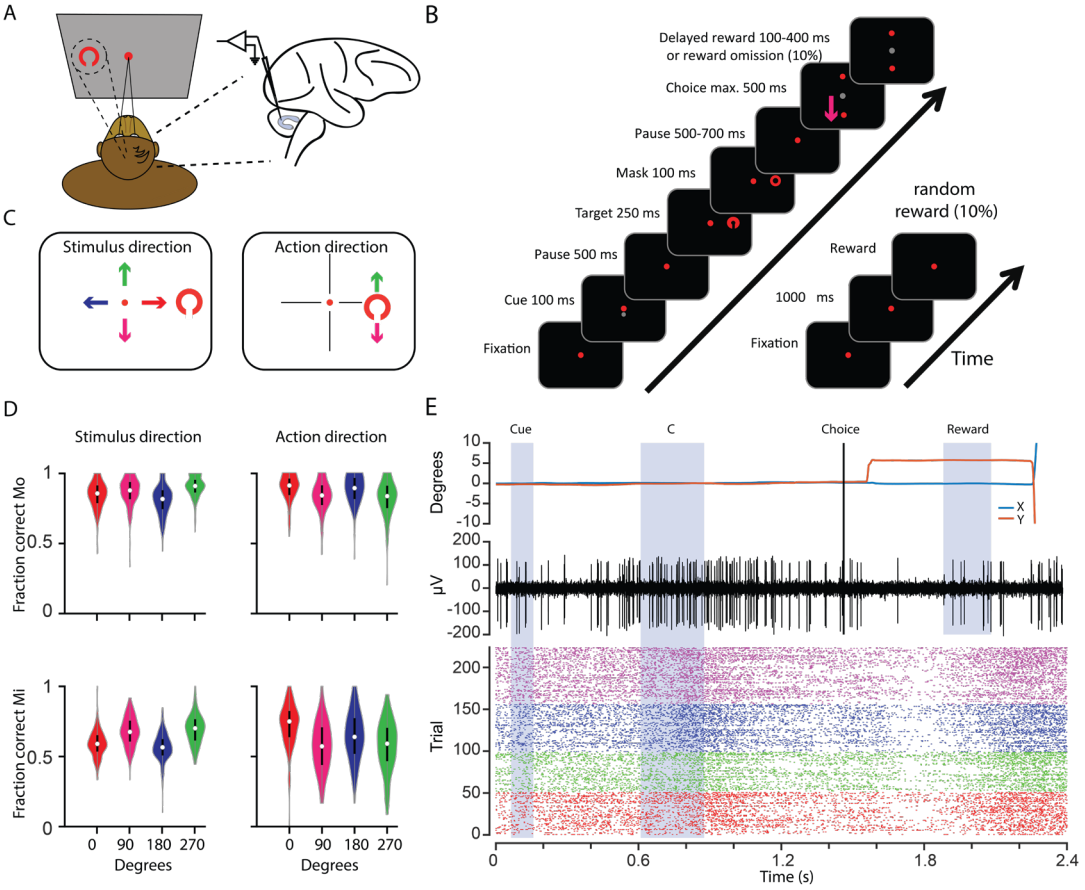

Figure 1. Overview of task variables, behavior and recordings. *A) Schematic drawing of the recording setup B) Step by step explanation of what the animal sees when performing the task. Left, regular and reward omission trials. Right, random reward trials. C) Explanation of the two forms of directionality in every trial. Left, the stimulus location, presented at ''Target 250 ms'' in B, represents the direction of the stimulus relative to the fixation point. Right, the action direction represents the direction of the gap of the Landolt C presented at ''Target 250 ms'' in B, this gap is always perpendicular to the stimulus location. The animal has to memorize the action direction so that at ''Choice max. 500 ms'' in B it can make a saccade, the action, to the target that is in the same direction as the gap. In this example that would be a downward saccade. D) Violin plot of task performance expressed as fraction of correct responses, based on the average during recording sessions. Split between animal, top/bottom plots, and form of directionality, left/right plots. Gray dot at the center indicates the median, black bar around it the interquartile range i.e. 50% of the distribution. E). Example recording of a neuron recorded in monkey Mo. Top panel shows eye position throughout the trial, shadings represent when a certain task event is taking place. Choice and reward are not continued downward in the bottom panel because they are at different times in the trials. Middle panel shows extracellular recording of a DN neuron that bursts in action potentials after the C stimulus and pauses after the saccade. This neuron is the same as ''Cell 2'' in* **Figure 2**. *Bottom panel shows a raster plot where every dot represents a spike. Trials are sorted and color-coded with colors representing the stimulus location of the trials.*

Neuronal responses are diverse and multimodal

The recorded population of DN neurons' action potential trains showed widely varying patterns of activity when the animal performed the Landolt C task (**Fig. 2**). Onset of activity modulation could be time locked to all epochs of the trial, e.g. some became active after the cue (Cell 1), at the onset of the stimulus (cell 2, 4 and 5) or at the offset of the stimulus (cell 3). The time between the onset of the stimulus and the saccade onset varied but averaged at ~1 second (**Fig. 1D**), therefore the plots aligned to C-onset and saccade onset show some overlap. Some cells displayed bursts of activity at the onset of the stimulus, and subsequently pause after the saccade (cell 1, 2, 3, and 5) or vice versa (cell 4). In most cells of the population activity was modulated throughout the trial, rather than only at a specific epoch, indicating the diverse multimodal character of these cells.

Modulation was determined based on a 200 ms sliding window moving in 100 ms steps. This method was used in two epochs, the stimulus epoch 0 - 800 ms after stimulus onset, and in the saccade epoch -200 to 200 ms after saccade onset (**Fig. 2** cell 5, black horizontal bars). Many cells remained active in some pattern until at least the saccade and even longer (**Fig. 2** cell 1, 2, 3, 4, 5). We classified cells as persistently active if more than half of the sliding windows are significant (see methods for details). There was a substantial overlap in the different epochs in which the population of neurons was active for every category (**Fig. 3A**). Peak responses were sorted for pausing cells and bursting cells, and aligned to time of peak response. Distributions of peak responses were different between cells and strongly distributed in time (**Fig. 3B, C**). We used a Kolmogorov-Smirnov (KS) test to assess if the population of peak timings for burst and pausing cells came from the same distribution. This was not the case for peak responses during the stimulus epoch, where pauses occurred earlier than bursts ($p<0.01$, KS test, **Fig. 3D**). During the saccade epoch the distribution of timing of bursts and pause was the same ($p = 0.24$, KS test, **Fig. 3E**).

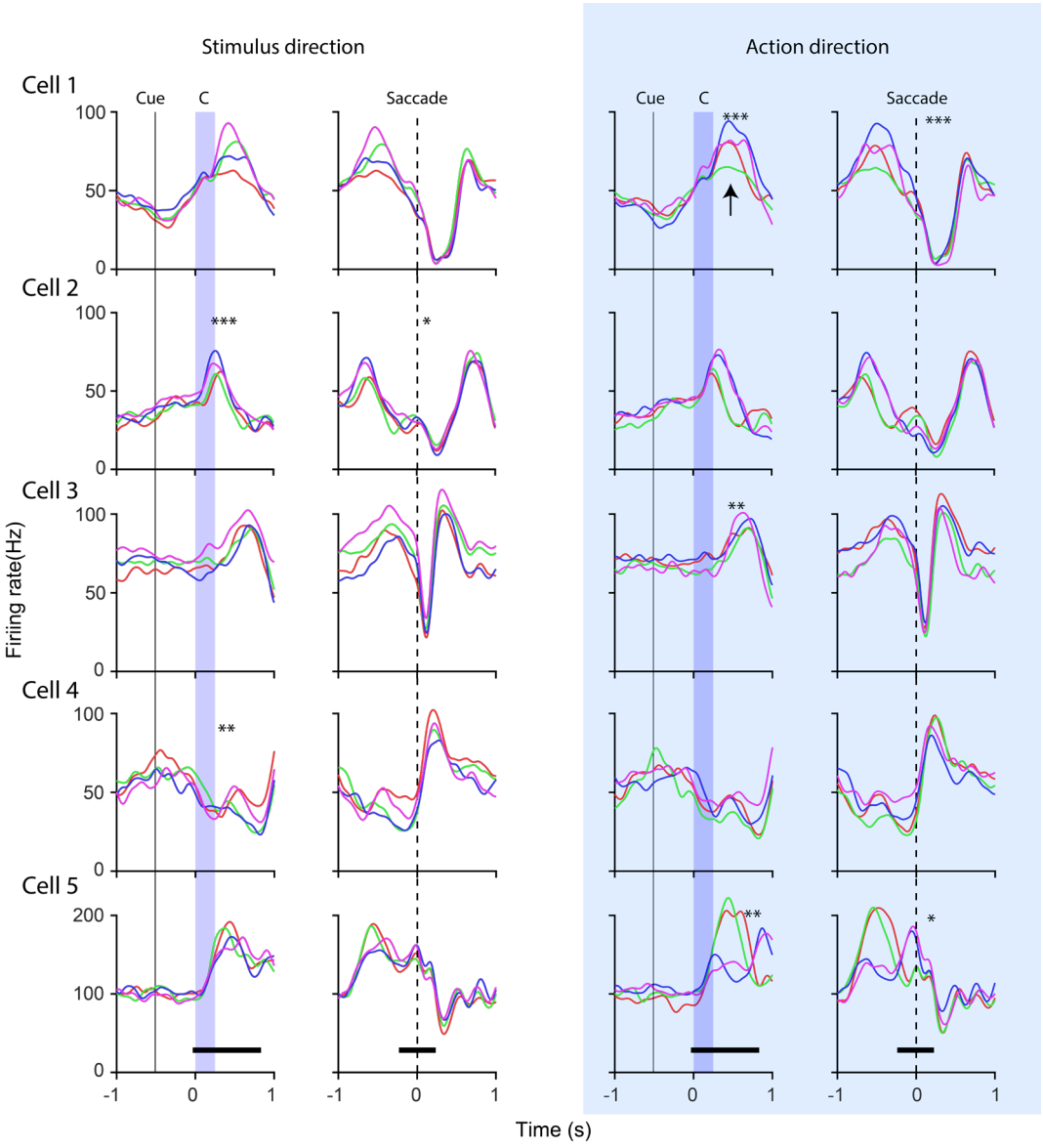

Figure 2. Examples of variability in firing rate modulation of individual DN cells. *DN neurons modulate their activity throughout the whole trial. Some cells show modulation preferences based on either the stimulus location (left two columns) or the action direction (right two columns, light blue shading). Colors represent either the stimulus location or action direction as in* **Fig. 1C**. *Black horizontal bars set in cell 5 represent the stimulus and the saccade epoch, during which direction selectivity was tested. Asterisks represent significance of direction selectivity based ANOVA; for details see methods. Black arrow indicates the time at which the variance between the firing rates for different directions is greatest. This point is the center of the window for ANOVA test for directional selectivity*

(see Methods).

Every trial has both a stimulus location and the action direction (**Fig. 1C**), sorting trials per directions can thus result in *two* possibilities for direction-selectivity. Since the action direction is always perpendicular to the stimulus location, these are inherently correlated and thus it can be expected that cells appear selective for both directions. We considered the direction sorting that showed the largest variance in firing rate between the different trial types as the preferred sorting, i.e., preferred stimulus location selectivity or preferred action direction-selectivity (see Methods for details, **Fig. 2**, cell 1 black arrow). The preferred direction sorting was determined independently in both the stimulus epoch and the saccade epoch. For every cell we found the time point of the maximum variance between the directions, and determined whether the cells preferred the stimulus or action direction sorting. **Figure 3F** shows a histogram with the time points of the maximum variance for the action and stimulus location preference in the recorded cells. Cells with directional preference for the stimulus location displayed their selectivity early, close to the presentation of the stimulus on average 370 ms (± 190 ms 1 SD unless specified otherwise, N = 47) after the onset presentation of the stimulus. Action direction preferring cells on the other hand had the maximum variance in firing rates closer to the saccade onset, 505 ms (± 171 ms, N = 88) after the presentation of the stimulus. These distributions were significantly different ($p < 0.001$, *t*-test). The same analysis was performed during the saccade period (**Fig. 3H**). From the distributions it can directly be observed that there was a larger fraction of the cells that preferred the stimulus location in the stimulus epoch (47/135, 35%) than in the saccade epoch (17/103, 17%, $p = 0.0016$, Chi^2 test). The mean timing of the maximum variance in firing rates from the onset of the saccade was -35 ms (± 128 ms 1 SD, N = 17) for stimulus location preferring cells, and 9 ms (± 109 ms, N = 86) for action direction preferring cells ($p = 0.15$, *t*-test, **Fig. 3H**). The timing of stimulus location and action direction preferring cells was also split between bursting and pausing cells, however no difference in timing of modulation could be detected (**Supplementary Figure 1**).

Preferred direction was determined for every cell as the direction of strongest modulation in both the stimulus and saccade epoch (See methods). These were split again between the cells that were selective for stimulus location and action direction (**Fig. 3G**). First, we tested if cells had circular uniformly distributed directional preferences. We found that during the stimulus presentation the stimulus location preferring cells clearly tended to have vertical preferences and action direction preferring cells horizontal for the stimulus and action direction respectively ($p = 2.96 * 10^{-5}$, and $p = 1.74 * 10^{-7}$ Omnibus test, **Fig. 3G**). The directional preference for stimulus location cells was different from that of the action direction cells during the stimulus presentation period ($p = 0.0097$, Watson-Williams test).

The same procedure was repeated for the saccade period. The stimulus location preferring cells had uniformly distributed directional preference, although more cells prefer upward or leftward directions. This might be explained by the relatively small sample size of this group ($p = 0.11$, Omnibus test, **Fig. 3I**, Left panel). Although they visually seem to be more evenly distributed, the action direction preferring cells were not uniformly distributed over all directions ($p = 1.3 * 10^{-6}$, Omnibus test, **Fig. 3I**, right panel). These groups did not have different overall directionality ($p = 0.78$, Watson-Williams test).

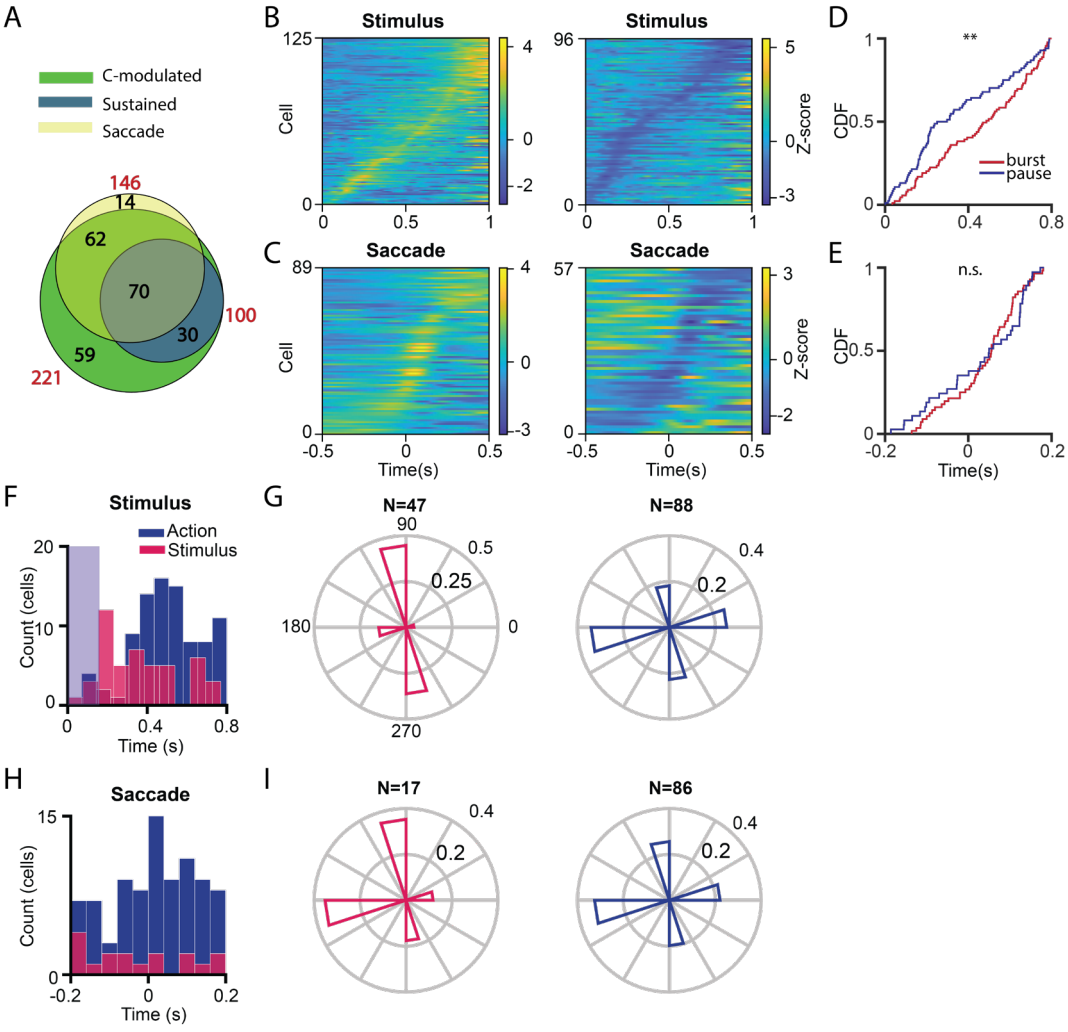

Figure 3. Distribution of modulation properties of DN neurons during peripheral Landolt C task. *A) Venn diagram showing the number of modulated neurons for every task epoch (red numbers). The sustained categories indicate that activity modulation in these cells bridges the stimulus and saccade epoch. Number of neurons for every subcategory is stated in black. B) Z-score of firing rates of bursting and pausing cells (left and right respectively) during the stimulus epoch (''C-modulated'' category in A). The time is relative to onset of the Landolt C. C) Same as B but for ''Saccade'' cells in A. The time is relative to saccade onset. D) Distribution of timing of peak responses of neuronal modulation of cells shown in B. Split between bursting and pausing cells. Asterisks indicate that these peak timings come from two different distributions KS test (see text for details). E) same as D but for timing of peak modulation in the saccade epoch. F) Histogram of the timing of peak variance in firing rates for different directions (black arrow in* **Figure 2***) split between cells that have a preferred direction for the action direction or the stimulus location. G) Normalized polar histogram of preferred directions of*

cells that preferred the stimulus location *(left) or the action direction (right). H) same as F for direction preference during saccade epoch. I) same as G for cells with direction preference during the saccade epoch.*

Together our results show a large diversity in neuronal responses in relation to the stimulus location and action direction. We found that the timing of responses was different for bursting and pausing cells during the stimulus epoch, but not during the saccade epoch. Furthermore, the timing was also related to the preference of direction sorting for stimulus location or action direction. In conclusion, the recorded cells were highly sensitive to all parameters of the task.

DCN cells also modulated during reward

DCN activity modulated long after the saccade, well into the period in which the animal received the reward (**Fig. 2**). To investigate if this activity is truly reward related, we added task manipulations and a video camera to track licking during reward delivery (**Fig. 1B**). On the basis of these manipulations, we made two main classifications of reward related neurons: sensory reward cells and reward expectation cells. Sensory reward cells were active when animals received a reward but not necessarily expected it, such as during trial and random reward, but not during reward omission (**Fig. 4A**). Reward expectation cells were active when a reward was expected, regardless of whether the reward was received, i.e., active during rewarded trials and reward omission but not during random rewards (**Fig. 4B**). It should be noted that the two example neurons shown in **Figure 4 A-B** follow the expected activity pattern in incorrect trials: the sensory neuron is not active, and the expectation neuron is active (**Supplementary Figure 2**). Since incorrect trials were not included for the classification of these cells, we do not know whether or when the animals become aware that they made an error. Reward modulation was determined in the same way as stimulus and saccade modulation, with a 100ms step sliding window 0 - 500 ms after reward onset, or 500 ms after the saccade in the case of reward omissions. Cells were only included if there were at least 5 trials in every category, 117/120 cells with video data met these criteria.

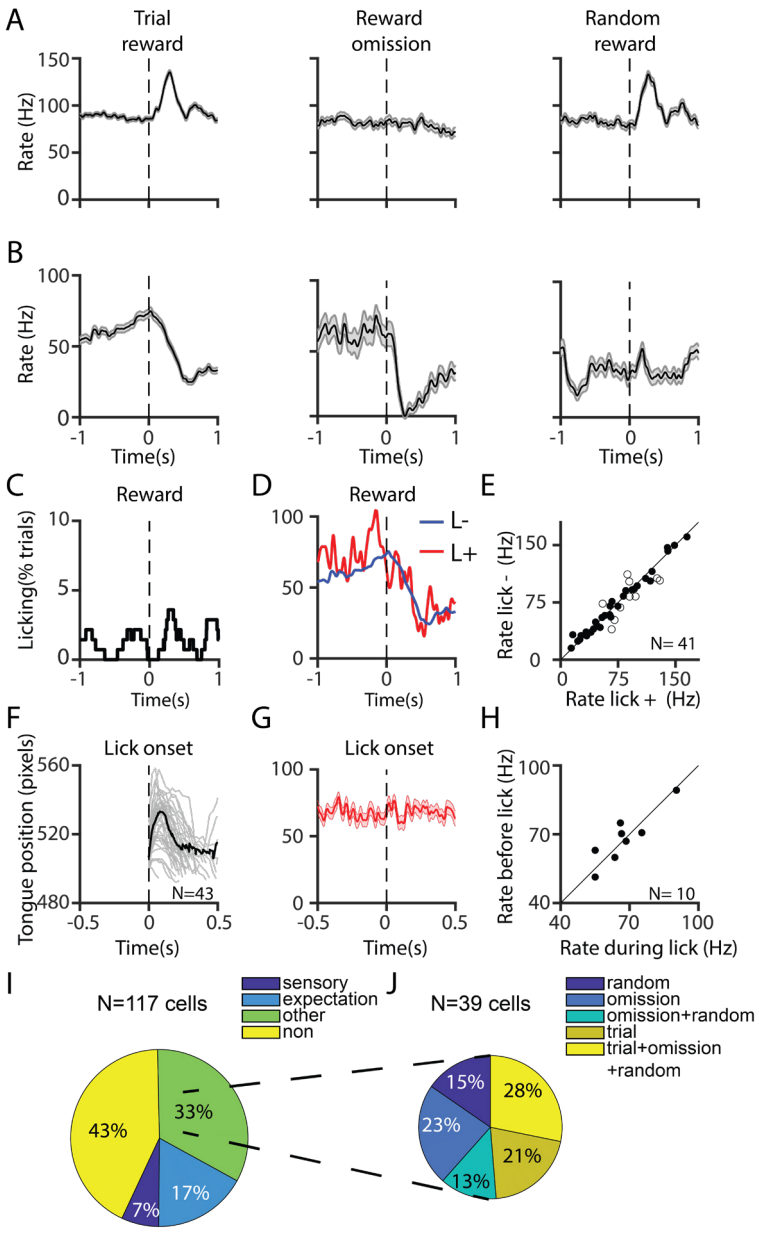

Figure 4. Reward associated modulation of DN neurons. *A) Example of bursting neurons with a pattern of activity that is indicative of reward sensation (modulating for trial and random rewards, not modulating for reward omissions, shaded area is SEM, for criteria of modulation see methods). B) Example of pausing neurons with a pattern of activity that is indicative of reward expectation (modulating for trial rewards and reward omission, not modulating for random reward rewards). C) Distribution of licking behavior around the reward. D) Average firing rate in trials with and without*

licking during the reward presentation. E) Average firing rate around the reward when there is licking during the reward window (Rate lick +) or no licking during the reward window (Rate lick -). Every dot represents one neuron, open dots are neurons where the firing rates are significantly different. For solid dots there is no significant difference. F) Example tongue movements during the recording of one neuron aligned to lick onset (grey traces) and average of all licks (black trace). G) Associated average firing rate during the licking behavior of the same cell as shown in F. H) Average firing rate before and during the lick of the cells that had significant modulation in E (open dots). Solid dots represent no significant difference, open dots represent significant differences in firing rate. I) Overview of the recorded population's responses to the different reward modulation categories. J). Overview for which types of trials the cells in the category ''Other'' shown in I modulated.

Animals showed licking behavior during the trials (**Fig. 4C**). To make sure that the reward related modulation that we observed was not due to the motor command for licking, which is represented in the cerebellum, we tested if these cells showed any lick related modulation during the reward window (Bryant et al., 2010). Mo licked during the reward window on 9% (± 15%) and Mi on 13 % (± 17%) of trials. **Fig4 D** Shows the firing rate of the cell in B during trials where the animal licks and during trials where it does not lick. Since there were a lot less trials where the animal licked, the average rate for licking trials was noisier, but showed the same modulation pattern. To quantify if the population of cells modulated their firing rate when there was licking during the reward window, we compared the firing rate in that window (0-500 ms after reward onset) for trials with licking to that without licking. 10/41 cells did seem to have different firing rates between licking and not licking trials (t-test, alpha = 0.05, open circles in **Fig. 4E**). Since trials with licking in the reward window were rarer than trials without licking, these cells could contain false positives. To further investigate if these cells were really modulated by licking, we identified lick events throughout the whole recording, thus not limiting the analysis to the reward window. We then aligned the lick events to lick onset (**Fig. 4F**) and compared the firing rate in a window of 500 ms before the lick with the firing rate in a window of 500 ms from the onset of the lick (**Fig. 4G**). None of the 10 earlier seemingly lick-related cells had a significantly different firing rate before the lick vs during the lick (**Fig. 4H**, black dots are not significant; t-test, alpha= 0.05). From this we concluded that activity of the population was not modulated by licking.

We found a diverse population of reward modulated neurons of which 7% percent modulated in a sensory fashion, 17% in a reward expecting fashion and 33% (**Fig. 4I**). The cells were classified in the other category if they had significant modulation in the reward window of at least of the three trial types (normal trial, reward omission and random reward). **Figure 4J** shows the different combinations of trial types that the cells can modulate for. Taken together, a large part of the population shows reward related activity.

DCN cells are highly multimodal

The subset of cells that was also recorded with video data allows for a summary of modulation types. Similarly to **Figure 3A**, where high multimodality was found between saccade and stimulus epoch modulating neurons, we now found the same when including cells that modulated for the reward conditions (reward sensation and reward expectation). Only 8/28 exclusively modulated for reward, the remaining cells either modulated during the stimulus, the saccade, or the reward epoch, or during any combination of these three (**Fig. 5**). These findings illustrate the high degree of multimodality that these cells possess and shed new light on how the lateral cerebellum encodes higher order functions.

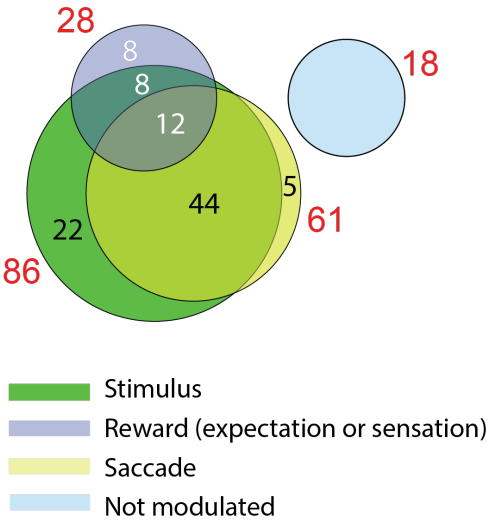

Figure 5. **Summary of cell categories.** *Colors indicate the task epochs in which the cells were significantly modulated. Red numbers represent the total number of cells indicated in the legend at the bottom. Black and white numbers indicate the individual categories.*

Anatomy of the network

After the electrophysiological experiments were finished, cholera toxin subunit B (CtB) as a retrograde tracer and BDA10k as an anterograde tracer were injected at the recording hotspots in the left DN. For now only CtB in monkey Mi has been stained, **Figure 6A** shows the injection spot at the lateral tip of the DN. Retrograde labeling of PCs could be detected in the cerebellar cortex' D1 zone (**Fig. 6A,B**). Moreover, labeling could also be found in the ventral lamina of the contralateral principal olive, corresponding with the D1 zone (Voogd et al., 2012) (**Fig. 6C,D**). Further analysis of the anterograde tracer will hopefully elucidate the thalamic nuclei with which this structure communicates.

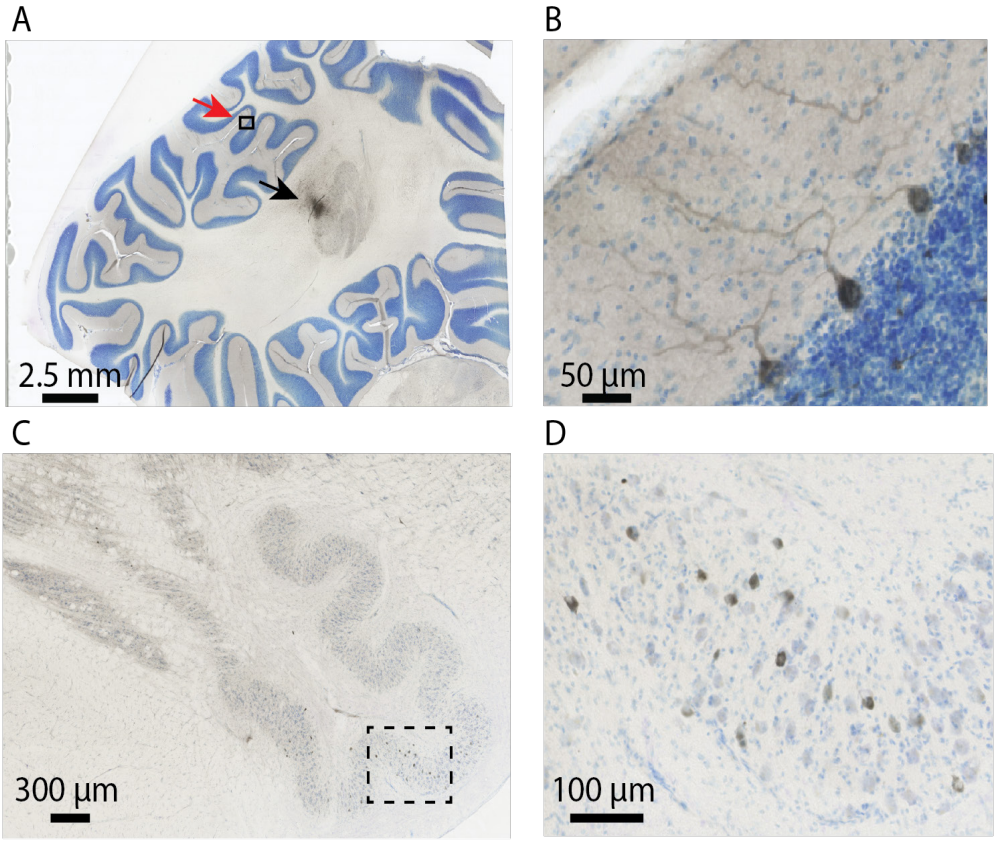

Figure 6. **Retrograde tracing with CtB of recorded DN cells.** *A) Coronal section of the cerebellum of monkey Mi showing the DN and cerebellar cortex (blue). Black arrow points at the Injections spot where CtB was stained with DAB. Red arrow points at the magnification shown in B. B) Magnification of retrogradely labeled purkinje cells in the D1 zone. C) Coronal section showing the ventral lamelle of the principal nucleus of the inferior olive, dashed box is magnified in D. D) magnification of retrogradely labeled IO cells.*

4.3 Discussion

Slowly but surely, the visual functions of the lateral cerebellum are becoming apparent. Primates have a highly developed visual system, which permits training them to do visual tasks that are similar in complexity as what humans do, and thus makes them the golden standard for cognitive neuroscience. In this study we used these properties by recording DN cells during a complex visual-motor Landolt C task. We found that DN cells have highly diverse activity patterns, most often relating to more than one task variable. As far as we know this is the first neurophysiological report of DN cells encoding the direction of a visual stimulus. Additionally, the DN neurons responded in a movement direction-selective manner more than half a second before an upcoming saccade. Lastly, they responded to reward or the absence thereof. Activity often bridged experimental epochs, similar as in PCs of the lateral cerebellum (**Chapter 3, Fig3**), therefore multi-modality seems to be one of the key properties of neurons in this brain region. Neurons were directionally tuned to either the stimulus location or the saccade direction, which was reflected in the temporal properties of these tunings (**Fig. 3F**). Interestingly, the FEF, an area that is bidirectionally connected with the D1 zone and thus the region under study, contains distinct populations of cells modulating to visual and motor stimuli (Gregoriou et al., 2012; Voogd et al., 2012). The reward modulation that we found is in accordance with the literature. The recorded DN neurons displayed properties such as reward expectation and sensation. Finally, retrograde labeling indicates that the recorded region is at least in part of the cerebellar D1 microcomplex.

The cerebellum is a highly multimodal structure receiving inputs from virtually every sensory modality and integrates them during performance of complex tasks. Multisensory integration is present in granule cells, which show enhanced spiking output when two sensory modalities are stimulated instead of one (Ishikawa et al., 2015). Integration and being able to select information from multiple streams is essential for associative learning. Huang et al (2013), hypothesized that granule cells even go so far as to integrate sensory and motor signals (Huang et al., 2013). Whether they integrate motor signals still remains an open question, nonetheless our results demonstrate that this appears to happen downstream in PCs (**Chapter 3**) and DN neurons. Primate fastigial nucleus neurons in the vestibulo-cerebellum also display multimodal profiles, encoding both vestibular and proprioceptive stimuli, tuned as a function of head-on-body position (Brooks and Cullen, 2009). Primate DN neurons also show similar responses in relation to arm movements, displaying both visual and/or auditory modulation and movement related discharges in the same spike trains (Chapman et al., 1986). These responses occur well before motor cortex responses when animals did the same task (Lamarre et al., 1981). Furthermore, enduring deficits of the initiation of movements on the basis of a sensory cue were observed after lesioning the DN (Spidalieri et al., 1983). These studies indicate that the DN might contribute to or even trigger the initiation of a movement.

The making of a decision between two saccade targets is frequently modeled as accumulation of evidence until a threshold is reached. In the context of perceptual decision making, selective ramping activity before a movement is interpreted as a signature of accumulation of evidence, which is considered a facet of motor preparation (for review see (Svoboda and Li, 2018)) (Shadlen and Newsome, 2001; Roitman and Shadlen, 2002; Hanks et al., 2015; Svoboda and Li, 2018). This model of perceptual decision making is well supported by neural evidence, indicating that this is a process that is prevalent throughout the brain (Ding and Gold, 2010, 2012; Hanks et al., 2015; Fan et al., 2018). Forebrain regions that express signatures of evidence accumulation receive input from the lateral cerebellum (Strick et al., 2009; Prevosto et al., 2010; Buckner et al., 2011; Bostan and

Strick, 2018). Furthermore, recent work in mice proves that persistent representation of information in the frontal cortex during motor planning, such as needed for evidence accumulation, is dependent on the cerebellum (Deverett et al., 2018, 2019). Perturbation of the fastigial nucleus (FN) disrupted preparatory activity in the frontal cortex, interestingly, the same was the case the other way around; perturbation of the cerebral cortex disrupted activity in the FN (Gao et al., 2018). Conversely, disruption of the DN did not have this effect. Building on this, Chabrol et al used a visual rather than whisker based task and did find a suppressing effect of DN silencing on preparatory activity in the frontal cortex (Chabrol et al., 2019). The task in the current study is arguably more cognitively demanding, and also depends on the visual system rather than whisker system. Therefore, cells recorded in this study might contribute to motor preparation of saccades in the FEF. FEF neurons encode multiple aspects of saccade processing, including target identification in covert visual searches (Monosov and Thompson, 2009) and decision making between multiple choices through evidence accumulation (Schall and Hanes, 1993; Hanes and Schall, 1996; Ding and Gold, 2012). Related properties are reflected in the activity of many of the presently recorded neurons, such as, the sustained activity spanning multiple epochs, and the direction-selectivity for saccades (**Fig. 3**). Moreover, the anatomical evidence indicates that the area under study is connected to the FEF.

The results of the anatomical tracing that are presented in this work indicate that the region where we recorded is part of the cerebellar D1 zone. This zone is known to connect with a multitude of eye movement related areas. Among those are the earlier mentioned FEF, the supplementary eye field (SEF), the parietal eye field (PEF) and even prefrontal cortex (Voogd and Ruigrok, 2012; Voogd et al., 2012). To understand the contribution of the DN we need to analyze the efferent projections labeled with BDA10k. On the basis of these preliminary results and the literature labeling can be expected in the superior colliculus (Kawamura et al., 1982; Voogd et al., 2012). Further anterograde labeling is expected in pulvinar and lateral geniculate nucleus of the thalamus (Petersen et al., 1987; O'Connor et al., 2002; Shipp, 2004; Hulme et al., 2010), the inferior olive, nucleus reticularis tegmentis ponti and red nucleus (Ignashchenkova et al., 2004; Voogd and Ruigrok, 2012; Voogd et al., 2012). Considering the DN neurons modulate for reward and that the cerebellar nuclei appear to project the ventral tegmental area (VTA) (Carta et al., 2019), anterograde labeling may also be expected in the VTA.

Functional connectivity and task related fMRI studies demonstrate that the cerebellum is an integrated part of the dorsal attention network (DAN) (Buckner et al., 2011; Brissenden et al., 2016, 2018; van Es et al., 2019). The D1 microcomplex of the cerebellum, in which the neurons in this study take part, is connected to areas like the FEF, SEF, PEF, all part of the DAN. Furthermore, a subset of neurons modulated their firing rate as a function of the location of the visual stimulus rather than the upcoming movement. Such mixing of visual and motor neurons in the same region is also observed in the FEF (Gregoriou et al., 2012). Therefore, this is the first physiological evidence that the cerebellum might contribute to DAN. The multifaceted aspects of the neurons under study deserve further investigation to clarify unanswered remaining questions such as: do the visual cells modulate for amplitude of attention shifts, and what are their properties in relation to top-down versus bottom-up attention shifts.

4.4 Methods

Animals

For these experiments we used two different monkeys (Macaca mulatta, referred to as monkeys Mi and Mo). Animals were painlessly head restrained through an implanted titanium head-post and trained to do the task in **Figure 1** Animals had for previous research been trained to focus on a fixation dot in the center of the monitor (frame rate: 100 Hz, 1152 x 864 pixels), placed at the viewing point distance of 52 cm. Eye movements were recorded in the dark with an infrared video eye tracker at 1000 Hz (Eyelink 1000 plus, SR Research) while the animal was head restrained through an implanted head-post. Standard Eyelink 5 point calibration with 10° eccentricity was used before every experiment. The left eye was tracked in all experiments

Surgical procedures

See Chapter 2 and methods section Chapter 3.

Landolt C task

A general outline of the task is provided in **Figure 1B**. When a trial started the animal had 500 ms to make a saccade to the target (red dot, 0.2 degree diameter). After which a cue was presented for 100 ms to give away the position of the upcoming C-stimulus. After the cue only the fixation dot was presented for 500 in which the monkey was not allowed to break fixation. If fixation was broken a new trial was started after a 1.5 s timeout. The C-stimulus was presented in 1 of 4 positions in **Fig. 1C**. The animal had to read the gap-direction of the C which was always perpendicular to the position of the C relative from the fixation dot. The stimulus was presented at 5 degrees eccentricity and had a diameter of 1 degree, walls of the C being 0.2 degree diameter and was presented for 250 ms. During the reading of the gap the animal had to maintain fixation on the fixation dot. The C-stimulus was masked for 100ms with a full circle to prevent the animal from gaining extra information from retinal after images. After the mask the fixation dot was only visible again for 500-700 ms (50 ms steps) during which the animal had to remember the direction of the gap. After the pause two saccade targets were presented, and the fixation dot turned gray, indicating that the animal was allowed to leave fixation and make a saccade to the target. To gain a reward the animal had to make a to the target earlier cued on basis of the gap-direction and ignore the other target. If the animal did not make a saccade and fixate for 100 ms within a circle with a diameter of 4 degrees of one of the two targets within 500 ms the trial was aborted. If not the animal received a juice reward.

Reward manipulations

Rewards were given after a delay period of 100-400 ms to be able to decouple recordings of neuronal activity from related to the reward from activity related to the saccade. Next to the standard trial rewards, randomly interleaved were 10% trials with omission of a reward. Another 10% of trials started the same as normal trials, but instead a random reward was given after 1000 ms fixation. Cells were only included for analysis of reward related behavior if every category had at least 5 trials.

Electrophysiology and behavioral recordings

Electrophysiology

Electrophysiology was recorded in the same way as in Chapter 3 with two exceptions. Instead of Purkinje cells, dentate nucleus cells were recorded and 1.5 Mohm instead of 2.5 Mohm tungsten electrodes were used.

Eye-tracking

Eye-tracking was recorded in the same way as in Chapter 5, saccadic adaptation experiments.

Oro-facial behavior

Oro-facial behavior was recorded in the same way as in Chapter 2. Licking during reward was classified as such if the tongue was visible for at least 50 ms during the reward window (0-500 ms after onset of the reward).

Motivation and controlled water intake

Animals were water deprived the day of the experiment and also partially water deprived on the day before the experiment depending on if their performance was insufficient otherwise. Water deprivation was done in consultation with the animal caretakers and in accordance with the rules of the Dutch law. During the task the animal was allowed to drink as reward for correctly executed trials much as he liked. Rewards were in the form of strawberry or tropical juice, depending on the animal's preference. The duration of reward determined the amount of juice, starting with a pulse of 100 ms. In every consecutively correct trial 50 ms up to a maximum 350 ms was added to motivate the animal to perform consistently. If the animal made an incorrect response no reward was given and the duration of the reward was reset to the initial 100 ms.

Data analysis

All analyses were performed off-line using custom programs written in Matlab (The Mathworks, Natick, MA, USA).

Eye movement analysis

Same as chapter 5, saccadic adaptation experiments.

Neuronal Modulation

Task modulation was determined in sliding windows of 200 ms during the epoch of interest. Windows moved in steps of 100 ms from 0 - 200 ms after the onset of the epoch of interest until -200 - 0 before the end of the window of interest. In this way a 0-500 epoch would be divided in 4

widows centered around 100, 200, 300 and 400 ms after onset of the epoch. Spike counts in the windows compared with the baseline window (-500 - 0 ms after the onset of the cue) by means of a one-way ANOVA with Tukey-Kramer post-hoc test. To get a more precise estimate of the activity during baseline spike counts in the baseline window were corrected for the larger length of the window rather than taking a smaller baseline window. If activity in one of the sliding windows was significantly different (alpha=0.05) from the activity in the baseline window the epoch was considered significantly modulated. In case of the stimulus epoch, if more than half of the windows were significantly different from the baseline window the cell was considered sustained active during the epoch. **Table2** provides an overview of all sliding windows.

Event	*Description*
Stimulus	*0-800 ms after C-onset. 200 ms sliding window with 100 ms steps*
Sustained	*Same as C-modulated window, more than half (minimum 5/8) of the sliding windows must be significant*
Saccade	*from 200 ms before until 200 ms after saccade onset. 200 ms sliding window with 100 ms steps*
Reward	*0-500 ms after reward. 200 ms sliding window with 100 ms steps*

Table 2. *Description of the sliding windows used to determine significant modulation for each category.*

Directional sorting and preferred direction

Trials were sorted twice into both stimulus location and action direction. From these sortings the average firing frequency was calculated based on a 50ms normal kernel separately for every direction and direction sorting. Resulting in 8 firing rates, 4 for the stimulus locations and 4 action directions. Cells were only included if there were at least 5 correct trials per direction. From the 4 stimulus locations the time point where the variance in firing rate between the four directions was the largest was determined in the epoch of interest, i.e., the point with the biggest difference between the direction with the lowest and the highest firing rate. In a 200 ms window around that time point an ANOVA is done on the number of spikes per direction to determine if the cell was direction-selective or not (alpha=0.05). The direction that shows the biggest change in firing rate from the baseline is selected as *preferred direction*. The same is done for the action direction. To determine if a cell preferably modulated for the stimulus location or action direction i.e., the preferred *direction sorting*, the ANOVA with the lowest p-value was selected. The stimulus location and action direction are inherently correlated since they are always perpendicular. Therefore, two significant ANOVAs were quite common, but does not necessarily mean that the cell actually is direction-selective for both sortings.

Statistics

If statistical testing involved two groups, a student's t-test was used. When more than two groups were involved, we used ANOVA with Tukey-Kramer post-hoc test. ANOVAs were one way unless specified otherwise. When comparing fractions, the Chi^2 for proportions was applied to determine significance. For circular statistics the circle stats toolbox for MATLAB was used. All statistical analysis was done in MATLAB.

Tracer injections

At the end of the experiments animals were injected in the recording with anterograde and retrograde tracers. As anterograde tracer we used 600 nl 10% BDA10k (Sigma-Aldrich, the Netherlands) and as retrograde tracer 600 nl 0.8 % CTB (Sigma-Aldrich, the Netherlands) both were dissolved in 0.01M Phosphate buffered saline. Injections were done on separate occasions so the survival times were tuned for optimal tracer spread. Injection with BDA10k was performed 25 and 27 days before perfusion in Mi and Mo respectively. The CTB injection was performed 18 and 19 days before perfusion in Mi and Mo respectively. Injection spots were the same locations as where the bulk of the DCN neurons were recorded. Injection position was verified with an electrode that was fixed to the injection line. For details on injection line fabrication and injection procedures see Chapter 2 section 7: pharmacological interventions.

Perfusion

Animals were transcardially perfused. Before the perfusion the animal is deeply anesthetized with fentanyl and pentobarbital. To prevent blood coagulation 2000 IE/kg of heparin was injected i.v. with at least 50 mL saline. First the animals were flushed with NaCl (0.9%), then tissue was fixed with 4% paraformaldehyde in 0.1 M PBS, (pH 7.6) followed by flush with PBS sucrose (5%, pH 7.6). Thereafter the brain is dissected out. If the brain was slightly soft it was post fixated in 4% PFA for a few days or up to one week. Then the brain is submerged in first 12.5% and then 25% sucrose PBS solution until it sinks at room temp.

Cutting and stainings

The brain was embedded in 14% gelatin and 10% sucrose and subsequently cut in 50 μm slices. For light-microscopy stainings of CtB in rhesus monkeys, the slices were incubated for 20 min in 3% H2O2 (in PBS) to remove endogenous peroxidase activity of blood. We used anti-CTB (goat, 1:15000, List labs) primary antibody and anti-goat-biotinylated secondary antibody (1:200, Vector). After washing, the sections were incubated in avidin-biotine complex (1:200 Avidine and Biotine in PBS, Vector) for 1.5 hours at RT and subsequently stained with 3,3'-Diaminobenzidine (DAB, 75mg/ml stock, 1:300, Sigma).

Acknowledgements

We thank Kor Brandsma and Anneke Ditewig for brilliant biotechnical assistance and animal caretaking; Beerend Winkelman for fruitful discussions; Masaki Tanaka and Jun Kunimatsu for sharing the design of the injectrode used for the tracer injections.

Contributions

N.A.F., A.B. and C.D.Z designed the experiments. N.A.F. trained the animals and performed and analyzed the electrophysiological experiments. N.A.F. and A.B. performed the tracer injections. N.A.F., A.B. Kor Brandsma, Anneke Ditewig, Tom Ruigrok and Erika Goedknecht performed the perfusions. Erika Goedknecht and Bas Hoogstraaten performed the anatomical stainings. N.A.F., B.H. and C.D.Z. analysed the stainings. N.A.F. wrote the chapter.

Ethical statement

All experimental and surgical procedures complied with the regulation from and were approved by the Royal Netherlands Academy of Arts and Sciences.

4.5 Supplementary data

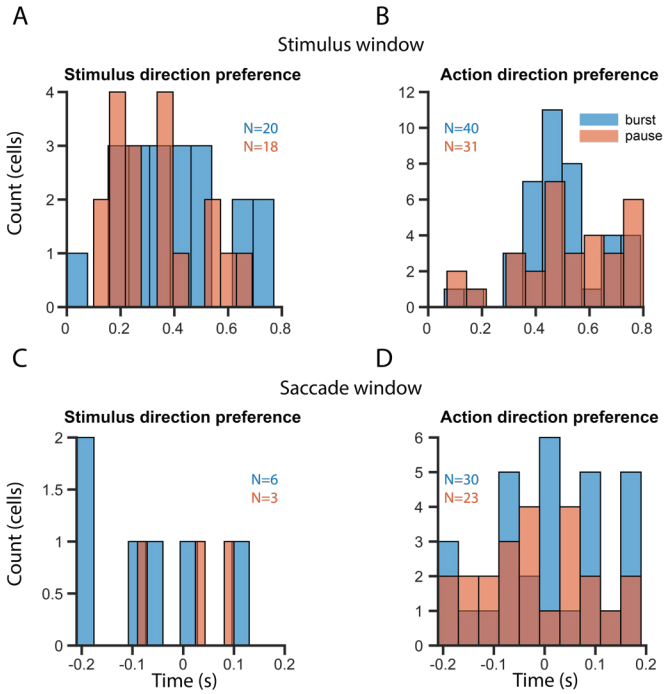

Supplementary Figure 1. Timing of peak response modulation split between bursting and pausing neurons. *A) Distribution of peak response of cells with stimulus location preference during the instruction period. p=0.25, all tests are t-tests. B) Same as A but for cells with action direction preference p=0.34. C) Same as A but for cells but during the saccade window. p= 0.35. D) Same as B but during the saccade window. p= 0.54.*

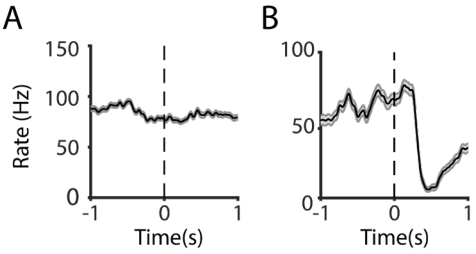

Supplementary Figure 2. Firing rate during incorrect trials aligned to the time the eye reached the incorrect target i.e. saccade offset. *A) Firing rates during incorrect trials of the same cell as in* **Figure 4A. B***) Same as A but for the same cell as in 4B.*

Chapter 5:

Glissades are altered by lesions to the oculomotor vermis but not by saccadic adaptation

Nico A. Fliermann[1,2], Alla Ignashchenkova[3], Mario Negrello[1], Peter Thier[3,4], Chris I. De Zeeuw[1,2], Aleksandra Badura[2]

Author affiliations:

[1]Netherlands Institute for Neuroscience, Amsterdam, The Netherlands.

[2]Department of Neuroscience, Erasmus MC, Rotterdam, The Netherlands.

[3]Department of Cognitive Neurology, Hertie Institute for Clinical Brain Research, Tübingen, Germany.

[4]Werner Reichardt Centre for Integrative Neuroscience (CIN), University of Tübingen, Tübingen, Germany.

Published as: Flierman, N.A., Ignashchenkova, A., Negrello, M., Thier, P., De Zeeuw, C.I., Badura, A., 2019. Glissades Are Altered by Lesions to the Oculomotor Vermis but Not by Saccadic Adaptation. *Front. Behav. Neurosci.* 13, 194. https://doi.org/10.3389/fnbeh.2019.00194

5.0 Abstract

Saccadic eye movements enable fast and precise scanning of the visual field. Therefore, accuracy and speed are crucial for processing visual information and are partially controlled by the posterior cerebellar vermis. Textbook saccades have a straight trajectory and a unimodal velocity profile, and hence have well-defined epochs of start and end. However, in practice only a fraction of saccades matches this description. One way in which a saccade can deviate from its trajectory is the presence of a saccadic overshoot or undershoot at the end of a saccadic eye movement just before fixation. This additional movement, known as a glissade, is regarded as a motor command error and was characterized decades ago but was almost never studied. Using rhesus macaques, we investigated the properties of glissades and changes to glissade kinematics following cerebellar lesions. Additionally, in monkeys with an intact cerebellum, we investigated whether the glissade amplitude can be modulated using multiple adaptation paradigms. Our results show that saccade kinematics are altered by the presence of a glissade, and that glissades do not appear to have any adaptive function as they do not bring the eye closer to the target. Quantification of these results establishes a detailed description of glissades. Further, we show that lesions to the posterior cerebellum have a deleterious effect on both saccade and glissade properties, which recovers over time. Finally, the saccadic adaptation experiments reveal that glissades cannot be modulated by this training paradigm. Together our work offers a functional study of glissades and provides new insight into the cerebellar involvement in this type of motor error.

5.1 Introduction

High-resolution vision is limited to the foveal region of the retina. Therefore, high acuity vision depends on saccadic eye movements to scan regions of interest in the visual field with high resolution. Since visual input is unavailable during saccades (Volkmann, 1962) and it is ethologically relevant to spend as little time blind as possible, gaze shifts need to have high velocity and accuracy. Saccades are some of the fastest movements that a body can produce, with durations shorter than 60 ms (Robinson, 1964), and amplitudes ranging from tenths of a degree (microsaccades) up to 60 degrees (Bahill et al., 1975c). The end-points of these ultra-fast movements regularly contain slow drifting overshoots or undershoots relative to fixation, which are referred to as glissades (Weber and Daroff, 1972; Bahill et al., 1975b; Hsu and Stark, 1978).

From a historic perspective the term glissade was first used by Weber and Daroff in the early 70's (Weber and Daroff, 1972) analogizing the long and slow post-saccadic drifts with a '*glissando*' on the piano, where the fingers glide from one note to another. The shorter duration, zero-latency "dynamic over- and undershoot", was initially referred to as a separate phenomenon. Indeed, Bahill and colleagues came up with two distinct models for each of these descriptions (Bahill and Stark, 1975; Bahill et al., 1975a). Later work often omitted the distinction due to empirical considerations, simply referring to both as a "glissade" (Kapoula et al., 1986; Nyström and Holmqvist, 2010). The main reason for the lack of distinction is that even if they are functionally distinguishable phenomena, the heterogeneity of the eye motion kinematics makes a meaningful separation virtually impossible in eye tracking data.

Here, we consider a glissade a drift-like movement that immediately follows the end of the decelerating phase of the saccade and before the eye settles on the final point (see Methods for details on the detection procedure and criteria). **Figure 1** shows examples of saccades without glissades (top panels) as well as saccades with glissadic overshoots (middle panels) and undershoots (middle and bottom panels; all saccades are aligned to the glissade onset) from the dataset used in this paper. Glissade duration, amplitudes and peak velocities occur in the same range as those of microsaccades (Tian et al., 2018).

Glissades have marked importance in the context of precision, programming, and the relationship of saccades to other eye movements. The study of glissades is timely: delineating the start and end of the saccade is an issue that repeatedly comes up in the recent surge of eye movement trackers with head-free and even freely moving subjects (Chukoskie et al., 2018; Macinnes et al., 2018; Wang et al., 2019) (for a review of commercially available eye tracking software used in research and commercial applications see: https://imotions.com/blog/top-eye-tracking-hardware-companies). This is particularly relevant for studies where eye movements are proposed to be used as a diagnostic criteria (Klin et al., 2009; Al-Wabil and Al-Sheaha, 2010). In these conditions stationary fixation preceding and following a saccade is the exception. More commonly the eye moves both before and after the saccade. These movements often comprise compensatory eye movement and other factors. Since modern technology and research makes frequent use of eye-tracking systems, segregating saccades becomes an important problem, which is anything but straightforward. In this context, recognizing glissades and understanding their basic properties and relationship to saccades is of high importance.

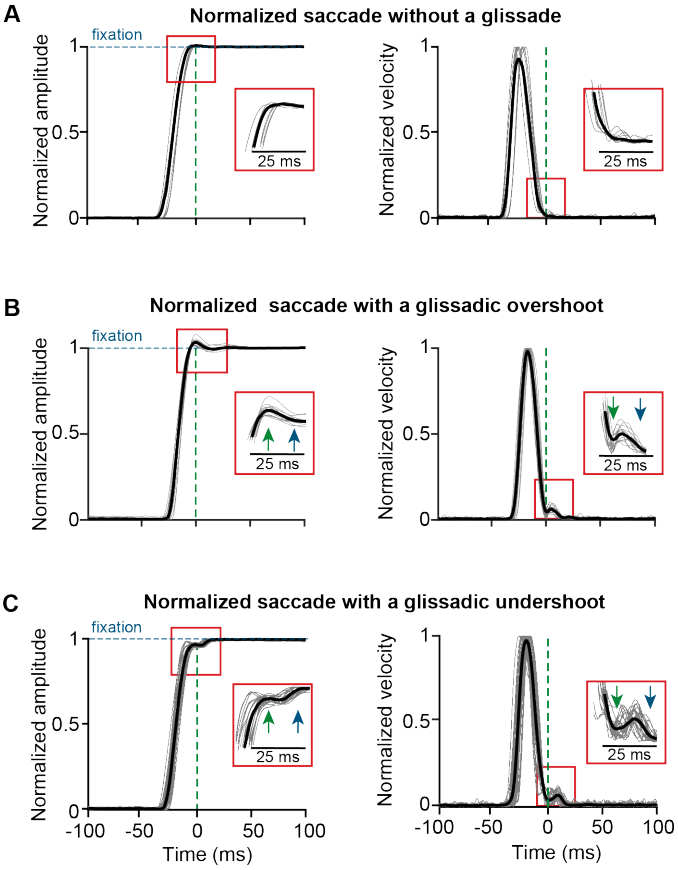

Figure 1. **Example traces of saccades normalized to fixation with and without the glissade**. *All saccades aligned to the onset of a glissade. A) Position and velocity traces of saccade (gray) and average (black) of saccades without a glissade; 59% of all saccades. B) Example traces of saccades with glissadic overshoot (35% of all saccades); inset shows glissade onset (green arrow) and offset (blue arrow). C) Example traces of saccades with a glissadic undershoot (6% of all saccades). Percentages were calculated from 3597 saccades from 4 monkeys (data collected with a scleral search coil). Traces were normalized to prevent the glissades from being concealed by the variability in saccade amplitude.*

So far the only physiological investigation of glissades describes the role of the lateral intraparietal cortex, an area that is known for visual saliency maps and attention, but also participates in the planning of saccades (O'Leary and Lisberger, 2012). The eye movements they study are in the range of 2-4°/s, whereas the eye movements in our study and those reported in the literature are around 20°/s (Nyström and Holmqvist, 2010). It is therefore possible that the 2012 study by O'Leary and Lisberger focuses more on the slow and long post-saccading drifts (Weber and Daroff, 1972), ignoring the short latency "dynamic over- and undershoots" in their definition of the glissade. This discrepancy makes the argument for unifying the two definitions even more pressing.

Little is known about the role of downstream structures, responsible for the execution of a

saccade, in the generation of glissades. One of the major hubs in this complex network for planning and execution of saccades is the cerebellum (**Fig. 2**). It is responsible for the fine-tuning of oculomotor performance and for keeping saccades accurate despite changes in the oculomotor system due to development, aging or disease (Golla et al., 2008; Beh et al., 2017). Lesions to the cerebellum have been shown to decrease saccadic accuracy and affect the amplitude and kinematic properties of saccades. Additionally, the cerebellum is also responsible for the adaptive lengthening and shortening of saccades based on a visual error, also known as saccadic adaptation (Pélisson et al., 2010). The posterior part of cerebellar vermis (lobules VIc, VII), also known as the oculomotor vermis (OMV), is a part of the cerebellum that is responsible for the control of saccadic eye movements. Lesions to this part of the cerebellum cause transient dysmetria (hypo- and/or hypermetria) and abolish the capacity for adaptive lengthening, but not shortening, of saccadic amplitudes through saccadic adaptation (Barash et al., 1999; Ignashchenkova et al., 2009).

The motoneuronal control of saccades has been studied in detail and is much better understood. It is commonly understood as consisting of two components, a phasic 'pulse' and a tonic 'step' (for a schematic overview of brain regions involved see **Figure 2**). The pulse brings the eyes to the new position and is characterized by a high frequency burst in the motoneurons (Sindermann et al., 1978; Scudder et al., 2002). The duration of this burst is approximately equal to the duration of the saccade, and it is accompanied by inhibition of the motoneuronal activity for the antagonist muscle. The step is a tonic activation which holds the eye in its new position (Van Gisbergen et al., 1981; Sparks, 2002). If the two components are matched, the saccade lands exactly on target. However, if the pulse is stronger than the step, the eye travels beyond its intended position and slowly drifts back producing an error, i.e. an overshooting glissade. The opposite can happen when the pulse is too weak and the eye drifts during the last part of the movement towards the target producing an undershooting glissade (Bahill et al., 1978). In this model, glissades appeared when there were pulse-step mismatches (Bahill and Stark, 1975; Bahill et al., 1975a).

The pulse and step are generated by a group of nuclei in the brainstem that are collectively called the brainstem burst generator (BBG; for review see: (Sparks, 2002). The superior colliculus (SC) and the OMV are the main inputs to the BBG that are responsible for executing the saccade (**Fig. 2**). The OMV influences eye movements through its Purkinje cell responses, which provide the sole output of the cerebellar cortex. Their activity correlates accurately with the eye velocity of the upcoming saccade and aligns with the saccade ending (Thier et al., 2002; Herzfeld et al., 2015). It is therefore hypothesized that the OMV is responsible for keeping the pulse of the motoneuron drive accurate (Optican and Robinson, 1980b). The OMV's Purkinje cells tonically inhibit a part of the cerebellar fastigial nucleus called the fastigial oculomotor region (FOR). Activity in the contraversive fastigial oculomotor region precedes the saccade, providing additional drive to the BBG and thus accelerating the eye movement. Later on, at the end of the movement, the ipsiversive fastigial oculomotor region becomes active, choking off the drive to the ipsiversive BBG and thus stopping the eye movement (Noda et al., 1990; Fuchs et al., 1993; Voogd et al., 2012). When both fastigial oculomotor regions are lesioned, saccades become hypermetric in all directions, leading to the hypothesis that the OMV is responsible for ending the saccade (Robinson et al., 1993; Quaia et al., 1999) (for an extensive review on what stops the saccades see: (Optican and Pretegiani, 2017).

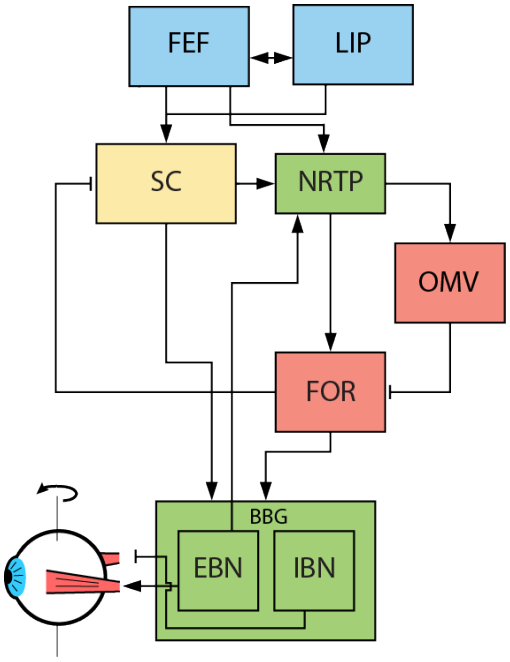

Figure 2. Overview of saccade related areas in the midbrain, brainstem, and cerebellum. *Saccade targets are jointly selected by cerebral cortex (blue) and SC (yellow). Subsequently, SC, brainstem (green) and cerebellum (red) execute the movement. SC provides drive to premotor nuclei and cerebellum via NRTP. Cerebellum provides additional drive to premotor nuclei through the FOR. EBN give feedback signal back to cerebellum about the progress of the saccade. FEF, frontal eye fields. LIP, lateral intraparietal cortex. SC, superior colliculus. NRTP, nucleus reticularis tegmenti pontis. OMV, oculomotor vermis. FOR, fastigial oculomotor region. EBN, excitatory burst neurons. IBN, inhibitory burst neurons. Blue areas are in the cerebral cortex, yellow areas represent the midbrain, green areas the brainstem, and red areas part of the cerebellum.*

Notably, alternative models exist but they are mostly a variation on the pulse-step model of the saccadic control. For example a pulse-slide-step incorporates a force to the pulse that precedes and continues during the saccade, a force of the step that holds the eye at its new position and a force that counteracts the long time constants of the visco-elastic elements of muscles and the eye itself, i.e. the slide force (together the muscles and the eye are commonly referred to as "the plant") (Collins, 1975; Miller and Robins, 1992). A full review of all models is out of the scope of this paper; for a comprehensive overview of the proposed models see (Scudder et al., 2002).

Since the cerebellum seems to be responsible for timely termination of the pulse part of the drive of the saccade, we hypothesized that OMV lesions could lead to inaccuracies at the end of the saccade, i.e. the glissades. Here, we have studied the effects of the OMV lesions on glissade kinematics and on their rate of occurrence in primates. Furthermore, we have investigated to what extent glissades can be adapted, since the adaptation of eye movements based on errors from prior movements is an ability that critically depends on the cerebellum (Dash and Thier, 2014). We

reasoned that during the glissade, a slower process of error feedback loop could be harnessed to adjust the step for endpoint correction. We hypothesized that if the contribution of the glissades were functional, it would be possible to observe a systematic contribution in the error distribution during an adaptation task.

5.2 Results

To study the role of the OMV in the formation and characteristics of glissades we used a dataset from a previously published OMV lesion-study of 4 rhesus macaques (B, E, R and S; (Ignashchenkova et al., 2009) and 2 of our own rhesus macaques (Mi and Mo). The aim of the original lesion study was to investigate the role of the OMV in spatial attention shifts, visual motion perception and the detection of luminance changes. Eye movements were tracked pre- and post-lesion using the sclera implanted search coil technique but the glissades were never analyzed (Judge et al., 1980). We used this dataset and analyzed saccades together with the occurrence and kinematics of glissades pre-lesion, early and late post-lesion. Saccades were classified in three categories; saccades without a glissade (**Fig. 1A**), saccades with a glissadic overshoot (**Fig. 1B**), and saccades with a glissadic undershoot (**Fig. 1C**). In the pre-lesion condition 59% of saccades did not have any form of glissade (**Fig. 1A**), 35% of saccades of all animals combined showed glissadic overshoots (**Fig. 1B**), and 6% of saccades showed glissadic undershoots (**Fig. 1C,** for percentage of individual animals see **Supplementary Table 1**). Glissadic undershoots had an average amplitude of 0.14 ± 0.08° and a duration of 13 ± 7 ms. Glissadic overshoots had an average amplitude of 0.21 ± 0.13° (SD) and a duration of 11 ± 5 ms. Because glissadic undershoots were relatively rare (**Supplementary Table 1**), in order to reach a significant power for our statistical comparisons we used glissadic overshoots alone in the analysis of the glissade endpoints, and pre- and post-lesion glissade comparisons. We do however present the analysis of the glissade kinematics separately for under- and overshoots, since these were not as constrained by the small size of the early post-lesion group particularly.

Notably, in our analysis we focused only on glissades immediately following the primary saccades. In accordance with previously published results, monkeys B, E, R and S used in the lesion studies displayed corrective/secondary saccades, particularly in the early post-lesion condition (Ignashchenkova et al., 2009). In the pre-lesion and late post-lesion condition, very few corrective saccades were detected, with the exception of monkey E who showed corrective saccades also in the baseline condition. These secondary saccades were not inspected for the presence or absence of glissades and are not included in any of our analysis.

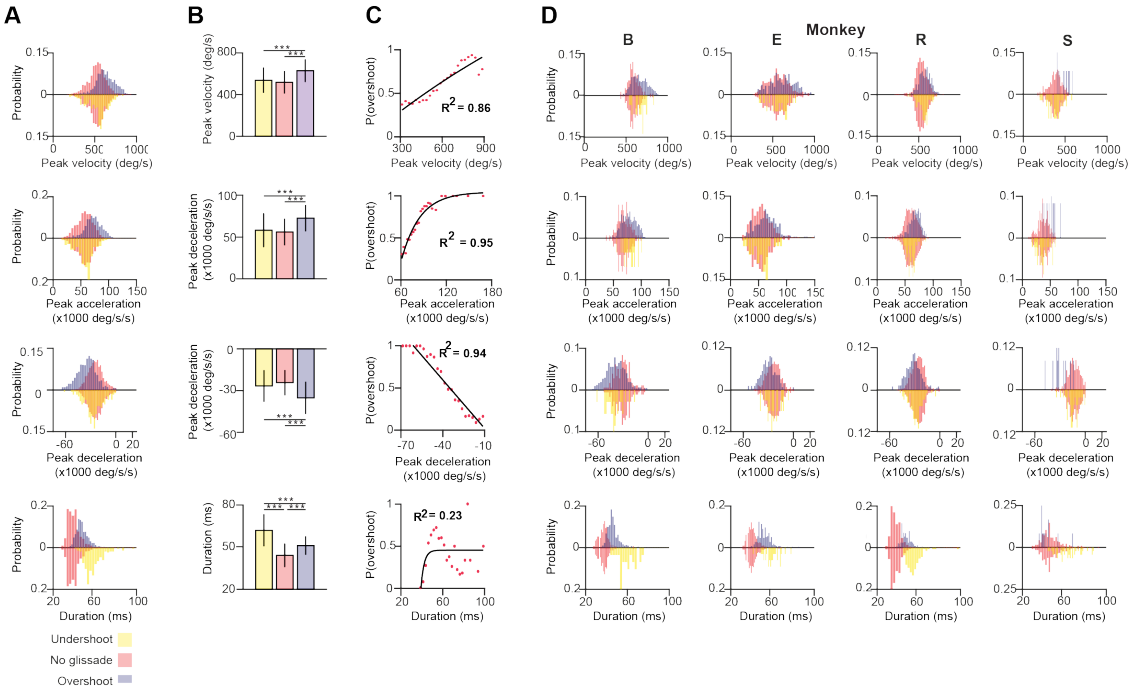

Figure 3. Kinematics of saccades with undershoot, overshoot or no glissade. *A) Probability density histograms of saccade kinematics of all animals combined. Red bars represent kinematic parameters of saccades without a glissade, purple bars represent saccades with glissadic overshoots and yellow bars saccades with glissadic undershoot. Red up and downward bars represent the same data to clearly compare the effect of undershoots and overshoots. B) Average kinematics of saccades from all animals with glissade ± SD. C) Linear or exponential regression analysis on the probability of having a saccadic with overshoots and kinematic parameters. D) Histograms of the same kinematic parameters as represented in A) for individual animals. "B," "E," "R," and "S" denote each of the four monkeys. '***' symbols denote p-values of <0.001.*

Saccades with and without a glissade before lesions

First, we compared the pre-lesion kinematic properties of saccades with and without glissadic over- and undershoots. Saccadic durations were measured as time from the onset of the saccade until complete fixation, including the glissade when present (blue arrow in **Fig. 1B, C**). **Figure 3A** shows distributions of the kinematic parameters pooled across all monkeys for saccades without glissades, saccades with undershoots, and saccades with overshoots (depicted by negatively and positively deflected histograms, respectively). Individual animals are represented in **Figure 3D** in the same fashion.

Saccades with glissadic overshoots of all animals combined had higher peak velocities, accelerations, decelerations than saccades with glissadic undershoots and saccades without glissades (**Fig. 3B**; all $p<0.001$). Saccades with glissadic undershoots on the other hand were not different

from saccades without glissades in the same categories ($p>0.01$). Saccades without glissades had the shortest durations, followed by saccades with glissadic overshoots. Lastly, saccades with glissadic undershoots had the longest durations ($p<0.001$ for all groups). Additionally, we explored the relation between the probability of a saccade having a glissadic overshoot and the same kinematic parameters of the saccade as discussed in **Figure 3A and B**. When binning peak velocities and calculating probabilities of glissadic overshoots associated with each bin, a regression model was fitted (**Fig. 3C**). High peak velocities showed a positive linear relationship with the probability of glissadic overshoots ($R^2 = 0.86$). Peak accelerations on the other hand showed a positive exponential relationship with the probability of glissadic overshoots ($R^2 = 0.95$). Peak decelerations also had a linear relationship with probability of glissadic overshoot ($R^2 = 0.94$). Lastly, glissadic durations did not show a clear relationship with probability of glissadic overshoots. The regression analysis was only performed for glissadic overshoot, because glissadic undershoots suffered from sample size constraints (**Supplementary Table 1**).

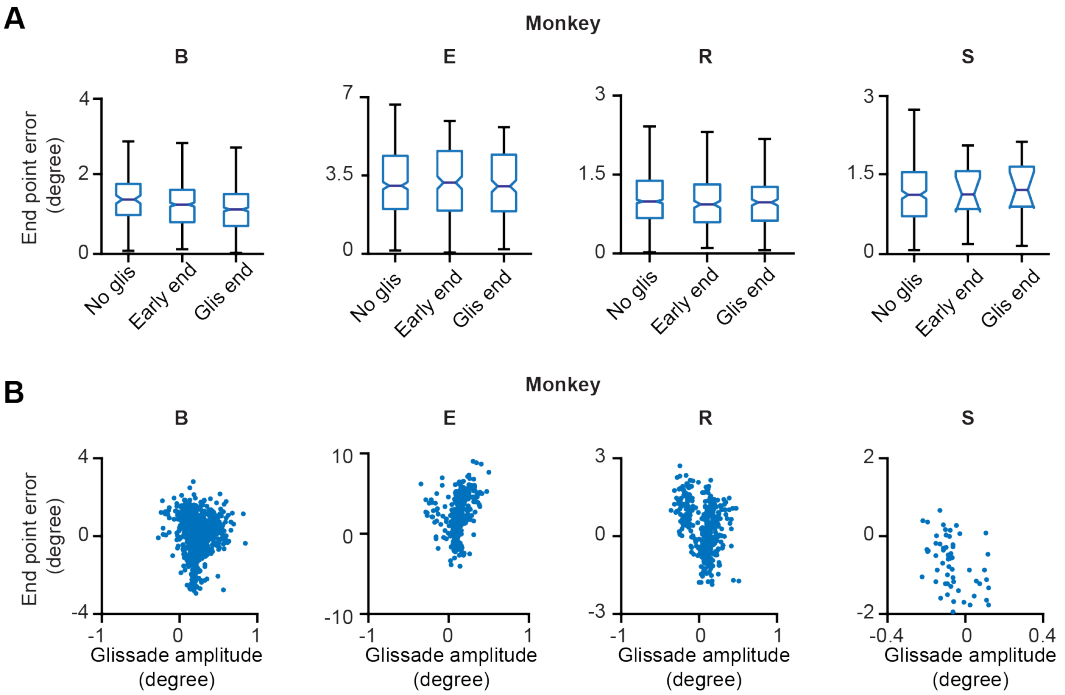

Figure 4. End point errors at onset and offset of the glissade and of saccades without a glissade. *A) The first box in every panel represents the average endpoint error of saccades without a glissade ("No glis"). The second box represents the end point error of the saccade at the onset of the overshooting glissade ("Early end"; green arrow in Figure 1B). The third box shows the end point error of the saccade at the end of the overshooting glissade ("Glis end"; blue arrow in Figure 1B). No significant differences were observed. B) Scatter plots of signed end point saccade errors (negative – hypometric saccades; positive – hypermetric saccades) and glissade amplitudes (negative – undershoots; positive – overshoots) of individual animals. See Supplementary Table 2 for p-values of A) and correlation coefficients of B).*

Next we explored whether glissades decrease endpoint errors. Endpoint errors were defined as the absolute position difference between the eye and the target:. We compared the endpoint errors at the beginning and end of overshooting glissades. No statistical difference was observed and thus the glissade did not contribute in bringing the eye closer to the target. There were also no differences when comparing endpoint errors of saccades with glissades where no glissade was present (**Fig. 4A** and **Supplementary Table 2** for p-values of the statistical tests). The end points of glissades and saccades were observed all around the target. Therefore, by chance, a hypermetric saccade with an overshooting glissade would somewhat decrease the end point error through the glissade. On the other hand a hypometric saccade with an overshooting glissade would increase the end point error. For this reason, we computed the coefficient of correlation between signed saccade endpoint (negative values represent hypometric saccades; positive values represent hypermetric saccades) and signed glissade amplitudes (negative values represent undershoots; positive values represent overshoots) (**Fig. 4B**). We found no consistent relationship between end point error and glissade amplitude (see **Supplementary Table 2** for correlation coefficient per each animal). This indicates that glissades do not provide additional accuracy by bringing the eye position closer to the desired endpoint.

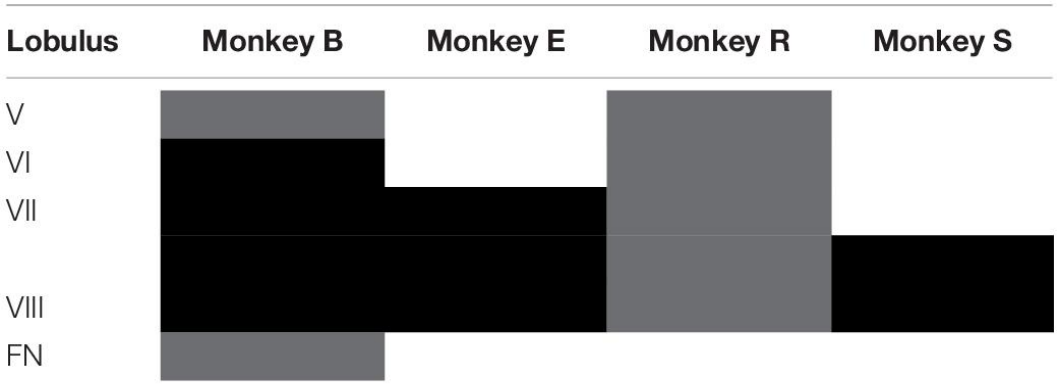

Gray boxes represent partial ablation of the lobule and black boxes represent complete ablation of the lobule. For additional details, see Ignashchenkova et al. (2009).

Table 1. Extent of the lesion for individual animals.

Recovery time from OMV lesion for overshooting glissades

Subsequently, we explored how both saccades and overshooting glissades change after lesions to the OMV. The extent of the lesions were distinct for individual monkeys, ranging from only partial ablation of lobules V-VIII of the OMV in monkey R to complete removal of lobules VI-VIII and partial removal of lob V in monkey B (for an overview of the extent of the lesion per monkey see **Table 1**). Lesions caused a clear but transient effect on saccadic amplitudes, which were extensively described in the original publication (Ignashchenkova et al., 2009).

Recovery of saccade amplitudes progressed exponentially in two out of four animals (**Fig. 5**, black lines show a significant exponential [(f(x) = a*exp(-x/b) +c; where $t_{1/2}$ = tau*ln(2), where tau = b in the previous formula] **Supplementary Table 3** shows R^2 and $t_{1/2}$ for all

animals). Exponential fits for saccades had a median half-life of 2.35 days ± 0.9 days (1 SD, unless otherwise specified), including only animals with a significant exponential fit (n=2; R,S). Monkey E showed a clear exponential decay in glissade amplitude. Two out of four monkeys (R, S) showed a significant exponential decay of fractions of saccades with a glissade. For monkey B, who did not have any significant fits, we used the average half-life of saccades amplitude of monkeys R and S (for all R^2 , p-values and half-life parameters see **Supplementary Table 3**).

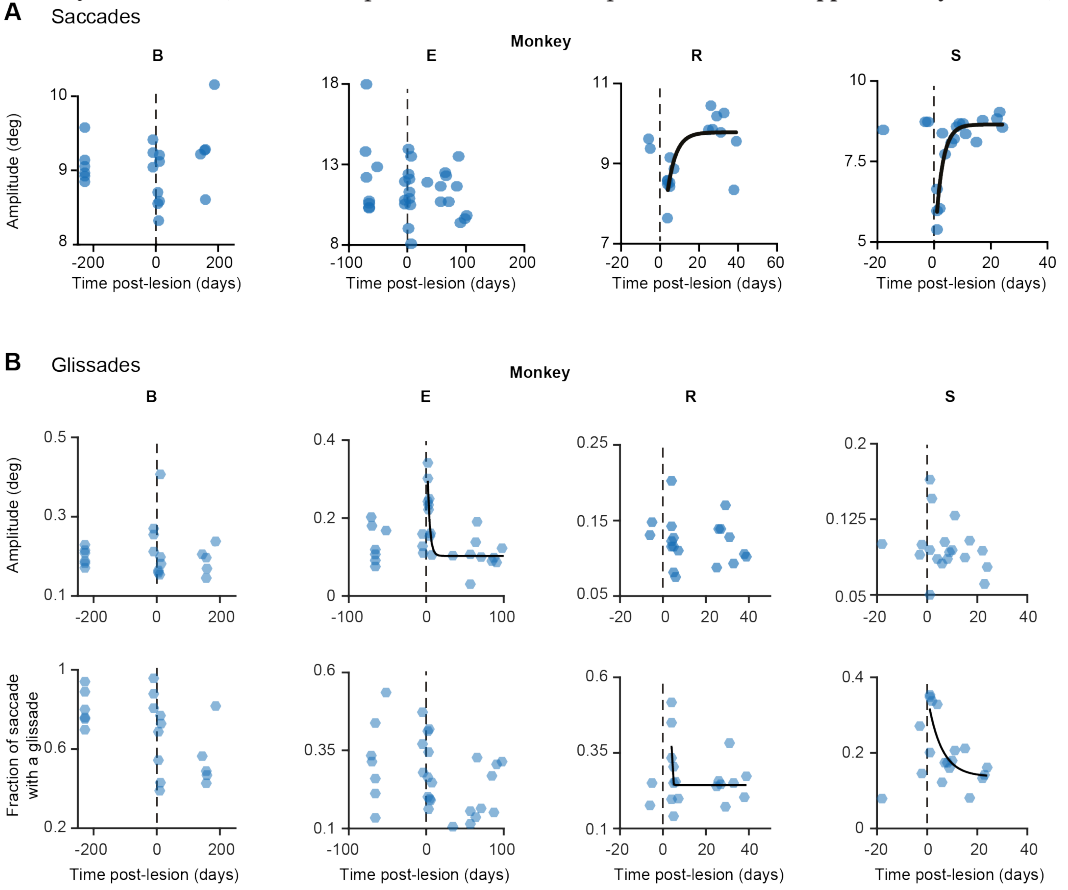

Figure 5. Development of lesion phenotypes over time. *A) Saccade amplitude per monkey plotted over time. Blue dots represent average saccade amplitude per experimental day including all directions pooled together, black fits represent exponential fit (f(x) = a*exp(−x/b) + c). B) Same as in A) but the hexagons indicate glissade amplitude and fraction. See Supplementary Table 3 for p-values and coefficient of determination. Fraction is defined as the number of saccades containing a glissadic overshoot. Only overshooting glissades were used for this analysis.*

Lesions of OMV result in mixed phenotypes

Based on the time course of the recovery period described above, we grouped the data in three time-epochs: pre-lesion, early post-lesion and late post-lesion. The early post-lesion group was defined as lesion date +3 times the half-life of exponential fit for saccades; the period after that was categorized as late post-lesion (monkeys R and S). Monkey E did not show exponential recovery of saccade deficits. Therefore we used the fit for glissade amplitude to determine the early and late post-lesion epochs. Monkey B did not have any significant fits, therefore we used the average half-life of saccades of monkeys R and S. Since the effect of the lesion varied substantially between monkeys, only significant results are described for each animal individually (**Fig. 6**). Only effects on glissadic overshoots are reported due to the earlier discussed constraints on glissadic undershoots.

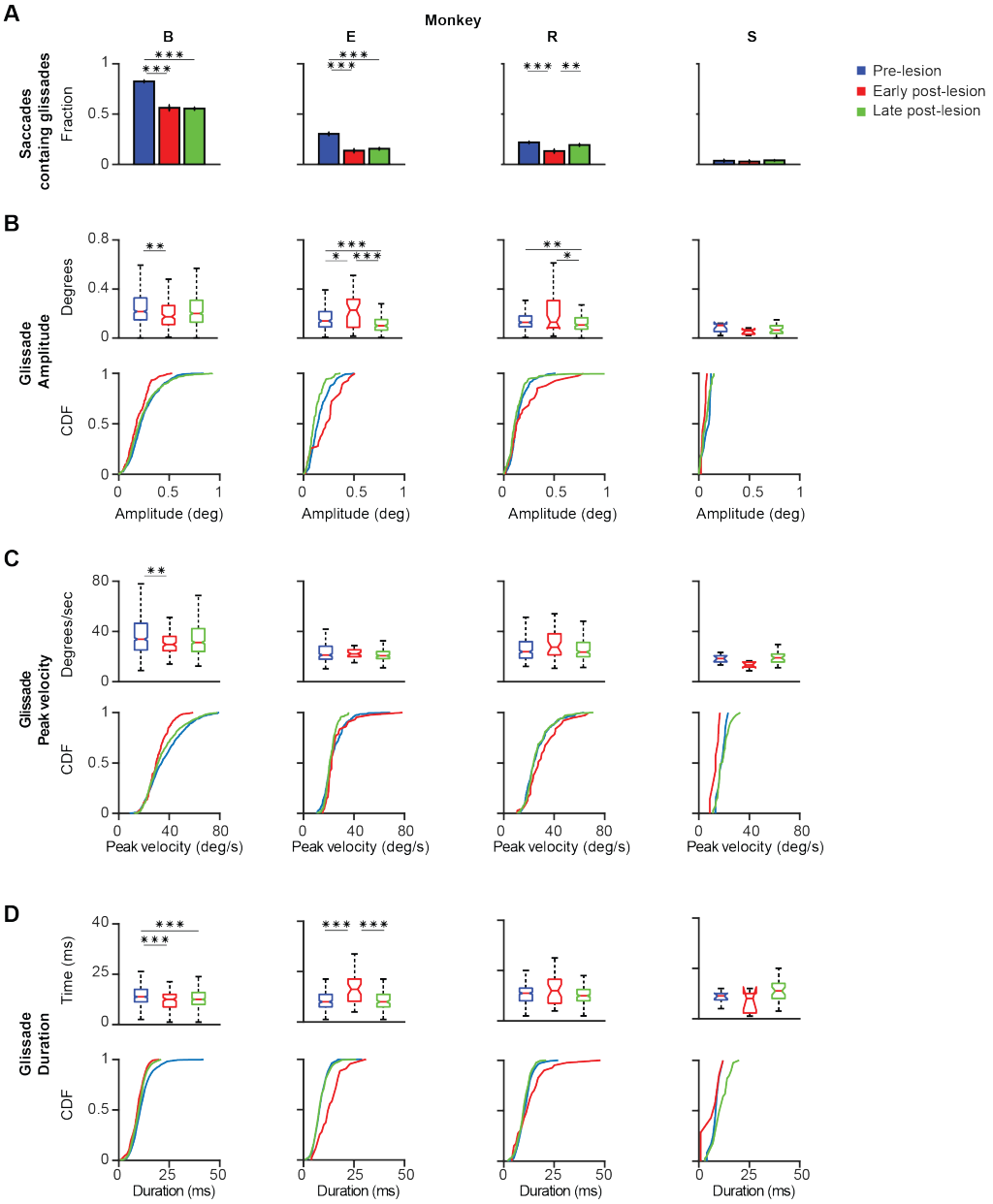

Figure 6. Post-lesion changes to glissadic overshoots. *Glissade kinematics were sorted in pre-, early, and late post-lesion groups. Early post-lesions were defined as the day of the lesion + 3 half-lives of the exponential fit in Figure 5, everything thereafter was classified as late post-lesion (for more details see section Results). Number of days that were classified as early post-lesion period is shown in the bottom row of Supplementary Table 3. A) Fractions of saccades with a glissade for individual monkeys. Error*

bars represent Jeffrey's interval for proportions. B) Box plots and [Cumulative Distribution Function (CDF)] of glissade amplitudes for individual monkeys. Boxes edges indicate 25th and 75th percentile, box midline indicates the median. Whiskers extend to the most extreme data points not considered outliers. C) Box plots and CDF of glissade velocities. D) Box plots and CDF of glissade durations. Only overshooting glissades were used for this analysis. See Supplementary Table 4 for p-values. '' symbols denote p-values of <0.05; '**' symbols denote p-values of <0.01; '***' symbols denote p-values of <0.001.*

Monkey B initially showed a very high fraction of saccades with glissades which decreased after the lesion and remained at this level in the late post-lesion period. Glissade amplitude initially decreased, but recovered in the late post-lesion period. It is notable that monkey B had a higher baseline fraction of glissades than the other animals. This could potentially be caused by repeated electrophysiological recordings of the SC that had been performed in this monkey prior to the current study (Ignashchenkova et al., 2004), see Methods and Discussion for details). However, it could also reflect the individual variability in glissades between animals. The glissadic peak velocity and duration of monkey B decreased early post-lesion. Glissadic durations showed a persistent decrease in the late post-lesion epoch, whereas glissadic peak velocity recovered to pre-lesion period values (for p-values see **Supplementary Table 4**).

Monkey E showed a decreased fraction of saccades with a glissade which stayed lowered in the late post-lesion period. Glissade amplitude decreased from early to late post-lesion period. Peak velocity is unaffected by the lesion. Glissade duration increased in the early post-lesion period and recovered to below their original values late post-lesion.

Monkey R's fraction of saccades with a glissade decreased early post-lesion which recovered to pre-lesion values in the late post-lesion period. Average amplitude showed a stark increase in variability of glissade amplitudes initially after the lesion. The glissade amplitude is decreased late post-lesion relative to early post-lesion. There was no effect on glissade peak velocity and duration.

Monkey S showed no change in glissade kinematics in any of the categories studied. This could be explained by the low percentage of glissadic overshoots that this animal made during all epochs of this study.

In summary, due to the large variability in the extent of the OMV lesions, the post-lesion changes to the kinematic parameters of glissades were highly heterogeneous. However, one common feature observed across several monkeys was that these effects regularly underwent a quick recovery to pre-lesion or close to pre-lesion values.

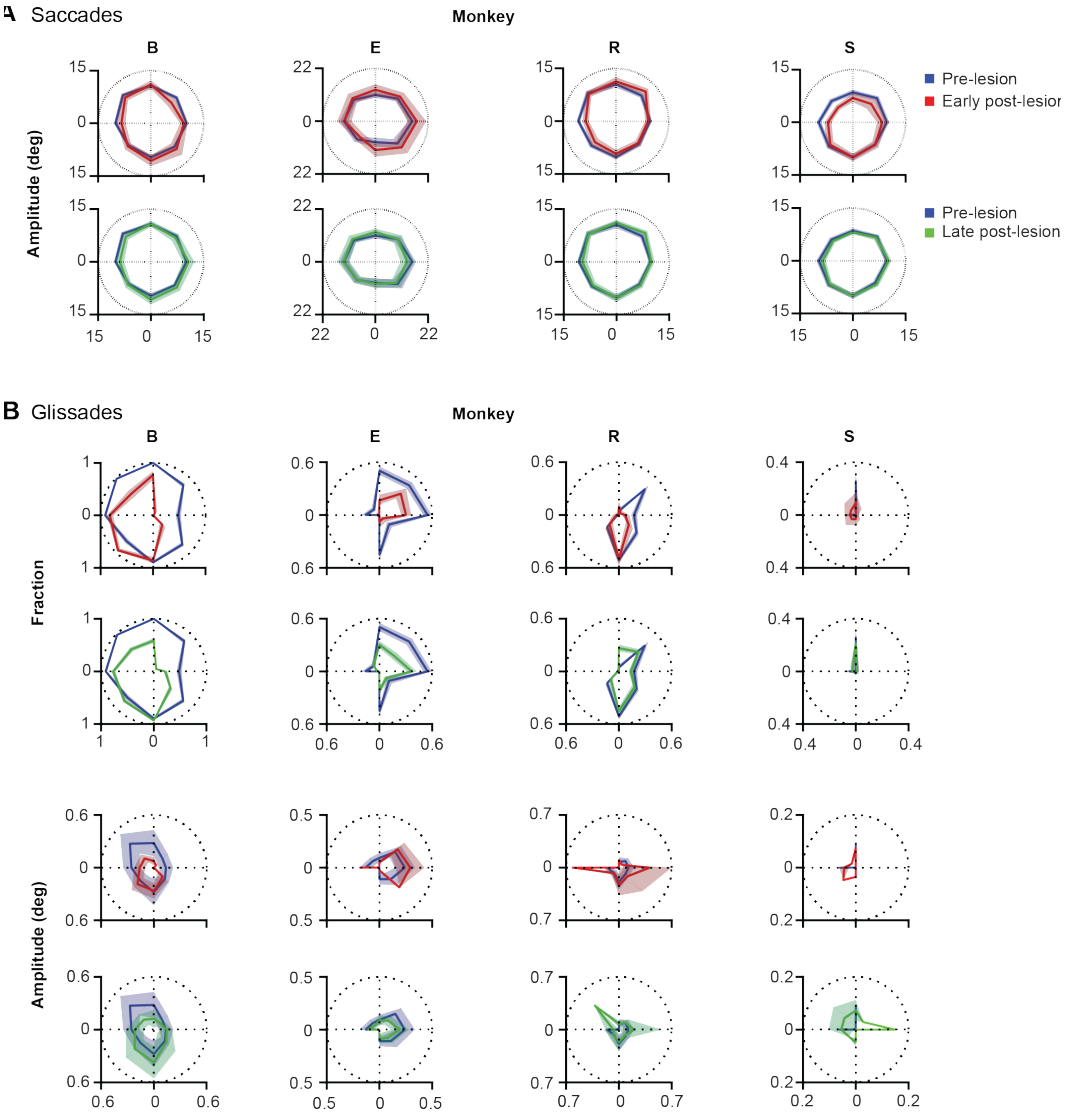

Figure 7. Direction specificity of lesion phenotype for glissades and saccades sorted for saccade direction. *A) Effect of lesion on saccade amplitude in different directions. Blue lines represent pre-lesion condition, red lines represent early post-lesion condition and green lines represent late post-lesion condition. B) Top two rows show fractions of saccade with a glissade sorted for saccades in each of the eight cardinal directions. Shading of fractions represents Jeffrey's interval. Bottom two rows show average glissade amplitude for saccades in each of the eight cardinal directions. Shading of amplitudes plots represent one standard deviation. Only overshooting glissades were used for this analysis. See Supplementary Table 5 for p-values and correlation coefficients between lesion time epochs.*

Direction specificity of glissadic overshoot amplitude and frequency sorted for saccade directions

Lesions to the OMV showed unique direction-dependent effects on saccade amplitudes (**Fig. 7A**). Monkey B primarily showed hypometria in the upper half of the visual field. Monkeys E showed hypermetria in the right quadrants. Monkey R showed hypometria in the bottom left quadrant and hypermetria in the top right quadrant. Finally, monkey S showed hypometria in the top quadrants (**Fig. 7A**).

To investigate whether the changes in glissade amplitude and fraction occurred in the same direction after the lesion, we calculated the fraction of saccades with a glissade and the average glissade amplitude per 8 saccade directions **(Fig. 7B**). This was done for all the lesion time epochs. To compare the directionality between time epochs, we calculated Pearson correlation coefficients of the directional distributions. First, we computed the correlation coefficient between the distribution of glissade amplitudes of the pre-lesion condition and the distribution of glissade amplitudes of the early post-lesion condition. If the correlation was significant, we concluded that glissade amplitudes in the different time epochs had a preference for the *same saccade directions*. If the correlation was non-significant, we concluded that the glissade amplitudes in the different time epochs had a preference for the *different saccade directions.* The same procedure was repeated for the other combinations of lesion time epochs: early-late and pre-late. The same analysis was also applied to the glissade numbers (fractions of saccade containing a glissade). We considered $p = 0.02$ as significant to correct for multiple testing, since we calculated correlations between the 3 groups (pre-early, pre-late, and early-late).

Monkey B showed no significant correlation in glissade amplitude and fraction between the pre- and early post-lesion period, but strong correlations in amplitude and fraction of glissade between early and late post-lesion ($R = 0.96, 0.94$; $p < 0.001$). This implies that the direction of amplitude and fraction of glissades changes from pre- to early post-lesion, but stays the same thereafter from early to late post-lesion (**Fig. 7B**, **Supplementary Table 5**).

In monkey E there was no correlation between amplitudes in any of the groups, showing glissade amplitudes changed in directional preference between all lesion epochs. A significant correlation between the fraction of glissades in the pre, early and late post-lesion existed, implying that the directional distribution of the glissade fraction was similar in all lesion epochs ($R= 0.83; 0.95; 0.82$, $p<0.02$ for all).

Monkey R showed no significant correlation in glissade amplitude between any of the groups thus implying that glissade amplitude in the different saccade directions changed between every lesion time epoch. Glissade fraction on the other hand was significantly correlated between the pre- and late post-lesion epochs ($R=0.86$, $p=0.007$) showing that the directionality of the fraction of glissades changed in the early post-lesion period and later recovered back to similar directionality in the late post-lesion period.

Monkey S showed no significant correlation in glissade amplitude between any of the groups, thus implying that glissade amplitude in the different saccade directions changed between every lesion time epoch. Glissade fraction, on the other hand, was significantly correlated between the pre- and late post-lesion epochs ($R=0.98$, $p<0.001$) showing that the directionality of the fraction of glissades changed in the early post-lesion period and later recovered back to similar directionality in the late post-lesion period.

When comparing glissadic overshoot direction with saccade direction it can be observed that glissades in all monkeys were in the opposite direction to the saccades that they were attached to (**Fig. 8A**). Relative glissade directions did not change after lesioning of the OMV in any of the monkeys. To test the difference in angles between pre-, early, and late post-lesion epochs, the circular analog to the Kruskal-Wallis test with Bonferroni correction was used (Fisher, 1995). **Figure 8B** shows circular means and circular standard deviations of relative glissade angles. The lesion had no effect on the direction of glissades in any of the experimental epochs (see **Supplementary Table 6** for p-values). These results show that glissade direction is strongly coupled to saccade direction, suggesting that glissades originate from the same motoneuronal drive signal as saccades.

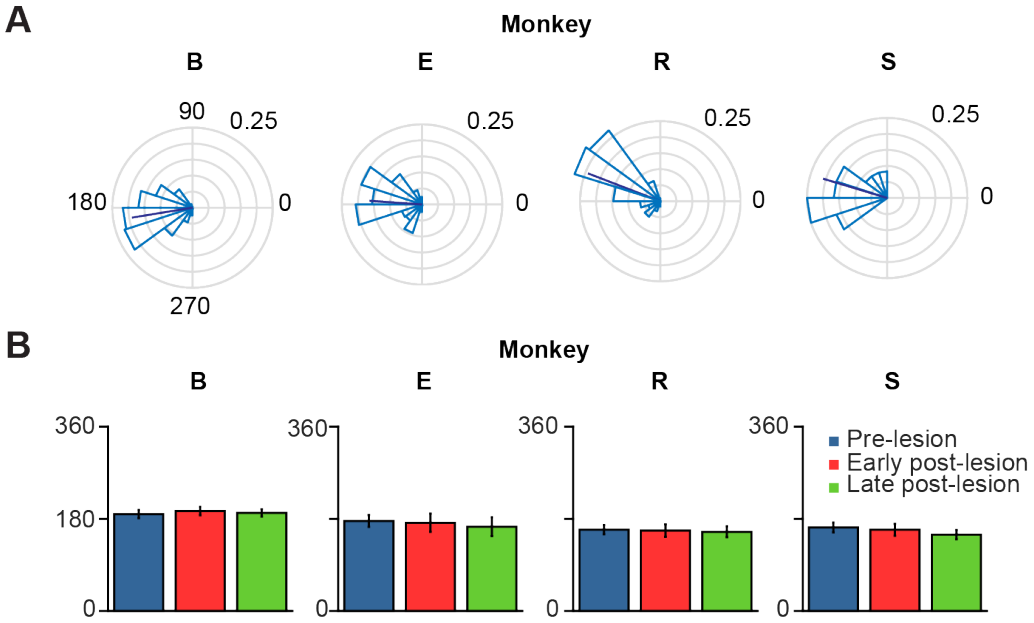

Figure 8. Polar plots of glissade angle relative to saccade. *A) Normalized polar histograms of glissade direction relative to saccade direction (all saccade directions set to 0°, glissade direction relative to saccade direction is defined as °saccade – °glissade) in the pre-lesion period. Dark blue line represents the average vector of all glissade angles. B) Mean glissade direction relative to saccade for pre-lesion and early and late post-lesion period. Only overshooting glissades were used for this analysis. Error bars represent one standard deviation. P-values of individual tests are i*n Supplementary Table 6.

Glissade characteristics during saccadic adaptation

Like many other movements, eye movements can be adapted by incorporating the errors from prior movements into the motor planning. This motor adaptation critically depends on the cerebellum (Optican and Robinson, 1980b; Tseng et al., 2007). Therefore, we set out to investigate whether glissades are adaptable by using a classical saccadic adaptation paradigm and one where the displacement was in the same amplitude range as a glissade. To that end we have used two monkeys

with an intact OMV (Mi, Mo), which we subjected to several saccade adaptation experiments. In these experiments eye position was tracked in the dark with infrared video eye tracker (Eyelink 1000 plus, SR Research). Video eye tracking can result in an overestimation of the glissades, because of pupil wobble in the iris. Fortunately, some discriminating features exist between pupil wobble and glissades. First, pupil wobble produces several peaks in the velocity profile, and second, the amplitude of pupil wobble is generally larger than that of glissades (Kimmel et al., 2012). **Figure 9A** shows the results of an outward saccadic adaptation experiment where the target jumped from 10 to 12°. We applied four experimental protocols (see Methods for details) performing both inward and outward adaptation experiments with a standard size adaptation step (2°, on a 10° primary saccade; where the amplitude of saccades gradually increased over time until it converged at 12° or decreased to reach 8°) and with a small adaptation step (0.5° on a 10° saccade; where the amplitude of saccades gradually increased over time until it converged at 10.5° or decreased to reach 9.5°) (McLaughlin, 1967; Pélisson et al., 2010). Although the saccade amplitudes robustly changed, glissade amplitudes from these saccades remained unaffected (**Fig. 9A**, right panel, black lines depict linear regression). Since these monkeys made comparable numbers of undershoots and overshoots, we analyzed them separately in the regression analysis. Neither of the monkeys showed any change in glissadic overshoot or undershoot amplitude over the course of the adaptation experiments in any of the adaptation protocols (**Fig. 9B** shows a matrix with the R^2 values of all adaptation experiments).

To investigate if saccadic adaptation had any effect on the frequency of occurrence of glissades, we compared the fraction of saccades with glissades at the beginning of the training to the fraction of saccades with glissades at the end of the adaptation (**Fig. 9C**). We pooled overshoots and undershoots when studying the fraction of saccades with glissades because we constrained the analysis to only the first and last 50 trials when most of the gain change in saccadic adaptation is noticeable. None of the experiments had an effect on the fraction of saccades with a glissade (**Fig. 9C** and **Supplementary Table 6** for R^2, p-values from z-test, and N numbers).

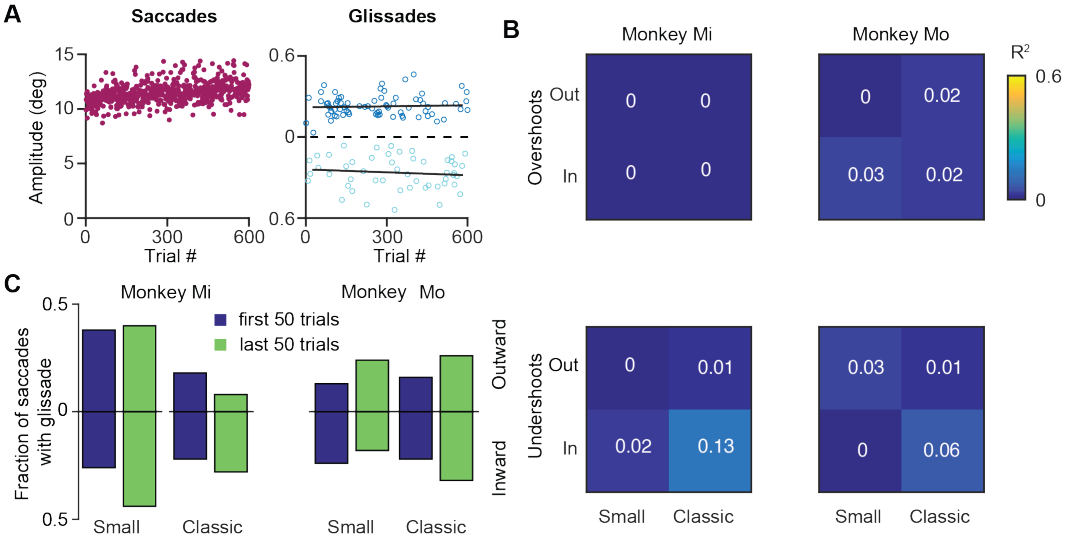

Figure 9. Effects of saccadic adaptation on glissades. *A) Example of a classical outward saccadic*

adaptation experiment from monkey Mo. Left panel, purple dots correspond to the saccade amplitudes gradually increasing over time. Right panel, dark blue dots display amplitude of the glissadic overshoots and light blue dots display amplitudes of the glissadic undershoots. Black lines represent a linear fit. B) Top panels display R2 of linear fits of glissadic overshoot amplitudes during inward and outward saccadic adaptation with a classical and small adaptation step. The bottom panels display the same for undershoots. Monkey Mi did not make any glissadic overshoots. Labels "Mi" and "Mo" denote each of the two monkeys. C) Fraction of saccades with overshooting and undershooting glissades pooled in the first and last 50 trials of the adaptation. Upward bars represent outward saccadic adaptation experiment and downward bars represent inward saccadic adaptation experiments for p-values see Supplementary Table 7.

5.3 Discussion

The cerebellum monitors the accuracy of eye movements and adjusts to errors in the gaze through saccadic adaptation (Optican and Robinson, 1980a; Shadmehr et al., 2010). We investigated whether glissades, the occasional overshoots and undershoots that accompany a saccade, are actively controlled by the cerebellum, and to what extent they are susceptible to sensorimotor adaptation. We found mixed evidence for cerebellar involvement in glissade control. On the one hand we found that cerebellar lesions did impact the characteristics of the glissades. However, these features could not be influenced by saccadic adaptation, even though this form of motor learning has been shown to prominently depend on an intact cerebellum (Takagi et al., 1998; Barash et al., 1999).

To find out whether the cerebellum influences the kinematics of glissades we used an eye movement dataset from a cerebellar lesion study performed on four monkeys, and new data of two monkeys with an intact cerebellum. Analyzing the pre-lesion eye movements, we established that saccades with a glissade had higher peak velocities, accelerations, decelerations and longer durations than saccades without a glissade (**Fig. 3**). Even though saccades with glissades took more time to reach fixation, the glissade itself did not contribute to bring the eye closer to the target (**Fig. 4**). These characteristics were consistent across all monkeys, indicating that glissades do not improve gaze accuracy. Furthermore, glissade direction was heavily dependent on saccade direction. Due to a substantial variation in lesion severity (**Table 1**) we identified a diverse phenotype of changes in the glissade profiles. Depending on the animal, changes in frequency of glissade occurrence, amplitude of glissades, peak velocity and duration could be observed (**Fig. 6**). Recovery of glissade abnormalities followed clear exponential progression in monkeys E, R and S. On average the acute recovery time was estimated at ~7 days post-lesion for those two monkeys. With the exception of monkey B, glissades were most pronounced in the early post-lesion period. Monkey B displayed an unusually high frequency of glissades in the pre-lesion condition. This monkey underwent repeated electrophysiological recordings from the SC. It is known that besides the brainstem, the SC also provides mossy fiber input to the OMV and that electrical stimulation of the SC is sufficient to elicit saccades (Sparks and Hartwich-Young, 1989). Further, it has been observed that muscimol injections in the intermediate layers of the SC can alter saccade trajectories (Aizawa and Wurtz, 1998). Considering this, we suspect that the high baseline frequency of glissades was a result of the incremental damage from SC experiments. Surprisingly, this initial high frequency of glissades was decreased post-lesion; we speculate that the cerebellum had initially overcompensated for the output of the damaged SC, which was diminished when the OMV was also lesioned. Similar phenotypes have been observed in other studies investigating double lesions. It has been shown that cats with

an ablated paravermis initially display tonic flexion of the ipsilateral limb, high stepping and ankle instability when walking, but recover from most of these deficits within 2-5 days. However, animals with pre-existing lesions to the red nucleus, which receives inputs from the cerebellum, showed no tonic flexion symptoms (Yul, 1972). Another example exists in the visual system, where unilateral cortical blindness, resulting in contralateral hemianopia (blindness to one half of the visual field), can be improved by lesioning of the ipsilateral SC; this has been reported as the Sprague effect (Sprague, 1966). Notably, this explanation for the higher baseline rate of the glissades is merely a hypothesis and further experiments with specific SC lesions are needed to establish a causal relationship. Although unlikely, we cannot exclude that this high fraction of glissades is merely a reflection of individual variability in monkeys. Interestingly, the recovery times of the changes to the glissades which we observed in our study were similar to the ones reported for the paravermal lesions discussed above. As seen in the results, the post-lesion increase in the fraction of saccades with a glissade was transient and recovered with a time course similar to that of the saccade recovery-time. The latter was in line with previous studies, which show that saccadic dysmetria is reversed quickly following lesions to the oculomotor vermis (Takagi et al., 1998; Barash et al., 1999; Ignashchenkova et al., 2009). The compensatory mechanism enabling the recovery is currently unknown, but two studies of natural lesions to the FOR in humans (e.g. through hemorrhage or tumor) do not show any recovery in saccadic dysmetria over time (Büttner et al., 1994; Straube et al., 1995). The FOR receives direct mossy fiber inputs from the same areas in the nucleus reticularis tegmenti pontis and paramedian pontine nucleus, which provide mossy fiber inputs to the OMV. Strikingly the mossy fiber projections to the OMV and FOR also share similar topographical organization (Yamada and Noda, 1987; Noda et al., 1990). Cells from the saccade region in the NTRP discharge 20-30 ms before the onset of a saccade in a direction-selective manner (Crandall and Keller, 1985). Additionally, the FOR receives collaterals from the part of the medial accessory olive that also provides climbing fibers towards the OMV (Ikeda et al., 1989; Noda et al., 1990). Therefore, these olivo-nuclear projections likely carry the same information as the OMV receives. Together these inputs could be utilized to compensate for the ablation of the OMV through plastic changes in the FOR.

To find out to what extent glissades are susceptible to sensorimotor adaptation we investigated whether glissades can be adapted using an inward or outward saccadic adaptation paradigm in two monkeys with intact OMV. We rationalized that even if glissades reflect a mismatch between pulse and step, a neural correlate of the mismatch could conceivably a posteriori correct for saccadic vector imprecision. Given that inward and outward adaptation paradigms rely on different structures and affect saccade kinematics in a different way, we tested both conditions. Based on Shadmehr's (Ethier et al., 2008) adaptation data, which suggest that inward adaptation affects saccade kinematics by decreasing the height of the pulse, we expected to see a change in the glissades in this test. However, we found that glissades were not susceptible to adaptation through either a standard saccadic adaptation paradigm (10% of primary saccade gain) or one where the adaptation step is in the same order of magnitude as the glissade itself (0.5°). Furthermore, the frequency of the glissades also remained unchanged in both outward and inward adaptation, even when we analyzed over- and undershoots separately.

From this, we conclude that glissades are not readily adaptable, at least using the classical saccadic adaptation paradigm. It remains an open question whether exponential target drift induced immediately at saccade offset (similar to visual perturbations used to elicit ocular following responses) could lead to glissade adaptation. Another manipulation that could affect the glissade kinematics and probability is a change in the spatiotemporal contrast, which we know can

be increased at low temporal frequencies (Westheimer and McKee, 1975). We hope to see future experiments addressing both of these questions.

The lesion dataset and the adaptation dataset were obtained using different eye tracking methods. The former with the sclera-embedded search coil technique and the latter using the video eye-tracking method. The method of eye tracking is of major importance when measuring glissades, since these movements are close to spatial and temporal resolution limits of most tracking methods. Advantages and disadvantages of different methods for precise eye tracking have been a topic of a discussion for some time (van der Geest and Frens, 2002; Kimmel et al., 2012) and some inconsistencies have been observed when measuring glissades with different eye tracking methods. Kimmel et al. (2012) compared the sclera-embedded search coil technique with the video eye tracking based on pupil center of mass by simultaneously recording from the same eye in macaque monkeys. They showed that pupil-based methods are more sensitive to recording post-saccadic oscillations (PSO). When the eye stops, the pupil occasionally wobbles in the iris at the end of the eye movement resulting in a PSO. Therefore, pupil-based eye trackers for saccades where pupil wobble is present display a signal which is a combination of actual eye movement and pupil wobble. These PSO's could easily be mistaken for glissades, although no actual movement of the eye takes place during this type of oscillation (Kimmel et al., 2012; Nyström et al., 2013). Based on these studies, the sclera-embedded search coil technique seems to be the preferred method for measuring glissades, since it does not suffer from errors resulting from wobble of the pupil inside the iris. In order to reduce errors resulting from our eye tracking approach we employed the following steps: (1) Glissades were distinguished from PSO's (and confirmed by an additional experimenter via visual inspection; see Methods for details) in that they showed a single rather than multiple peak(s) in their velocity profile and that their amplitude and velocity were lower than those of PSO's (Kimmel et al., 2012); (2) Saccades within each experiment were shuffled so that the analysis was blinded to the trail number. This way the glissades were labeled without a priori knowledge of whether they belonged to saccades recorded at the beginning or at the end of the experiment. Taken together, the distinct velocity profiles allowed us to mark glissades alone and ignore PSO's, and trial shuffling ensured impartial analysis. Therefore, we are confident that the observed lack of changes in the glissade amplitude and fraction, in any conditions throughout the adaptation, was not due to any systematic mislabeling of the PSO's.

It is possible that other cerebellar or non-cerebellar regions play a role in glissade formation. A systems model by (Bahill et al., 1978) suggests that glissades are a product of errors in the width of the pulse (i.e. duration) in the pulse-step control signal of saccades. In Bahill's model, the pulse brings the eye quickly to the new target and the step keeps the gaze fixed in the new position. The production of a consistently accurate pulse is dependent on the OMV (Optican and Robinson, 1980a), whereas the step component is dependent on the flocculus, nucleus prepositus hypoglossi and medial vestibular nuclei (Sparks, 2002). Indeed, lesion studies of the flocculus cause inability to keep the gaze in an eccentric position (Zee et al., 1981). The gaze drift after a saccade in floculecotomied monkeys has a duration of 40-150 ms, whereas glissades are in the range of 10-40 ms. Furthermore, post-saccadic ocular following of a persistent full-motion stimulus is dependent on the flocculus (Optican and Miles, 1985; Optican et al., 1986). Onset of following has an initial latency of 50-60 ms after the saccade, which is nullified after adaptation and is also abolished after flocculectomy. Glissades on the other hand are always appended directly to the saccade and their direction is strongly coupled to the direction of the saccade.

In Bahill's framework, a mismatch between the amplitude of the pulse and the step explain the direction and amplitude of the glissades. Moreover, it is presumed that the step results from the neural integration of the pulse. Systematic pulse integration errors would lead to systematic changes in glissades, meaning glissades of similar saccades should have a similar direction (over- or undershooting). In our case, we have discovered that saccadic adaptation paradigms did not affect glissade systematically, meaning that whichever neural process matches the pulse and the step, an inherent source of variability results in a stable proportion of glissades, with kinematic parameters largely independent of target error of the initial saccade.

We argue that our data suggest that glissades are a product of an imprecision of the pulse integration, as the parameters of the glissade do not seem to be independently controlled. An undershooting glissade occurs when the pulse is insufficient to match the step and thus the eye slowly drifts to the step equilibrium position. Conversely, in overshooting saccades the pulse is in excess, adding an overshoot at the end of the saccade back to the encoded step amplitude. Presumably, the OMV keeps saccade amplitudes accurate by complementing the drive of the pulse width, hence the commonly observed hypometrias after lesions of the OMV. It has been hypothesized that the OMV achieves this by tracking the saccade as it progresses and choking off the drive and stopping the pulse when the target is reached (Optican and Pretegiani, 2017). Consequently, when the OMV is ablated, saccades become hypometric, as we argued, due to inaccurate termination of the pulse. The glissades kinematics however do not show such consistent change. In our experiments two out of four monkeys display more prominent glissades (monkey E and R). This change is far less dramatic than the saccade impairment. In the other two monkeys, glissade fraction is either stable or decreases (for a possible explanation of this phenomena in monkey B see the discussion above). That in itself suggests that the OMV does not play any functional role in determining glissade parameters. In order to fully investigate the role of the cerebellum in the glissades more studies are needed, specifically in the contributions of the flocculonodular lobe.

In summary, our results show that saccades with glissades had a longer duration, higher peak velocities, and faster peak decelerations and accelerations. Lesioning the OMV had an effect on glissade frequency, amplitude, peak velocities and duration. Furthermore, these effects recovered in an exponential fashion over the course of days. Glissade deficits, like saccades, were more pronounced in some directions. Lastly, glissades were not adaptable using either a classical inward or outward saccadic adaptation paradigm, nor in an adaptation paradigm with adaptation step commensurate with the glissade. Taken together, our findings indicate that glissades are the consequence of an error of the oculomotor system, rather than a functional movement controlled by the cerebellum. Specifically, it seems likely that glissades are a pulse integration error of the pulse-step command caused by inaccurate termination of the pulse.

5.4 Materials and Methods

Experimental animals and tasks in the lesion studies

For the lesion experiments, eye movements of four monkeys (Macaca mulatta, referred to as monkeys B, E, R, and S) were recorded using the scleral search coil tracking method (Judge et al., 1980) (spatial resolution < 0.1°, temporal resolution 1 ms). Animals were painlessly head restrained through an implanted head-post and trained to make visually guided saccades to targets (white

spot with a diameter of 0.33° and a luminance of 12 cd/m^2) while seated 22 cm from a computer monitor (21-in monitor; Flexscan F760i-W; frame rate: 72 Hz; 1280x1024 pixels). The eye was tracked unilaterally in all experiments. Data was collected from: both right and left eye but never simultaneously. Scleral search coils were calibrated by having the animal make visually guided eye movements to 9 points on the screen at different locations. The animal was visually monitored by an infrared camera inside the setup that allowed the experimenter to make sure that the animals were looking at the target. For details on surgical procedures and OMV lesions see (Ignashchenkova et al., 2009).

Fixation targets were presented for 500 ms after which saccade targets appeared. The saccade targets had an eccentricity of 10° and were presented in one of eight different (0 – 315°) directions for a duration of 700 ms. Monkeys were trained to make saccades to the target for a fluid reward (water or juice, depending on the monkey's preference) that they received if they moved their eyes to the target within 400 ms after its appearance.

Saccades were considered to be correctly executed when the animal fixated its gaze within a square region around the target of 2 - 2.5° side length. Animals were allowed to make a secondary saccade as long as fixation was reached inside the square window within 400 ms after the appearance of the target. Only primary saccades were considered for analysis. These values for the fixation window around the saccade targets were determined bearing in mind that our monkeys will undergo cerebellar lesions and their saccades will be very inaccurate after this procedure. Therefore, in the early days following the lesion the fixation size window was extended 2 - 4 fold.

Experimental animals and tasks in the saccadic adaptation

For the saccadic adaptation experiment we used two different monkeys (Macaca mulatta, referred to as monkeys Mi and Mo). Animals were painlessly head restrained through an implanted titanium head-post and trained to make visually guided saccades to targets. The eye was tracked unilaterally in all experiments. Data was collected from the right eye in both monkeys.

The intra-saccadic step paradigm (McLaughlin, 1967) was applied for adaptive shortening or lengthening of saccades. Animals were trained to focus on a fixation dot in the center of the monitor (frame rate: 100 Hz, 1152 x 864 pixels), placed at the viewing point distance of 52 cm. Eye movements were recorded in the dark with an infrared video eye tracker at 1000 Hz (Eyelink 1000 plus, SR Research) while the animal was head restrained through an implanted head-post. Standard Eyelink 5 point calibration with 10° eccentricity was used before every experiment. The right eye was tracked in all experiments. At the start of an adaptation trial, when fixation was detected, a saccade target appeared horizontal and ipsilateral from the fixation point in the periphery of the visual field at 10° eccentricity. The target was displaced inward or outward when the velocity of the eye exceeded 30°/second. Target displacements could have different amplitudes; classical inward or outward adaptation displacements were 2° (10° to 8° for inward adaptation; 10° to 12° for outward adaptation), whereas small saccadic adaptation displacements were 0.5° (10° to 9.5° for inward adaptation; 10° to 10.5° for outward adaptation). Each experiment contained between 550 and 600 trials. Saccades were considered to be correctly executed when the animal fixated its gaze within a circle region around the target of 3° diameter.

Data Analysis

Eye movement data were analyzed using custom written MATLAB programs (MathWorks Inc.). Saccade onset and offset were detected on the basis of an adaptive velocity threshold, which consisted of 3 standard deviations (std) of the noise during fixation. Position traces were differentiated with the 'diff' function of MATLAB ($y = x_{i+1} - x_i$). Acceleration was acquired by further differentiating the velocity signal. We used a Savitzky-Golay filter for smoothing of the raw traces and a median filter for further smoothing of acceleration signals.

Only glissades immediately following the primary saccades were considered in this analysis. In accordance with previously published results, monkeys B, E, R and S displayed some number of corrective/secondary saccades, particularly in the early post-lesion condition (Ignashchenkova et al., 2009). In the pre-lesion and late post-lesion condition, very few corrective saccades were detected, with the exception of monkey E who showed corrective saccades also in the baseline condition.

All glissades were selected by hand, based on the position and velocity profile of the eye movement by a single analyst. Selection of glissades was done without knowing which animal the file belonged to or whether it was from pre- or post-lesion. For the saccadic adaptation experiments, the trials were shuffled so the analyst did not know he was looking at saccades from the beginning of the adaptation or from the end. To be classified as a glissade, an overshoot or undershoot had to stand out clearly from the background noise as determined by the 3 std baseline criterion; either in the form of a clearly distinguishable peak, directly attached to the saccade (**Fig. 1B**), or as a shoulder visible as a deflection (**Fig. 1C**) from the normal deceleration profile.

Post saccadic oscillations (PSO) are a phenomenon that can be present in the signal of video eye trackers. PSO's are distinguishable from glissades because PSO's show multiple peaks in the velocity profile whereas glissades show only one. Additionally, PSO's are of higher velocity and amplitude than glissades (Kimmel et al., 2012). These features allow the analyst to mark glissades and ignore PSO's. Glissades were classified as undershoots or overshoots relative to the fixation. If the early end of the saccade, i.e., the start of the glissade, passed the eventual fixation point, it was classified as an overshoot, whereas if after the early end of the saccade the eye moved further toward the fixation point, it was classified as an undershoot.

Statistics

If statistical testing involved two groups, a student's t-test was used unless the assumptions of normality and equality of variance were violated (Kolmogorov-Smirnov test or F-test for equal variances $p<0.05$). In these cases, a Wilcoxon rank sum test was used. When more than two groups were involved, we used ANOVA with Bonferroni correction, unless any of the previously mentioned assumptions were violated; in which case we used the Friedman test. In cases of fractions, error bars represent Jeffreys interval and the z-test for proportions was used to determine significance. For circular statistics we used the *circle stats* toolbox for MATLAB. Since there is no post-hoc test available for circular ANOVA, we performed the test on all groups individually and Bonferroni corrected the p-value (alpha = alpha/ number of hypotheses). All statistical analysis was done using MATLAB.

To estimate the recovery times of the effect of the lesion on saccade amplitudes, glissade amplitudes and fraction of saccades with a glissade, we calculated the half-life of an exponential fit to

these parameters. The formula [f(x) = a*exp(-x/b) +c] was used for the exponential fit. Subsequently, the half-life ($t_{1/2}$) was calculated with [$t_{1/2}$ = tau*ln(2)], where tau is b in the exponential function. The early post-lesion time interval was defined as 3 * $t_{1/2}$ based on the exponential fit to the saccade amplitudes in monkeys R and S. In monkey E we calculated the half-life from the glissade amplitudes, since there was no significant fit to saccade amplitudes. Monkey B did not have significant fits to either saccades or glissades. Therefore, we used an average half-life of the fits to saccade amplitudes from monkeys R and S to define the early post-lesion interval.

Error bars or shadings signify one standard deviation unless otherwise specified. Box and whisker plots contain median with box edges indicating the 25th and 75th percentile and the whiskers extend to the most extreme data points not considered outliers. Outliers determined as values larger or smaller than median ± 2.7 SD (standard value for whiskers in MATLAB).

To evaluate whether lesions affected glissade parameters (e.g. glissade amplitude) related to the eight cardinal saccade directions, we replotted the rose plots, shown in **Figure 7**, as histograms which resulted in two distributions. We then calculated the Pearson's correlation coefficient between the independent variables of the distributions.

For saccadic adaptation experiments, a linear regression was fitted using all glissadic over- or undershoots (analyzed separately) to analyse the glissade amplitude during the adaptation. To calculate the fraction of saccades with a glissade we used the first 50 and last 50 trials and applied z-test for proportions test to obtain the statistics.

Acknowledgements

N.F. and A.I. designed and performed the experiments. N.F. analyzed the data. A.B, C.Z. and P.T. supervised the project. M.N. and C.Z. suggested the hypothesis and provided conceptual feedback. N.F., C.Z. and A.B. wrote the manuscript. We would like to thank Kor Brandsma and Anneke Ditewig for excellent technical assistance and Amy Hassett for proofreading the manuscript.

Conflict of Interest:

None declared.

Ethical statement

All experimental and surgical procedures complied with the NIH Guide for Care and Use of Laboratory Animals (National Institutes of Health, Bethesda, Maryland), and were approved by the institutional animal care and use committee of Tübingen (RP Tübingen, FG Tierschutz; lesion studies) and of the Royal Netherlands Academy of Arts and Sciences (saccadic adaptation studies).

Funding

This work was supported by the Dutch Organisation for Medical Sciences, Life Sciences, and Social and Behavioural Sciences, NeuroBasic, ERC-adv, and C7 programs of the EU (C.Z.); Dutch Organisation for Medical Sciences, Life Sciences (A.B.)

5.5 Supplementary data

	Boris		**Elvis**		**Rocky**		**Spock**	
	N		**N**		**N**		**N**	
total	882	100%	874	100%	1473	100%	364	100%
overshoots	704	80%	256	29%	300	20%	12	3%
undershoots	29	3%	33	4%	108	7%	46	13%
no glis	149	17%	306	35%	1065	72%	306	84%

Supplementary Table 1: *Percentage of saccades with glissade undershoots or overshoots in the pre-lesion condition.*

ANOVA	*No glis - Early end*	*Early end - Glis end*	*No glis - Glis end*	*Correlation coefficient*
B	1	0.30	0.37	-0.008
E	0.52	1	0.96	0.32
R	0.07	0.44	1	-0.38
S	1	1	1	-0.42

Supplementary Table 2*: p-values of ANOVA and correlation coefficients shown in* **Figure 4**.

	B			**E**			**R**			**S**		
	R^2	**$t_{1/2}$**	**p**	**R^2**	**$t_{1/2}$**	**p**	**R^2**	**$t_{1/2}$**	**p**	**R^2**	**$t_{1/2}$**	**p**
Saccade amplitude	0.34	~	0.19	0.07	~	0.54	0.62	3	**0.001**	0.85	1.7	**>0.001**
Glissade amplitude	0	~	0.94	0.81	2	**>0.001**	0.19	~	0.08	0.11	~	0.21
Glissade fraction	0.018	~	0.41	0.17	~	0.19	0.34	0.2	**0.02**	0.6	3.8	**0.003**
Time early post-lesion	7 days			6 days			9 days			6 days		

Supplementary Table 3*: Decay time constants, coefficients of determination and p-values from regression analysis on saccade amplitude, glissade amplitude and glissade fraction over time for exponential fits (black lines) in* **Figure 5**. *Decay time constants were calculated only for significant fits (significant p-values indicated in bold).*

	B (N=149)			**E (N= 43)**		
	Pre- early	*Early- late*	*Pre- late*	*Pre- early*	*Early- late*	*Pre- late*
Fractions	**<0.001**	0.83	**<0.001**	**<0.001**	0.39	**<0.001**
Amplitude	**0.002**	0.07	0.34	**0.045**	**<0.001**	**<0.001**
Velocity	**0.002**	0.85	0.05	1	0.16	0.22
Duration	**<0.001**	0.59	**<0.001**	**<0.001**	**<0.001**	1
	R (N=41)			**S (N=20)**		
	Pre- early	*Early- late*	*Pre- late*	*Pre- early*	*Early- late*	*Pre- late*
Fractions	**<0.001**	**0.01**	0.13	0.69	0.49	0.77
Amplitude	1	**0.02**	**0.002**	0.20	0.83	0.59
Velocity	0.15	0.19	1	0.06	0.005	1
Duration	0.49	0.65	1	1	0.10	0.14

Supplementary Table 4*: Comparison of glissade kinematics between lesion groups. p-values of data reported in* **Figure 6.** *Fractions were tested with z-test for proportions. Amplitude, velocity, and duration were compared by ANOVA's with Bonferroni corrections as a post-hoc test. n's in top row represent the number of glissades used per group (pre, early, late). Significant p-values indicated in bold.*

		B			**E**			**R**			**S**		
		Pre-Early	*Pre-Late*	*Early-Late*	*Pre-Early*	*Pre-Late*	*Early-Late*	*Pre-Early*	*Pre-Late*	*Early-Late*	*Pre-Early*	*Pre-Late*	*Early-Late*
Fraction	R	0.55	0.44	0.94	0.83	0.95	0.82	0.69	0.86	0.73	0.77	0.98	0.80
	p	0.16	0.28	**<0.001**	**0.01**	**<0.001**	**0.01**	0.06	**0.007**	0.04	0.02	**<0.001**	0.02
Amplitude	R	0.23	0.09	0.96	0.85	0.87	0.71	0.54	0.40	0.09	0.64	0.10	-0.08
	p	0.61	0.85	**<0.001**	0.03	0.02	0.11	0.22	0.37	0.85	0.09	0.81	0.86

Supplementary Table 5*: Statistical analysis of the data presented in* **Figure 7***. Fraction denotes the fraction of saccades with a glissade in respect to saccades in each of the eight cardinal directions. Glissade amplitude was calculated for glissade containing saccades in each of the eight cardinal directions. We replotted the rose plots as histograms which resulted in two distributions (for example, pre and early). From these we calculated the correlation coefficient between those two distributions. R-values represent Pearson correlation for the fraction and amplitude as defined above compared between different lesion time epochs (pre-lesion vs early post-lesion, i.e. Pre-Early; pre-lesion vs late post-lesion, i.e. Pre-Late; and early post-lesion vs late post-lesion, i.e. Early-Late) P-values represent significance of the correlation coefficient (significant p-values indicated in Bold).*

	pre-early	*early-late*	*pre-late*
B	0.94	0.41	0.28
E	0.42	0.38	0.52
R	0.85	0.84	1
S	0.51t	0.68	0.21

Supplementary Table 6*: Glissade direction relative to saccade direction compared between pre-lesion, early and late post-lesion. p-values of circular Kruskal-Wallis test of* **Figure 8B***. Tests were considered significant when p<0.0167 (Bonferroni correction for 3 tests).*

Monkeys	*Outward*		*Inward*	
	Classic	*Small*	*Classic*	*Small*
	P-value z-test			
Mi	0.14	0.84	0.49	0.06
Mo	0.22	0.05	0.26	0.46
	# trials			
Mi	600	565	600	600
Mo	600	600	600	600

Supplementary Table 7*: Coefficient of determination (R^2) for regression between glissade amplitude, p-values of z-test for proportions used to compare first and last 50 trials and the number of trials per saccadic adaptation experiment* **Figure 9B**.

Chapter 6:

General discussion

Living in social groups has several costs and benefits. Larger groups provide protection from predators, opportunities for learning strategies for environmental adaptation and increased chances for mating. On the other hand, living in smaller groups causes less competition for resources like food. Individuals living in large groups also require a certain level of social cognition that makes dealing with hierarchy possible. They need access to information about hierarchical positions of fellow group members, their behavior and emotional disposition (Emery, 2000). As most people intuitively know, many of these traits can be read from the eyes. Moreover, catching someone looking at us evokes a reaction that is initially detected subconsciously (Senju and Johnson, 2009; Stein et al., 2011). For macaques and most other primates direct eye contact is considered threatening and thus something that is generally avoided (Van Hooff, 1967; Harrod et al., 2020). The tolerance for eye contact varies as a function of social structure, where primates with a more egalitarian social structure have a higher tolerance for eye contact (Harrod et al., 2020). Macaques have low tolerance for eye contact, placing them roughly between chimps and gorillas, with gorillas being slightly less and chimps slightly more tolerant. Out of 88 primate species humans are the only ones that have a white sclera, making it easy to discern their gaze direction (Kobayashi and Kohshima, 1997). Since in many primate species direct eye contact is threatening, a dark sclera helps obscure gaze direction and thus makes it easier to read relevant social cues from other faces without being noticed. Accordingly, monkeys that viewed pictures of other monkeys that had their eyes averted made more eye contact with the picture, than with pictures of monkeys who looked directly at them (Keating and Keating, 1982). Clearly, planning of eye movements is heavily influenced by social cues.

For adequate visual perception and visually-guided decision making, it is essential to separate relevant from irrelevant visual information. We understand our visual world by shifting attention overtly to stimuli by moving our eyes and aligning the fovea with the target of interest. This is however not always advantageous. As explained above, it can be desirable to avoid direct eye contact. To improve access to visual information, perception outside the fovea can be enhanced through covert attention shifts, giving it more weight in the visual processing stream (Lowet et al., 2018). Covert attention shifts are faster than overt attention shifts and decrease reaction times for overt attention shifts (Posner, 1980). A wealth of neuroimaging evidence exists that implies that mechanisms of covert attention overlap with those that control the programming of saccades (Corbetta et al., 1998; Nobre et al., 2000). This is collectively called the ''premotor theory of attention'' and proposes that the same circuit that is used for generating movements, also is active during attention shifts, rather than a separate substrate that regulates attention (Rizzolatti et al., 1987). In **Chapter 4** I investigate how saccade planning on the basis of a stimulus to which no direct eye movements are allowed is represented in the dentate nucleus (DN) of the cerebellum.

Another approach to avoid improper eye contact is by looking away from a stimulus. In **Chapter 3** we study this in an isolated non-social paradigm called the pro- and antisaccade task, where a saccade to the mirror position of an appearing target must be made. The subject has to suppress a reflexive saccade to the target and invert the target vector to make a saccade to the unmarked mirror position. Meanwhile Purkinje cells (PCs) in the oculomotor vermis (OMV) and lateral cerebellum are recorded. Given the high stakes of oculomotor behavior in the social context but also in life and death situations, such as taking part in traffic, it is imperative that saccades are both fast and precise. To this end the OMV of the cerebellum continuously monitors and adjusts the saccades on the basis of end-point errors. In a lesion study of the OMV we review the quality of movement execution before and after the lesion (**Chapter 5**). Taken together, both planning and

execution relies heavily on the cerebellum. This is illustrated by the fact that patients with autism, a disorder affecting cerebellar development (Courchesne et al., 1994; Wang et al., 2014), suffer from problems with all the above mentioned facets of saccade planning: covert attention shifts (Townsend et al., 1996a), volitional saccades such as antisaccades (Goldberg et al., 2002), and inaccuracies in saccade kinematics performance (Johnson et al., 2012). Saccadic adaptation, a form of sensorimotor learning critically dependent on the OMV, is also deficient in people with autism (Johnson et al., 2013; Mosconi et al., 2013). Lastly, deficits to saccade related tasks are also present in dyslexia, a disorder that also involves cerebellar development (Nicolson et al., 2001; Freedman et al., 2017).

6.1 Primate research anno 2021

Primate research is a shrinking branch of neuroscience research. During the entire time I spent working on this thesis I was the sole researcher in the Netherlands doing cerebellar experiments on non-human primates (NHP). In recent years there has been international backlash against doing NHP research, going as far as researchers being bullied into giving up their primate research lines[1]. Regardless, many prominent researchers see its necessity, and keep doing primate research, moving their research lines to different countries such as China, where acceptance of NHP research by the public and authorities is much higher than in Europe[1]. The Dutch government wants to be a world leader in animal-free innovations by 2025, according to the national committee advice on animal research policy[2]. Moreover, recently, a petition was offered to the European Commission calling for an immediate ban on animal testing in general[3]. These developments illustrate the current sentiment surrounding animal research. The COVID-19 crisis, during which part of this thesis was written, can be solved through a vaccine. This is presently impossible to develop without animal research (Genzel et al., 2020). Cynomolgus macaques have similar lung pathology and virus shedding from the upper respiratory tract as humans, and are therefore an important COVID-19 animal model (Rockx et al., 2020). This high similarity and close evolutionary proximity to humans is one of the key values of NHP research (Mantini et al., 2013). Critically, NHPs represent the best available model of the human brain. Developments of new drugs, understanding infectious diseases and neuroscience are the most important research areas where NHPs are still needed according to the EU SCHEER report (Hoet et al., 2017). Essential clinical advances such as the recent breakthrough in which visual cortex implants were used for a 1024 pixel neuroprosthesis, enabling artificial vision, would not have been possible without NHPs (Chen et al., 2020).

These developments would not have been possible without decades of research on the cellular properties and mechanisms underlying the function of the brain. Basic neuroscience research on primates has led to much more insights than just the understanding of perception. Important cognitive functions such as decision making, working memory, reward representation and expectation, neural coding of categories, attentional deployment, recognition of objects or faces and many more are all examples of domains where NHPs provided essential insights. For example, the mechanisms underpinning attention in NHPs have been significant for understanding

1 https://www.sciencemag.org/news/2020/01/animal-rights-conflict-prompts-leading-researcher-leave-germany-china retrieved: 13-01-2021

2 https://www.ncadierproevenbeleid.nl/documenten/rapport/2016/12/15/ncad-advies-transitie-naar-proefdiervrij-onderzoek retrieved: 13-01-2021

3 https://www.transitieproefdiervrijeinnovatie.nl/documenten/rapporten/18/06/01/tpi-philosophy-and-approach retrieved: 13-01-2021

and treating patients with ADHD (Roelfsema and Treue, 2014). Therefore, it would be misguiding to distinguish ethical approval for clinical versus fundamental research; indeed many of the current therapies depend on earlier fundamental research. This thesis contributes to the understanding of the cerebellum performing cognitive and motor functions (**Chapter 3, 4 & 5**). The cerebellum's participation in cognitive and mental disorders is only recently starting to gain serious attention (Schmahmann, 1991; Schmahmann and Sherman, 1998; Wang et al., 2014). Consequently, knowledge of the physiology of healthy cognitive processes enables the invention of therapies aimed at normalizing the diseased brain state rather than treating symptoms.

To minimize harm when doing research on NHPs it is important to keep improving methodologies. The three R's. Replacement, Reduction and Refinement are the main pillars of improving animal research. In **Chapter 2** I outline the methods used in the current thesis. This will be published as a chapter in the book Neuromethods, expected 2021. Sharing of, and continually improving methodology is important for both the animals and science, as these refinements of methods enable more precise results and reduction in harm to the animals (Lemon, 2018). For instance, with the recent advances in 3D printing it is possible to print metals and thus make affordable and reliable implants on basis of the contour of the skull of the animal rather than bending premade implants during the surgery. This leaves less space for infection between the skull and the implant and thus promotes longevity of the implant (Chen et al., 2017). To this end developments to improve methodology are an active part of many research groups that work with primates.

6.2 Visual processing and planning of saccades

Volitional saccades such as memory guided saccade or antisaccades depend on the lateral cerebellum (Ohki et al., 2009; Kunimatsu et al., 2016). The behavioral tasks we study in **Chapter 3 & 4** require saccades that have similar mental demands. There are several similarities between the tasks. First, the decoding of a visual stimulus, second, memorizing the direction of an upcoming action until a go-cue, and last, to plan and initiate the movement and receive a reward. An important difference between the tasks is that in the Landolt C task the stimulus is in the periphery of the visual field, whereas in the pro- and antisaccade task it is presented centrally. Also, the Landolt C task has more extensive delay periods and different reward categories, including reward omissions and task irrelevant random rewards. Regardless, highly comparable properties are observed in the electrophysiological recordings. PCs and DN neurons exhibit responses in the action potential firing at short latency from the onset of the visual stimulus that provides instruction about the location of an upcoming saccade. Additionally, both cell types show direction-selectivity in their firing rate modulation, PCs notably with their complex spike responses. The activity modulation further also bridges the epochs of visual instruction and the saccade execution in both cell types, where timing of peak modulation of different cells is spread out over the trial. Since DN neurons are downstream of PCs, it is possible that DN neurons in the Landolt C task receive inputs from the same PCs in the pro- and antisaccade task. Furthermore, the modulation seems to be stronger in DN neurons, arguably because of the heavy convergence of PCs on DN neurons (Person and Raman, 2012). Beside the retrograde labeling of PCs in the D1 zone, coming from the DN, additional preliminary observations from the retrograde tracing in the DN show extensive labeling in Crus I/II (**Fig. 1**). This is approximately the same region as where PCs were recorded during the pro- and antisaccade task (**Chapter 4, Fig. 1**). In conclusion, the behavior and recordings of the Landolt C and pro- and antisaccade tasks seem to be derived at least partially from the same neuronal circuits.

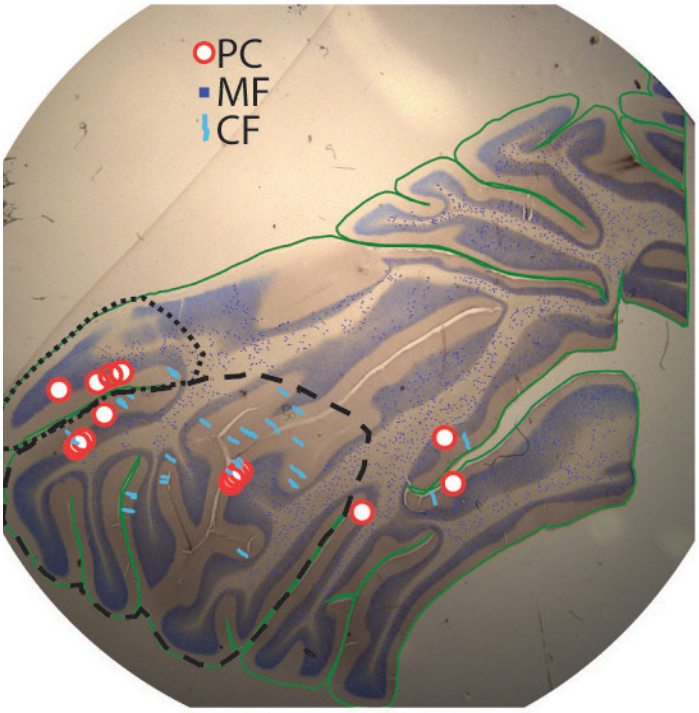

Figure 1. Retrograde labeling of afferents from the PC layer to dentate nucleus. *Dotted area indicates Crus I and the dashed area indicates Crus II. Abbreviations: CF, climbing fiber; MF, mossy fiber; PC, Purkinje cell.*

Around the turn of the millennium two landmark papers by Strick and colleagues provided direct evidence for the existence of closed loops between the lateral cerebellum and the prefrontal cortex (Middleton and Strick, 2001; Kelly and Strick, 2003). In these publications they described the different regions of the DN as output channels with distinct functions and cortical targets. PCs in Crus I/II project through the DN via the thalamus to the dlPFC (i.e., Brodmann's area 46), and back via the pontine nuclei (PN), a loop which participates in non-motor behavior. A second pathway that they studied is from the arm area of the primary motor cortex (M1) through the PN to lateral hemispheres of lobule IV-VI, which projects back through the thalamus to M1 (Kelly and Strick, 2003). These so-called cortico-cerebellar loops have become a hot topic in the cerebellar field and their physiological and behavioral properties are a target of many investigations (Ramnani, 2006). During the execution of the complex saccade tasks studied in this thesis multiple of these loops might be engaged sequentially.

The retrogradely labeled neurons from DN to Crus I/II are possibly part of a parallel loop with the dlPFC. Neurons in the same general area are connected with the dlPFC (Kelly and Strick, 2003). Lesions to the dlPFC cause an increase in deficits of memory guided saccades as a function of how long the saccade target has to be remembered, showing that the dlPFC participates in the working memory storage of saccades. This memory storage is maintained by persistent firing of dlPFC cells (Gaymard et al., 1998; Bruinsma, 2020; van Vugt et al., 2020). In the Landolt C task,

a delay of at least 500 ms exists between the offset of the visual stimulus and the presentation of the saccade targets. In this period the animals have to remember the saccade direction. Perhaps the neurons labeled in **Figure 1** are part of a loop between Crus I/II and the dlPFC that participate in facilitating bridging this delay period (**Fig. 2A**). Furthermore, lesions to the dlPFC also cause deficits in antisaccades, conceivably because the dlPFC suppresses cells in the SC and FEF that would otherwise initiate a reflexive prosaccade (Munoz and Everling, 2004). Hence, in the Landolt C task the dlPFC might suppress reflexive saccades to the peripheral Landolt C, something the monkeys were very much inclined to do during training. Preparatory activity in the DN of mice is very similar to that in the anterolateral motor cortex (ALM), this preparatory motor cortex preparatory activity is maintained on the basis of persistent firing of a cerebro-cerebellar loop with the DN (Chabrol et al., 2019). Both in the Crus I/II PCs recorded during the pro- and antisaccade task and the DN neurons recorded in the Landolt C task sustained activity bridges the instruction and saccade execution epochs. Consequently, it is possible that the Crus I/II output channels through the DN towards the dlPFC contributes to maintenance of working memory traces for the upcoming saccade.

The initial part of both the pro- and antisaccade task and the Landolt C task requires the decoding of a visual stimulus. Indeed, in both tasks following the onset of the stimulus, neurons become active after short delays. In the Landolt C task, the perception of the stimulus can be enhanced by making covert attention shifts towards the target (Moore and Zirnsak, 2017). A physiologically defined sub-population of DN neurons (**Chapter 4, Fig. 3**), which are active during the stimulus epoch in the Landolt C task, show specific modulation favoring the direction of the stimulus rather than the upcoming saccade. As discussed in **Chapter 4**, these neurons are part of the D1 zone, which connects with the FEF, and could thus form a visual output channel of the DN (**Fig. 2B**) (Lynch and Tian, 2006; Prevosto et al., 2010; Voogd et al., 2012). The FEF resides at the intersection between visual attention processing and motor responses (Schafer and Moore, 2007; Gregoriou et al., 2012). A striking duality exists in the relation of cells toward visual attention and saccades. Sato and Schall argue that the first type is part of an attentional saliency map that indicates the location of relevant stimuli, whereas the second type may code the motor command for saccades (Sato and Schall, 2003). It should be noted that these are not the only types of responses in the FEF, a continuum of cells from purely visual to purely motor has been observed, which is also the case in the superior colliculus (SC) (Bruce and Goldberg, 1985; Awh et al., 2006; Ignashchenkova et al., 2009). The DN visually direction-selective neurons might be connected to the cells in the FEF that are selective for visual attention. Given the cerebro-cerebellar loops, these could then feed back into the DN.

In a parallel loop similar to the visually selective neurons, the motor cells in the DN-FEF connection might be addressed. These are the cells in the Landolt C task selective for saccade directions and are temporarily closer to the execution of the saccade then the visually selective cells (**Chapter 4, Fig. 3**). The cerebro-cerebellar loop between the fastigial nucleus (FN) and ALM is essential for motor preparation in mice. Perturbation of the FN disrupted preparatory activity in the frontal cortex. Interestingly, the same was the case the other way around; perturbation of the cerebellar cortex disrupted activity in the FN (Gao et al., 2018). Conversely, disruption of the DN did not have this effect. Building upon this Chabrol and colleagues used a visual rather than whisker-based task and did find a suppressing effect of DN silencing on preparatory activity in the ALM (Chabrol et al., 2019). The tasks in the current study also depends on the visual system rather than the whisker system.

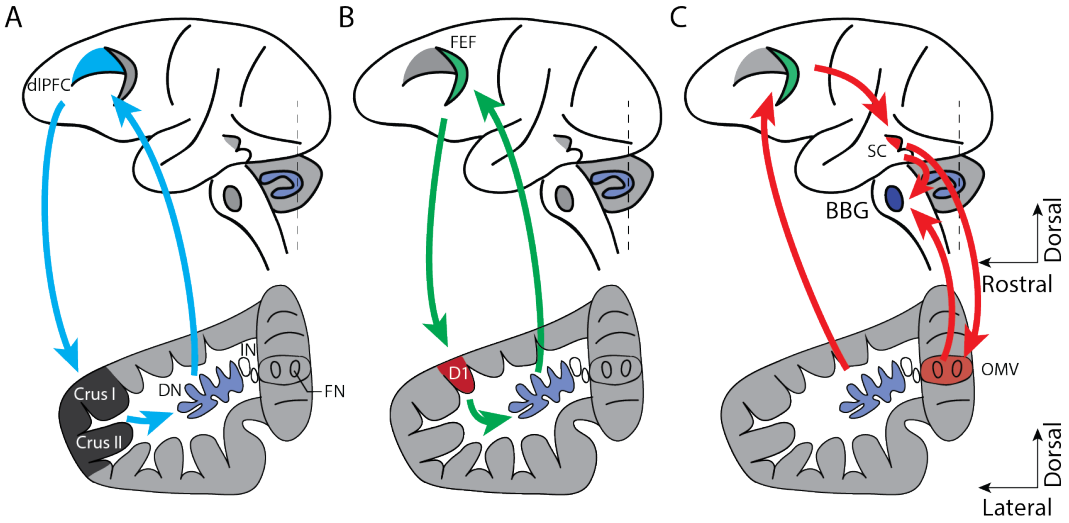

Figure 2. Hypothetical cerebro-cerebellar for saccade planning and execution. *Sagittal section of the cerebrum and coronal section of the cerebellum at the dashed line. A) Loop between Crus I/II the DN and the dlPFC. B) Loop of the D1 zone, the DN and the FEF. C) Possible output channel of the DN to contribute to initiating saccades. Abbreviations: BBG, Brainstem burst generator; dlPFC, dorsolateral Prefrontal Cortex; DN, dentate nucleus; IN, interposed nuclei; FN, fastigial nucleus; FEF, frontal eye fields; OMV, Oculomotor Vermis; SC, Superior Colliculus*

Therefore, cells recorded in this study might contribute to motor preparation of saccades in the FEF. Although motor and visual processes in the FEF can be separated during normal visually guided behavior, oculomotor selection and visual attention are typically coincident (Awh et al., 2006). Saccade cells in the DN convey delay activity related to self-timing of saccades and deficits to the lateral cerebellar cortex cause timing deficits (Ohki et al., 2009; Ashmore and Sommer, 2013). The DN with both its visual and motor cells which are active in order could support bridging both visual and motor processes by sequently engaging several cerebro-cerebellar loops.

6.3 Initiation and execution of the saccade

When visual cues are decoded and the go cue is presented a saccade must be initiated. Experimental lesions of the FEF, superior colliculus and striate visual cortex have indicated that none are necessary for the initiation of saccades to visual target (Sparks, 1986). However combined lesions of the SC and FEF are detrimental for visually guided saccade initiation (Schiller et al., 1980). A saccade is evoked when the activity of movement related neurons in the FEF reaches a threshold. However, when this buildup is interrupted the saccade is withheld (Brown et al., 2008). In relation to arm movements DN neurons show very similar responses as the DN neurons observed in **Chapter 4**, displaying both visual and/or auditory modulation and movement related discharges in the same spike trains (Chapman et al., 1986). These responses occur well before responses in the motor cortex during the same task (Lamarre et al., 1981). Furthermore, enduring deficits of the initiation of movements on the basis of a sensory cue were observed after lesioning the DN (Spidalieri et al., 1983). Therefore, output of the saccade selective DN neurons recorded in the Landolt C task might contribute to the build-up of FEF activity to a threshold, which when reached, initiates the saccade in concert with modulations in the SC (**Fig. 2C**). This is possibly a similar process to the DN-ALM loop described above maintaining motor preparation and setting network activity for the initiation of specific movements (Gao et al., 2018; Svoboda and Li, 2018). The SC provides the initial drive of the saccade to the brainstem burst generator (BBG), which contains premotor burst neurons. This drive is supplemented by the cerebellum, since the initial drive by the SC is insufficient (Optican and Quaia, 2002). Subsequently, the drive to the BBG is choked off by the OMV and the saccade is ended (Quaia et al., 1999). When the OMV is lesioned, there is an increase in *glissades* (**Chapter 5**). This is likely the product of the improper termination of the drive to the BBG in the absence of the OMV (Optican and Pretegiani, 2017; Flierman et al., 2019). Keeping execution of saccade precise regardless of aging and disease has been attributed to the OMV (Golla et al., 2008). In the scheme in **Fig 2** the OMV represent the final output of the cerebro-cerebellar loops controlling saccades by its connections to the eye muscles via the BBG.

6.4 Reward modulation in the lateral cerebellum

The idea that reward is a distributed signal that affects neural activity throughout the brain is only recently embraced by the cerebellar field, although it has been a concept in the cerebral literature for longer (Schultz and Dickinson, 2000; Chubykin et al., 2013; Hunt and Hayden, 2017). The rate of saccadic adaptation, a classical model for cerebellum dependent motor adaptation, is influenced by rewards. Besides, reaction times in rewarded conditions were shorter (Kojima and Soetedjo, 2017). Reward related signals have been found in granule cells and complex spikes and thus reach the cerebellar cortex through both the climbing fiber (CF) and the mossy fiber (MF) pathway (Wagner et al., 2017; Kostadinov et al., 2019). CFs relay expected reward magnitude (Larry et al., 2019) and granule cells convey trial rewards, reward anticipation, and reward omission. In the DN neurons recorded in **Chapter 4**, we observe similar types of reward related modulation. Cells become specifically active in situations where reward might be expected or in situations where reward can be sensed, but is not necessarily expected (**Chapter 4 Fig. 4**). This implies that the MF and CF signals are relayed through all cerebellar cortical layers up onto the output channels in the DN. It appears that beside the encoding of sensory prediction errors by the cerebellum, which are the driver of motor adaptation in most current models, reward prediction errors are also present

(Thoroughman and Shadmehr, 2000; Herzfeld et al., 2018; Heffley and Hull, 2019; Medina, 2019). A motor adaptation study where the quality of the sensory prediction errors was degraded, showed that reward prediction errors could take over the motor learning (Izawa and Shadmehr, 2011). Classical views of sensorimotor learning dictate that the reward circuits involving the basal ganglia care about action selection, and the cerebellum cares about precise execution of the action (Doya, 2000; Gurney et al., 2001; Friend and Kravitz, 2014). However, there is a growing body of evidence suggesting that the basal ganglia and cerebellum interact via reciprocal connections during goal-directed behavior (Bostan and Strick, 2018; Kunimatsu et al., 2018; Carta et al., 2019). Therefore, there might not be such a neat division between systems that select and execute action, as the cerebellum likely participates in both.

The evolutionary expansion of the lateral cerebellum in primates has been attributed to increasing demands of higher cognitive functions and connectivity with the frontal cortex (Kelly and Strick, 2003; Smaers et al., 2011, 2018). Classical cerebellar associative learning, such as in eyeblink conditioning relies on the prediction of an upcoming event (Leggio and Molinari, 2015; Broersen, 2019). Eyeblink condition however, is based on the sensory feedback of an air puff to the eye. In the case of higher cognitive functions sensory feedback to evaluate the associated reaction is not present. Therefore, associative learning in these situations, such as for instance the social consequence of direct eye contact, could be learned based on reward predictions rather than sensory predictions (Sokolov et al., 2017). The capacity to evaluate predictions in this way enables cerebellar associative learning in a non-motor context.

6.5 Upbound and downbound modules in the cerebellum

A novel theory founded on the difference in baseline firing frequency of simples spikes between Zebrin II(+) and Zebrin II(-) expressing regions suggests that cerebellar microzones are divided into two types of modules; microzones that rely predominantly on PC-LTP to increase firing rates, i.e., upbound modules, and microzones that rely predominantly on PC-LTD and interneuronal activity to decrease firing rates, i.e., downbound modules (De Zeeuw, 2021). Zebrin II(+) zones, PCs of which have a relatively low intrinsic firing frequency of 50-75 Hz *in vivo* (Zhou et al., 2014), belong to the upbound category, and Zebrin(-) zones, PCs of which have higher frequencies between 75-110 Hz, belong to the downbound group (Zhou et al., 2014; De Zeeuw, 2021). VOR adaptation and eye blink conditioning are two types of cerebellum-dependent motor learning that are controlled by upbound and downbound modules, respectively (Lisberger et al., 1994; ten Brinke et al., 2015). The PCs recorded during the pro- and antisaccade in **Chapter 3** are located in lateral cerebellum. This region is predominantly, but not exclusively, Zebrin II(+), a feature that is highly conserved among species (Luo et al., 2017; Sugihara, 2018). The average firing rate of the neurons recorded there was roughly 70 Hz. This implies that the recordings were probably made to a substantial extent in the upbound modules of the D zones. The medial cerebellum had similar average firing rates as the lateral cerebellum. The Zebrin pattern in the medial cerebellum is also striped, implying also both upbound and downbound modules (Sillitoe et al., 2004). During saccades to a target, PCs show both pausing and bursting activity, which together as a population can perfectly predict motion of the eye (Herzfeld et al., 2015). Saccadic adaptation experiments show that both bursts and pauses can be modulated bidirectionally, i.e., both can become weaker or stronger (Catz et al., 2008; Herzfeld et al., 2018). These physiological findings confirm the presence of both upbound and downbound modules that can be expected based on Zebrin stainings. Saccades are highly

demanding movements because of the conflict between precision and high peak velocities. Thus, the presence of both types of modules for the control of this behavior may enable maximum dynamic range for firing rate modulation and learning, further subserving temporal precision. Finally, during the Landolt C task we probably recorded the DN neurons (**Chapter 4**) downstream of the PCs in the lateral cerebellum that were engaged in the pro- and antisaccade task (**Chapter 3**). Therefore, these PCs are probably also predominantly, but not exclusively, located in upbound modules. Thus, our data support the theory that can explain how the physiological and molecular heterogeneity observed throughout the cerebellum can help to control and acquire different types of behavior.

6.6 Conclusion

In this thesis I study motor and premotor processes in the cerebellum in relation to saccade planning and execution. We find that cerebellar Purkinje cells in Crus I/II (i.e., lateral cerebellum), but not the OMV (i.e., medial cerebellum), discriminate between pro- and antisaccades. These cells become active at short latency from the onset of a visual cue, and maintain their activity throughout the trial. Strikingly, DN cells in a peripheral Landolt C task exhibit highly similar responses. Moreover, the DN population is split in cells that show selective responses toward the direction of a visual stimulus, and the direction of the upcoming movement. The same duality also exists in the FEF, a saccade hub crucial in planning and initiating movements. The anatomical tracer experiments indicate that interconnectivity exists between the DN neurons recorded here and the FEF. Furthermore, these experiments show that the population of PCs recorded in the pro- and antisaccade task is, at least in part, the same population of PCs that provide input to the DN during the Landolt C task. Thus, these cell populations likely partake in connected cerebro-cerebellar loops for saccade planning and execution. Finally, the reward related modulation that is present in some of the same DN cells as the visual and motor related components provides additional confirmation that the cerebellum does not exclusively depend on sensory prediction errors for learning, but also on reward prediction errors.

References

Adams, D. L., Economides, J. R., Jocson, C. M., Parker, J. M., and Horton, J. C. (2011). A watertight acrylic-free titanium recording chamber for electrophysiology in behaving monkeys. *J. Neurophysiol.* 106, 1581–1590.

Adewole, D. O., Serruya, M. D., Harris, J. P., Burrell, J. C., Petrov, D., Chen, H. I., et al. (2016). The Evolution of Neuroprosthetic Interfaces. *Crit. Rev. Biomed. Eng.* 44, 123–152.

Aggarwal, V., Tenore, F., Acharya, S., Schieber, M. H., and Thakor, N. V. (2009). Cortical decoding of individual finger and wrist kinematics for an upper-limb neuroprosthesis. *Conf. Proc. IEEE Eng. Med. Biol. Soc.* 2009, 4535–4538.

Aizawa, H., and Wurtz, R. H. (1998). Reversible inactivation of monkey superior colliculus. I. Curvature of saccadic trajectory. *J. Neurophysiol.* 79, 2082–2096.

Aizenman, C. D., and Linden, D. J. (1999). Regulation of the rebound depolarization and spontaneous firing patterns of deep nuclear neurons in slices of rat cerebellum. *J. Neurophysiol.* 82, 1697–1709.

Albert, S. T., Hadjiosif, A. M., Jang, J., Zimnik, A. J., Soteropoulos, D. S., Baker, S. N., et al. (2020). Postural control of arm and fingers through integration of movement commands. *Elife* 9. doi:10.7554/eLife.52507.

Allen, G. (1997). Attentional Activation of the Cerebellum Independent of Motor Involvement. *Science* 275, 1940–1943.

Alviña, K., Walter, J. T., Kohn, A., Ellis-Davies, G., and Khodakhah, K. (2008). Questioning the role of rebound firing in the cerebellum. *Nat. Neurosci.* 11, 1256–1258.

Al-Wabil, A., and Al-Sheaha, M. (2010). "Towards an Interactive Screening Program for Developmental Dyslexia: Eye Movement Analysis in Reading Arabic Texts," in *Lecture Notes in Computer Science*, 25–32.

Amador, N., Schlag-Rey, M., and Schlag, J. (1998). Primate antisaccades. I. Behavioral characteristics. *J. Neurophysiol.* 80, 1775–1786.

Andreasen, N. C., Paradiso, S., and O'Leary, D. S. (1998). "Cognitive dysmetria" as an integrative theory of schizophrenia: a dysfunction in cortical-subcortical-cerebellar circuitry? *Schizophr. Bull.* 24, 203–218.

Angelaki, D. E., Yakusheva, T. A., Green, A. M., Dickman, J. D., and Blazquez, P. M. (2010). Computation of egomotion in the macaque cerebellar vermis. *Cerebellum* 9, 174–182.

Apps, R., and Garwicz, M. (2000). Precise matching of olivo-cortical divergence and cortico-nuclear convergence between somatotopically corresponding areas in the medial C1 and medial C3 zones of the paravermal cerebellum: Cerebellar olivo-cortico-nuclear connections. *Eur. J. Neurosci.* 12, 205–214.

Apps, R., and Garwicz, M. (2005). Anatomical and physiological foundations of cerebellar information processing. *Nat. Rev. Neurosci.* 6, 297–311.

Apps, R., and Hawkes, R. (2009). Cerebellar cortical organization: a one-map hypothesis. *Nat. Rev. Neurosci.* 10, 670–681.

Ashmore, R. C., and Sommer, M. A. (2013). Delay activity of saccade-related neurons in the caudal dentate nucleus of the macaque cerebellum. *J. Neurophysiol.* 109, 2129–2144.

Avila, E., Lakshminarasimhan, K. J., DeAngelis, G. C., and Angelaki, D. E. (2019). Visual and Vestibular Selectivity for Self-Motion in Macaque Posterior Parietal Area 7a. *Cereb. Cortex* 29, 3932–3947.

Awh, E., Armstrong, K. M., and Moore, T. (2006). Visual and oculomotor selection: links, causes and implications for spatial attention. *Trends Cogn. Sci.* 10, 124–130.

Badura, A., Schonewille, M., Voges, K., Galliano, E., Renier, N., Gao, Z., et al. (2013). Climbing fiber input shapes reciprocity of Purkinje cell firing. *Neuron* 78, 700–713.

Bagnall, M. W., Zingg, B., Sakatos, A., Moghadam, S. H., Zeilhofer, H. U., and du Lac, S. (2009). Glycinergic projection neurons of the cerebellum. *J. Neurosci.* 29, 10104–10110.

Bahill, A. T., Clark, M. R., and Stark, L. (1975a). Dynamic overshoot in saccadic eye movements is caused by neurological control signal reversals. *Exp. Neurol.* 48, 107–122.

Bahill, A. T., Clark, M. R., and Stark, L. (1975b). Glissades—eye movements generated by mismatched

components of the saccadic motoneuronal control signal. *Math. Biosci.* 26, 303–318.

Bahill, A. T., Clark, M. R., and Stark, L. (1975c). The main sequence, a tool for studying human eye movements. *Math. Biosci.* 24, 191–204.

Bahill, A. T., Hsu, F. K., and Stark, L. (1978). Glissadic overshoots are due to pulse width errors. *Arch. Neurol.* 35, 138–142.

Bahill, A. T., and Stark, L. (1975). Overlapping saccades and glissades are produced by fatigue in the saccadic eye movement system. *Exp. Neurol.* 48, 95–106.

Baier, B., Dieterich, M., Stoeter, P., Birklein, F., and Müller, N. G. (2010). Anatomical Correlate of Impaired Covert Visual Attentional Processes in Patients with Cerebellar Lesions. *J. Neurosci.* doi:10.1523/JNEUROSCI.0487-09.2010.

Baier, B., Müller, N. G., and Dieterich, M. (2014). What part of the cerebellum contributes to a visuospatial working memory task? *Ann. Neurol.* 76, 754–757.

Baizer, J. S. (2014). Unique Features of the Human Brainstem and Cerebellum. *Front. Hum. Neurosci.* 8, 202.

Bala, P. C., Eisenreich, B. R., Yoo, S. B. M., Hayden, B. Y., Park, H. S., and Zimmermann, J. (2020). OpenMonkeyStudio: Automated Markerless Pose Estimation in Freely Moving Macaques. 2020.01.31.928861. doi:10.1101/2020.01.31.928861.

Balsters, J. H., Cussans, E., Diedrichsen, J., Phillips, K. A., Preuss, T. M., Rilling, J. K., et al. (2010). Evolution of the cerebellar cortex: the selective expansion of prefrontal-projecting cerebellar lobules. *Neuroimage* 49, 2045–2052.

Barash, S., Melikyan, A., Sivakov, A., Zhang, M., Glickstein, M., and Thier, P. (1999). Saccadic dysmetria and adaptation after lesions of the cerebellar cortex. *J. Neurosci.* 19, 10931–10939.

Barton, R. A. (2012). Embodied cognitive evolution and the cerebellum. *Philos. Trans. R. Soc. Lond. B Biol. Sci.* 367, 2097–2107.

Barton, R. A., and Venditti, C. (2014). Rapid evolution of the cerebellum in humans and other great apes. *Curr. Biol.* 24, 2440–2444.

Beh, S. C., Frohman, T. C., and Frohman, E. M. (2017). Cerebellar Control of Eye Movements. *J. Neuroophthalmol.* 37, 87–98.

Berger, M., Agha, N. S., and Gail, A. (2020). Wireless recording from unrestrained monkeys reveals motor goal encoding beyond immediate reach in frontoparietal cortex. *Elife* 9. doi:10.7554/eLife.51322.

Bliss-Moreau, E., Theil, J. H., and Moadab, G. (2013). Efficient cooperative restraint training with rhesus macaques. *J. Appl. Anim. Welf. Sci.* 16, 98–117.

Bosse, M. L., Tainturier, M. J., and Valdois, S. (2007). Developmental dyslexia: The visual attention span deficit hypothesis. *Cognition* 104, 198–230.

Bostan, A. C., and Strick, P. L. (2018). The basal ganglia and the cerebellum: nodes in an integrated network. *Nat. Rev. Neurosci.* 19, 338–350.

Braitenberg, V., Heck, D., and Sultan, F. (1997). Waiting for the ultimate theory of the cerebellum. *Behav. Brain Sci.* 20, 267–271.

Bral, A., and Mommaerts, M. Y. (2016). In vivo biofunctionalization of titanium patient-specific implants with nano hydroxyapatite and other nano calcium phosphate coatings: A systematic review. *J. Craniomaxillofac. Surg.* 44, 400–412.

Brissenden, J. A., Levin, E. J., Osher, D. E., Halko, M. A., and Somers, D. C. (2016). Functional Evidence for a Cerebellar Node of the Dorsal Attention Network. *J. Neurosci.* 36, 6083–6096.

Brissenden, J. A., Tobyne, S. M., Osher, D. E., Levin, E. J., Halko, M. A., and Somers, D. C. (2018). Topographic Cortico-cerebellar Networks Revealed by Visual Attention and Working Memory. *Curr. Biol.* 28, 3364–3372.e5.

Broersen, R. (2019). Timing in the Cerebellum During Motor Learning: From neuron to athlete to patient.

Brooks, J. X., and Cullen, K. E. (2009). Multimodal integration in rostral fastigial nucleus provides an estimate of body movement. *J. Neurosci.* 29, 10499–10511.

Brown, J. W., Hanes, D. P., Schall, J. D., and Stuphorn, V. (2008). Relation of frontal eye field activity to saccade initiation during a countermanding task. *Exp. Brain Res.* 190, 135–151.

Bruce, C. J., and Goldberg, M. E. (1985). Primate frontal eye fields. I. Single neurons discharging before saccades. *J. Neurophysiol.* 53. Available at: http://jn.physiology.org/content/jn/53/3/603.full.pdf.

Bruinsma, B. (2020). Cortical contributions to cognitive control.

Brunamonti, E., Chiricozzi, F. R., Clausi, S., Olivito, G., Giusti, M. A., Molinari, M., et al. (2014). Cerebellar damage impairs executive control and monitoring of movement generation. *PLoS One* 9, e85997.

Bryant, J. L., Boughter, J. D., Gong, S., LeDoux, M. S., and Heck, D. H. (2010). Cerebellar cortical output encodes temporal aspects of rhythmic licking movements and is necessary for normal licking frequency: Cerebellum and fluid licking. *Eur. J. Neurosci.* 32, 41–52.

Buchli, R., Boesiger, P., and Meier, D. (1988). Heating effects of metallic implants by MRI examinations. *Magn. Reson. Med.* 7, 255–261.

Buckner, R. L. (2013). The cerebellum and cognitive function: 25 years of insight from anatomy and neuroimaging. *Neuron* 80, 807–815.

Buckner, R. L., Krienen, F. M., Castellanos, A., Diaz, J. C., and Yeo, B. T. T. (2011). The organization of the human cerebellum estimated by intrinsic functional connectivity. *J. Neurophysiol.* 106, 2322–2345.

Bullock, T. H., Hopkins, C. D., and Fay, R. R. (2006). *Electroreception*. Springer Science & Business Media.

Bunge, S. A., Wallis, J. D., Parker, A., Brass, M., Crone, E. A., Hoshi, E., et al. (2005). Neural circuitry underlying rule use in humans and nonhuman primates. *J. Neurosci.* 25, 10347–10350.

Büttner, U., Straube, A., and Spuler, A. (1994). Saccadic dysmetria and "intact" smooth pursuit eye movements after bilateral deep cerebellar nuclei lesions. *J. Neurol. Neurosurg. Psychiatry* 57, 832–834.

Caesar, K., Thomsen, K., and Lauritzen, M. (2003). Dissociation of spikes, synaptic activity, and activity-dependent increments in rat cerebellar blood flow by tonic synaptic inhibition. *Proc. Natl. Acad. Sci. U. S. A.* 100, 16000–16005.

Caligiore, D., Pezzulo, G., Baldassarre, G., Bostan, A. C., Strick, P. L., Doya, K., et al. (2017). Consensus Paper: Towards a Systems-Level View of Cerebellar Function: the Interplay Between Cerebellum, Basal Ganglia, and Cortex. *Cerebellum* 16, 203–229.

Carta, I., Chen, C. H., Schott, A. L., Dorizan, S., and Khodakhah, K. (2019). Cerebellar modulation of the reward circuitry and social behavior. *Science* 363. doi:10.1126/science.aav0581.

Catz, N., Dicke, P. W., and Thier, P. (2005). Cerebellar complex spike firing is suitable to induce as well as to stabilize motor learning. *Curr. Biol.* 15, 2179–2189.

Catz, N., Dicke, P. W., and Thier, P. (2008). Cerebellar-dependent motor learning is based on pruning a Purkinje cell population response. *Proc. Natl. Acad. Sci. U. S. A.* 105, 7309–7314.

Chabrol, F. P., Blot, A., and Mrsic-Flogel, T. D. (2019). Cerebellar Contribution to Preparatory Activity in Motor Neocortex. *Neuron* 103, 506–519.e4.

Chapman, C. E., Spidalieri, G., and Lamarre, Y. (1986). Activity of dentate neurons during arm movements triggered by visual, auditory, and somesthetic stimuli in the monkey. *J. Neurophysiol.* 55, 203–226.

Chen, C.-Y., Hoffmann, K.-P., Distler, C., and Hafed, Z. M. (2019). The Foveal Visual Representation of the Primate Superior Colliculus. *Curr. Biol.* 29, 2109–2119.e7.

Chen, S., Augustine, G. J., and Chadderton, P. (2016). The cerebellum linearly encodes whisker position during voluntary movement. *Elife* 5, 1–16.

Chen, X., Possel, J. K., Wacongne, C., van Ham, A. F., Klink, P. C., and Roelfsema, P. R. (2017). 3D printing and modelling of customized implants and surgical guides for non-human primates. *J. Neurosci. Methods* 286, 38–55.

Chen, X., Wang, F., Fernandez, E., and Roelfsema, P. R. (2020). Shape perception via a high-channel-count neuroprosthesis in monkey visual cortex. *Science* 370, 1191–1196.

Chernov, M. M., Friedman, R. M., Chen, G., Stoner, G. R., and Roe, A. W. (2018). Functionally specific optogenetic modulation in primate visual cortex. *Proc. Natl. Acad. Sci. U. S. A.* 115, 10505–10510.

Chubykin, A. A., Roach, E. B., Bear, M. F., and Shuler, M. G. H. (2013). A cholinergic mechanism for reward timing within primary visual cortex. *Neuron* 77, 723–735.

Chukoskie, L., Guo, S., Ho, E., Zheng, Y., Chen, Q., Meng, V., et al. (2018). Quantifying Gaze Behavior During Real-World Interactions Using Automated Object, Face, and Fixation Detection. *IEEE Transactions on Cognitive and Developmental Systems* 10, 1143–1152. doi:10.1109/tcds.2018.2821566.

Clark, D. A., Mitra, P. P., and Wang, S. S. (2001). Scalable architecture in mammalian brains. *Nature* 411, 189–193.

Coe, B. C., and Munoz, D. P. (2017). Mechanisms of saccade suppression revealed in the anti-saccade task. *Philos. Trans. R. Soc. Lond. B Biol. Sci.* 372. doi:10.1098/rstb.2016.0192.

Collins, C. C. (1975). The human oculomotor control system. *Basic mechanisms of ocular motility and their clinical implications*, 145–180.

Coltz, J. D., Johnson, M. T., and Ebner, T. J. (1999). Cerebellar Purkinje cell simple spike discharge encodes movement velocity in primates during visuomotor arm tracking. *J. Neurosci.* 19, 1782–1803.

Connolly, J. D., Goodale, M. A., Menon, R. S., and Munoz, D. P. (2002). Human fMRI evidence for the neural correlates of preparatory set. *Nat. Neurosci.* 5, 1345–1352.

Corbetta, M., Akbudak, E., Conturo, T. E., Snyder, A. Z., Ollinger, J. M., Drury, H. A., et al. (1998). A common network of functional areas for attention and eye movements. *Neuron* 21, 761–773.

Cotti, J., Panouilleres, M., Munoz, D. P., Vercher, J.-L., Pélisson, D., and Guillaume, A. (2009). Adaptation of reactive and voluntary saccades: different patterns of adaptation revealed in the antisaccade task. *J. Physiol.* 587, 127–138.

Courchesne, E., Townsend, J., Akshoomoff, N. A., Saitoh, O., Yeung-Courchesne, R., Lincoln, A. J., et al. (1994). Impairment in shifting attention in autistic and cerebellar patients. *Behav. Neurosci.* 108, 848–865.

Craighero, L., Nascimben, M., and Fadiga, L. (2004). Eye position affects orienting of visuospatial attention. *Curr. Biol.* 14, 331–333.

Crandall, W. F., and Keller, E. L. (1985). Visual and oculomotor signals in nucleus reticularis tegmenti pontis in alert monkey. *J. Neurophysiol.* 54, 1326–1345.

Cullen, K. E., and Brooks, J. X. (2015). Neural correlates of sensory prediction errors in monkeys: evidence for internal models of voluntary self-motion in the cerebellum. *Cerebellum* 14, 31–34.

Cutsuridis, V., Kumari, V., and Ettinger, U. (2014). Antisaccade performance in schizophrenia: a neural model of decision making in the superior colliculus. *Front. Neurosci.* 8, 13.

Dacre, J., Colligan, M., Ammer, J., Schiemann, J., Clarke, T., Chamosa-Pino, V., et al. (2019). Cerebellar-recipient motor thalamus drives behavioral context-specific movement initiation. *bioRxiv*, 802124. doi:10.1101/802124.

D'Angelo, E., and Casali, S. (2012). Seeking a unified framework for cerebellar function and dysfunction: from circuit operations to cognition. *Front. Neural Circuits* 6, 116.

Dash, S., and Thier, P. (2014). "Chapter 6 - Cerebellum-Dependent Motor Learning: Lessons from Adaptation of Eye Movements in Primates," in *Progress in Brain Research*, ed. N. Ramnani (Elsevier), 121–155.

Deaner, R. O., van Schaik, C. P., and Johnson, V. (2006). Do Some Taxa Have Better Domain-General Cognition than others? A Meta-Analysis of Nonhuman Primate Studies. *Evol. Psychol.* 4, 147470490600400114.

Dean, P., Porrill, J., Ekerot, C.-F., and Jörntell, H. (2010). The cerebellar microcircuit as an adaptive filter: experimental and computational evidence. *Nat. Rev. Neurosci.* 11, 30–43.

Deffains, M., Nguyen, T. H., Orignac, H., Biendon, N., Dovero, S., Bezard, E., et al. (2020). In vivo electrophysiological validation of DREADD-based modulation of pallidal neurons in the non-human primate. *Eur. J. Neurosci.* doi:10.1111/ejn.14746.

De Gruijl, J. R., Hoogland, T. M., and De Zeeuw, C. I. (2014). Behavioral correlates of complex spike synchrony in cerebellar microzones. *J. Neurosci.* 34, 8937–8947.

Dehnhardt, G., Mauck, B., and Bleckmann, H. (1998). Seal whiskers detect water movements. *Nature* 394, 235–236.

De Schutter, E. (2019). Fallacies of Mice Experiments. *Neuroinformatics* 17, 181–183.

De Schutter, E., and Steuber, V. (2009). Patterns and pauses in Purkinje cell simple spike trains: experiments, modeling and theory. *Neuroscience* 162, 816–826.

Desmond, J. E., and Fiez, J. A. (1998). Neuroimaging studies of the cerebellum: language, learning and memory. *Trends Cogn. Sci.* 2, 355–362.

Desmurget, M., and Grafton, S. (2000). Forward modeling allows feedback control for fast reaching movements. *Trends Cogn. Sci.* 4, 423–431.

de Solages, C., Szapiro, G., Brunel, N., Hakim, V., Isope, P., Buisseret, P., et al. (2008). High-frequency organization and synchrony of activity in the purkinje cell layer of the cerebellum. *Neuron* 58, 775–788.

DeSouza, J. F. X., Menon, R. S., and Everling, S. (2003). Preparatory set associated with pro-saccades and anti-saccades in humans investigated with event-related FMRI. *J. Neurophysiol.* 89, 1016–1023.

Deverett, B., Kislin, M., Tank, D. W., and Wang, S. S.-H. (2019). Cerebellar disruption impairs working memory during evidence accumulation. *Nat. Commun.* 10, 3128.

Deverett, B., Koay, S. A., Oostland, M., and Wang, S. S.-H. (2018). Cerebellar involvement in an evidence-accumulation decision-making task. *Elife* 7. doi:10.7554/eLife.36781.

De Zeeuw, C. I. (2020). Bidirectional learning in upbound and downbound microzones of the cerebellum. *Nature Neuroscience Reviews*. doi:In press.

De Zeeuw, C. I. (2021). Bidirectional learning in upbound and downbound microzones of the cerebellum. *Nat. Rev. Neurosci.* 22, 92–110.

De Zeeuw, C. I., Chorev, E., Devor, A., Manor, Y., Van Der Giessen, R. S., De Jeu, M. T., et al. (2003). Deformation of Network Connectivity in the Inferior Olive of Connexin 36-Deficient Mice Is Compensated by Morphological and Electrophysiological Changes at the Single Neuron Level. *J. Neurosci.* 23, 4700–4711.

De Zeeuw, C. I., Hoebeek, F. E., Bosman, L. W. J., Schonewille, M., Witter, L., and Koekkoek, S. K. (2011). Spatiotemporal firing patterns in the cerebellum. *Nat. Rev. Neurosci.* 12, 327–344.

Diamond, A. (2013). Executive functions. *Annu. Rev. Psychol.* 64, 135–168.

Ding, L., and Gold, J. I. (2010). Caudate encodes multiple computations for perceptual decisions. *J. Neurosci.* 30, 15747–15759.

Ding, L., and Gold, J. I. (2012). Neural correlates of perceptual decision making before, during, and after decision commitment in monkey frontal eye field. *Cereb. Cortex* 22, 1052–1067.

Dow, B. M., Snyder, A. Z., Vautin, R. G., and Bauer, R. (1981). Magnification factor and receptive field size in foveal striate cortex of the monkey. *Exp. Brain Res.* 44, 213–228.

Doya, K. (1999). What are the computations of the cerebellum, the basal ganglia and the cerebral cortex? *Neural Netw.* 12, 961–974.

Doya, K. (2000). Complementary roles of basal ganglia and cerebellum in learning and motor control. *Curr. Opin. Neurobiol.* 10, 732–739.

Doyle, M., and Walker, R. (2001). Curved saccade trajectories: voluntary and reflexive saccades curve away from irrelevant distractors. *Exp. Brain Res.* 139, 333–344.

Dubowitz, D. J., and Scadeng, M. (2011). Suppl 2: A Frameless Stereotaxic MRI Technique for Macaque Neuroscience Studies. *Open Neuroimag. J.* 5, 198.

Ekerot, C. F., Jörntell, H., and Garwicz, M. (1995). Functional relation between corticonuclear input and movements evoked on microstimulation in cerebellar nucleus interpositus anterior in the cat. *Exp. Brain Res.* 106, 365–376.

Emery, N. J. (2000). The eyes have it: The neuroethology, function and evolution of social gaze. *Neurosci. Biobehav. Rev.* 24, 581–604.

Ethier, V., Zee, D. S., and Shadmehr, R. (2008). Changes in control of saccades during gain adaptation. *J. Neurosci.* 28, 13929–13937.

Everling, S., Dorris, M. C., Klein, R. M., and Munoz, D. P. (1999a). Role of primate superior colliculus in preparation and execution of anti-saccades and pro-saccades. *J. Neurosci.* 19, 2740–2754.

Everling, S., Dorris, M. C., and Munoz, D. P. (1999b). "Neuronal Activity in Monkey Superior Colliculus during an Antisaccade Task," in *Current Oculomotor Research: Physiological and Psychological Aspects*, eds. W. Becker, H. Deubel, and T. Mergner (Boston, MA: Springer US), 17–23.

Everling, S., and Fischer, B. (1998). The antisaccade: a review of basic research and clinical studies. *Neuropsychologia* 36, 885–899.

Everling, S., and Johnston, K. (2013). Control of the superior colliculus by the lateral prefrontal cortex. *Philos. Trans. R. Soc. Lond. B Biol. Sci.* 368, 20130068.

Everling, S., and Munoz, D. P. (2000). Neuronal correlates for preparatory set associated with pro-saccades and anti-saccades in the primate frontal eye field. *J. Neurosci.* 20, 387–400.

Fan, Y., Gold, J. I., and Ding, L. (2018). Ongoing, rational calibration of reward-driven perceptual biases. *Elife* 7. doi:10.7554/eLife.36018.

Farris, S. M. (2011). Are mushroom bodies cerebellum-like structures? *Arthropod Struct. Dev.* 40, 368–379.

Fernström, A.-L., Fredlund, H., Spångberg, M., and Westlund, K. (2009). Positive reinforcement training in rhesus macaques-training progress as a result of training frequency. *Am. J. Primatol.* 71, 373–379.

Fisher, N. I. (1995). *Statistical Analysis of Circular Data*. Cambridge University Press.

Flierman, N. A., Ignashchenkova, A., Negrello, M., Thier, P., De Zeeuw, C. I., and Badura, A. (2019). Glissades Are Altered by Lesions to the Oculomotor Vermis but Not by Saccadic Adaptation. *Front. Behav. Neurosci.* 13, 194.

Freedman, E. G., Molholm, S., Gray, M. J., Belyusar, D., and Foxe, J. J. (2017). Saccade adaptation deficits in developmental dyslexia suggest disruption of cerebellar-dependent learning. *J. Neurodev. Disord.* 9, 36.

Frens, M. A., and van der Geest, J. N. (2002). Scleral search coils influence saccade dynamics. *J. Neurophysiol.* 88, 692–698.

Frey, S., Pandya, D. N., Chakravarty, M. M., Bailey, L., Petrides, M., and Collins, D. L. (2011). An MRI based average macaque monkey stereotaxic atlas and space (MNI monkey space). *Neuroimage* 55, 1435–1442.

Friend, D. M., and Kravitz, A. V. (2014). Working together: basal ganglia pathways in action selection. *Trends Neurosci.* 37, 301–303.

Fuchs, A. F. (1967). Saccadic and smooth pursuit eye movements in the monkey. *J. Physiol.* 191, 609–631.

Fuchs, A. F., Brettler, S., and Ling, L. (2010). Head-free gaze shifts provide further insights into the role of the medial cerebellum in the control of primate saccadic eye movements. *J. Neurophysiol.* 103, 2158–2173.

Fuchs, A. F., Robinson, F. R., and Straube, A. (1993). Role of the caudal fastigial nucleus in saccade generation. I. Neuronal discharge pattern. *J. Neurophysiol.* 70, 1723–1740.

Funahashi, S., Chafee, M. V., and Goldman-Rakic, P. S. (1993). Prefrontal neuronal activity in rhesus monkeys performing a delayed anti-saccade task. *Nature* 365, 753–756.

Gao, Z., Davis, C., Thomas, A. M., Economo, M. N., Abrego, A. M., Svoboda, K., et al. (2018). A cortico-cerebellar loop for motor planning. *Nature* 563, 113–116.

Gao, Z., Thomas, A. M., Economo, M. N., Abrego, A. M., Svoboda, K., De Zeeuw, C. I., et al. (2019). Response to "Fallacies of Mice Experiments." *Neuroinformatics* 17, 475–478. doi:10.1007/s12021-019-09433-y.

Gao, Z., van Beugen, B. J., and De Zeeuw, C. I. (2012). Distributed synergistic plasticity and cerebellar learning. *Nat. Rev. Neurosci.* 13, 619–635.

Gaymard, B., Ploner, C. J., Rivaud, S., Vermersch, a. I., and Pierrot-Deseilligny, C. (1998). Cortical control of saccades. *Exp. Brain Res.* 123, 159–163.

Genzel, L., Adan, R., Berns, A., van den Beucken, J. J. J. P., Blokland, A., Boddeke, E. H. W. G. M., et al. (2020). How the COVID-19 pandemic highlights the necessity of animal research. *Curr. Biol.* 30, R1014–R1018.

Gerrits, N. M., and Voogd, J. (1989). The Topographical Organization of Climbing and Mossy Fiber Afferents in the Flocculus and the Ventral Paraflocculus in Rabbit, Cat and Monkey. *The Olivocerebellar System in Motor Control*, 26–29. doi:10.1007/978-3-642-73920-0_3.

Giovannucci, A., Badura, A., Deverett, B., Najafi, F., Pereira, T. D., Gao, Z., et al. (2017). Cerebellar granule cells acquire a widespread predictive feedback signal during motor learning. *Nat. Neurosci.* 20, 727–734.

Goldberg, M. C., Lasker, A. G., Zee, D. S., Garth, E., Tien, A., and Landa, R. J. (2002). Deficits in the initiation of eye movements in the absence of a visual target in adolescents with high functioning autism. *Neuropsychologia* 40, 2039–2049.

Goldring, J., and Fischer, B. (1997). Reaction times of vertical prosaccades and antisaccades in gap and overlap tasks. *Exp. Brain Res.* 113, 88–103.

Golla, H., Tziridis, K., Haarmeier, T., Catz, N., Barash, S., and Thier, P. (2008). Reduced saccadic resilience and impaired saccadic adaptation due to cerebellar disease. *Eur. J. Neurosci.* 27, 132–144.

Gottlieb, J., and Goldberg, M. E. (1999). Activity of neurons in the lateral intraparietal area of the monkey during an antisaccade task. *Nat. Neurosci.* 2, 906–912.

Gregoriou, G. G., Gotts, S. J., and Desimone, R. (2012). Cell-type-specific synchronization of neural activity in FEF with V4 during attention. *Neuron* 73, 581–594.

Gross, C. G. (2009). *A Hole in the Head More Tales in the History of Neuroscience*. The MIT Press.

Guo, A., Zhang, K., Ren, Q. Z., Su, H. F., and Chen, N. N. (2016). "Functional Connectivity Mapping of Decision-Making in Drosophila Melanogaster," in *Advances in Cognitive Neurodynamics (V)* (Springer, Singapore), 35–40.

Gurney, K., Prescott, T. J., and Redgrave, P. (2001). A computational model of action selection in the basal ganglia. I. A new functional anatomy. *Biol. Cybern.* 84, 401–410.

Guthrie, B. L., Porter, J. D., and Sparks, D. L. (1983). Corollary discharge provides accurate eye position information to the oculomotor system. *Science* 221, 1193–1195.

Hakvoort Schwerdtfeger, R. M., Alahyane, N., Brien, D. C., Coe, B. C., Stroman, P. W., and Munoz, D. P. (2012). Preparatory neural networks are impaired in adults with attention-deficit/hyperactivity disorder during the antisaccade task. *Neuroimage Clin* 2, 63–78.

Hale, M. E. (2019). Toward Diversification of Species Models in Neuroscience. *Biotechnol. Bioprocess Eng.* 93, 166–168.

Hallett, P. E. (1978). Primary and secondary saccades to goals defined by instructions. *Vision Res.* 18, 1279–1296.

Hanes, D. P., and Schall, J. D. (1996). Neural control of voluntary movement initiation. *Science* 274, 427–430.

Hanke, F. D., Hanke, W., Scholtyssek, C., and Dehnhardt, G. (2009). Basic mechanisms in pinniped vision. *Exp. Brain Res.* 199, 299–311.

Hanks, T. D., Kopec, C. D., Brunton, B. W., Duan, C. A., Erlich, J. C., and Brody, C. D. (2015). Distinct relationships of parietal and prefrontal cortices to evidence accumulation. *Nature* 520, 220–223.

Hanning, N. M., and Deubel, H. (2020). Attention capture outside the oculomotor range. *Curr. Biol.* 30, R1353–R1355.

Harrod, E. G., Coe, C. L., and Niedenthal, P. M. (2020). Social Structure Predicts Eye Contact Tolerance in Nonhuman Primates: Evidence from a Crowd-Sourcing Approach. *Sci. Rep.* 10, 6971.

Harvey, C. D., Coen, P., and Tank, D. W. (2012). Choice-specific sequences in parietal cortex during a virtual-navigation decision task. *Nature* 484, 62–68.

Head, H., and Holmes, G. (1911). SENSORY DISTURBANCES FROM CEREBRAL LESIONS. *Brain* 34, 102–254.

Heck, D. H., Thach, W. T., and Keating, J. G. (2007). On-beam synchrony in the cerebellum as the mechanism for the timing and coordination of movement. *Proc. Natl. Acad. Sci. U. S. A.* 104, 7658–7663.

Heffley, W., and Hull, C. (2019). Classical conditioning drives learned reward prediction signals in climbing fibers across the lateral cerebellum. *Elife* 8. doi:10.7554/eLife.46764.

Heffley, W., Song, E. Y., Xu, Z., Taylor, B. N., Hughes, M. A., McKinney, A., et al. (2018). Coordinated cerebellar climbing fiber activity signals learned sensorimotor predictions. *Nat. Neurosci.* 21, 1431–1441.

Heimbauer, L. A., Conway, C. M., Christiansen, M. H., Beran, M. J., and Owren, M. J. (2012). A Serial Reaction Time (SRT) task with symmetrical joystick responding for nonhuman primates. *Behav. Res. Methods* 44, 733–741.

Heiney, S. A., Kim, J., Augustine, G. J., and Medina, J. F. (2014). Precise control of movement kinematics by optogenetic inhibition of Purkinje cell activity. *J. Neurosci.* 34, 2321–2330.

Henschke, J. U., Dylda, E., Katsanevaki, D., Dupuy, N., Currie, S. P., Amvrosiadis, T., et al. (2020). Reward Association Enhances Stimulus-Specific Representations in Primary Visual Cortex. *Curr. Biol.* 30, 1866–1880.e5.

Herzfeld, D. J., Kojima, Y., Soetedjo, R., and Shadmehr, R. (2015). Encoding of action by the Purkinje cells

of the cerebellum. *Nature* 526, 439–442.

Herzfeld, D. J., Kojima, Y., Soetedjo, R., and Shadmehr, R. (2018). Encoding of error and learning to correct that error by the Purkinje cells of the cerebellum. *Nat. Neurosci.* 21, 736–743.

Herzfeld, D. J., and Shadmehr, R. (2014). Cerebellum estimates the sensory state of the body. *Trends Cogn. Sci.* 18, 66–67.

Hodos, W. (2009). "Evolution of Cerebellum," in *Encyclopedia of Neuroscience*, eds. M. D. Binder, N. Hirokawa, and U. Windhorst (Berlin, Heidelberg: Springer Berlin Heidelberg), 1240–1243.

Hoet, P., Krätke, R., Testai, E., and Vermeire, T. (2017). SCHEER (Scientific Committee on Health, Environmental and Emerging Risks), Final Opinion on "The need for non-human primates in biomedical research, production and testing of products and devices (update 2017)", 18 May 2017. Available at: https://ec.europa.eu/health/sites/health/files/scientific_committees/scheer/docs/scheer_o_004.pdf.

Holmes, G. (1917). THE SYMPTOMS OF ACUTE CEREBELLAR INJURIES DUE TO GUNSHOT INJURIES. *Brain* 40, 461–535.

Hong, S., Negrello, M., Junker, M., Smilgin, A., Thier, P., and De Schutter, E. (2016). Multiplexed coding by cerebellar Purkinje neurons. *Elife* 5, 1–19.

Hoogland, T. M., De Gruijl, J. R., Witter, L., Canto, C. B., and De Zeeuw, C. I. (2015). Role of Synchronous Activation of Cerebellar Purkinje Cell Ensembles in Multi-joint Movement Control. *Curr. Biol.* 25, 1157–1165.

Hsu, B. T. F., and Stark, L. (1978). Glissadic Overshoots Are Due to Pulse Width Errors Glissades. *Arch Neurol.*

Huang, C.-C., Sugino, K., Shima, Y., Guo, C., Bai, S., Mensh, B. D., et al. (2013). Convergence of pontine and proprioceptive streams onto multimodal cerebellar granule cells. *Elife* 2, e00400.

Huber, G., Heynen, S., Imsand, C., vom Hagen, F., Muehlfriedel, R., Tanimoto, N., et al. (2010). Novel rodent models for macular research. *PLoS One* 5, e13403.

Huberman, A. D., and Niell, C. M. (2011). What can mice tell us about how vision works? *Trends Neurosci.* 34, 464–473.

Huk, A., Bonnen, K., and He, B. J. (2018). Beyond Trial-Based Paradigms: Continuous Behavior, Ongoing Neural Activity, and Natural Stimuli. *J. Neurosci.* 38, 7551–7558.

Hull, C., and Regehr, W. G. (2012). Identification of an inhibitory circuit that regulates cerebellar Golgi cell activity. *Neuron* 73, 149–158.

Hulme, O. J., Whiteley, L., and Shipp, S. (2010). Spatially distributed encoding of covert attentional shifts in human thalamus. *J. Neurophysiol.* 104, 3644–3656.

Hunt, L. T., and Hayden, B. Y. (2017). A distributed, hierarchical and recurrent framework for reward-based choice. *Nat. Rev. Neurosci.* 18, 172–182.

Hutchison, R. M., and Everling, S. (2012). Monkey in the middle: why non-human primates are needed to bridge the gap in resting-state investigations. *Front. Neuroanat.* 6, 29.

Huynh, V., Ngo, N. K., and Golden, T. D. (2019). Surface Activation and Pretreatments for Biocompatible Metals and Alloys Used in Biomedical Applications. *Int. J. Biomater.* 2019, 3806504.

Ignashchenkova, A., Dash, S., Dicke, P. W., Haarmeier, T., Glickstein, M., and Thier, P. (2009). Normal spatial attention but impaired saccades and visual motion perception after lesions of the monkey cerebellum. *J. Neurophysiol.* 102, 3156–3168.

Ignashchenkova, A., Dicke, P. W., Haarmeier, T., and Thier, P. (2004). Neuron-specific contribution of the superior colliculus to overt and covert shifts of attention. *Nat. Neurosci.* 7, 56–64.

Ikeda, Y., Noda, H., and Sugita, S. (1989). Olivocerebellar and cerebelloolivary connections of the oculomotor region of the fastigial nucleus in the macaque monkey. *J. Comp. Neurol.* 284, 463–488.

Ikegaya, Y., Aaron, G., Cossart, R., Aronov, D., Lampl, I., Ferster, D., et al. (2004). Synfire chains and cortical songs: temporal modules of cortical activity. *Science* 304, 559–564.

Inoshita, T., and Hirano, T. (2018). Occurrence of long-term depression in the cerebellar flocculus during adaptation of optokinetic response. *Elife* 7. doi:10.7554/eLife.36209.

Ishikawa, T., Shimuta, M., and Häusser, M. (2015). Multimodal sensory integration in single cerebellar granule cells in vivo. *Elife* 4. doi:10.7554/eLife.12916.

Ito, M. (2001). Cerebellar long-term depression: characterization, signal transduction, and functional roles. *Physiol. Rev.* 81, 1143–1195.

Ito, M. (2008). Control of mental activities by internal models in the cerebellum. *Nat. Rev. Neurosci.* 9, 304–313.

Ivry, R. B., and Diener, H. C. (1991). Impaired velocity perception in patients with lesions of the cerebellum. *J. Cogn. Neurosci.* 3, 355–366.

Izawa, J., and Shadmehr, R. (2011). Learning from sensory and reward prediction errors during motor adaptation. *PLoS Comput. Biol.* 7, e1002012.

Jansen, J., and Jansen, J. (1969). *Biology of Marine Mammals*.

Jazayeri, M., Lindbloom-Brown, Z., and Horwitz, G. D. (2012). Saccadic eye movements evoked by optogenetic activation of primate V1. *Nat. Neurosci.* 15, 1368–1370.

Jennings, C. G., Landman, R., Zhou, Y., Sharma, J., Hyman, J., Movshon, J. A., et al. (2016). Opportunities and challenges in modeling human brain disorders in transgenic primates. *Nat. Neurosci.* 19, 1123–1130.

Jin, D. Z., Fujii, N., and Graybiel, A. M. (2009). Neural representation of time in cortico-basal ganglia circuits. *Proc. Natl. Acad. Sci. U. S. A.* 106, 19156–19161.

Johnson, B. P., Rinehart, N. J., Papadopoulos, N., Tonge, B., Millist, L., White, O., et al. (2012). A closer look at visually guided saccades in autism and Asperger's disorder. *Front. Integr. Neurosci.* 6, 99.

Johnson, B. P., Rinehart, N. J., White, O., Millist, L., and Fielding, J. (2013). Saccade adaptation in autism and Asperger's disorder. *Neuroscience* 243, 76–87.

Judge, S. J., Richmond, B. J., and Chu, F. C. (1980). Implantation of magnetic search coils for measurement of eye position: an improved method. *Vision Res.* 20, 535–538.

Junker, M., Endres, D., Sun, Z. P., Dicke, P. W., Giese, M., and Thier, P. (2018). Learning from the past: A reverberation of past errors in the cerebellar climbing fiber signal. *PLoS Biol.* 16, e2004344.

Kapoula, Z. A., Robinson, D. A., and Hain, T. C. (1986). Motion of the eye immediately after a saccade. *Experimental Brain Research* 61. doi:10.1007/bf00239527.

Kawamura, S., Hattori, S., Higo, S., and Matsuyama, T. (1982). The cerebellar projections to the superior colliculus and pretectum in the cat: an autoradiographic and horseradish peroxidase study. *Neuroscience* 7, 1673–1689.

Keating, C. F., and Keating, E. G. (1982). Visual scan patterns of rhesus monkeys viewing faces. *Perception* 11, 211–219.

Keifer, J., and Summers, C. H. (2016). Putting the "Biology" Back into "Neurobiology": The Strength of Diversity in Animal Model Systems for Neuroscience Research. *Front. Syst. Neurosci.* 10. doi:10.3389/fnsys.2016.00069.

Kelly, E., Meng, F., Fujita, H., Morgado, F., Kazemi, Y., Rice, L. C., et al. (2020). Regulation of autism-relevant behaviors by cerebellar-prefrontal cortical circuits. *Nat. Neurosci.* doi:10.1038/s41593-020-0665-z.

Kelly, R. M., and Strick, P. L. (2003). Cerebellar Loops with Motor Cortex and Prefrontal Cortex of a Nonhuman Primate. *J. Neurosci.* 23, 8432–8444.

Khilkevich, A., Zambrano, J., Richards, M.-M., and Mauk, M. D. (2018). Cerebellar implementation of movement sequences through feedback. *Elife* 7. doi:10.7554/eLife.37443.

Kikinis, R., Pieper, S. D., and Vosburgh, K. G. (2014). 3D Slicer: A Platform for Subject-Specific Image Analysis, Visualization, and Clinical Support. *Intraoperative Imaging and Image-Guided Therapy*, 277–289. doi:10.1007/978-1-4614-7657-3_19.

Kimmel, D. L., Mammo, D., and Newsome, W. T. (2012). Tracking the eye non-invasively: simultaneous comparison of the scleral search coil and optical tracking techniques in the macaque monkey. *Front. Behav. Neurosci.* 6, 49.

Klin, A., Lin, D. J., Gorrindo, P., Ramsay, G., and Jones, W. (2009). Two-year-olds with autism orient to non-social contingencies rather than biological motion. *Nature* 459, 257–261.

Knöll, J., Pillow, J. W., and Huk, A. C. (2018). Lawful tracking of visual motion in humans, macaques, and marmosets in a naturalistic, continuous, and untrained behavioral context. *Proc. Natl. Acad. Sci. U. S. A.* 115, E10486–E10494.

Kobayashi, H., and Kohshima, S. (1997). Unique morphology of the human eye. *Nature* 387, 767–768.

Kojima, Y., and Soetedjo, R. (2017). Selective reward affects the rate of saccade adaptation. *Neuroscience* 355, 113–125.

Kornhuber, H. H. (1971). Motor functions of cerebellum and basal ganglia: the cerebellocortical saccadic (ballistic) clock, the cerebellonuclear hold regulator, and the basal ganglia ramp (voluntary speed smooth movement) generator. *Kybernetik* 8, 157–162.

Kostadinov, D., Beau, M., Pozo, M. B., and Häusser, M. (2019). Predictive and reactive reward signals conveyed by climbing fiber inputs to cerebellar Purkinje cells. *Nat. Neurosci.* 22, 950–962.

Krieg, W. J. S. (1967). The Comparative Anatomy and Histology of the Cerebellum From Myxinoids Through Birds. *JAMA* 201, 784–785.

Kunimatsu, J., Suzuki, T. W., Ohmae, S., and Tanaka, M. (2018). Different contributions of preparatory activity in the basal ganglia and cerebellum for self-timing. *Elife* 7. doi:10.7554/eLife.35676.

Kunimatsu, J., Suzuki, T. W., and Tanaka, M. (2016). Implications of Lateral Cerebellum in Proactive Control of Saccades. *Journal of Neuroscience* 36, 7066–7074.

Kunimatsu, J., and Tanaka, M. (2010). Roles of the primate motor thalamus in the generation of antisaccades. *J. Neurosci.* 30, 5108–5117.

Lakshminarasimhan, K. J., Avila, E., Neyhart, E., DeAngelis, G. C., Pitkow, X., and Angelaki, D. E. (2020). Tracking the Mind's Eye: Primate Gaze Behavior during Virtual Visuomotor Navigation Reflects Belief Dynamics. *Neuron* 106, 662–674.e5.

Lamarre, Y., Spidalieri, G., and Lund, J. P. (1981). Patterns of muscular and motor cortical activity during a simple arm movement in the monkey. *Can. J. Physiol. Pharmacol.* 59, 748–756.

Lanz, F., Lanz, X., Scherly, A., Moret, V., Gaillard, A., Gruner, P., et al. (2013). Refined methodology for implantation of a head fixation device and chronic recording chambers in non-human primates. *J. Neurosci. Methods* 219, 262–270.

Larry, N., Yarkoni, M., Lixenberg, A., and Joshua, M. (2019). Cerebellar climbing fibers encode expected reward size. *Elife* 8. doi:10.7554/eLife.46870.

Larsell, O. (1952). The morphogenesis and adult pattern of the lobules and fissures of the cerebellum of the white rat. *J. Comp. Neurol.* 97, 281–356.

Laule, G. E., Bloomsmith, M. A., and Schapiro, S. J. (2003). The use of positive reinforcement training techniques to enhance the care, management, and welfare of primates in the laboratory. *J. Appl. Anim. Welf. Sci.* 6, 163–173.

Laurens, J., and Angelaki, D. E. (2020). Simple spike dynamics of Purkinje cells in the macaque vestibulo-cerebellum during passive whole-body self-motion. *Proc. Natl. Acad. Sci. U. S. A.* 117, 3232–3238.

Laurens, J., Meng, H., and Angelaki, D. E. (2013a). Computation of linear acceleration through an internal model in the macaque cerebellum. *Nat. Neurosci.* 16, 1701–1708.

Laurens, J., Meng, H., and Angelaki, D. E. (2013b). Neural representation of orientation relative to gravity in the macaque cerebellum. *Neuron* 80, 1508–1518.

Leggio, M., and Molinari, M. (2015). Cerebellar sequencing: a trick for predicting the future. *Cerebellum* 14, 35–38.

Leiner, H. C. (2010). Solving the mystery of the human cerebellum. *Neuropsychol. Rev.* Available at: https://idp.springer.com/authorize/casa?redirect_uri=https://link.springer.com/article/10.1007/s11065-010-9140-z&casa_token=hoviTvB7GXQAAAAA:b7mlC_SzCZBvMtbnrPressn7MEjASoy-V2G0nUXOWQLaUi9htn-8PEWtnE80rmlf3BFwI1a2Ji7XiL06cw.

Leiner, H. C., Leiner, A. L., and Dow, R. S. (1986). Does the cerebellum contribute to mental skills? *Behav. Neurosci.* 100, 443–454.

Leiner, H. C., Leiner, A. L., and Dow, R. S. (1993). Cognitive and language functions of the human cerebellum. *Trends Neurosci.* 16, 444–447.

Lemon, R. N. (2018). Applying the 3Rs to neuroscience research involving nonhuman primates. *Drug Discov. Today* 23, 1574–1577.

Lepore, F. E. (1994). Harvey Cushing, Gordon Holmes, and the neurological lessons of World War I. *Arch. Neurol.* 51, 711–722.

Lévy-Bencheton, D., Pisella, L., Salemme, R., Tilikete, C., and Pélisson, D. (2013). Plastic modification of anti-saccades: adaptation of saccadic eye movements aimed at a virtual target. *J. Neurosci.* 33, 13489–13497.

Lewis, R. F., Zee, D. S., Hayman, M. R., and Tamargo, R. J. (2001). Oculomotor function in the rhesus monkey after deafferentation of the extraocular muscles. *Exp. Brain Res.* 141, 349–358.

Lisberger, S. G., Pavelko, T. A., Bronte-Stewart, H. M., and Stone, L. S. (1994). Neural basis for motor learning in the vestibuloocular reflex of primates. II. Changes in the responses of horizontal gaze velocity Purkinje cells in the cerebellar flocculus and ventral paraflocculus. *J. Neurophysiol.* 72, 954–973.

Liu, X., Yu, S.-Y., Flierman, N., Loyola, S., Kamermans, M., Hoogland, T. M., et al. (2020). OptiFlex: video-based animal pose estimation using deep learning enhanced by optical flow. *bioRxiv*, 2020.04.04.025494. doi:10.1101/2020.04.04.025494.

Llinás, R., and Mühlethaler, M. (1988). Electrophysiology of guinea-pig cerebellar nuclear cells in the in vitro brain stem-cerebellar preparation. *J. Physiol.* 404, 241–258.

Logothetis, N. K., Pauls, J., Augath, M., Trinath, T., and Oeltermann, A. (2001). Neurophysiological investigation of the basis of the fMRI signal. *Nature* 412, 150–157.

Lowet, E., Gomes, B., Srinivasan, K., Zhou, H., Schafer, R. J., and Desimone, R. (2018). Enhanced Neural Processing by Covert Attention only during Microsaccades Directed toward the Attended Stimulus. *Neuron* 99, 207–214.e3.

Luo, Y., Fujita, H., Nedelescu, H., Biswas, M. S., Sato, C., Ying, S., et al. (2017). Lobular homology in cerebellar hemispheres of humans, non-human primates and rodents: a structural, axonal tracing and molecular expression analysis. *Brain Struct. Funct.* 222, 2449–2472.

Lynch, J. C., and Tian, J.-R. (2006). Cortico-cortical networks and cortico-subcortical loops for the higher control of eye movements. *Prog. Brain Res.* 151, 461–501.

Machado, C. J., and Nelson, E. E. (2011). Eye-tracking with nonhuman primates is now more accessible than ever before. *Am. J. Primatol.* 73, 562–569.

Macinnes, J. J., Iqbal, S., Pearson, J., and Johnson, E. N. (2018). Wearable Eye-tracking for Research: Automated dynamic gaze mapping and accuracy/precision comparisons across devices. *bioRxiv*, 299925. doi:10.1101/299925.

Mantini, D., Corbetta, M., Romani, G. L., Orban, G. A., and Vanduffel, W. (2013). Evolutionarily novel functional networks in the human brain? *J. Neurosci.* 33, 3259–3275.

Manto, M., Bower, J. M., Conforto, A. B., Delgado-García, J. M., da Guarda, S. N. F., Gerwig, M., et al. (2012). Consensus paper: roles of the cerebellum in motor control–the diversity of ideas on cerebellar involvement in movement. *Cerebellum* 11, 457–487.

Marple-Horvat, D. E., and Stein, J. F. (1990). Neuronal activity in the lateral cerebellum of trained monkeys, related to visual stimuli or to eye movements. *J. Physiol.* 428, 595–614.

Mathis, A., Mamidanna, P., Cury, K. M., Abe, T., Murthy, V. N., Mathis, M. W., et al. (2018). DeepLabCut: markerless pose estimation of user-defined body parts with deep learning. *Nat. Neurosci.* 21, 1281–1289.

Maximino, C., do Carmo Silva, R. X., da Silva, S. de N. S., dos Santos Rodrigues, L. do S., Barbosa, H., de Carvalho, T. S., et al. (2015). Non-mammalian models in behavioral neuroscience: consequences for biological psychiatry. *Front. Behav. Neurosci.* 9. doi:10.3389/fnbeh.2015.00233.

McAndrew, R. M., Lingo VanGilder, J. L., Naufel, S. N., and Helms Tillery, S. I. (2012). Individualized recording chambers for non-human primate neurophysiology. *J. Neurosci. Methods* 207, 86–90.

McDevitt, C. J., Ebner, T. J., and Bloedel, J. R. (1987). Relationships between simultaneously recorded Purkinje cells and nuclear neurons. *Brain Res.* 425, 1–13.

McElligott, J. G., and Keller, E. L. (1984). Cerebellar vermis involvement in monkey saccadic eye movements: microstimulation. *Exp. Neurol.* 86, 543–558.

McLaughlin, S. C. (1967). Parametric adjustment in saccadic eye movements. *Percept. Psychophys.* 2, 359–362.

McMillan, J. L., Perlman, J. E., Galvan, A., Wichmann, T., and Bloomsmith, M. A. (2014). Refining the pole-and-collar method of restraint: emphasizing the use of positive training techniques with rhesus macaques (Macaca mulatta). *J. Am. Assoc. Lab. Anim. Sci.* 53, 61–68.

Medina, J. F. (2019). Teaching the cerebellum about reward. *Nat. Neurosci.* 22, 846–848.

Medina, J. F., and Lisberger, S. G. (2009). Encoding and decoding of learned smooth-pursuit eye movements in the floccular complex of the monkey cerebellum. *J. Neurophysiol.* 102, 2039–2054.

Miall, R. C., Weir, D. J., and Stein, J. F. (1987). Visuo-motor tracking during reversible inactivation of the cerebellum. *Exp. Brain Res.* 65, 455–464.

Miall, R. C., Weir, D. J., Wolpert, D. M., and Stein, J. F. (1993). Is the cerebellum a smith predictor? *J. Mot. Behav.* 25, 203–216.

Middleton, F. A., and Strick, P. L. (2000). Basal ganglia and cerebellar loops: motor and cognitive circuits. *Brain Res. Brain Res. Rev.* 31, 236–250.

Middleton, F. A., and Strick, P. L. (2001). Cerebellar projections to the prefrontal cortex of the primate. *J. Neurosci.* 21, 700–712.

Miller, J. M., and Robins, D. (1992). Extraocular muscle forces in alert monkey. *Vision Res.* 32, 1099–1113.

Mitchell, A. S., Thiele, A., Petkov, C. I., Roberts, A., Robbins, T. W., Schultz, W., et al. (2018). Continued need for non-human primate neuroscience research. *Curr. Biol.* 28, R1186.

Mitchell, J. P., Macrae, C. N., and Gilchrist, I. D. (2002). Working memory and the suppression of reflexive saccades. *J. Cogn. Neurosci.* 14, 95–103.

Mitz, A. R., Bartolo, R., Saunders, R. C., Browning, P. G., Talbot, T., and Averbeck, B. B. (2017). High channel count single-unit recordings from nonhuman primate frontal cortex. *J. Neurosci. Methods* 289, 39–47.

Mokler, A., and Fischer, B. (1999). The recognition and correction of involuntary prosaccades in an antisaccade task. *Exp. Brain Res.* 125, 511–516.

Monosov, I. E., and Thompson, K. G. (2009). Frontal eye field activity enhances object identification during covert visual search. *J. Neurophysiol.* 102, 3656–3672.

Monsivais, P., Clark, B. A., Roth, A., and Häusser, M. (2005). Determinants of action potential propagation in cerebellar Purkinje cell axons. *J. Neurosci.* 25, 464–472.

Monzée, J., Drew, T., and Smith, A. M. (2004). Effects of muscimol inactivation of the cerebellar nuclei on precision grip. *J. Neurophysiol.* 91, 1240–1249.

Moore, T., Armstrong, K. M., and Fallah, M. (2003). Visuomotor origins of covert spatial attention. *Neuron* 40, 671–683.

Moore, T., and Zirnsak, M. (2017). Neural Mechanisms of Selective Visual Attention. *Annu. Rev. Psychol.* 68, 47–72.

Mosconi, M. W., Luna, B., Kay-Stacey, M., Nowinski, C. V., Rubin, L. H., Scudder, C., et al. (2013). Saccade adaptation abnormalities implicate dysfunction of cerebellar-dependent learning mechanisms in Autism Spectrum Disorders (ASD). *PLoS One* 8, e63709.

Mugnaini, E. (1983). The length of cerebellar parallel fibers in chicken and rhesus monkey. *J. Comp. Neurol.* 220, 7–15.

Mulliken, G. H., Bichot, N. P., Ghadooshahy, A., Sharma, J., Kornblith, S., Philcock, M., et al. (2015). Custom-fit radiolucent cranial implants for neurophysiological recording and stimulation. *J. Neurosci. Methods* 241, 146–154.

Munoz, D. P., and Everling, S. (2004). Look away: the anti-saccade task and the voluntary control of eye movement. *Nat. Rev. Neurosci.* 5, 218–228.

Napper, R. M., and Harvey, R. J. (1988). Number of parallel fiber synapses on an individual Purkinje cell in the cerebellum of the rat. *J. Comp. Neurol.* 274, 168–177.

Nicolson, R. I., Fawcett, A. J., and Dean, P. (2001). Developmental dyslexia: the cerebellar deficit hypothesis. *Trends Neurosci.* 24, 508–511.

Nieuwenhuys, R. (1967). Comparative anatomy of the cerebellum. *Prog. Brain Res.* 25, 1–93.

Nieuwenhuys, R., Donkelaar, H. J. T., and Nicholson, C. (1998). *The Central Nervous System of Vertebrates: Volume 1 / Volume 2 / Volume 3*. Springer, Berlin, Heidelberg.

Nobre, A. C., Gitelman, D. R., Dias, E. C., and Mesulam, M. M. (2000). Covert Visual Spatial Orienting and Saccades: Overlapping Neural Systems. *Neuroimage* 11, 210–216.

Noda, H., and Fujikado, T. (1987). Involvement of Purkinje cells in evoking saccadic eye movements by microstimulation of the posterior cerebellar vermis of monkeys. *J. Neurophysiol.* 57, 1247–1261.

Noda, H., Sugita, S., and Ikeda, Y. (1990). Afferent and efferent connections of the oculomotor region of the fastigial nucleus in the macaque monkey. *J. Comp. Neurol.* 302, 330–348.

Norris, S. A., Hathaway, E. N., Taylor, J. A., and Thach, W. T. (2011). Cerebellar inactivation impairs memory of learned prism gaze-reach calibrations. *J. Neurophysiol.* 105, 2248–2259.

Nyström, M., and Holmqvist, K. (2010). An adaptive algorithm for fixation, saccade, and glissade detection in eyetracking data. *Behav. Res. Methods* 42, 188–204.

Nyström, M., Hooge, I., and Holmqvist, K. (2013). Post-saccadic oscillations in eye movement data recorded with pupil-based eye trackers reflect motion of the pupil inside the iris. *Vision Res.* 92, 59–66.

O'Connor, D. H., Fukui, M. M., Pinsk, M. A., and Kastner, S. (2002). Attention modulates responses in the human lateral geniculate nucleus. *Nat. Neurosci.* 5, 1203–1209.

Ohki, M., Kitazawa, H., Hiramatsu, T., Kaga, K., Kitamura, T., Yamada, J., et al. (2009). Role of primate cerebellar hemisphere in voluntary eye movement control revealed by lesion effects. *J. Neurophysiol.* 101, 934–947.

Ohtsuka, K., and Noda, H. (1995). Discharge properties of Purkinje cells in the oculomotor vermis during visually guided saccades in the macaque monkey. *J. Neurophysiol.* 74, 1828–1840.

Ojakangas, C. L., and Ebner, T. J. (1992). Purkinje cell complex and simple spike changes during a voluntary arm movement learning task in the monkey. *Journal of Neurophysiology* 68, 2222–2236. doi:10.1152/jn.1992.68.6.2222.

O'Leary, J. G., and Lisberger, S. G. (2012). Role of the lateral intraparietal area in modulation of the strength of sensory-motor transmission for visually guided movements. *J. Neurosci.* 32, 9745–9754.

Optican, L. M., and Miles, F. A. (1985). Visually induced adaptive changes in primate saccadic oculomotor control signals. *J. Neurophysiol.* 54, 940–958.

Optican, L. M., and Pretegiani, E. (2017). What stops a saccade? *Philos. Trans. R. Soc. Lond. B Biol. Sci.* 372. doi:10.1098/rstb.2016.0194.

Optican, L. M., and Quaia, C. (2002). Distributed model of collicular and cerebellar function during saccades. *Ann. N. Y. Acad. Sci.* 956, 164–177.

Optican, L. M., and Robinson, D. A. (1980a). Cerebellar-dependent adaptive control of primate saccadic system. *J. Neurophysiol.* 44, 1058–1076.

Optican, L. M., and Robinson, D. A. (1980b). Cerebellar-dependent adaptive control of primate saccadic system. *J. Neurophysiol.* 44, 1058–1076.

Optican, L. M., Zee, D. S., and Miles, F. A. (1986). Floccular lesions abolish adaptive control of post-saccadic ocular drift in primates. *Exp. Brain Res.* 64, 596–598.

Ormianer, Z., Laufer, B. Z., Nissan, J., and Gross, M. (2000). An investigation of heat transfer to the implant-bone interface related to exothermic heat generation during setting of autopolymerizing acrylic resins applied directly to an implant abutment. *Int. J. Oral Maxillofac. Implants* 15, 837–842.

Ortiz-Rios, M., Haag, M., Balezeau, F., Frey, S., Thiele, A., Murphy, K., et al. (2018). Improved methods for MRI-compatible implants in nonhuman primates. *J. Neurosci. Methods* 308, 377–389.

Overton, J. A., Cooke, D. F., Goldring, A. B., Lucero, S. A., Weatherford, C., and Recanzone, G. H. (2017). Improved methods for acrylic-free implants in nonhuman primates for neuroscience research. *J. Neurophysiol.* 118, 3252–3270.

Palay, S. L., and Chan-Palay, V. (1974). *Cerebellar Cortex: Cytology and Organization*. Springer, Berlin, Heidelberg.

Palkovits, M., Mezey, E., Hámori, J., and Szentágothai, J. (1977). Quantitative histological analysis of the cerebellar nuclei in the cat. I. Numerical data on cells and on synapses. *Exp. Brain Res.* 28, 189–209.

Passingham, R. (2009). How good is the macaque monkey model of the human brain? *Current Opinion in Neurobiology* 19, 6–11. doi:10.1016/j.conb.2009.01.002.

Paulin, M. G. (2005). Evolution of the cerebellum as a neuronal machine for Bayesian state estimation. *J. Neural Eng.* 2, S219–S234.

Paxinos, G., Huang, X.-F., and Toga, A. W. (2000). The Rhesus Monkey Brain in Stereotaxic Coordinates.

Available at: https://ro.uow.edu.au/hbspapers/3613 [Accessed May 19, 2020].

Pélisson, D., Alahyane, N., Panouillères, M., and Tilikete, C. (2010). Sensorimotor adaptation of saccadic eye movements. *Neurosci. Biobehav. Rev.* 34, 1103–1120.

Person, A. L., and Raman, I. M. (2011). Purkinje neuron synchrony elicits time-locked spiking in the cerebellar nuclei. *Nature* 481, 502–505.

Person, A. L., and Raman, I. M. (2012). Synchrony and neural coding in cerebellar circuits. *Front. Neural Circuits* 6, 97.

Peterburs, J., Gajda, K., Koch, B., Schwarz, M., Hoffmann, K.-P., Daum, I., et al. (2012). Cerebellar lesions alter performance monitoring on the antisaccade task–an event-related potentials study. *Neuropsychologia* 50, 379–389.

Petersen, S. E., Robinson, D. L., and Morris, J. D. (1987). Contributions of the pulvinar to visual spatial attention. *Neuropsychologia* 25, 97–105.

Piu, P., Pretegiani, E., Rosini, F., Serchi, V., Zaino, D., Chiantini, T., et al. (2019). The cerebellum improves the precision of antisaccades by a latency-duration trade-off. *Prog. Brain Res.* 249, 125–139.

Popa, L. S., Hewitt, A. L., and Ebner, T. J. (2012). Predictive and feedback performance errors are signaled in the simple spike discharge of individual Purkinje cells. *J. Neurosci.* 32, 15345–15358.

Popa, L. S., Streng, M. L., and Ebner, T. J. (2017). Long-Term Predictive and Feedback Encoding of Motor Signals in the Simple Spike Discharge of Purkinje Cells. *eNeuro* 4. doi:10.1523/ENEURO.0036-17.2017.

Popa, L. S., Streng, M. L., Hewitt, A. L., and Ebner, T. J. (2016). The Errors of Our Ways: Understanding Error Representations in Cerebellar-Dependent Motor Learning. *Cerebellum* 15, 93–103.

Prescott, M. J., Brown, V. J., Flecknell, P. A., Gaffan, D., Garrod, K., Lemon, R. N., et al. (2010). Refinement of the use of food and fluid control as motivational tools for macaques used in behavioural neuroscience research: report of a Working Group of the NC3Rs. *J. Neurosci. Methods* 193, 167–188.

Prevosto, V., Graf, W., and Ugolini, G. (2010). Cerebellar inputs to intraparietal cortex areas LIP and MIP: functional frameworks for adaptive control of eye movements, reaching, and arm/eye/head movement coordination. *Cereb. Cortex* 20, 214–228.

Procyk, E., Wilson, C. R. E., Stoll, F. M., Faraut, M. C. M., Petrides, M., and Amiez, C. (2016). Midcingulate Motor Map and Feedback Detection: Converging Data from Humans and Monkeys. *Cereb. Cortex* 26, 467–476.

Quaia, C., Lefèvre, P., and Optican, L. M. (1999). Model of the control of saccades by superior colliculus and cerebellum. *J. Neurophysiol.* 82, 999–1018.

Rajan, A. T., Boback, J. L., Dammann, J. F., Tenore, F. V., Wester, B. A., Otto, K. J., et al. (2015). The effects of chronic intracortical microstimulation on neural tissue and fine motor behavior. *Journal of Neural Engineering* 12, 066018. doi:10.1088/1741-2560/12/6/066018.

Ramirez, J. E., and Stell, B. M. (2016). Calcium Imaging Reveals Coordinated Simple Spike Pauses in Populations of Cerebellar Purkinje Cells. *Cell Rep.* 17, 3125–3132.

Ramnani, N. (2006). The primate cortico-cerebellar system: anatomy and function. *Nat. Rev. Neurosci.* 7, 511–522.

Reato, D., Tara, E., and Khodakhah, K. (2016). "Chapter 2 - Deep Cerebellar Nuclei Rebound Firing In Vivo: Much Ado About Almost Nothing?," in *The Neuronal Codes of the Cerebellum*, ed. D. H. Heck (San Diego: Academic Press), 27–51.

Reinhardt, V. (2003). Working with rather than against macaques during blood collection. *J. Appl. Anim. Welf. Sci.* 6, 189–197.

Reinhardt, V. (2004). Common husbandry-related variables in biomedical research with animals. *Lab. Anim.* 38, 213–235.

Reveley, C., Gruslys, A., Ye, F. Q., Glen, D., Samaha, J., E Russ, B., et al. (2017). Three-Dimensional Digital Template Atlas of the Macaque Brain. *Cereb. Cortex* 27, 4463–4477.

Rispal-Padel, L., Cicirata, F., and Pons, C. (1982). Cerebellar nuclear topography of simple and synergistic movements in the alert baboon (Papio papio). *Exp. Brain Res.* 47, 365–380.

Rizzolatti, G., Riggio, L., Dascola, I., and Umiltá, C. (1987). Reorienting attention across the horizontal and vertical meridians: evidence in favor of a premotor theory of attention. *Neuropsychologia* 25, 31–40.

Robinson, D. A. (1963). A METHOD OF MEASURING EYE MOVEMENT USING A SCLERAL SEARCH COIL IN A MAGNETIC FIELD. *IEEE Trans. Biomed. Eng.* 10, 137–145.

Robinson, D. A. (1964). THE MECHANICS OF HUMAN SACCADIC EYE MOVEMENT. *J. Physiol.* 174, 245–264.

Robinson, F. R., Straube, A., and Fuchs, A. F. (1993). Role of the caudal fastigial nucleus in saccade generation. II. Effects of muscimol inactivation. *J. Neurophysiol.* 70, 1741–1758.

Rockx, B., Kuiken, T., Herfst, S., Bestebroer, T., Lamers, M. M., Oude Munnink, B. B., et al. (2020). Comparative pathogenesis of COVID-19, MERS, and SARS in a nonhuman primate model. *Science* 368, 1012–1015.

Roelfsema, P. R., and Treue, S. (2014). Basic neuroscience research with nonhuman primates: a small but indispensable component of biomedical research. *Neuron* 82, 1200–1204.

Roitman, J. D., and Shadlen, M. N. (2002). Response of neurons in the lateral intraparietal area during a combined visual discrimination reaction time task. *J. Neurosci.* 22, 9475–9489.

Ron, S., and Robinson, D. A. (1973). Eye movements evoked by cerebellar stimulation in the alert monkey. *J. Neurophysiol.* 36, 1004–1022.

Rowland, N. C., and Jaeger, D. (2005). Coding of tactile response properties in the rat deep cerebellar nuclei. *J. Neurophysiol.* 94, 1236–1251.

Ruigrok, T. J. (1997). Cerebellar nuclei: the olivary connection. *Prog. Brain Res.* 114, 167–192.

Ryan, A. M., Freeman, S. M., Murai, T., Lau, A. R., Palumbo, M. C., Hogrefe, C. E., et al. (2019). Non-invasive Eye Tracking Methods for New World and Old World Monkeys. *Front. Behav. Neurosci.* 13, 39.

Saleem, K. S., and Logothetis, N. K. (2012). *A Combined MRI and Histology Atlas of the Rhesus Monkey Brain in Stereotaxic Coordinates*. Academic Press.

Sato, T. R., and Schall, J. D. (2003). Effects of stimulus-response compatibility on neural selection in frontal eye field. *Neuron* 38, 637–648.

Scerra, V. E., Costello, M. G., Salinas, E., and Stanford, T. R. (2019). All-or-None Context Dependence Delineates Limits of FEF Visual Target Selection. *Curr. Biol.* 29, 294–305.e3.

Schafer, R. J., and Moore, T. (2007). Attention governs action in the primate frontal eye field. *Neuron* 56, 541–551.

Schall, J. D., and Hanes, D. P. (1993). Neural basis of saccade target selection in frontal eye field during visual search. *Nature*.

SCHEER, (Scientific Committee on Health, Environmental and Emerging Risks) (2017). Final Opinion on "The need for non-human primates in biomedical research, production and testing of products and devices (update 2017)."

Schiller, P. H., True, S. D., and Conway, J. L. (1980). Deficits in eye movements following frontal eye-field and superior colliculus ablations. *J. Neurophysiol.* 44, 1175–1189.

Schlag-Rey, M., Amador, N., Sanchez, H., and Schlag, J. (1997). Antisaccade performance predicted by neuronal activity in the supplementary eye field. *Nature* 390, 398–401.

Schmahmann, J. D. (1991). An emerging concept. The cerebellar contribution to higher function. *Arch. Neurol.* 48, 1178–1187.

Schmahmann, J. D. (2004). Disorders of the cerebellum: ataxia, dysmetria of thought, and the cerebellar cognitive affective syndrome. *J. Neuropsychiatry Clin. Neurosci.* 16, 367–378.

Schmahmann, J. D. (2016). "A Brief History of the Cerebellum," in *Essentials of Cerebellum and Cerebellar Disorders: A Primer For Graduate Students*, eds. D. L. Gruol, N. Koibuchi, M. Manto, M. Molinari, J. D. Schmahmann, and Y. Shen (Cham: Springer International Publishing), 5–20.

Schmahmann, J. D., and Sherman, J. C. (1998). The cerebellar cognitive affective syndrome. *Brain* 121, 561–579.

Scholtyssek, C., Kelber, A., and Dehnhardt, G. (2008). Brightness discrimination in the harbor seal (Phoca vitulina). *Vision Res.* 48, 96–103.

Schultz, S. R., Kitamura, K., Post-Uiterweer, A., Krupic, J., and Häusser, M. (2009). Spatial pattern coding of sensory information by climbing fiber-evoked calcium signals in networks of neighboring cerebellar Purkinje cells. *J. Neurosci.* 29, 8005–8015.

Schultz, W., and Dickinson, A. (2000). Neuronal coding of prediction errors. *Annu. Rev. Neurosci.* 23, 473–500.

Scudder, C. A., Kaneko, C. R., and Fuchs, A. F. (2002). The brainstem burst generator for saccadic eye movements. *Exp. Brain Res.* 142, 439–462.

Sedaghat-Nejad, E., Herzfeld, D. J., Hage, P., Karbasi, K., Palin, T., Wang, X., et al. (2019). Behavioral training of marmosets and electrophysiological recording from the cerebellum. *J. Neurophysiol.* 122, 1502–1517.

Seidemann, E., Chen, Y., Bai, Y., Chen, S. C., Mehta, P., Kajs, B. L., et al. (2016). Calcium imaging with genetically encoded indicators in behaving primates. *Elife* 5. doi:10.7554/eLife.16178.

Sendhilnathan, N., Ipata, A. E., and Goldberg, M. E. (2020). Neural Correlates of Reinforcement Learning in Mid-lateral Cerebellum. *Neuron* 106, 188–198.e5.

Senju, A., and Johnson, M. H. (2009). The eye contact effect: mechanisms and development. *Trends Cogn. Sci.* 13, 127–134.

Sereno, M. I., Diedrichsen, J., Tachrount, M., Testa-Silva, G., d'Arceuil, H., and De Zeeuw, C. (2020). The human cerebellum has almost 80% of the surface area of the neocortex. *Proc. Natl. Acad. Sci. U. S. A.* 117, 19538–19543.

Shadlen, M. N., and Newsome, W. T. (2001). Neural basis of a perceptual decision in the parietal cortex (area LIP) of the rhesus monkey. *J. Neurophysiol.* 86, 1916–1936.

Shadmehr, R. (2017). Learning to Predict and Control the Physics of Our Movements. *J. Neurosci.* 37, 1663–1671.

Shadmehr, R., Smith, M. A., and Krakauer, J. W. (2010). Error correction, sensory prediction, and adaptation in motor control. *Annu. Rev. Neurosci.* 33, 89–108.

Shepherd, G. M. ed. (2004). *The synaptic organization of the brain, 5th ed*. New York, NY, US: Oxford University Press The synaptic organization of the brain.

Sherrington, C. (1952). *The Integrative Action of the Nervous System*. CUP Archive.

Shin, S. L., Hoebeek, F. E., Schonewille, M., De Zeeuw, C. I., Aertsen, A., and De Schutter, E. (2007). Regular patterns in cerebellar Purkinje cell simple spike trains. *PLoS One* 2, 1–9.

Shipp, S. (2004). The brain circuitry of attention. *Trends Cogn. Sci.* 8, 223–230.

Sillitoe, R. V., Malz, C. R., Rockland, K., and Hawkes, R. (2004). Antigenic compartmentation of the primate and tree shrew cerebellum: a common topography of zebrin II in Macaca mulatta and Tupaia belangeri. *J. Anat.* 204, 257–269.

Simpson, J. I., Belton, T., Suh, M., and Winkelman, B. (2002). Complex spike activity in the flocculus signals more than the eye can see. *Ann. N. Y. Acad. Sci.* 978, 232–236.

Sindermann, F., Geiselmann, B., and Fischler, M. (1978). Single motor unit activity in extraocular muscles in man during fixation and saccades. *Electroencephalogr. Clin. Neurophysiol.* 45, 64–73.

Smaers, J. B., Steele, J., and Zilles, K. (2011). Modeling the evolution of cortico-cerebellar systems in primates. *Ann. N. Y. Acad. Sci.* 1225, 176–190.

Smaers, J. B., Turner, A. H., Gómez-Robles, A., and Sherwood, C. C. (2018). A cerebellar substrate for cognition evolved multiple times independently in mammals. *Elife* 7. doi:10.7554/eLife.35696.

Smaers, J. B., and Vanier, D. R. (2019). Brain size expansion in primates and humans is explained by a selective modular expansion of the cortico-cerebellar system. *Cortex* 118, 292–305.

Soetedjo, R., Kojima, Y., and Fuchs, A. F. (2019). How cerebellar motor learning keeps saccades accurate. *J. Neurophysiol.* 121, 2153–2162.

Sokolov, A. A., Miall, R. C., and Ivry, R. B. (2017). The Cerebellum: Adaptive Prediction for Movement and Cognition. *Trends Cogn. Sci.* 21, 313–332.

Sparks, D. L. (1986). Translation of sensory signals into commands for control of saccadic eye movements: role of primate superior colliculus. *Physiol. Rev.* 66, 118–171.

Sparks, D. L. (2002). The brainstem control of saccadic eye movements. *Nat. Rev. Neurosci.* 3, 952–964.

Sparks, D. L., and Hartwich-Young, R. (1989). The deep layers of the superior colliculus. *Rev. Oculomot. Res.* 3, 213–255.

Spidalieri, G., Busby, L., and Lamarre, Y. (1983). Fast ballistic arm movements triggered by visual, auditory, and somesthetic stimuli in the monkey. II. Effects of unilateral dentate lesion on discharge of precentral cortical neurons and reaction time. *J. Neurophysiol.* 50, 1359–1379.

Spira, M. E., and Hai, A. (2013). Multi-electrode array technologies for neuroscience and cardiology. *Nat. Nanotechnol.* 8, 83–94.

Sprague, J. M. (1966). Interaction of cortex and superior colliculus in mediation of visually guided behavior in the cat. *Science* 153, 1544–1547.

Stein, T., Senju, A., Peelen, M. V., and Sterzer, P. (2011). Eye contact facilitates awareness of faces during interocular suppression. *Cognition* 119, 307–311.

Stern, S., Kirst, C., and Bargmann, C. I. (2017). Neuromodulatory Control of Long-Term Behavioral Patterns and Individuality across Development. *Cell* 171. doi:10.1016/j.cell.2017.10.041.

Stoodley, C. J., D'Mello, A. M., Ellegood, J., Jakkamsetti, V., Liu, P., Nebel, M. B., et al. (2017). Altered cerebellar connectivity in autism and cerebellar-mediated rescue of autism-related behaviors in mice. *Nat. Neurosci.* 20, 1744–1751.

Straube, A., Deubel, H., Spuler, A., and Büttner, U. (1995). Differential Effect of a Bilateral Deep Cerebellar Nuclei Lesion on Externally and Internally Triggered Saccades in Humans. *Neuroophthalmology* 15, 67–74.

Streng, M. L., Popa, L. S., and Ebner, T. J. (2018). Modulation of sensory prediction error in Purkinje cells during visual feedback manipulations. *Nat. Commun.* 9, 1099.

Strick, P. L., Dum, R. P., and Fiez, J. A. (2009). Cerebellum and nonmotor function. *Annu. Rev. Neurosci.* 32, 413–434.

Striemer, C. L., Cantelmi, D., Cusimano, M. D., Danckert, J. A., and Schweizer, T. A. (2015). Deficits in reflexive covert attention following cerebellar injury. *Front. Hum. Neurosci.* 9, 1–10.

Sugihara, I. (2018). Crus I in the Rodent Cerebellum: Its Homology to Crus I and II in the Primate Cerebellum and Its Anatomical Uniqueness Among Neighboring Lobules. *Cerebellum* 17, 49–55.

Sultan, F., Hamodeh, S., and Baizer, J. S. (2010). The human dentate nucleus: a complex shape untangled. *Neuroscience* 167, 965–968.

Sun, Z., Smilgin, A., Junker, M., Dicke, P. W., and Thier, P. (2017). The same oculomotor vermal Purkinje cells encode the different kinematics of saccades and of smooth pursuit eye movements. *Sci. Rep.* 7, 40613.

Surmenev, R. A., Surmeneva, M. A., and Ivanova, A. A. (2014). Significance of calcium phosphate coatings for the enhancement of new bone osteogenesis–a review. *Acta Biomater.* 10, 557–579.

Suvrathan, A., and Raymond, J. L. (2018). Depressed by Learning-Heterogeneity of the Plasticity Rules at Parallel Fiber Synapses onto Purkinje Cells. *Cerebellum* 17, 747–755.

Svoboda, K., and Li, N. (2018). Neural mechanisms of movement planning: motor cortex and beyond. *Curr. Opin. Neurobiol.* 49, 33–41.

Takagi, M., Zee, D. S., Tamargo, R. J., Kojima, Y., Robinson, F. R., and Soetedjo, R. (1998). Effects of Lesions of the Oculomotor Vermis on Eye Movements in Primate : Saccades. *Journal of neurophysiology*, 1911–1931.

Tanaka, H., Harada, M., Arai, M., and Hirata, K. (2003). Cognitive dysfunction in cortical cerebellar atrophy correlates with impairment of the inhibitory system. *Neuropsychobiology* 47, 206–211.

Tanaka, M. (2006). Inactivation of the central thalamus delays self-timed saccades. *Nat. Neurosci.* 9, 20–22.

Tek, P., Chiganos, T. C., Mohammed, J. S., Eddington, D. T., Fall, C. P., Ifft, P., et al. (2008). Rapid prototyping for neuroscience and neural engineering. *J. Neurosci. Methods* 172, 263–269.

ten Brinke, M. M., Boele, H.-J., Spanke, J. K., Potters, J.-W., Kornysheva, K., Wulff, P., et al. (2015). Evolving Models of Pavlovian Conditioning: Cerebellar Cortical Dynamics in Awake Behaving Mice. *Cell Rep.* 13, 1977–1988.

Ten Brinke, M. M., Heiney, S. A., Wang, X., Proietti-Onori, M., Boele, H.-J., Bakermans, J., et al. (2017). Dynamic modulation of activity in cerebellar nuclei neurons during pavlovian eyeblink conditioning in mice. *Elife* 6. doi:10.7554/eLife.28132.

Thach, W. T. (2007). On the mechanism of cerebellar contributions to cognition. *Cerebellum* 6, 163–167.

Thier, P., Dicke, P. W., Haas, R., Thielert, C.-D., and Catz, N. (2002). The role of the oculomotor vermis in the control of saccadic eye movements. *Ann. N. Y. Acad. Sci.* 978, 50–62.

Thier, P., and Möck, M. (2006). The oculomotor role of the pontine nuclei and the nucleus reticularis tegmenti pontis. *Prog. Brain Res.* 151, 293–320.

Thoroughman, K. A., and Shadmehr, R. (2000). Learning of action through adaptive combination of motor primitives. *Nature* 407, 742–747.

Tian, X., Yoshida, M., and Hafed, Z. M. (2018). Dynamics of fixational eye position and microsaccades during spatial cueing: the case of express microsaccades. *J. Neurophysiol.* 119, 1962–1980.

Townsend, J., Courchesne, E., and Egaas, B. (1996a). Slowed orienting of covert visual-spatial attention in autism: Specific deficits associated with cerebellar and parietal abnormality. *Dev. Psychopathol.* 8, 563.

Townsend, J., Harris, N. S., and Courchesne, E. (1996b). Visual attention abnormalities in autism: delayed orienting to location. *J. Int. Neuropsychol. Soc.* 2, 541–550.

Tseng, Y.-W., Diedrichsen, J., Krakauer, J. W., Shadmehr, R., and Bastian, A. J. (2007). Sensory prediction errors drive cerebellum-dependent adaptation of reaching. *J. Neurophysiol.* 98, 54–62.

Tsutsui, K.-I., Hosokawa, T., Yamada, M., and Iijima, T. (2016). Representation of Functional Category in the Monkey Prefrontal Cortex and Its Rule-Dependent Use for Behavioral Selection. *J. Neurosci.* 36, 3038–3048.

Uusisaari, M. Y., and Knöpfel, T. (2012). Diversity of neuronal elements and circuitry in the cerebellar nuclei. *Cerebellum* 11, 420–421.

van der Geest, J. N., and Frens, M. A. (2002). Recording eye movements with video-oculography and scleral search coils: a direct comparison of two methods. *J. Neurosci. Methods* 114, 185–195.

Van Der Giessen, R. S., Koekkoek, S. K., van Dorp, S., De Gruijl, J. R., Cupido, A., Khosrovani, S., et al. (2008). Role of olivary electrical coupling in cerebellar motor learning. *Neuron* 58, 599–612.

van Dorp, S., and De Zeeuw, C. I. (2014). Variable timing of synaptic transmission in cerebellar unipolar brush cells. *Proc. Natl. Acad. Sci. U. S. A.* 111, 5403–5408.

van Es, D. M., van der Zwaag, W., and Knapen, T. (2019). Topographic Maps of Visual Space in the Human Cerebellum. *Curr. Biol.* 29, 1689–1694.e3.

Van Essen, D. C., Donahue, C. J., and Glasser, M. F. (2018). Development and Evolution of Cerebral and Cerebellar Cortex. *Brain Behav. Evol.* 91, 158–169.

Van Gisbergen, J. A., Robinson, D. A., and Gielen, S. (1981). A quantitative analysis of generation of saccadic eye movements by burst neurons. *J. Neurophysiol.* 45, 417–442.

Van Hooff, J. A. R. A. M. (1967). "The Facial Displays of the Catarrhine Monkeys and Apes," in *Primate ethology , (pp*, ed. D. Morris, 7–68.

van Vugt, B., van Kerkoerle, T., Vartak, D., and Roelfsema, P. R. (2020). The Contribution of AMPA and NMDA Receptors to Persistent Firing in the Dorsolateral Prefrontal Cortex in Working Memory. *J. Neurosci.* 40, 2458–2470.

Volkmann, F. C. (1962). Vision during voluntary saccadic eye movements. *J. Opt. Soc. Am.* 52, 571–578.

Voogd, J., and De Zeeuw, C. I. (2020). Cerebellum: What is in a Name? Historical Origins and First Use of This Anatomical Term. *Cerebellum* 19, 550–561.

Voogd, J., and Marani, E. (2016). "Gross Anatomy of the Cerebellum," in *Essentials of Cerebellum and Cerebellar Disorders: A Primer For Graduate Students*, eds. D. L. Gruol, N. Koibuchi, M. Manto, M. Molinari, J. D. Schmahmann, and Y. Shen (Cham: Springer International Publishing), 33–38.

Voogd, J., and Ruigrok, T. J. H. (2012). "Cerebellum and Precerebellar Nuclei," in *The Human Nervous System*, eds. J. K. Mai and G. Paxinos (Elsevier Academic Press).

Voogd, J., Schraa-Tam, C. K. L., van der Geest, J. N., and De Zeeuw, C. I. (2012). Visuomotor cerebellum in human and nonhuman primates. *Cerebellum* 11, 392–410.

Wagner, M. J., Kim, T. H., Savall, J., Schnitzer, M. J., and Luo, L. (2017). Cerebellar granule cells encode the expectation of reward. *Nature* 544, 96–100.

Wang, J.-J., Kim, J. H., and Ebner, T. J. (1987). Climbing fiber afferent modulation during a visually guided, multi-joint arm movement in the monkey. *Brain Research* 410, 323–329. doi:10.1016/0006-8993(87)90331-3.

Wang, Q., Ding, S.-L., Li, Y., Royall, J., Feng, D., Lesnar, P., et al. (2020a). The Allen Mouse Brain Common Coordinate Framework: A 3D Reference Atlas. *Cell* 181, 936–953.e20.

Wang, S. S. H., Kloth, A. D., and Badura, A. (2014). The Cerebellum, Sensitive Periods, and Autism. *Neuron* 83, 518–532.

Wang, X., Ley, A., Koch, S., Lindlbauer, D., Hays, J., Holmqvist, K., et al. (2019). The Mental Image Revealed by Gaze Tracking. *Proceedings of the 2019 CHI Conference on Human Factors in Computing Systems - CHI '19*. doi:10.1145/3290605.3300839.

Wang, X., Yu, S.-Y., Ren, Z., De Zeeuw, C., and Gao, Z. (2020b). A Novel FN-MdV Pathway and Its Role in Cerebellar Multimodular Control of Sensorimotor Behavior. doi:10.21203/rs.3.rs-43736/v1.

Wardak, C., Olivier, E., and Duhamel, J.-R. (2011). The relationship between spatial attention and saccades in the frontoparietal network of the monkey. *Eur. J. Neurosci.* 33, 1973–1981.

Weber, R. B., and Daroff, R. B. (1972). Corrective movements following refixation saccades: type and control system analysis. *Vision Res.* 12, 467–475.

Welch, J. M., Lu, J., Rodriguiz, R. M., Trotta, N. C., Peca, J., Ding, J. D., et al. (2007). Cortico-striatal synaptic defects and OCD-like behaviours in Sapap3-mutant mice. *Nature* 448, 894–900.

Welsh, J. P., Lang, E. J., Suglhara, I., and Llinas, R. (1995). Dynamic organization of motor control within the olivocerebellar system. *Nature* 374, 453–457.

Westheimer, G., and Blair, S. M. (1974). Function Organization of primate oculomotor system revealed by cerebellectomy. *Exp. Brain Res.* 21, 463–472.

Westlund, K. (2015). Training laboratory primates–benefits and techniques. *Primate Biology* 2, 119.

Whiting, B. A., and Barton, R. A. (2003). The evolution of the cortico-cerebellar complex in primates: anatomical connections predict patterns of correlated evolution. *J. Hum. Evol.* 44, 3–10.

Witter, L., Canto, C. B., Hoogland, T. M., de Gruijl, J. R., and De Zeeuw, C. I. (2013). Strength and timing of motor responses mediated by rebound firing in the cerebellar nuclei after Purkinje cell activation. *Front. Neural Circuits* 7, 133.

Wulff, P., Schonewille, M., Renzi, M., Viltono, L., Sassoè-Pognetto, M., Badura, A., et al. (2009). Synaptic inhibition of Purkinje cells mediates consolidation of vestibulo-cerebellar motor learning. *Nat. Neurosci.* 12, 1042–1049.

Yakhnitsa, V., and Barmack, N. H. (2006). Antiphasic Purkinje cell responses in mouse uvula-nodulus are sensitive to static roll-tilt and topographically organized. *Neuroscience* 143, 615–626.

Yamada, J., and Noda, H. (1987). Afferent and efferent connections of the oculomotor cerebellar vermis in the macaque monkey. *J. Comp. Neurol.* 265, 224–241.

Yang, Y., and Lisberger, S. G. (2014). Purkinje-cell plasticity and cerebellar motor learning are graded by complex-spike duration. *Nature* 510, 529–532.

Yeo, B. T. T., Krienen, F. M., Sepulcre, J., Sabuncu, M. R., Lashkari, D., Hollinshead, M., et al. (2011). The organization of the human cerebral cortex estimated by intrinsic functional connectivity. *J. Neurophysiol.* 106, 1125–1165.

Yu, F., Jiang, Q.-J., Sun, X.-Y., and Zhang, R.-W. (2015). A new case of complete primary cerebellar agenesis: clinical and imaging findings in a living patient. *Brain* 138, e353–e353.

Yul, J. (1972). The Pathway Mediating flexion After Cerebellar Ablation or Ipsilateral Limb Paravermal Cortical Cooling in Cats. *Experimental Neurology* 36, 549–562.

Yushkevich, P. A., Piven, J., Hazlett, H. C., Smith, R. G., Ho, S., Gee, J. C., et al. (2006). User-guided 3D active contour segmentation of anatomical structures: significantly improved efficiency and reliability. *Neuroimage* 31, 1116–1128.

Zee, D. S., Optican, L. M., Cook, J. D., Robinson, D. A., and Engel, W. K. (1976). Slow saccades in spinocerebellar degeneration. *Arch. Neurol.* 33, 243–251.

Zee, D. S., Yamazaki, A., Butler, P. H., and Gücer, G. (1981). Effects of ablation of flocculus and paraflocculus of eye movements in primate. *J. Neurophysiol.* 46, 878–899.

Zeki, S. M. (1978). The cortical projections of foveal striate cortex in the rhesus monkey. *J. Physiol.* 277, 227–244.

Zhang, M., and Barash, S. (2000). Neuronal switching of sensorimotor transformations for antisaccades.

Nature 408, 971–975.

Zhou, H., Lin, Z., Voges, K., Ju, C., Gao, Z., Bosman, L. W. J., et al. (2014). Cerebellar modules operate at different frequencies. *Elife* 3, e02536.

English summary

Saccades are the fast eye movements with which the fovea, the part of the retina where visual acuity is highest, is aligned with a subject of interest. In this thesis I study the relationship between the cerebellum and the steps necessary to produce an accurate saccadic eye movement. To this end rhesus macaques were trained in several different saccade tasks. I start this thesis with a detailed description of techniques that are used to perform behavioral and electrophysiological experiments in non-human primates (**Chapter 2**). This chapter covers how structural imaging techniques can be used to design implants and offers a concise description of surgical techniques to implant those. Furthermore, I provide an overview of experimental techniques to measure eye movements, oro-facial movements, extracellular recordings on single units, and pharmacological interventions.

In the following chapters I use the methods mentioned above to study the relationship between activity patterns of cells in the cerebellum and visually guided behavior. Cerebellar activity has historically been studied mostly in the context of non-volitional motor behavior, such as posture or reflexive (eye) movements. In **Chapter 3** I provide a detailed description on how Purkinje cells in the lateral and medial cerebellum contribute to execution of the pro- and antisaccade task. This task requires a decision between a reflexive movement (prosaccade) and the volitional suppression of one to make an opposite movement (antisaccade). Primates were trained to make this decision on the basis of a visual cue (instruction). In line with prior findings on the cognitive functions of the lateral cerebellum, Purkinje cells in this region were more active during the instruction period than those in the medial cerebellum, which is commonly associated with movement execution. Furthermore, activity of lateral neurons was more likely to bridge the period from instruction to execution, highlighting its function in motor planning.

Subsequently, I investigate the properties of neural activity in cells one synapse downstream of the dentate nucleus, which receives input from Purkinje cells (**Chapter 4**). The central question of this chapter is: which visual functions are executed by the dentate nucleus to plan a saccade? During neural measurements, primates performed a direction dependent task in which they had to read the gap of a Landolt C presented in the periphery of the visual field. Thereafter, they had to show that they had read the C by performing a saccade to the correct target. The neurons exhibit, congruent with the pro- and antisaccade task, modulation of activity throughout the entire task, including the part where the animal receives a reward. In the majority of neurons activity modulations are dependent on the direction of the Landolt C, or the thereupon following saccace. These data provide new insights into how the cerebellum integrates direction dependent visual information to correctly initiate and execute movements. A dye was infused in the area under study to investigate which brain regions send information to it. The stained cells are a specific group of Purkinje cells in the cerebellar cortex (shown on the cover) and neurons in the ventral lamina of the inferior olivary complex in the brainstem. These neurons are part of the D-zones of the cerebellum, which have prominent connections with the visual and attention controlling areas in the cerebral cortex. Both the anatomical and physiological data imply that the cerebellum partakes in the integration of visual perception and motor behavior.

The final experimental chapter of this thesis covers how glissades, the slow gliding movements at the end of the saccade, are under influence of the oculomotor vermis (OMV) of the cerebellum (**Chapter 5**). Local lesions are a tool to assess whether a structure is necessary for execution of a particular behavior. Lesions to the OMV generally cause an increase in the rate of

occurrence of glissades. Glissade speed, duration and amplitude, are also altered by lesioning the OMV, which often rapidly recovers in the days after the lesion. In a series of behavioral experiments on primates with an intact OMV, I tested whether it is possible to elicit motor adaptation of glissades through an adapted version of the intersaccadic step paradigm. This appears not to be the case. The results of adaptation and lesion experiments imply that glissades are a motor error rather than a functional movement.

In the general discussion, (**Chapter 6**) I discuss the results of this thesis in the context of the functions and activity of other brain regions and how they come to initiate and execute movement. Recent research measuring the activity of multiple regions at the same time, shows that the areas under study in this thesis do not operate in isolation. These areas form a loop with, among others, the frontal and parietal eye fields. In this loop information is exchanged bidirectionally, which appears necessary for adequate movement planning and execution. Until recently the cerebellum was regarded primarily as a motor execution oriented structure. The results from this thesis contribute to the understanding of which properties of the cerebellum underlie the whole sequence of events in the brain relating to motor function; from interpreting a stimulus to the proper planning and execution of an eye movement.

Nederlandse samenvatting

Saccade zijn zeer snelle oogbewegingen waarmee de fovea, het deel van de retina waarmee zicht het scherpst is, op een onderwerp wordt gericht. In dit proefschrift onderzoek ik de bijdrage van het cerebellum aan de stappen die gemaakt moeten worden om een correcte saccade te plannen en uit te voeren. Om dit te onderzoeken zijn rhesus makaken getrained op een aantal verschillende saccade taken. Ik begin met een gedetailleerde beschrijving van de technieken die gebruikt worden in dit proefschrift om de gedrags en elektrofysiologische experimenten in niet-humane primaten uit te kunnen voeren (**Hoofdstuk 2**). Dit hoofdstuk behandelt hoe op basis van structurele beeldvormingstechnieken implantaten ontworpen kunnen worden voor fixatie en elektrofysiologische en een beknopte samenvatting van chirurgische technieken om deze te kunnen implanteren. Daarnaast geef ik een overzicht van experimentele technieken om metingen aan oogbewegingen, mond- en gezichtsbewegingen, elektrofysiologische aan individuele cellen, en farmacologische interventies te kunnen uitvoeren

In de hierop volgende hoofdstukken gebruik ik de hierboven beschreven technieken om de relatie tussen activiteitenpatronen van cellen in het cerebellum en verschillende vormen van visueel gestuurd gedrag te bestuderen. Van oudsher wordt het cerebellum vooral bestudeerd in de context van onbewust geïnitieerde motoriek, zoals de spierspanning die nodig is voor het behouden van postuur of reflexmatige bewegingen. In **Hoofdstuk 3** geef ik een gedetailleerde beschrijving van de bijdrage van Purkinje cellen in het mediale en laterale cerebellum aan het uitvoeren van de pro- en antisaccade taak. Deze taak vereist het maken van een keuze tussen reflexive oogbeweging (prosaccade) of het bewust onderdrukken van deze om een oogbeweging de andere kant op te maken (antisaccade). Primaten waren getraind om op basis van een visuele stimulus (instructie) deze keuze te maken. In lijn met eerdere bevindingen over de cognitieve functies van het laterale cerebellar bleek dat Purkinje cellen in dit gebied actievere ware tijdens de instructie periode, dan cellen in het meer uitvoeringsgerichte mediale cerebellum. Daarnaast hebben cellen in het lateral cerebellum vaker activiteits patronen die de periode van instructie tot de executie overbruggen, wat de bijdrage van dit gebied aan motor planning benadrukt.

Vervolgens onderzoek ik de activiteit van cellen een synapse verder in de nucleus dentatus, die informatie ontvangen van de Purkinje cellen (**Hoofdstuk 4**). De vraag die ik wil beantwoorden in dit hoofdstuk is: welke visuele functies voert de nucleus dentatus uit om een saccade te kunnen plannen? Tijdens de elektrofysiologische metingen voeren de primaten een richtingsafhankelijk taak uit, waarbij ze de richting van de opening van een in de peripherie van het visuele veld gepresenteerde Landolt C moeten lezen. Daarna kunnen ze aan de hand van een saccade naar het doel aan de correcte kant laten zien dat ze de C goed gelezen hebben. Er zijn, net als in het geval van de pro- en antisaccade taak, veranderingen in activiteit te zien over de hele periode van de taak, inclusief de periode wanneer de aap een beloning krijgt. In een groot gedeelte van de cellen is de activiteits modulatie afhankelijk van de richting van de Landolt C, of de richting van de daaropvolgende saccade. Deze data geeft nieuw inzicht in hoe het cerebellum directie afhankelijke visuele informatie integreert voor het correct initiëren en uitvoeren van een beweging. Om te onderzoeken van welke andere hersengebieden de hier gemeten cellen informatie ontvangen is er een kleurstof ingebracht. De cellen die hierdoor aangekleurd zijn een specifieke groep Purkinje cellen in de cerebellaire schors (zie voorkant) en cellen in de ventrale lamina van de complexus olivaris inferior in de hersenstam. Deze gebieden zijn deel van de D-zones van het cerebellum, welke sterke connecties heeft met visuele en aandacht aansturende gebieden in de cerebrale schors. Zowel de anatomische als the

fysiologische data impliceren dat het cerebellum deelneemt aan de integratie van visuele percetie wat leidend tot motorisch gedrag.

Het laatste hoofdstuk gaat over hoe glissades, langzame glijdende bewegingen aan het einde van de saccade, onder invloed staan van de oculomotor vermis (OMV) van het cerebellum (**Hoofdstuk 5**). Lokale lesies geven inzicht in of een hersengebied nodig is voor het uitvoeren van een bepaald gedrag. Lesies aan de OMV veroorzaken een toename van hoe vaak glissades voorkomen. Glissades snelheid, duur en amplitude zijn allemaal aangedaan door lesies aan de OMV, wat snel weer herstelt in de dagen na de lesie. In een set gedrag experimenten aan primaten met een intacte OMV toets ik of het mogelijk is motor adaptatie van glissades te induceren door middel van een aangepaste versie van het inter-saccadische stap taak. De resultaten impliceren dat glissades geen functionele beweging zijn maar een motorische fout.

Het brein is een groot complex netwerk, in de general discussion (**Hoofdstuk 6**) plaats ik de resultaten van dit proefschrift in de context met wat andere hersengebieden doen en hoe deze gezamenlijk komen tot het produceren van beweging. Recent onderzoek dat metingen beschrijft van meerdere hersengebieden tegelijk, laat zien dat ook de gebieden die in dit proefschrift gemeten zijn niet in isolatie functioneren. Ze vormen een circuit met onder andere de frontale en pariëtale oog velden, waarin informatie bijde kanten op uitgewisseld wordt. Het hele circuit is noodzakelijk om saccades te kunnen plannen en uitvoeren. Het cerebellum werd tot voor kort gezien als een structuur die zich voornamelijk bezighield met het uitvoeren van bewegingen. De resultaten in dit proefschrift dragen bij aan het in kaart brengen van welke eigenschappen van het cerebellum ten grondslag liggen aan de hele sequentie van gebeurtenissen in het brein betrokken bij motoriek; van het interpreteren van een stimulus tot het plannen en uitvoeren van een oogbeweging.

Publications

Liu, X., Yu, S.-Y., **Flierman, N.A.**, Loyola, S., Kamermans, M., Hoogland, T.M., De Zeeuw, C.I., (2021). OptiFlex: Multi-Frame Animal Pose Estimation Combining Deep Learning With Optical Flow. Front. Cell. Neurosci. 15, 621252.

Flierman, N.A., de Zeeuw, C.I., Badura, A.,(Expected 2021). Measuring cerebellar processing and sensorimotor functions in non-human primates, in: Silitoe, R. (Ed.), Neuromethods. Springer. *Accepted*.

Avila, E.O., **Flierman, N.A.**, Holland, P.J., Roelfsema, P., Frens, M.A., Badura, A., De Zeeuw, C.I., (2021). Purkinje Cell Activity During Suppression of Voluntary Eye Movements in Rhesus Macaques. bioRxiv.

Flierman, N.A., Ignashchenkova, A., Negrello, M., Thier, P., De Zeeuw, C.I., Badura, A., (2019). Glissades Are Altered by Lesions to the Oculomotor Vermis but Not by Saccadic Adaptation. Front. Behav. Neurosci. 13, 194.

Wouterlood, F.G., van Oort, S., Bloemhard, L., **Flierman, N.A.**, Spijkerman, J., Wright, C.I., Beliën, J.A.M., Groenewegen, H.J., (2018). Neurochemical fingerprinting of amygdalostriatal and intra-amygdaloid projections: a tracing–immunofluorescence study in the rat. J. Chem. Neuroanat. 94, 154–172.